



**University of  
Nottingham**

UK | CHINA | MALAYSIA

**Design, Synthesis and Application of a  
Library of Novel Bioactive Surfactants  
as a Tool for the Production of  
Functionalised Microparticles**

Valentina Cuzzucoli Crucitti, MSci

Thesis submitted to the University of Nottingham for the degree

of Doctor of Philosophy

December 2020



**Biomaterials  
Discovery**

# Abstract

The development of novel biomaterials needs to move towards a rational design from both a research and commercial point of view. In this context, the rise of combinatorial chemistry approaches and analytical high-throughput methods have been a breakthrough in the design and screening of new materials. In the polymer chemistry field, these methods led to the synthesis of libraries of novel polymers with significant savings in time, materials waste, and labour. Additionally, in the biomaterials screening process, it is important to find new biological alternative tests in order to have a deeper understanding on the interaction of the biomaterials with their immediate extracellular environment and, consequently, derive more realistic biological models/assays that mimic real human conditions.

In the work presented here, it was reported the synthesis of novel amphiphilic copolymers presenting target chemistry and biological properties. For the first time, this polymeric amphiphiles were used in a flow-focusing microfluidic apparatus where they acted as surfactants for the production of a library of monodisperse microparticles with bio-instructive surface, to be used as potential 3D platform for controlling surface-cell response.

In Chapter 3, a library of new polymeric surfactant materials was designed and synthesised by using a high-throughput synthesiser. In addition, in this chapter, the combination of a novel high-throughput analytical technique

and the use of a machine learning analysis delivered 'on-demand' product property assessment.

Chapter 4 outlines how the use of designed polymeric surfactants and droplet microfluidics can exert control over both the surface chemistry and size distribution of microparticle materials, demonstrating their critical importance for controlling surface-cell response.

In Chapter 5 the main aim was to develop and synthesise cationic random and block amphiphilic copolymers, by using two different radical polymerisation techniques. Also, the ability to self-assemble in water and to act as surfactant were investigated using the droplets microfluidics setup previously discussed.

# Acknowledgment

Firstly, I would like to thank my supervisors Professor Derek Irvine, Professor Morgan Alexander and Professor Ricky Wildman for their support and advice. Their encouragement and patience helped me to persist in this journey called PhD. I particularly would like to thank Derek for always being available when needed and for his contribution in the researcher I have become in these four years. A huge thank goes to Dr. Adam Dundas, without whom this project could not be as successful. His infinite patience and positivity helped me to persevere with the microfluidics and with this project. I would thank Arsalan Latif and Joris Meurs who performed the fibroblast attachment/proliferation and the protein attachment assay, respectively. I need to thank, also, Ana Alves Costa Pacheco who kindly helped and trained on the use of scCO<sub>2</sub> and Dr. Marion Limo who performed the analysis with the DLS plate reader. I would like to give a special mention to Dr. Jean Dubern who trained me and support me in the microbiology lab. A special thank you to Dr. Benjamin Muir and Dr. Shaun Howard who gave me the opportunity to visit their research lab in the CSIRO facilities. I will always remember my stay in Melbourne as one of the happiest moments of my PhD and for this I am very grateful.

I would thank all the people from the Next Generation Biomaterials Discovery Programme Grant, the B10/B10a lab and anyone who has contributed to my journey in these 4 years. Thanks for the support and the assistance throughout my project.

I would like to extend my deepest gratitude to the people who made my stay in Nottingham memorable. To Dara O'Brien my companion of misadventures and adventure without whom my PhD would not be the same. Thanks for your immense support, for dedicating me your time when I most needed and, most of all, for being you.

Finally, thanks to my parents, Lina and Rocco, and my sisters Valeria e Giuliana for your endless love and for always believing in me. Last but not least, my immense gratitude goes to my husband Vincenzo for his unconditional love which helped me to grow and mature in the person I am today. Thanks for always being there, listening through the tough times and encouraging me to be the best version of myself. None of this could have happen without you.

# List of Publications

## First Author Papers:

- Cuzzucoli Crucitti V., Migneco L. M., Piozzi A., Taresco V., Garnett M., Argent R. H., Francolini I., 'Intermolecular Interaction and Solid State Characterization of Abietic Acid/Chitosan Solid Dispersion Possessing Antimicrobial and Antioxidant Properties', European Journal of Pharmaceutics and Biopharmaceutics, 2018.
- Dundas A., Cuzzucoli Crucitti V., Haas S., Duber J. F., Latif A., Romero M., Sanni O., Ghaemmaghami A. M., Williams P., Alexander M., Wildman R., Irvine D. J., 'Achieving Microparticles with Cell-Instructive Surface Chemistry by Using Tunable Co-Polymer Surfactants', Advanced Functional Materials, 2020.

## Co-author Papers:

- Alvarez-Paino M., Amer M., Nasir A., Cuzzucoli Crucitti V., Needham D., Denning C., Alexander M., Rose F. R. A. J., Alexander C., 'Polymer Microparticles with Defined Surface Chemistry and Topography Mediate the Formation of Stem Cell Aggregates and Cardiomyocyte Function', ACS Applied Materials and Interfaces, 2019.
- Vasey C., Pearce A. K., Sodano F., Cavanagh R., Abelha T., Cuzzucoli Crucitti V., Anane-Adjei A. B., Ashford M. B., Gellert P. R., Taresco V., Alexander C., 'Amphiphilic Tri- and Tetra- Block Co-polymers

Combining Versatile Functionality with Facile Assembly into Cytocompatible Nanoparticles', *Biomaterials Science*, 2019.

- Pearce A. K., Vasey C. E., Anane-Adjei A. B., Sodano F., Cuzzucoli Crucitti V., Irvine D. J., Howdle S. M., Alexander C., Taresco V., 'Versatile, Highly Controlled Synthesis of Hybrid (Meth)acrylate-Polyester-Carbonates and their Exploitation in Tandem Post-Polymerization-Functionalization', *Macromolecular Chemistry and Physics*, 2019.
- Vallieres C., Hook A. L., He Y., Cuzzucoli Crucitti V., Figueredo G., Davies C. R., Burroughs L., Winkler D. A., Wildman R. D., Irvine D. J., Alexander M., Avery S. V., 'Discovery of (Meth)Acrylate Polymers that Resist Colonization by Fungi Associated with Pathogenesis and Biodeterioration', *Science Advances*, 2020.

### In progress

- Cuzzucoli Crucitti V., Contreas L., Taresco V., Howard S. C., Dundas A. A., Limo M. J., Williams P. M., Williams P., Alexander R.M., Wildman R. D., Muir B. W., Irvine D. J., 'Generation and Characterization of a Library of Novel Biologically Active Functional Surfactants using Combined High-Throughput Methods'

# Table of Contents

ABSTRACT .....	I
ACKNOWLEDGMENT .....	III
LIST OF PUBLICATIONS .....	V
<b>First Author Papers:.....</b>	<b>v</b>
<b>Co-author Papers:.....</b>	<b>v</b>
<b>In progress.....</b>	<b>vi</b>
TABLE OF CONTENTS.....	VII
LIST OF FIGURES.....	XV
LIST OF TABLES.....	XXVI
LIST OF ABBREVIATIONS.....	XXX
<b>1 INTRODUCTION .....</b>	<b>1</b>
<b>1.1 Polymer and Polymerisations .....</b>	<b>1</b>
1.1.1 Free Radical Polymerisation.....	2
1.1.1.1 Radical Polymerisation in the Presence of Chain Transfer Agent (CTA) .....	5
1.1.1.1.1 Thiol-mediated Free Radical Polymerisation .....	7
1.1.1.1.2 Catalytic Chain Transfer Polymerisation (CCTP).....	9
1.1.2 Reversible-Deactivation Radical Polymerization.....	13
1.1.2.1 Atom Transfer Radical Polymerisation (ATRP) .....	14

<b>1.2</b>	<b>Surfactant.....</b>	<b>17</b>
<b>1.3</b>	<b>Amphiphilic Copolymers.....</b>	<b>20</b>
1.3.1	Comb-graft Copolymers .....	21
1.3.2	Block Copolymers.....	25
<b>1.4</b>	<b>Polymers Applied to Medical Applications .....</b>	<b>27</b>
<b>1.5</b>	<b>Biomaterials Challenge.....</b>	<b>29</b>
<b>1.6</b>	<b>Combinatorial and High-Throughput Processing .....</b>	<b>31</b>
1.6.1	HT and Combinatorial Processing in Polymer Science .....	32
1.6.2	HT and Combinatorial Processing in Biomaterial Discovery .....	35
<b>1.7</b>	<b>Microfluidic Processing.....</b>	<b>38</b>
1.7.1	Physics of Droplets Production .....	41
1.7.2	Droplets Generation.....	43
1.7.3	Surfactants in Droplet-based Microfluidics.....	46
1.7.4	Microfluidics vs Conventional Methods.....	48
<b>2</b>	<b>MATERIALS AND METHODS .....</b>	<b>50</b>
<b>2.1</b>	<b>Chemical Synthesis.....</b>	<b>50</b>
2.1.1	Materials .....	50
2.1.1.1	Free Radical Polymerisation Controlled by CTA.....	50
2.1.1.2	Polymerisation via ATRP .....	52
2.1.2	Nuclear Magnetic Resonance Spectroscopy .....	53
2.1.3	Gel Permeation Chromatography .....	57
2.1.4	Automated Synthesiser: Chemspeed Swing Robot.....	60
<b>2.2</b>	<b>Polymer Microarray .....</b>	<b>62</b>
2.2.1	Materials .....	62

2.2.2	Printing Substrate Preparation .....	63
2.2.3	Microarray Printing .....	64
<b>2.3</b>	<b>Self-assembling Characterisation.....</b>	<b>66</b>
2.3.1	Nanoprecipitation Method .....	66
2.3.1.1	Ink-jet Printer .....	67
2.3.2	Dynamic Light Scattering.....	68
2.3.3	Zeta Potential .....	70
<b>2.4</b>	<b>Microparticles Production and Characterisation .....</b>	<b>71</b>
2.4.1	Materials .....	71
2.4.2	Microfluidics.....	71
2.4.3	Scanning Electron Microscopy .....	72
2.4.3.1	Size Characterisation.....	73
2.4.4	Time of Flight Secondary Ion Mass Spectrometry .....	74
<b>3</b>	<b>SYNTHESIS AND CHARACTERISATION OF AMPHIPHILIC RANDOM COPOLYMERS VIA TRADITIONAL AND HIGH-THROUGHPUT METHODS.....</b>	<b>76</b>
<b>3.1</b>	<b>Introduction .....</b>	<b>76</b>
3.1.1	Aims and Objectives.....	79
<b>3.2</b>	<b>Methods.....</b>	<b>80</b>
3.2.1	Polymer Microarray Production and 2D Biological Assay .....	80
3.2.2	Synthesis and Characterisation .....	83
3.2.2.1	CCTP Performed via Conventional Thermal Polymerisation Method .....	83
3.2.2.2	High-Throughput Synthesis of Polymer Libraries via Automated Synthesiser .....	85
3.2.2.2.1	Initial Parallel Polymerisation Screen Containing 42 Polymerisations Using CCTP at 1.5 g Scale.....	85

3.2.2.2.2	Optimisation of CCTP Parallel Polymerisation for 10 Monomers which Exhibited No Conversion in the Initial Screening at 1.5g Scale .....	87
3.2.2.2.3	Scale Up of 4 Selected Parallel Polymerisation Conducted via CCTP from 1.5g to 10 g Scale .....	88
3.2.2.2.4	General Procedure for the Parallel Polymerisation of 12 Auto-synthesiser based Polymerisations Conducted Using a Thiol Control Agents at 1.5 g scale	89
3.2.2.3	Nuclear Magnetic Resonance Analysis ( <sup>1</sup> H and <sup>13</sup> C-NMR) .....	90
3.2.3	High-Throughput (HT) Critical Aggregation Concentration Analysis (CAC) .....	94
3.2.4	Predictive Computational Model Development on Surfactants Self-Assembling Properties .....	96
<b>3.3</b>	<b>Results and Discussions .....</b>	<b>99</b>
3.3.1	2D Microarray Screening.....	99
3.3.2	CCTP Performed <i>via</i> Conventional Thermal Polymerisation Method .....	103
3.3.3	Synthesis of a Library of Surfactants via HT Method .....	112
3.3.3.1	High-Throughput Synthesis of Polymer Libraries via Automated Synthesiser .....	113
3.3.3.2	Copolymer Characterisation Results.....	117
3.3.3.3	HT Polymerisation Scalability – from 1.5g to 10 g .....	120
3.3.3.4	Thiol-mediated Free Radical Polymerisation via High-Throughput Synthesis	122
3.3.4	HT Evaluation of Critical Aggregation Concentration .....	124
3.3.5	Predictive Computational Model Development on Surfactants Self-Assembling Properties .....	132
<b>3.4</b>	<b>Conclusions .....</b>	<b>136</b>
<b>3.5</b>	<b>Appendix.....</b>	<b>138</b>

4	FABRICATION OF MICROPARTICLES VIA DROPLETS MICROFLUIDICS	
	PROCESSING AND THEIR BIOLOGICAL APPLICATIONS.....	158
<b>4.1</b>	<b>Introduction .....</b>	<b>158</b>
4.1.1	Aim and objectives.....	164
<b>4.2</b>	<b>Methods.....</b>	<b>166</b>
4.2.1	Microfluidic Microparticle Production .....	166
4.2.2	Microparticles Characterisation.....	167
4.2.3	<sup>1</sup> H-NMR method to Assess Leaching Materials.....	167
4.2.4	Leaching test with Cytotoxicity Assay .....	168
4.2.5	Bacterial Biofilm Formation .....	169
4.2.5.1	Statistical Analysis.....	171
4.2.6	Protein attachment Assay <i>via</i> Nano ESI-MS/MS.....	171
4.2.7	Fibroblast Attachment and Proliferation Assay .....	173
4.2.7.1	Cell Culture.....	173
4.2.7.2	Cytotoxicity .....	173
4.2.7.3	Cell Attachment .....	174
4.2.7.4	Cell Proliferation .....	174
4.2.7.5	Statistical Analysis.....	174
<b>4.3</b>	<b>Results and Discussions .....</b>	<b>175</b>
4.3.1	Microparticles Production.....	175
4.3.1.1	Initial Flow Optimisation.....	176
4.3.1.2	Flow Optimisation for HPhOPA Based Surfactant.....	178
4.3.1.3	SEM Characterisation for MPs Produced by Varying Hydrophilic Chain Length. 180	
4.3.1.4	SEM Characterisation for MPs Produced with Different Major Chemistry Components .....	182

4.3.1.5	Use of the HT produced Surfactants within an MPs Formation Screening Program	185
4.3.1.6	Microparticles leaching	189
4.3.1.7	Microparticle Surface Characterisation	192
4.3.2	Biological Performance of Functionalised Polymer Microparticles	195
4.3.2.1	Bacterial Biofilm Formation Assay	196
4.3.2.2	Human Skin Fibroblasts Attachment and Proliferation	204
<b>4.4</b>	<b>Conclusions</b>	<b>208</b>
<b>4.5</b>	<b>Appendix</b>	<b>210</b>
<b>5</b>	<b>SYNTHESIS AND CHARACTERISATION OF AMPHIPHILIC COPOLYMERS USING AN ALTERNATIVE HYDROPHILIC MONOMER: REPLACING PEG SIDE CHAIN WITH A TERTIARY AMINE</b>	<b>212</b>
<b>5.1</b>	<b>Introduction</b>	<b>212</b>
5.1.1	Aim and Objectives	214
<b>5.2</b>	<b>Methods</b>	<b>215</b>
5.2.1	Thiol-mediated Free Radical Polymerisation	215
5.2.2	ATRP of EGDPEA- <i>b</i> -DMAEMA	218
5.2.2.1	Synthesis of EGDPEA Macroinitiator	218
5.2.2.2	Synthesis of EGDPEA- <i>b</i> -DMAEMA	220
5.2.3	ATRP of HPhOPA- <i>b</i> -DMAEMA	221
5.2.3.1	Synthesis of HPhOPA Macroinitiator	221
5.2.3.2	Synthesis of HPhOPA- <i>b</i> -DMAEMA	223
5.2.4	ATRP of EA- <i>b</i> -DMAEMA	224
5.2.4.1	Synthesis of EA Macroinitiator	224
5.2.4.2	Synthesis of EA- <i>b</i> -DMAEMA	226

5.2.5	Dynamic Light Scattering.....	227
5.2.5.1	Critical Aggregation Concentration (CAC) Analysis.....	227
5.2.5.2	Zeta Potential.....	228
5.2.5.3	Protein Corona Binding Assay.....	228
5.2.6	Particles Production.....	229
5.2.6.1	Microfluidics.....	229
5.2.7	Microparticles Characterisation.....	229
<b>5.3</b>	<b>Results and Discussions.....</b>	<b>230</b>
5.3.1	Positively Charged Amphiphilic Random Copolymers.....	230
5.3.1.1	Comparison Random Copolymers.....	232
5.3.2	Positively Charged Block Copolymers.....	234
5.3.2.1	Synthesis of the Macromonomers.....	235
5.3.2.1.1	Synthesis of poly(EA).....	235
5.3.2.1.2	Synthesis of poly(EGDPEA).....	237
5.3.2.1.3	Synthesis of the poly(HPhOPA).....	241
5.3.2.2	Synthesis of the second block DMAEMA.....	245
5.3.2.3	Comparison Random and Block Architecture.....	248
5.3.3	Microfluidics.....	249
5.3.3.1	Microparticles Production with DMAEMA Based Random Copolymers..	249
5.3.3.2	Microparticles Production with DMAEMA Based Amphiphilic Block Copolymers.....	256
5.3.4	Microparticle Surface Characterisation.....	262
5.3.5	Protein Corona Binding Assay.....	266
<b>5.4</b>	<b>Conclusions.....</b>	<b>270</b>
<b>5.5</b>	<b>Appendix.....</b>	<b>272</b>
<b>6</b>	<b>CONCLUSIONS.....</b>	<b>280</b>

6.1	Summary.....	280
6.2	Recommendation for Future Work.....	283
7	REFERENCES.....	286

## List of Figures

Figure 1.1 Structure of bis[(difluoroboryl) diphenylglyoximato]cobalt(II) (PhCoBF) .....	10
Figure 1.2 CCTP catalytic cycle of Methyl Methacrylate (MMA), the cobaloxime catalyst go through to the oxidation state $\text{Co}^{\text{II}}$ to $\text{Co}^{\text{III}}$ .....	11
Figure 1.3 Schematic representation of a surfactant. The blue part represents the hydrophilic head; the red part represents the hydrophobic tail .....	17
Figure 1.4 Schematic plot of surface tension versus log of the concentration for an aqueous solution of a surfactant. It is also represented with a schematic illustration of aggregates formation with an increase of surfactant concentration.....	19
Figure 1.5 Methods of synthesis of branched graft copolymers. ....	22
Figure 1.6 Different alternating structures of block copolymers.....	25
Figure 1.7 Example of automated equipment for chemical process. <sup>155</sup> .....	32
Figure 1.8 Example of a typical polymer microarray. <sup>176</sup> .....	36
Figure 1.9 squeezing, dripping and jetting regimes into the microfluidics channel are affected by capillary number.....	42
Figure 1.10 Summary of materials adopted for the fabrication of microfluidics chip. Image adapted with permission from Ren et al. <sup>221</sup> Copyright 2013 American Chemical Society.....	44
Figure 1.11 Two principle microfluidic geometries for ‘droplets microfluidics’ .....	46

Figure 2.1 Spectroscopic analysis via $^1\text{H-NMR}$ to calculate the conversion of monomer in polymer and the molar ratio of one component in the copolymer contents. EA-co-mPEGMA <sub>300</sub> was used as example.....	55
Figure 2.2 Spectroscopic analysis via $^1\text{H-NMR}$ to calculate EGDPEA-co-mPEGMA/PEGMA comonomer ratio. ....	56
Figure 2.3 How GPC separates molecules of different sizes. ....	58
Figure 2.4 Chemspeed Swing robot used in this thesis work.....	60
Figure 2.5 Schematic steps process of printing polymer microarray which consist in (a) withdrawing monomer solution from a source plate using 946MP6B Arrayit quilled metal pins (b) transferring monomer solution to pHEMA substrate (c) photopolymerisation of the monomer spots by UV-light and (d) completed polymer microarray with polymer spots. ....	65
Figure 2.6 Schematic of particle size characterisation from the SEM images (a). Bandpass filter (FFT) (b) find edges (c) and threshold (d) commands was used in order to enable the Hough Circle Transform plugin within the ImageJ (Fiji software) (e). ....	73
Figure 3.1 Structures of the main monomers (a-g) and copolymers (h-m) adopted in the biological characterisation.....	91
Figure 3.2 (a) Structures of the monomers used for printing polymer microarrays showing major hydrophobic monomers in the blue panel and the minor hydrophilic monomers in the red panel. Chain lengths were either $n = 6$ or $9/10$ for PEGMA monomers or $m = 2, 4/5$ or $9/10$ for mPEGMA (b) Heat map variation in monomers entity; 1-12 variation in co-monomers concentration) of the polymer microarray showing attachment of mCherry	

labelled *P. aeruginosa* from high (red) to low (white) showing data from  $n = 6$ ,  $N = 2$  repeats. Narrow columns to the left or right indicate  $\pm 1$  standard deviation. (c) Copolymer data for EGDPEA with a range of different PEG-based hydrophilic chains, showing attachment of *P. aeruginosa* across a sequential copolymer series  $n = 6$  technical repeats and  $N = 2$  biological repeats and (d) Copolymer data for HPhOPA with a range of different PEG-based hydrophilic chains, showing attachment of *P. aeruginosa* across a sequential copolymer series  $n = 6$ ,  $N = 2$ . Data was normalized respect to the highest fluorescence intensity value (EGDPEA-co-mPEGMA<sub>500</sub> 50:50), corresponding to the highest *P. aeruginosa* biofilm spot coverage. ....101

Figure 3.3 Possible intermolecular hydrogen transfer reactions in the FRP of EGDPEA.....107

Figure 3.4 Study of the monomer conversion in the EGDPEA-co-mPEGMA<sub>300</sub> copolymer by NMR (a-b) and (c) GPC chromatogram of the final pure copolymer after 70h. ((EGDPEA:mPEGMA300):cyclohexanone 1:3 v/v at 75°C for 18h, 40h and 70h using 1% wt/wt of AIBN (EGDPEA:mPEGMA<sub>300</sub>)). .....109

Figure 3.5 Structures of the monomers and the scale of clogP used to assess the hydrophobicity level of each monomer.....112

Figure 3.6 Conversion of polymerisation determined by means of <sup>1</sup>H-NMR spectroscopy varying the solvent/monomer ratio.....114

Figure 3.7 Resulted conversions, determined by means of <sup>1</sup>H-NMR spectroscopy, from a further screening related to the decreasing the catalyst concentrations (i.e. 650 ppm and 450 ppm).....116

Figure 3.8 (a) Comparison of the % conversion of CCT polymerisations in small scale (1.5g) and large scale (10g) determined by means of <sup>1</sup>H-NMR spectroscopy. (b) Comparison of Mn of the copolymers obtained in small scale (1.5g) and large scale obtained. ....122

Figure 3.9 CAC of iBMA-co-MePEGMA, an example of plot of the intensity of scattered light (kilo counts per second) as a function of concentration (µg/mL). The data showed that the scattering detected for the surfactant concentrations below the CMC is similar to deionised water. After the CMC was reached, the scattering intensity shows a linear increase with concentration. The intersection between the 2 lines, at 4.93 µg/mL, corresponds to the CAC/CMC.....126

Figure 3.10 the logarithmic values of the calculated CACs were plotted against the value of the LogP of 14 HB monomers. CACs of 4 surfactants with HB monomers in the rectangle (a, b, c and d) were excluded from the trend. ....128

Figure 4.1 Section of the <sup>1</sup>H-NMR Spectra for HMDA monomer peak which defines the vinyl methacrylate double bond peaks at: 6.4 ppm, 6.1 ppm 5.8 ppm.....168

Figure 4.2 Schematic of the experimental microfluidics setup. The organic and aqueous phase were pumped with 3 syringe pumps and connected to the device via polytetrafluoroethylene tubes. A high-speed video camera was applied to observe the droplet formation through the flow focusing microfluidic chip. The droplets were collected in a glass vessel with water and shine by UV-Vis. At the bottom of the picture, it was included a generic

schematic of the chemistry used in this set up. The result in the application of the custom-made functionalised surfactants with an inert diacrylate monomer is the formation of cross-linked MPs (60-70  $\mu\text{m}$ ) with a low-density PEG-layer on the surface (around 10 nm). .....175

Figure 4.3 Flow diagram of an oil-in-water microfluidics system with HMDA core material and EGDPEA-co-mPEGMA<sub>300</sub>.  $\circ$  denotes idealistic dripping behaviour,  $\square$  denotes jetting behaviour,  $\diamond$  denotes formation of satellite droplets,  $\diamond$  denotes flow rates which caused wall wetting events and  $\Delta$  denotes large dripping. The Black square denotes the region of flow rates that produces monodisperse emulsions. Images show examples of dripping, jetting, satellite droplet formation and wall wetting events, respectively. ....177

Figure 4.4 Flow diagram of an oil-in-water microfluidics system with HMDA core material and HPhOPA-co-mPEGMA<sub>300</sub>.  $\circ$  denotes idealistic dripping behaviour,  $\square$  denotes jetting behaviour,  $\diamond$  denotes formation of satellite droplets,  $\diamond$  denotes flow rates which caused wall wetting events and  $\Delta$  denotes large dripping. The Black square denotes the region of flow rates that produces monodisperse emulsions. Images show examples of dripping, jetting, satellite droplet formation and wall wetting events, respectively. ....179

Figure 4.5 SEM of polymer microparticles produced using surfactants with different hydrophilic PEGMA/mPEGMA chains showing graphically the sizes of the images A-D (A) Monodisperse particles made from surfactant EGDPEA-co-mPEGMA<sub>300</sub> and a HMDA core with size  $64.30 \pm 1.33 \mu\text{m}$  (CV =

2.1 %) (B) Monodisperse particles made from surfactant EGDPEA-co-mPEGMA<sub>500</sub> and a HMDA core with size  $57.81 \pm 0.77 \mu\text{m}$  (CV = 1.3 %) (C) Monodisperse particles made from surfactant EGDPEA-co-PEGMA<sub>360</sub> and a HMDA core with size  $65.24 \pm 2.74 \mu\text{m}$  (CV = 4.2 %) (D) Monodisperse particles made from surfactant PVA and a HMDA core with size  $61.60 \pm 2.93 \mu\text{m}$  (CV = 4.8 %) .....181

Figure 4.6 SEM images of polymer microparticles produced using a droplets approach showing graphically the sizes of the images A-D size of particles shown in images A-E.(A) Monodisperse particles made with EGDPEA-co-mPEGMA<sub>300</sub> surfactant with a core made from HMDA and a size of  $64.30 \pm 1.33 \mu\text{m}$  (CV = 2.1 %) (B) Particles made with EGDPEA-co-mPEGMA<sub>300</sub> and HPhOPA-co-mPEGMA<sub>300</sub> in a 1:1 ratio with a core made from HMDA and a size of  $62.2 \pm 5.2 \mu\text{m}$  (CV = 8.4 %) (C) Particles produced with HPhOPA-co-mPEGMA<sub>300</sub> with a core made from HMDA with a size of  $62.42 \pm 1.66 \mu\text{m}$  (CV = 2.7 %) (D) Particles made with PVA surfactant with a core made from HMDA with a size of  $61.60 \pm 2.93 \mu\text{m}$  (CV = 4.8 %) (E) Particles made with only HMDA core material with no surfactant with a size of  $73.09 \pm 11.63 \mu\text{m}$  (CV = 15.9 %).....183

Figure 4.7 Size and % CV of the MPs produced by using surfactants using the automated synthesiser. EGDPEA and HPhOPA were not included as they had already been assessed.....185

Figure 4.8 SEM pictures at X250 and X650 resolution of the MPs produced with HA-co-mPEGMA<sub>300</sub> (A-C) and with THFuA-co-mPEGMA<sub>300</sub> (B-D) .....187

Figure 4.9 SEM pictures at X250 and X650 resolution of the MPs produced with NMEMA-co-mPEGMA<sub>300</sub> (A-C) and with DMPAm-co-mPEGMA<sub>300</sub> (B-D).  
.....188

Figure 4.10 <sup>1</sup>H-NMR spectrum showing minimal amount of leaching from particles when exposed to deuterated chloroform. Internal control used is TMS. Peaks in expanded section refer to acrylate bond protons, which facilitated calculation of the concentration of HMDA (0.5 mM). .....189

Figure 4.11 LIVE/DEAD cell viability study using MRC-5 (ATCC® CCL171™) human lung fibroblast cells. Particles produced with different photoinitiator content up to 5 wt % were used across a range of different particle concentrations. Cells grown on tissue culture plastic (TCP) and cells treated with Triton-X were used as positive and negative controls respectively. Measurements taken over N = 3 biological repeats. ....191

Figure 4.12 ToF-SIMS data showing intensities of: a) the key ions associated to the hydrophobic comonomers within the surfactant structures compared to the intensity of the same ions present in the HMDA spectra and b) the key ion associated to mPEGMA<sub>300</sub> (C<sub>3</sub>H<sub>7</sub>O<sup>+</sup>) present on the surface of each MPs. Ion images for each MPs are shown in Figure Appendix 4-1. ....194

Figure 4.13 Schematic representation of biofilm formation. Biofilm formation can be divided into five stages: Initial reversible attachment (1), irreversible attachment (2-3), maturation (4) and dispersion (5). During later stages, the biofilm is mature, forming characteristic “mushroom” structures due the polysaccharides. Finally, some cells start to detach, and the biofilm (shown in yellow) will disperse.<sup>345</sup> .....197

Figure 4.14 a) Surface coverage by single species (*P. aeruginosa*) biofilms quantified after 24 h incubation on particles coated with EGDPEA-co-mPEGMA<sub>300</sub>, HPhOPA-co-mPEGMA<sub>300</sub>:EGDPEA-co-mPEGMA<sub>300</sub>, HPhOPA-co-mPEGMA<sub>300</sub>, none and PVA surfactants respectively in RPMI. Quantification was performed on fluorescence images acquired on the 48 well-plate considering an area of 568 x 568  $\mu\text{m}$ . Error bars equal  $\pm 1$  SD unit, n = 3. Particle data were normalised for surface area and then to the non-surfactant (HMDA) control for comparison b) confocal microscopy images for mcherry tagged *P. aeruginosa* growing on each polymer surface. Each image is 295 x 295  $\mu\text{m}$ .....198

Figure 4.15 % Sequence Peptides Coverage of BSA quantified after overnight protein extraction and digestion from particles coated with EGDPEA-co-mPEGMA<sub>300</sub>, EGDPEA-co-mPEGMA<sub>300</sub>:HPhOPA-co-mPEGMA<sub>300</sub>, HPhOPA-co-mPEGMA<sub>300</sub>, none (HMDA core alone) and PVA surfactants. Quantification was performed using nanoESI-MS/MS and ion mass peaks in the mass spectra were confronted with tabled peptides mass ions. Error bars equal  $\pm 1$  SD unit, n = 3).....203

Figure 4.16 ToxiLight™ non-destructive cytotoxicity bioassay study using human skin fibroblasts (CRL-2522, ATCC). The assay measures the release of adenylate kinase (AK) from cells with compromised cell membranes. The AK catalyses conversion from ADP to ATP is detected through bioluminescence and the emitted light intensity is linearly related cell viability. n=6; ANOVA; p $\leq$ 0.05.....206

Figure 4.17 Human skin fibroblasts (CRL-2522, ATCC) attachment using CyQuant NF Assay, 24 h post seeding [n=6; analysis of variance (ANOVA);  $p \leq 0.05$ ] on polymer MPs in comparison to tissue culture plastic (PS flat). On the bottom confocal images of the human skin fibroblasts attachment obtained fixing (with PFA 4%) and staining with Phalloidin 488 and DAPI. b) Human skin fibroblasts (CRL-2522, ATCC) proliferation over 72 h using Click-iT™ Edu microplate assay [n=6; analysis of variance (ANOVA);  $p \leq 0.05$ ] on polymer MPS in comparison to tissue culture plastic (PS flat). .....206

Figure 5.1 GPC chromatogram and <sup>1</sup>H-NMR spectra of poly(Ethyl Acrylate). .....236

Figure 5.2 Cell view experiments for the solubility study of EGDPEA in scCO<sub>2</sub>. Below 1550 psi and 40°C the monomer is not soluble as it is possible observe from the figure a. Above 1550 psi and 40°C the monomer starts being soluble (figure b) and interacting with solvent. ....240

Figure 5.3 <sup>1</sup>H-NMR spectra of the pure poly(EGDPEA) using two different purification methods. ....241

Figure 5.4 <sup>1</sup>H-NMR spectra with peaks assignment and the GPC chromatogram of poly(HPhOPA).....244

Figure 5.5 <sup>1</sup>H-NMR spectra and the respective GPC chromatogram of the block copolymers HPhOPA-b-DMAEMA, EGDPEA-b-DMAEMA and EA-b-DMAEMA. ....247

Figure 5.6 Flow diagram of an O/W microfluidics system with HMDA core material and EGDPEA-co-DMAEMA (a), HPhOPA-co-DMAEMA (b) and EA-co-DMAEMA (c). In the diagram: ○ denotes idealistic dripping behaviour, □

denotes jetting behaviour,  $\square$  denotes formation of satellite droplets,  $\diamond$  denotes flow rates which caused wall wetting events and  $\Delta$  denotes large dripping. The Black square denotes the region of flow rates that produces monodisperse emulsions. Images show examples of dripping, jetting, satellite droplet formation and wall wetting events, respectively. ....251

Figure 5.7 Plot with size summary and the Coefficient of Variation (%) for the surfactants EGDPEA-co-DMAEMA and EA-co-DMAEMA produced by analysing the SEM images of the polymer MPs. ....254

Figure 5.8 Flow diagram of an O/W microfluidics system with HMDA core material and EA-b-DMAEMA (a) EGDPEA-b-DMAEMA (b) as surfactants. In the diagram:  $\circ$  denotes idealistic dripping behaviour,  $\square$  denotes jetting behaviour,  $\square$  denotes formation of satellite droplets,  $\diamond$  denotes flow rates which caused wall wetting events and  $\Delta$  denotes large dripping. The Black square denotes the region of flow rates that produces monodisperse emulsions. Images show examples of dripping, jetting, satellite droplet formation and wall wetting events, respectively. ....257

Figure 5.9 Plot with size summary and the Coefficient of Variation (CV %) for the surfactants EGDPEA-b-DMAEMA and EA-b-DMAEMA produced by analysing the SEM images of the polymer MPs. ....258

Figure 5.10 Plot with size summary and the Coefficient of Variation (%) for the mixed system formed by the surfactants (EGDPEA-b-DMAEMA/EGDPEA-co-DMAEMA)<sub>50/50</sub> and (EA-b-DMAEMA/EA-co-DMAEMA)<sub>50/50</sub> produced by analysing the SEM images of the polymer MPs. ....261

Figure 5.11 ToF-SIMS data showing intensities and the related images of the key ions associated to the (a) EGDPEA:DMAEMA and (b) EA:DMAEMA comonomers within the surfactant structure compared to the intensity of the same ions present in the core HMDA particles spectra.....264

Figure 5.12 Protein corona binding studies of the follow copolymers EGDPEA-co-mPEGMA<sub>300</sub>, EGDPEA-co-DMAEMA, EGDPEA-b-DMAEMA, HPhOPA-co-mPEGMA<sub>300</sub> and HPhOPA-co-DMAEMA with representative DLS traces of each polymer architectures after incubation in 2 wt% of BSA, confirming stability to aggregation in these conditions. Correlograms of the DLS traces and sizes as Intensity, Volume and Number are shown in Figure Appendix 5-12 and 5-13. ....267

## List of Tables

Table 2.1 Monomers used for the synthesis of surfactants using a CTA for the control of the polymerisation. ....	51
Table 3.1 Percentage conversions, calculated ratios and Mn for synthesised polymer surfactants based on EGDPEA-co-PEGMA <sub>360</sub> ((EGDPEA:PEGMA <sub>360</sub> ):cyclohexanone 1:3 v/v at 75°C for 18h using 0.5% wt/wt of AIBN (EGDPEA:PEGMA <sub>360</sub> )).....	104
Table 3.2 Percentage conversions, calculated ratios and Mn for synthesised polymer surfactants based on EGDPEA-co-mPEGMA <sub>300</sub> ((EGDPEA:mPEGMA <sub>300</sub> ):cyclohexanone 1:3 v/v at 75°C for 18h using 0.5% wt/wt of AIBN (EGDPEA:mPEGMA <sub>300</sub> )).....	106
Table 3.3 Percentage conversions and calculated ratios for synthesised polymer surfactants showing a range of different hydrophilic chains (PEGMA <sub>360</sub> , PEGMA <sub>500</sub> , mPEGMA <sub>300</sub> and mPEGMA <sub>500</sub> ) and also different major comonomer materials (EGDPEA + HPhOPA) (comonomers:cyclohexanone 1:3 v/v at 75°C for 18h using 0.5% wt/wt of AIBN).....	110
Table 3.4 Mn, Đ and final copolymer ratios of the initial screening reactions with CCTP with target feed ratio of 90:10 mol/mol.....	118
Table 3.5 Mn, Đ and Copolymer Ratio of the reactions with the altered CCTP catalyst concentrations. ....	118
Table 3.6 Conversion, Mn, Đ and final copolymer ratio of the scale up reactions with CCTP with a target feed ratio of 90:10 % mol/mol. ....	121

Table 3.7 Conversion, $M_n$ , $\bar{D}$ and final copolymer ratio for iBMA, iBuMA, DMA, DMAPA, DMPAm and F7BMA based mPEGMA <sub>300</sub> copolymers with a target feed ratio of 90:10 % mol/mol.....	123
Table 3.8 HT-CAC and final copolymer ratios of the surfactants produced in high-throughput method using either CCTP or thiol mediated free radical polymerisation.....	127
Table 3.9 size of the surfactants, produced in high-throughput method using either CCTP or thiol mediated free radical polymerisation, at the CAC of each single copolymers and above the CAC using 100 $\mu\text{g}/\text{mL}$ as fixed concentration. Each experiment was conducted using a DLS-plate reader at 25°C and preparing the emulsion/suspension in DI water (as described in Section 3.2.3).....	130
Table 5.1 Percentage conversions, calculated ratios (HyB:DMAEMA), $M_n$ and the physical characterisation of the nanoaggregates (size, CAC and zeta potential) for the synthesised polymer surfactants EA-co-DMAEMA, EGDPEA-co-DMAEMA and HPhOPA-co-DMAEMA. The DLS analysis were performed at 25°C and the Intensity (%) values were registered and analysed. The suspension/emulsion were prepared in DI water at pH of around 7. All the obtained conversions <sup>a</sup> were above 90%. .....	231
Table 5.2 Summary of the physicochemical characterisation data of the amphiphilic copolymers using DMAEMA as the hydrophilic component. The DLS analysis were performed at 25°C and the Intensity (%) values were registered and analysed. The suspension/emulsion were prepared in DI water at pH of around 7. ....	232

Table 5.3 Summary of the physicochemical characterisation data of the amphiphilic copolymers using mPEGMA <sub>300</sub> as the hydrophilic component. The DLS analysis were performed at 25°C and the Intensity (%) values were registered and analysed. The suspension/emulsion were prepared in DI water at pH of around 7. ....	233
Table 5.4 Summary of the polymerisation of EA via ATRP considering a theoretical $M_n$ of 13,000 g mol <sup>-1</sup> .....	236
Table 5.5 Summary of the polymerisation of EGDPEA via ATRP considering a theoretical $M_n$ of 15,000 g mol <sup>-1</sup> .....	238
Table 5.6 Summary of the polymerisation of HPhOPA via ATRP conducted for 24 h and considering a theoretical $M_n$ of 15,000 g mol <sup>-1</sup> .....	242
Table 5.7 Summary of the ATRP and the physical characterisation of the nanoaggregates (size, CAC and zeta potential) of EA-b-DMAEMA, EGDPEA-b-DMAEMA and HPhOPA-b-DMAEMA. ATRP was conducted using a molar ratio Initiator:Cu(I)Cl:Cu(II)Cl:HMTETA of 1:2:0.4:1.2 and aiming at a molar ratio Macroinitiator:DMAEMA of 90:10 % mol/mol. physical characterisation of the nanoaggregates (size, CAC and zeta potential). The DLS analysis were performed at 25°C and the Intensity (%) values were registered and analysed. The suspension/emulsion were prepared in DI water at pH of around 7. ....	246
Table 5.8 Summary of the physicochemical characterisation data of the amphiphilic block copolymers using DMAEMA as the hydrophilic component. The DLS analysis were performed at 25°C and the Intensity (%)	

values were registered and analysed. The suspension/emulsion were prepared in DI water at pH of around 7.....248

Table 5.9 Summary of the physicochemical characterisation data of the amphiphilic random copolymers using DMAEMA as the hydrophilic component.....248

## List of Abbreviations

FRP	Free Radical Polymerisation
MWt	Molecular Weight
CTA	Chain Transfer Agent
$C_s$	Chain Transfer Constant
$D_{pn}$	Degree of Polymerisation
CCTP	Catalytic Chain Transfer Polymerisation
PhCoBF	Bis[(difluoroboryl)diphenylglyoximato]cobalt (II)
RDRP	Reversible-Deactivation Radical Polymerisation
ATRP	Atom Transfer Polymerisation
RAFT	Reversible Addition Fragmentation Transfer Polymerisation
NMP	Nitroxide-Mediated Radical Polymerisation
PEG	Poly(ethylene glycol)
Water-in-oil	W/O
Oil-in-water	O/W
PVA	Poly(vinyl alcohol)
CAC	Critical Aggregation Concentration
CMC	Critical Micelle Aggregation
HT	High-throughput
MPs	Microparticles
NPs	Nanoparticles
<i>Re</i>	Reynolds number

$Ca$	Capillary number
FFD	Flow Focusing Device
PEGMA	Poly(ethylene glycol) methacrylate
mPEGMA	Poly(ethylene glycol) methyl ether methacrylate
AIBN	2, 2' Azobis (2-methylproprionitrile)
BzSH	Benzyl mercaptan
EGDPEA	Ethylene glycol dicyclopenthenyl ether acrylate
HPhOPA	Hydroxy-3-phenoxypropyl acrylate
EGPhEA	Ethylene glycol phenyl ether acrylate
THFuA	Tetrafurfuryl acrylate
EA	Ethyl acrylate
DMAEMA	2-(dimethylamino)ethyl methacrylate
NMR	Nuclear Magnetic Resonance
GPC	Gel Permeation Chromatography
SEC	Size Exclusion Chromatography
$\bar{D}$	Polydispersity
RI	Refractive Index
$M_n$	Number average molecular weight
$M_w$	Weight average molecular weight
polyHEMA	Poly[2-(hydroxy ethyl) methacrylate]
DLS	Dynamic Light Scattering
Z	Zeta potential
SEM	Scanning Electron Microscopy

ToF-SIMS	Time of Flight Secondary Ion Mass Spectrometry
HyB	Hydrophobic
Conv	Conversion
BSA	Bovine Serum Albumin
BAR	Bacteria Attachment Resistance
HMDA	1,6-hexanediol diacrylate
$Q_d$	Flow disperse phase
$Q_c$	Flow continuous phase
CV	Coefficient of Variation

# 1 Introduction

## 1.1 Polymer and Polymerisations

A polymer can be defined as a large molecule, or macromolecule, composed of many small repetitive units. The single molecules that represent the repetitive unit are called monomers and they are linked to each other by a chemical bond formed after a process called polymerisation. Staudinger has been one of the pioneers of the polymer chemistry science. In fact, he coined the word polymer in 1920<sup>1</sup> and, since then, synthetic polymeric materials have experienced a rapid development, which is one of the most remarkable achievements regarding science and technology in the 20th century.<sup>2</sup>

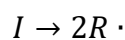
During the polymerisation process more than one monomer can be used and by varying the nature of the starting materials and the technique used, a large variation of monomer compositions can be obtained. Polymers that are composed of only one monomer type are called homopolymers whereas, polymers that are composed of two or more monomers are called copolymers. Homo- and copolymers can be generally synthesised by using two classes of polymerisations: chain-growth polymerisation and step-growth polymerisation. In the case of step-growth polymerisation, the mechanism is simply an extension of a conventional condensation reaction in which, usually, a small molecule such as H<sub>2</sub>O or HCl is formed as sub product when the polymer is formed. Example of step-growth polymerisations are polycondensation<sup>3,4</sup> and Michael-addition.<sup>5</sup>

While, in the chain-growth polymerisation an active molecule (e.g. ion or radical, conventionally coming from initiator species) reacts with monomers forming a polymer chain with a large molecular weight in a very short period of time. Chain-growth polymerisations are classified in 4 major subcategories: free-radical polymerisation, cationic polymerisation, anionic polymerisation and ring opening polymerisation (that can be activated by different mechanisms).

### 1.1.1 Free Radical Polymerisation

Free radical polymerisation (FRP) is a method of polymerisation which belongs to the chain-growth polymerisations.<sup>6</sup> In FRP, a polymeric chain is formed by the addition of monomeric species to the radical activated chain end thus, allowing the polymer chain to grow.<sup>6</sup>

The mechanism of such polymerisation technique comprises of three primary processes: initiation, propagation and termination.<sup>7</sup> Initiation takes place by cleavage of an initiator compound, either thermally, photochemically or chemically (Scheme 1.1).

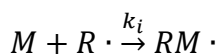


*Scheme 1.1 The homolytic cleavage of an initiator compounds.*

Different class of initiators are available, amongst the most used are azo compounds and peroxides.

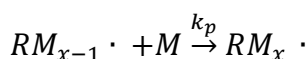
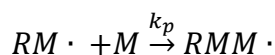
This new radical species can react with the double bond of the monomer yielding to a primary polymer radical (Scheme 1.2). In fact, one of the

prerequisites for the FRP is that the monomer bears a C=C as vinyl monomers, (meth)acrylates etc.



Scheme 1.2 The initiation process which involves the formation of a primary radical.

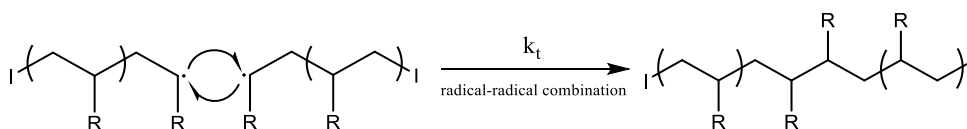
The propagation occurs when a series of monomers sequentially add to a primary radical or to a radical at the end of the growing polymer chain (Scheme 1.3).



Scheme 1.3 The propagation process: addition of a monomeric species to the primary radical (a) or a formed polymeric chain (b).

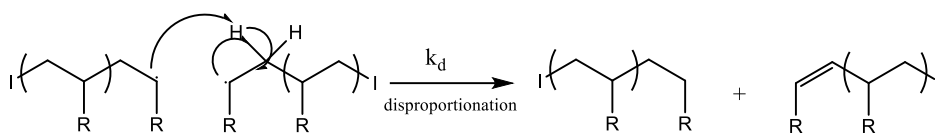
The propagation step proceeds by the radical monomer species continuing to react with the double bond of further monomers, increasing the chain length and, hence, the molecular weight (MWt).

The last step is the termination which can occur by two mechanisms: a) radical-radical combination and b) disproportionation. In the radical-radical combination scenario, two radical chains combine to produce a dead polymer with a high MWt (Scheme 1.4).



Scheme 1.4 The radical-radical combination of a radical polymeric chain where a new C-C bond is formed by the combination of two radical chains.

In the disproportionation, one polymeric radical extract a hydride species from the chain of a second polymer resulting in one saturated chain end and one olefinic chain end (Scheme 1.5).



*Scheme 1.5 The disproportionation process of two polymeric radical chains which is followed by the formation of a saturated chain end and an olefinic chain end.*

An additional step to be considered in the mechanism of the FRPs is the chain transfer process, which is commonly described as the transfer of a radical, from a polymeric chain to another molecule such as solvent, monomer or polymer and Chain Transfer Agent (CTA). This process will be discussed in more details in the following section 1.1.1.1.

A key advantage of this particular polymerisation is that: a) it does not require stringent process conditions and b) it can be used for the (co)polymerisation of a wide range of vinyl monomers. Today, nearly 50% of all commercial synthetic polymers are prepared using radical chemistry, providing a broad spectrum of materials for a range of markets.<sup>8</sup> However, the major limitation of FRP is the poor control over some of the key elements of the mechanism that would allow the preparation of well-defined polymers with controlled molecular weight, polydispersity, composition and chain architecture.<sup>9</sup> For instance, the propagation is rapid and high molecular weight (MWt) polymers are formed even at very low level of conversion. In addition, when FRP is scaled up at industry level, it is highly important to have control over the polymerisation, so undesired and potentially dangerous effects do not occur.<sup>10</sup> For instance, during the propagation phase, the viscosity of the medium can increase, as the polymer is produced, resulting in the decreasing of the termination

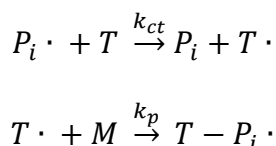
processes rate. This may lead to a higher radical concentration, consequently, the temperature and pressure increase within the reaction vessel which may result in an explosion. This undesired and uncontrolled cascade of events is called the Trommsdorf- Norrish effect,<sup>11</sup> or gel effect. It can be stopped by means of applying some precautions: stopping the polymerisation either at low conversion or low MWt and/or using solvents to reduce the reaction medium viscosity and/or adding chain transfer agents (CTA).<sup>7</sup> This latter strategy is employed to control MWt because the chain transfer agent reacts with a growing chain to yield a new polymer-terminated chain.<sup>7</sup> Typical CTAs used in industry are thiols. However, in the last few decades a number of new strategies were developed, such as the use of inorganic catalyst, to enhance the process of chain transfer to monomer opening.<sup>12</sup> In particular, it was found that porphyrins or benzoporphyrins substituted cobalt catalysts facilitated the production of low molecular weight polymers, with little to no reduction in overall yield in polymer.<sup>12,13</sup>

Another important chapter in the development of new strategies to overcome FRP limitations, in terms of MWt control and achievable architecture, is the development of Reversible-Deactivation Radical Polymerisation (RDRP), cationic and anionic polymerisations.<sup>14</sup>

#### *1.1.1.1 Radical Polymerisation in the Presence of Chain Transfer Agent (CTA)*

The control over the molecular weight of polymers is a subject of increasing interest because many of the polymers properties, such as physical and

mechanical properties, strongly depend on the chain length.<sup>15</sup> In the conventional FRP, since the control of the polymer chain length is difficult to attain, the classical method for controlling MWt is the addition of a CTA to the polymerisation medium.<sup>16</sup> As mentioned in the previous section, the reaction between the polymeric radical and the transfer agent is known as the chain transfer reaction. The typical mechanism, in which a CTA is involved, proceeds via hydrogen abstraction between the growing radical polymer chain ( $P_i \cdot$ ) and the transfer agent ( $T$ ). This forms a dead polymer chain and leaves a free radical on the CTA fragment which can be used for the initiation of other monomers (Scheme 1.6).<sup>15</sup>



*Scheme 1.6 The chain transfer mechanism.*

Due to the mechanism of action, usually, the CTAs introduce new functionalities to the polymeric backbone (see the “T” species in the figure above). This is often undesirable and may need to be removed in order to render the polymer suitable for its intended applications. Common CTAs include thiols, disulfides, halomethanes and other molecules with a readily abstractable hydrogen atom.

The general chain transfer constant,  $C_s$ , is defined as the ratio between the chain transfer and the propagation rate coefficients,  $k_{ct}/k_p$ , and is a measure of the reactivity of a chain transfer agent. The higher is  $C_s$ , the lower is the concentration of the CTA required to achieve a particular MWt reduction.<sup>17</sup>

The decrease in the MWt that will be attained by the addition of a CTA is quantitatively given by the Mayo equation (Equation 1.1), which expresses the reciprocal of the polymerisation degree ( $D_{Pn}$ ) as a function of the rate of the chain growth and the chain termination.<sup>18</sup>

$$\frac{1}{D_{Pn}} = \frac{1 + \alpha}{(D_{Pn})_0} + C_s \frac{[CTA]}{[M]}$$

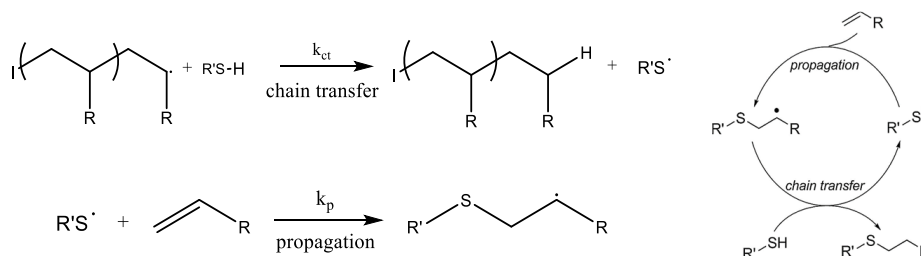
*Equation 1.1 The Mayo equation.*

In the Equation 1.1,  $(D_{Pn})_0$  is the Polymerisation degree in the absence of chain transfer agent,  $[CTA]$  is the concentration of the chain transfer agent,  $[M]$  is the monomer concentration and  $\alpha$  is the fraction of termination by disproportionation.

#### *1.1.1.1.1 Thiol-mediated Free Radical Polymerisation*

Thiol-mediated Free Radical Polymerisation is a chain-growth radical polymerisation involving a reaction between a multifunctional thiol and -ene (vinyl) monomers such as methyl methacrylate and styrene.<sup>17,19,20</sup> This kind of polymerisation exhibits several unique properties that have made them the focus of considerable recent investigations.<sup>19</sup> In fact, thiols have been employed as efficient, nearly ideal, chain transfer agents thanks to the high efficiency in the control of the chain length.<sup>20</sup> This is attributed to a combination of the weakness of the S–H bond, and the high reactivity of the thiyl radicals ( $RS\cdot$ ) towards the double bonds.<sup>21</sup> The weakness of the S-H bond explains the high reactivity of these compounds towards chains carrying macroradicals, leading to high value of chain transfer constants, regardless of the monomer employed. The high reactivity of the thiyl

radicals explains the chain transfer behaviour of thiols, which leads to a large decrease in the polymer molecular weight, without a significant change in the polymerisation rate.<sup>22</sup> Generally, the thiol-mediated polymerisation is conducted under standard radical conditions. Under such conditions, it proceeds *via* a typical FRP process with initiation, propagation and termination steps. Initiation involves the formation of radicals by cleavage of the radical initiators as in the FRP.<sup>23,24</sup> In the propagation step, there is the formation of a thiyl radical ( $R'S\cdot$ ), after the transfer of the radical from a growing radical polymer chain to a thiol functional group. Subsequently, this thiyl radical is added across the C=C bond of a monomeric species forming a thioether (Scheme 1.7). Possible termination reaction involves typical radical-radical coupling process.



Scheme 1.7 Propagation process which involves the chain transfer of a radical with consequent formation of a thyl radical which is initiating a new monomer.<sup>23</sup>

Two interesting examples of thiol-mediated radical polymerisation were proposed by Mandal's group.<sup>25,26</sup> By using thiols as CTA, they have prepared functional materials based either on polyhedral oligomeric silsesquioxanes (POSS) or water-soluble amphiphilic peptide-poly (1-vinylimidazole). The adoption of hybrid thiols as CTA has shown, in both works, control over the molecular weight as well as the possibility to tune thermal and amphiphilic properties.

As mentioned earlier, thiol-mediated polymerisation has renewed interest in the recent years, in particular, to obtain low-molecular weight polymers.<sup>17,20</sup> Low molecular weight polymers, due to the low viscosity and similar thermal properties to the monomeric precursors, are appealing to different applications (e.g. coatings, surfactants, etc.).<sup>27–29</sup> However, when using thiols as CTA some disadvantages have to be taken into account. Low molecular weight polymers can be achieved by employing high concentration of thiols, with potential toxicity. Finally, the formation of a thioether functionality, in the polymer chain-end group, might affect the physical properties of the final polymer.<sup>17</sup>

#### *1.1.1.1.2 Catalytic Chain Transfer Polymerisation (CCTP)*

In the last three decades, CCTP has been recognised as a successful method for producing low molecular weight functional polymers *via* FRP.<sup>30</sup> In fact, Smirnov and Marchenko discovered a method in which they could both control the MWt of polymers using certain low-spin Co<sup>II</sup> complexes, in particular Co<sup>II</sup> porphyrins, and enhance the process of chain transfer to polymeric radical species.<sup>31</sup> Improvement in the catalyst technology led to cobalt catalysts being very efficient, active and not sensitive to hydrolysis and oxidation. To date, the most widely used catalyst in the CCTP is the one commonly denoted as bis[(difluoroboryl) diphenylglyoximato]cobalt(II) (PhCoBF) (Figure 1.1)

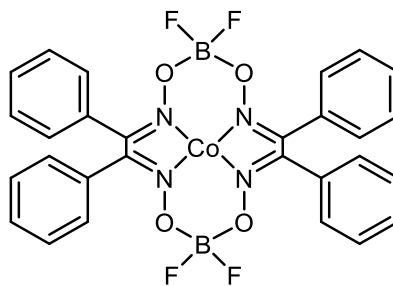


Figure 1.1 Structure of bis[(difluoroboryl) diphenylglyoximate]cobalt(II) (PhCoBF)

One of the most striking features of CCTP is the exceptionally fast rate at which it takes place.<sup>32</sup> The MWt of a polymer can be reduced from tens of thousands to several hundred Dalton (Da), utilising only ppm concentrations of cobalt catalyst.<sup>33</sup> The chemistry of low molecular weight oligomers has been relatively unexplored for several reasons. Previous routes to produce oligomers involved complicated and expensive chemistry, while, thiol chain termination required high levels of toxic or malodorous side products making the use of these CTA unacceptable in certain applications.<sup>16</sup> On the other hand, RDRP (will be explained in detailed in section 1.1.2.1) required high levels of initiator or catalyst because each initiator leads to only one macromonomer, making them commercially unattractive when low molecular weights are required. Furthermore, unlike other methods of controlling FRP, including Reverse Addition-Fragmentation chain-Transfer polymerisation (RAFT), Nitroxide-mediated radical polymerisation (NMP) and Atom Transfer Radical polymerisation (ATRP), CCTP does not leave any fragment of the control agent on the terminated polymer, but instead generates a terminal double bond.<sup>34,35</sup> This chain end functionality can be further exploited in a second radical polymerisation step. Thus, this polymerisation technique is a very efficient and versatile strategy which has

---

found applications in a wide range of fields.<sup>30</sup> For instance, Haddleton and co-workers used CCTP, in the first stage to synthesise a vinyl-terminated poly(methyl methacrylate) macromolecule, carried out in emulsion, that was subsequently used *in situ* as a chain-transfer agent for the reversible addition-fragmentation chain transfer polymerisation of various methacrylic monomers.<sup>36</sup> Using a similar approach, the same group produced polymerizable surfactants based on a small library of methacrylate monomers, by combining CCTP with sulfur-free reversible addition-fragmentation chain transfer polymerisation in emulsion.<sup>37</sup>

All the studies conducted to understand the mechanism behind the CCTP indicates that it proceeds via a two-step radical process (Figure 1.2).<sup>30,38–40</sup>

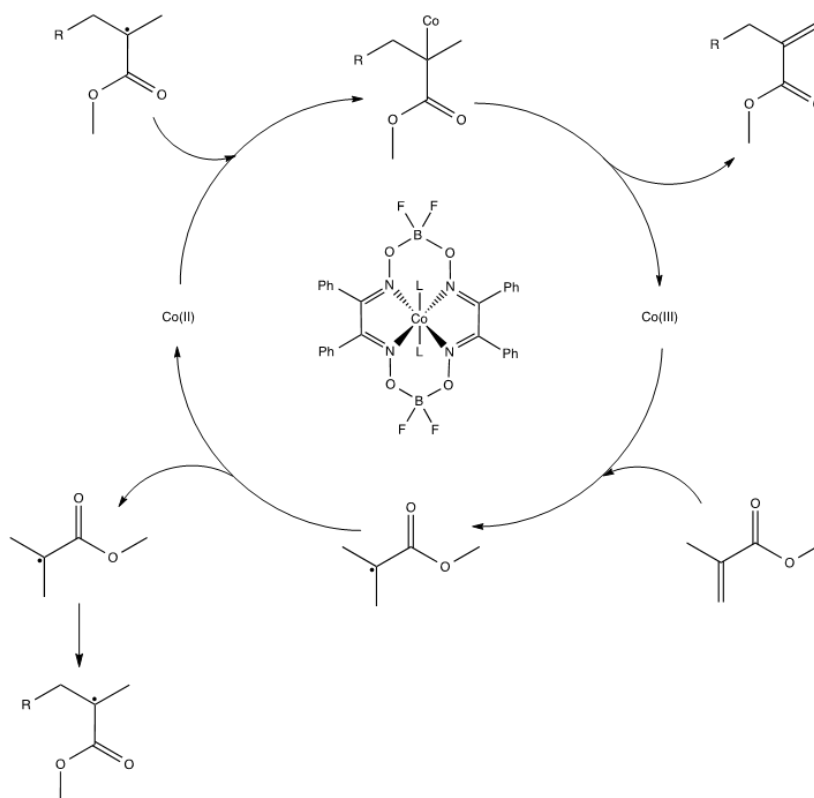


Figure 1.2 CCTP catalytic cycle of Methyl Methacrylate (MMA), the cobaloxime catalyst go through to the oxidation state  $\text{Co}^{\text{II}}$  to  $\text{Co}^{\text{III}}$ .

Firstly, the  $\text{Co}^{\text{II}}$  complex abstracts a hydride species from the growing molecule leading to an intermediate  $\text{Co}^{\text{III}}\text{H}$  complex, called cobalt hydride, and a dead polymer chain terminated with a double bond. The  $\text{Co-H}$  species are very reactive and, in the case of methacrylates and/or monomers with an  $\alpha$ -methyl group, it reacts with a monomeric molecule yielding back to the original  $\text{Co}^{\text{II}}$  catalyst and a monomeric radical, which can start growing. However, for monomers without any  $\alpha$ -methyl group near the  $\text{C}=\text{C}$ , the mechanism is slightly different due to the lack of an  $\alpha$ -methyl group. It is thought that in this case a hydrogen is abstracted from a secondary position in the polymer backbone, which is less sterically and electronically favourable. This also means that the polymer formed is not terminated with a vinyl group and instead a double bond is present between the penultimate and last repeating units. Hydrogen abstraction at the  $\alpha$ -methyl substituent is more efficient and monomers containing an  $\alpha$ -methyl group are therefore very active in CCTP.<sup>39</sup>

An unwanted side reaction, which takes active catalyst out the cycle itself, is the  $\text{Co-C}$  bonding between the catalyst and the radical chain which does not form part of the catalytic cycle of CCTP.<sup>32</sup> For methacrylates, cobalt-carbon bonding is negligible and has no significant effect on the polymerisation.<sup>41</sup> However, monomers forming secondary radicals (such as styrene and acrylates) a significant amount of  $\text{Co}^{\text{II}}$  can be trapped as a  $\text{Co}^{\text{III}}-\text{R}_n$  complex.

Nevertheless, CCTP does have its disadvantages, the catalyst may need to be removed after the reaction by precipitation of the polymer. This often

requires large volumes of organic solvent, which is not very environmentally friendly. Often the precipitation needs to be carried out more than once or the polymer may still have traces of catalyst left which affects the colour of the product.

### 1.1.2 Reversible-Deactivation Radical Polymerization

The concept of Reversible-Deactivation Radical Polymerisation (RDRP) was born in the attempt to overcome one of the disadvantages of FRP related to the control of the polydispersity, chain architectures and composition. In particular, these types of polymerisations are propagated by radicals that are deactivated reversibly, bringing them into active dormant equilibria incapable of being terminated by disproportionation and combination.<sup>42</sup> RDRP polymerisations have witnessed a rapid growth in the synthesis of polymers. Their advantages are as follows:

- initiation process and rate of active dormant chain equilibrium are rapid compared to propagation
- linear increase in molecular weight during the polymerisation with monomer conversion
- target molecular weight with narrow  $\bar{D}$  values ( $<1.50$ )
- re-initiation of the polymer/macromonomer (allowing the synthesis of block copolymers and other complex architectures).<sup>7,9</sup> RDRP are different from the free radical polymerisation processes because of the dynamic equilibrium between a low concentration of active propagating chains and predominant amount of dormant chains. A dormant chain is

a polymeric chain unable to propagate or terminate. Since the equilibrium is shifted towards dormant species, the concentration of propagating chains decreases, and termination becomes less significant compared to the propagation step.<sup>14</sup>

A number of RDRP methods have been developed so far and, the three most promising are: Nitroxide-mediated Radical Polymerisation (NMP), Atom Transfer Radical Polymerisation (ATRP) and Reversible Addition Fragmentation Chain Transfer (RAFT) polymerisation. In particular, in the present work ATRP has been studied and evaluated for its ability to build random and, especially block copolymers adopting inorganic catalyst.

#### *1.1.2.1 Atom Transfer Radical Polymerisation (ATRP)*

ATRP is one of the most adopted RDRP techniques and it uses transition-metal as catalysts in the control over its mechanism.<sup>43</sup> The transition metals that have been explored in the ATRP chemistry are ruthenium/aluminium alkoxide-based, iron-based, nickel-based. However, the most used so far, are copper-based catalysts.<sup>44</sup> They are usually in the halide form and complexed with a ligand to improve their solubility in the reaction medium.<sup>45</sup> Ligands are amines-based molecules with either linear or complex (e.g. tetradentate, tridentate, etc.) structures which play a role in the activity of the metal halide catalysts.<sup>45</sup> The monomers that generally are suitable for this technique are (meth)acrylate monomers, styrenes and acrylonitrile. Other components involved in the ATRP system are initiators.



Since ATRP has been discovered, its technology has improved considerably. One of the main points addressed so far is the higher concentration of catalyst used, often equimolar to the initiator.<sup>43</sup> In this regard, the research has focused on finding solutions to either remove the catalyst by adding purification steps (including passing the polymer solution through silica or neutral alumina columns, stirring with an ion-exchange resin, clay, precipitation of polymers into a nonsolvent, or the use of a heterogeneous catalyst that could be isolated after polymerisation) or trying to lower the level of catalyst, to ppm amount, by increasing the activity of the catalyst (e.g. involving the continuous regeneration of the deactivator).<sup>47</sup> With the aim to pursue the latter strategy, polymerisation procedures like ARGET, ICAR, SARA and eATRP have been developed.<sup>48–51</sup> Thanks to this constant progress, and also, the ability of such method to produce polymers with different architectures, ATRP has become one of the techniques of election for the synthesis of polymers in a variety of applications.<sup>35,47,52</sup> In particular, Alvarez-Paino et al. have shown the use of ARGET ATRP to functionalise biodegradable PLA microparticles.<sup>53</sup> They functionalised the microparticles with an alkyl halide, which acted as initiator, and, subsequently, grew poly(N-(3-aminopropyl)-methacrylamide hydrochloride) and poly(ethylene glycol) methacrylate (PEGMA). Based on the different synthesised surface chemistry, these materials were found to be useful for long term 3D co-culture with mammalian cells, and a subset of the microparticles was supportive of cell attachment, growth, and cardiomyocyte contraction.

## 1.2 Surfactant

Surfactants are a class of materials that have become vital for everyday life. In fact, the technology of surfactants has seen a huge development in the last three decades, spreading their use in many industries spanning from the pharmaceuticals and medical to the petroleum and detergents<sup>54–59</sup>. The high interest connected to these materials is mainly related to their ability to modify the surface properties of liquids, typically water (the name surfactant is the contraction of the term **surface-active agents**). This inherent property generates from their particular structures which is formed by at least one lyophilic ('solvent-loving') group and one lyophobic ('solvent-hating') group. If the solvent is water or an aqueous solution then, the terms would be 'hydrophilic' and 'hydrophobic', respectively (Figure 1.3).

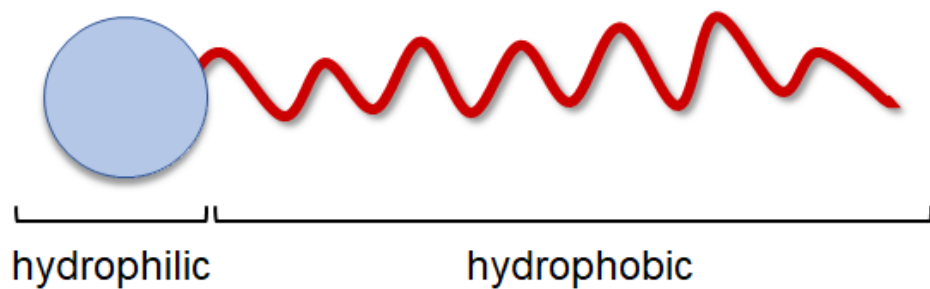


*Figure 1.3 Schematic representation of a surfactant. The blue part represents the hydrophilic head; the red part represents the hydrophobic tail*

This dual characteristic of surfactant molecules gives them a wide range of properties connected to two key features: 1) adsorption at interfaces and 2) self-assembly in solution.

In a solution, molecules on the top surface layer are attracted into the bulk, leading to an imbalance between the attractive intermolecular interactions at the liquid surface. This imbalance generates an excess of free energy at the surface, forcing the liquid surface to contract and, reducing the exposed surface area.<sup>60,61</sup> This tendency of liquid to shrink into the minimum surface possible is called surface tension ( $\gamma$ ) (units  $\text{J m}^{-2}$  or  $\text{N m}^{-1}$ ). Surfactant molecules have the ability to adsorb onto surfaces significantly, altering/decreasing the surface tension, and so the free energy, at the interface.<sup>62–66</sup> Importantly, the tendency of surfactants to self-assemble in solution depends on their concentration in the liquid phase. A dramatic decreasing of surface tension is observable when the surfactant concentration is increasing until a Critical Aggregation Concentration (CAC)<sup>67,68</sup> is reached. This concentration represents the point where a homogenous layer of surfactants molecules is formed at the liquid/air interface. Beyond this point the interface is saturated by surfactants molecules, therefore, aggregates are formed (Figure 1.4). If these aggregates assume a well-defined structure called micelle, the concentration, where the micelle development is detectable, is called Critical Micelle Concentration (CMC).<sup>69</sup>

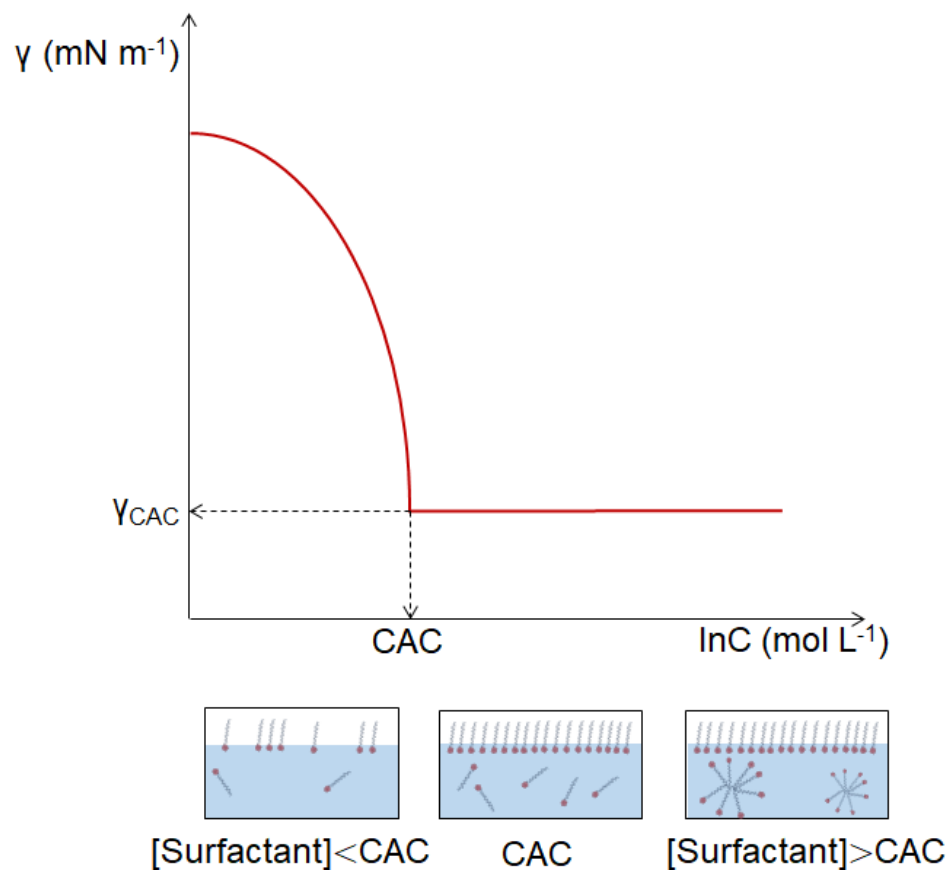


Figure 1.4 Schematic plot of surface tension versus log of the concentration for an aqueous solution of a surfactant. It is also represented with a schematic illustration of aggregates formation with an increase of surfactant concentration.

Traditionally, surfactants are classified in three different categories: ionic, non-ionic and zwitterionic.<sup>70</sup> Ionic surfactants present the hydrophilic polar segment with a charge. The charge can be either positive or negative and, based on this, they are called cationic and anionic, respectively. Anionic surfactants are widely used for industrial applications, such as cleaning and pesticide formulations.<sup>71,72</sup> Examples of anionic surfactant groups include sulfonic acid salts, alcohol sulphates, alkylbenzene sulfonates, phosphoric acid esters, and carboxylic acid salts<sup>73</sup>. Cationic surfactants, exhibiting a positive charge at the hydrophilic part, are less exploited as detergents since

they bind too strongly to fabrics. However, they are used in hair products and as antimicrobial agents.<sup>74,75</sup>

Zwitterionic surfactants are surfactants that carry both a positive and a negative charge on the backbone. These charges can either be permanent or dependent to the pH value. Often the cationic compound is either an amine or a quaternary ammonium cation.<sup>76,77</sup>

Non-ionic surfactants, unlike the aforementioned categories, are comprised of neutral hydrophilic and hydrophobic groups. They are extensively used in many fields thanks to their inherent low toxicity, good compatibility with other type of surfactants and their weak ability to be adsorbed into surfaces which makes easier their removal.<sup>61,78</sup>

Recently, polymeric surfactants have received an increasing attention in the surfactant field, thanks to their unique formation of self-assembled structures and for the higher structural complexity (number and distribution of hydrophilic/hydrophobic units).<sup>79,80</sup> Polymeric surfactants, which present a hydrophilic/hydrophobic dualism in the backbone, are addressed as amphiphilic polymers in the literature.

### 1.3 Amphiphilic Copolymers

Polymers endowed with hydrophobic and hydrophilic segments, in the polymeric chain, are called amphiphilic. In fact, the adjective amphiphilic derives from Greek and it means “loving both”. In the case of amphiphilic copolymers, this dual affection is related to the affinity towards a water and an oil phase. They have been extensively used in different applications

spanning from drug delivery, oil-recovery and food products.<sup>81–87</sup> However, thanks to this “duality” the amphiphilic polymeric chains can migrate to the liquid-liquid interfaces and be used as surfactants or stabilisers for emulsions or dispersions.<sup>88,89</sup> In fact, unlike low molecular weight amphiphilic molecules, polymers have the advantage of being more stable when adsorbing at a surface. This is possible because of more anchor points along the chain towards the surface, allowing the use of lower concentrations for these amphiphilic materials in formulations.<sup>90,91</sup> In addition, the stability of the self-assembled structure is linked to the amphiphilic polymer’s physical properties which depend on its chemical structures, hydrophilic-hydrophobic balances, molecular weights and functional moieties.<sup>91–93</sup> Thanks to the development of different controlled polymerisation techniques, e.g. anionic or RDRP, amphiphilic copolymers have been prepared in various chemical structures, including linear block copolymers, graft copolymers, dendritic polymers, star-like polymers, and cyclic polymers, among others.<sup>94–97</sup> In the present work, linear, graft and block copolymers were taken into account as two different architectures able to generate different self-assembling systems.

### 1.3.1 Comb-graft Copolymers

Graft copolymers are formed by two or more different monomers with different chemical nature (e.g. hydrophobic, hydrophilic, etc.).<sup>98</sup> The monomers, which side chain or brush have a different chemical composition of the backbone, are randomly organised along the polymer chain assuming

a comb-shaped architecture. Graft copolymers have a high relevance thanks to their low viscosity which is a significant advantage during the manufacturing process.<sup>99</sup> The low viscosity, compared to linear structures with the same molecular weights, is associated to their particular branched structure.<sup>100</sup>

Graft copolymers have many structural variables (comonomer composition, backbone length, side chain length, grafting density, distribution of the side chains, etc.). They can be synthesised using three different process: grafting onto, grafting from and grafting through (Figure 1.5).<sup>98</sup>

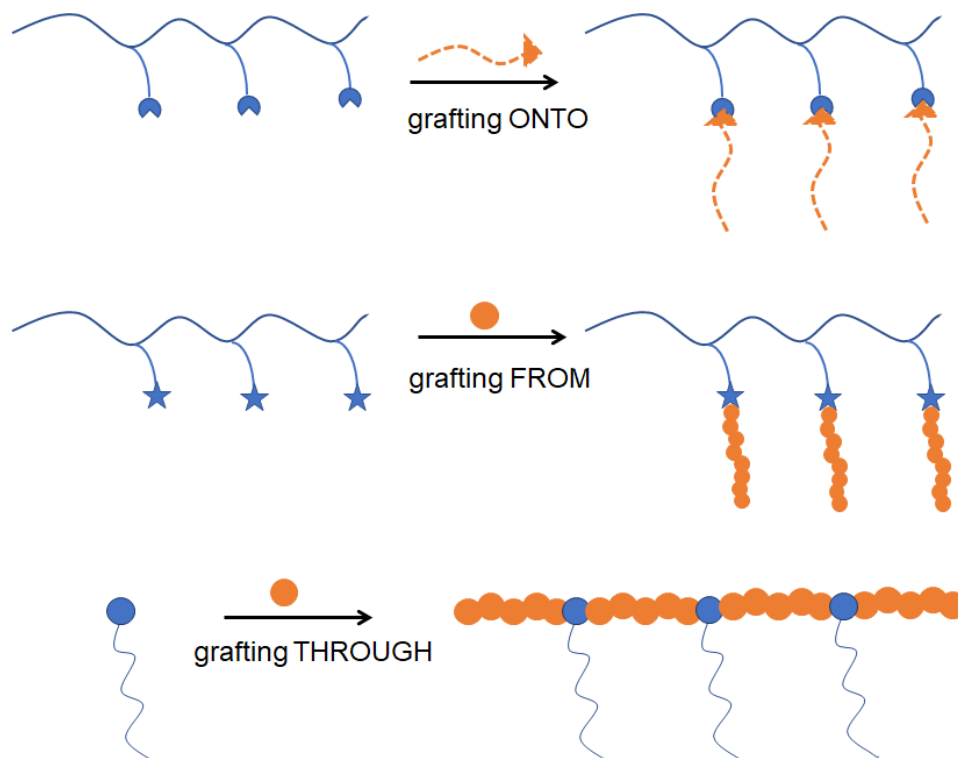


Figure 1.5 Methods of synthesis of branched graft copolymers.

*Grafting onto* is the process that sees a chemical bonding between pre-formed polymeric chains, having target functional groups, and other polymeric chains with active chain-ends. An example of *grafting onto* method is the ring oxirane opening reaction to introduce azide groups in

copolymers (glycidyl methacrylate)-co-(methyl methacrylate) performed by Matyjaszewski group.<sup>101</sup> The synthesis of brush copolymers by a *grafting onto* click technique is followed, adding a polymeric alkyne to the azide groups present in the polymeric side chain by click reaction.

In the *Grafting from* method, the polymeric side chain is modified in order to become the activation site of the polymerisation of a second monomer.

The number of grafted chains can be controlled by the number of active sites generated along the backbone, assuming that each one of them participate in the formation of one branch.<sup>98</sup> A variety of examples of the synthesis of comb-like copolymers can be reported using this versatile method. Russel et al. have shown a successful strategy for the ATRP of amphiphilic copolymers using poly(chlorotrifluoroethylene) oligomers as ATRP initiator and styrene and tert-butyl acrylate as monomers for the subsequent grafting.<sup>102</sup>

*Grafting through* or *Macromonomer method* is the method applied for the synthesis of the random comb-like graft copolymers in the present thesis work. In particular, macromonomer species, with polymerisable end groups, are reacted with monomers and initiator species resulting in copolymers.<sup>100,103,104</sup> The factors that are affecting the reactivity ratio are:

- the intrinsic reactivity of the macromonomer and the comonomer based on their chemical nature.
- the diffusion or excluded volume associated with the large size of the macromonomer.

- The potential incompatibility of the macromonomer and propagating comonomer chain due to thermodynamic repulsive interactions.<sup>105–107</sup>

In this method, the synthesis of macromonomers have been one of the main points of investigation, in particular new controlled polymerisation techniques have been used to aim at producing macromonomers with a variety of chemistry.<sup>108</sup> ATRP and anionic polymerisations have demonstrated to be versatile techniques,<sup>98,108</sup> alternatively, the use of industrially proven free-radical polymerisation techniques such as CCTP, also, allows the synthesis of low molecular weight macromonomers.<sup>104</sup> Macromonomers such as polyethylene,<sup>109</sup> poly(ethylene oxide),<sup>110</sup> polysiloxanes,<sup>103,111</sup> poly(lactic acid),<sup>112</sup> polycaprolactone<sup>113,114</sup> and poly(ethylene glycol) (PEG)<sup>115</sup> have been copolymerised with monomers such as styrene, methyl methacrylate and ethyl methacrylate in order to tune the final physical and chemical properties of the materials.

## 1.3.2 Block Copolymers

Block copolymers have a distinguishing architecture where monomeric units are arranged in distinctive blocks along the polymer backbone. Each block is linked to the other by a chemical bond as a result of the polymerisation mechanism.<sup>116</sup> The alternation order of each block (A and B) can be grouped in different structures among these: AB diblock, ABA/BAB triblock, alternating block and tapered block (Figure 1.6).

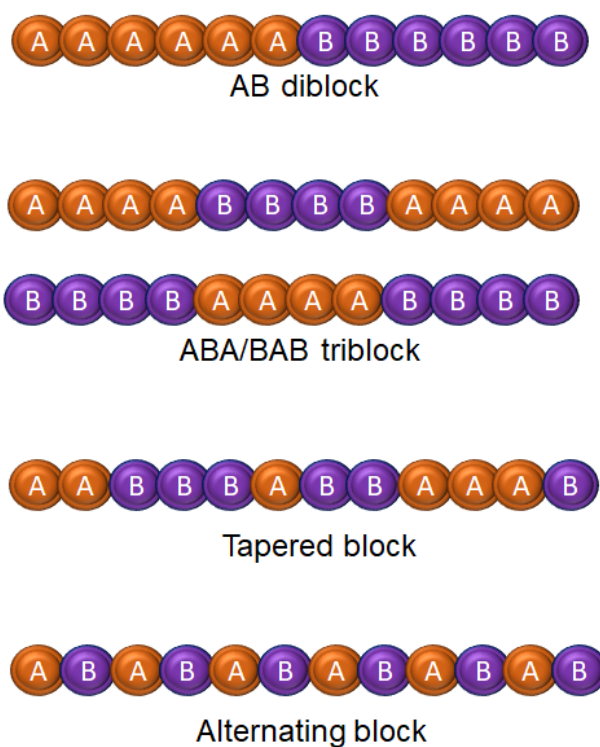


Figure 1.6 Different alternating structures of block copolymers.

Block copolymers, when in bulk, can assume different morphologies including spherical, cylindrical and lamellar. This is possible by manipulating the alternation of monomer units, along with other parameters such as solubility parameter, the degree of polymerisation and the volume fraction (between the hydrophilic and hydrophobic segments).<sup>91,116,117</sup>

On the other hand, the block copolymer amphiphiles undergo to a different self-assembling process when in aqueous solution. In fact, the driving force is to minimise energetically unfavourable hydrophobic-water interactions.<sup>83</sup> In this case, the morphologies are primarily determined by the so called ‘packing parameter’.<sup>116</sup> By controlling the factors that are able to change the packing parameter such as monomer composition and concentration, water content, common solvent, and additives, a wide range of morphologies have been reported including spherical micelles, cylindrical, bi-continuous, lamella, vesicles, tubules, etc.

Nowadays the synthetic pathways are mainly focused on two different strategies: the use of RDRP to add different monomeric units in sequence and coupling reactions which use the active chain-ends to add different chain segments.<sup>97</sup> This thesis work has been focused on the RDRP strategies, in particular, due to their suitability with a variety of monomers and chemistry and, also, the easy experimental setup.<sup>9,118</sup> The polymerisation mechanism of RDRP has been already introduced in the Section 1.1.2, therefore, it will not be discussed in the present paragraph. However, over the last two decades, numerous literatures have described the synthesis of block copolymers using techniques such as ATRP, RAFT, nitroxide-mediated polymerisation and many others.<sup>96,119</sup>

Polymer chain ends equipped with an alkyl halide enables ATRP to prepare block copolymers through the addition of a second monomer. For example, Alexander’s group showed the design and the synthesis of a new PEG-based block copolymers *via* ATRP for the delivery of the cytotoxic camptothecin

into tumour cells that overexpress Luteinizing Hormone Releasing Hormone Receptor (LHRHR).<sup>120</sup> Matyjaszewski et al. reported the preparation of poly(*n*-butyl acrylate-*b*-methyl methacrylate) (PBA-*b*-PMMA) by activators regenerated by electron transfer atom transfer radical polymerisation (ARGET ATRP) with ppm levels of Cu catalyst.<sup>121</sup> Controlled polymerisation was realised using tris(2-pyridylmethyl) amine (TPMA) as a ligand because of its strong binding interaction to copper. This new ARGET system was also successfully applied to the efficient synthesis of styrene and *n*-butyl acrylate block copolymers.<sup>122</sup> Later on, miniemulsion ARGET ATRP was developed by the same group and used for the preparation of homopolymers and block copolymers.<sup>123,124</sup> Finally, Constantinou et al. have prepared a small library of tri-block copolymers (ABC) at different monomers molar composition using Group Transfer Polymerisation to investigate the thermo- and pH-responsiveness of the resultant materials.<sup>125</sup> These copolymers were made of non-ionic hydrophilic penta(ethylene glycol) methyl ether methacrylate (PEGMA), 2-(diethylamino)ethyl methacrylate (DEAEMA), which acted as comonomers with thermo- and pH-responsive properties (hydrophilic at alkaline pH and hydrophobic at acidic pH) and *n*-butyl methacrylate (BuMA) behaving as the non-ionic hydrophobic counterpart to promote self-assembly.

#### 1.4 Polymers Applied to Medical Applications

The numerous advances achieved in the area of synthetic polymeric materials have allowed for significant improvements in the medical field. In

this field, polymers have become materials of choice for drug and gene delivery, tissue engineering, manufacturing of medical devices and vaccine/anti-toxin therapeutics.<sup>126–132</sup> The advantage of polymers, used as biomaterials, is attributed to the possibility to tailor a wide range of properties like molecular weight, cross-linking degree, degree of crystallisation, co-polymers, blends and additional bioactive surface functionalisation.<sup>132</sup> Amongst other advantages, biodegradation, as a more advanced property of some polymers, finds application in an increasing number of fields from suture materials to vascular stents, because these devices may need to degrade after they have fulfilled their function.<sup>127,131</sup> Stiffness, topography and elasticity along with toxicity and biocompatibility are primary characteristics to be taken into account in the choice of substrate for cell differentiation *in vitro* and *in vivo*.<sup>133,134</sup> An interesting example regarding the important role of the modification and tuning of materials properties, in the design of biomaterials, is presented by Jones et al.<sup>135</sup> They developed degradable antimicrobial coatings of urinary medical devices using blends made of poly( $\epsilon$ -caprolactone) (PCL) and poly(vinylpyrrolidone)-iodine (PVP-I). In fact, they proposed to reduce the incidence of medical device related infection by offering surface/local antimicrobial activity (PVP-I) facilitated by the removal of attached microorganisms by the biodegradation of PCL.

Finally, in the drug delivery research one of the most active fields is the stimuli-responsive “smart” polymers, where polymers are able to respond

to changes in the surrounding environments by altering their properties.<sup>136,137</sup>

## 1.5 Biomaterials Challenge

Biomaterial design and manufacturing have, amongst all the challenges,<sup>138–141</sup> tried to evolve throughout the years, addressing the different requests from both the academia and industry. In the first generation, biomaterials were developed in order to ‘achieve a suitable combination of physical properties to match those of the replaced tissue with a minimal toxic response in the host’.<sup>141</sup> In other words, the main properties required for biomaterials were biological inertness, to reduce any response from our body, after the introduction of the foreign body, with optimal mechanical properties.<sup>140,142</sup> Subsequently, the interest moved towards a second generation of materials able to show biological response, in order to achieve an action and reaction in the physiological environment (allowing materials to be resorbed into the body and expelled with time through non-toxic breakdown products).<sup>140,143</sup> Finally, in the third-generation, specific cellular responses at the molecular level were sought.<sup>144</sup>

Along with the development process of biomaterials from the first to the third generation, researchers have also tried to tackle the problem associated to the translation from a small-scale lab design to a large-scale, which includes the commercialisation of such materials.<sup>145</sup> Ideally, for a biomaterial being selected as a commercial candidate has to respond to two critical questions that a commercial sponsor must address: a) the scalability

of the chemistry and b) the environmental/health and safety regulations.<sup>146</sup> For instance, if the biomaterial of interest is biodegradable, the mechanism and kinetics of degradation need to be characterised and understood properly in order to identify the chemical breakdown products.<sup>147</sup> The process of addressing these issues is based upon long trial and error experiments, that require the use of many animals and large numbers of human clinical trials. These result prohibitively expensive and most of the time fail with the non-commercialisation of the product.<sup>145,146</sup> In this regard, the total number of published researches concerning the concept of “biomaterials” in peer-review journals is taking into consideration, they have been over 60,000 in the last 20 years (searching on Scopus<sup>148</sup> using ‘biomaterial’ as keyword). However, to date only a small number of these materials are currently being used or developed commercially, e.g. polylactides and glycolides, polycaprolactone and polypropylene.<sup>139,147</sup> Nevertheless, they have shown a series of limitations and have not always provide the ideal combination of physical, chemical and biological properties.<sup>139</sup> For this reason, the development of novel biomaterials through a rational design, fulfilled from both a research and commercial point of view, is vital.

Moreover, in the last decade great interest has grown in the development of predictive *in vitro* tests based upon human cells that are sufficiently reliable and cost effective.<sup>149,150</sup> There are different points to address regarding the strategy of *in vitro* tests to ensure relevance to eventual *in vivo* applications:<sup>140</sup> a) correlation of the same mature cell phenotype

between *in vivo* and *in vitro*; b) when testing the biomaterials, it is important to monitor the status and response of cell cycles in culture and the cell phenotype; c) examine molecular changes, in terms of pattern of protein expression, during the exposure with the biomaterials; d) perform 3D cellular assay. This latter point has risen to a particular attention to find an alternative to the well-established 2D *in vitro* assays. In fact, it has been observed that correlation of results between 2D cultures, typically in tissue culture plastic, and real live *in vivo* scenario are in most of the cases very different.<sup>151</sup> In particular, it is well known that flat and hard plastic or glass substrates, usually used for *in vitro* cell culture, are not representative of the cellular environment found in the human body.<sup>152</sup>

As a consequence, it is important to find new *in vitro* alternative tests in order to have a deeper understanding on the interaction of cells with their immediate extracellular environment and, consequently, derive more realistic biological models/assays that mimic real conditions.<sup>130</sup>

## 1.6 Combinatorial and High-Throughput Processing

The rise of combinatorial chemistry approaches and high-throughput (HT) methods have been a breakthrough in the redefinition of the process of research and development in a number of fields.<sup>153</sup> These include the pharmaceutical sector,<sup>154</sup> where the drug discovery process has been improved largely thanks to the application of automated screenings; the area of biomaterial development (discovery),<sup>153</sup> where these methodologies have improved the identification of lead candidates by

screening a large number of molecules/materials against specific biological response.

Polymer chemistry have, also, benefitted from these methods, where a wide variety of monomers with different molecular structures and polymerisation techniques have been tested.<sup>155–157</sup>

### 1.6.1 HT and Combinatorial Processing in Polymer Science

The application of high-throughput methods and combinatorial chemistry in the polymer chemistry field have led to the synthesis of libraries of polymers delivering significant savings in time and labour.<sup>158–161</sup> By employing a synthetic robot (Figure 1.7), which is able to dispense solutions, mix and modify parameters (e.g. T, pH, t, etc.), it is possible to perform completely automated and less time-consuming workflows.<sup>162</sup>



Figure 1.7 Example of automated equipment for chemical process.<sup>155</sup>

When compared to the traditional synthetic approaches, the advantages of producing these HT libraries are in the rapid identification of a small number of promising candidates, or “hit” candidates, with chemical, physical and biological properties of interest.<sup>163,164</sup> In addition, polymer chemistry is very well suited for combinatorial approaches due to the diversity of parameters that can be varied systematically, e.g., monomers, initiators, catalysts, solvent, targeted molecular weight, functional groups and architecture.<sup>156</sup> In this regard, free radical polymerisation is of particular interest for its application in a HT screening pipeline. It does not require stringent process conditions/pre-preparation of reagents and it can be used for the (co)polymerisation of a wide range of vinyl-bearing moiety monomers (including acrylates, (meth)acrylates, (meth)acrylamide, etc).<sup>8</sup> Bradley’s group was one of the first group to apply FRP to an automated synthesiser.<sup>165</sup> They performed the polymerisation in suspension of styrene, divinyl benzene and vinylbenzyl chloride in order to produce polymeric beads. The resulting size distribution of such beads was reproducible and showed that automation can be a pathway for the rapid design of polymeric beads and, to optimise polymerisation conditions. Copolymers have, also, been prepared in an automated fashion by Baudis et al. using methyl methacrylate as a base monomer for the copolymerisation with the comonomers styrene, N-vinylpyrrolidone, 4-vinylpyridine and 2-carboxyethyl acrylate.<sup>166</sup> Up to 48 parallel polymerisations were performed showing that the generation of the four different polymer libraries can be generated in about one month after optimising all the conditions. This

corresponds to an increase of throughput by a factor of about 10 when compared to classical experimentation.

Unfortunately, the relative low level of control over the FRP polymerisation mechanism often makes difficult the use of FRP in HT processes where the target is the screening of well-defined polymers with controlled molecular weight, polydispersity, composition and chain architecture. For these types of molecular targets, examples of HT RDRP, such as RAFT and ATRP, have been shown in literature reporting high degree of success in reaching the set targeted  $M_n$  and  $\bar{D}$  in a controlled way.<sup>167–169</sup> For instance, one of the first example of automated/parallel RAFT is the work presented by Schubert's group where they successfully synthesised poly(methyl methacrylate)s aiming at a molecular weight of  $10,000 \text{ g mol}^{-1}$ .<sup>170</sup> By screening different conditions, well-controlled polymers with narrow polydispersity were obtained hinting that parallel synthesis can be successfully applied to RDRP. Another interesting example of parallel RDRP is the one showed by Pan et al. In this particular work, they have replaced a traditional automated synthesiser with a DNA synthesiser preparing well-defined homopolymers and block copolymers by photo-ATRP.<sup>171</sup> Photo-ATRP has been selected because of its mild conditions, reactivity at room temperature, tolerance to oxygen and no need to introduce radical initiators. In order to extend the applications of such polymers, a series of DNA-polymer hybrids have been prepared to assess the direct compatibility of this method with DNA synthesis. This protocol, thus, provides a convenient alternative option for non-experts in synthetic polymer

chemistry to obtain highly controlled bioconjugates without any degassing procedures. A similar example was developed by Gurnani et al., where a protocol was established for the preparation of a library of well-defined homo-polymers, block- and statistical copolymers *via* RAFT polymerisation by exploiting thermocycler technology.<sup>172</sup>

However, to date, there are no examples of HT screenings which have been specifically aimed at testing and demonstrating the suitability of a controlled radical polymerisation which is robust enough to be readily and easily scaled-up to an industrial manufacturing level. On commercial scale, polymerisation control can be achieved successfully, yielding to a new functionalised polymer-terminated chain, by the use of a chain transfer agents (CTAs).<sup>7,118</sup>

### 1.6.2 HT and Combinatorial Processing in Biomaterial Discovery

To date, the biomedical field has relied on reduced sources of materials which have severely limited product development and increased the demand to find effective and less cost- and time-consuming solutions.<sup>145</sup> HT methods have been to be successful for materials screening, in particular, to speed up the rational design and optimisation of materials.<sup>173</sup> One HT platform, which have demonstrated in the past to be a powerful tool for genomic and drug discovery, that can be promising adopted for the material discovery is the microarray.<sup>153</sup> A microarray is a platform where hundreds of materials can be deposited onto solid substrate in discrete locations, in the form of spots, representing a unique and parallel experiment.<sup>174</sup> This

results in hundreds to thousands of independent measurements on a system being conducted simultaneously in a single screen.<sup>175</sup> Recently, the microarray has been exploited for the high-throughput discovery of polymers. In fact, by replacing biomolecules (e.g. DNA, proteins, etc.) with monomers it allows the formation of a combinatorial library of polymer spots (Figure 1.8).<sup>176</sup>



Figure 1.8 Example of a typical polymer microarray.<sup>176</sup>

Importantly, individual polymers are spatially resolved, which enables the high throughput, cost-effective and parallel screening of every member of large libraries of polymers identifying new biomaterials when tested for different biological assays.<sup>176</sup> Polymer microarrays are typically formed by contact or ink-jet printing. Printing involves the use of a robot moving a metallic pin or a nozzle, which is dipped into a solution and then spotted onto the substrate surface by either making contact or ink-jetting, respectively. The microarray format proved to be a valuable platform for

the material-cell interactions being tested in cell culture with ease (bacteria, fungi, human cells, cancer cells, etc.).<sup>177–180</sup> The results in the screening of many polymeric materials, using the appropriate choice of bioassay, identify the ‘hit’ materials suitable for the scale-up process. The creation of a diverse range of polymeric materials is an important requirement for producing biomaterials ideally suited to the unique and specific requirements of every medical application.<sup>181</sup> A typical array formed by this method is the one published by Anderson et al. where they identify an array which allow different levels of human embryonic stem cell attachment and spreading, cell-type specific growth, and growth factor–specific proliferation.<sup>182</sup> Celiz et al. have applied this approach to identify the polymeric substrate, among more than 900 polymers tested, that achieves human pluripotent stem cells (hPSC) pluripotency and expansion and, subsequently, the multilineage differentiation into representatives of the three germ layers, namely cardiomyocytes, hepatocyte-like cells and neural progenitors.<sup>183</sup> Samples have been fixed and stained for OCT4 expression (an indicator of pluripotency) and images have been acquired using an automated fluorescence microscope. The screening process allowed them to find the lead candidate that fulfilled all the current culture requirements for the clinical use providing an alternative to commercially available hPSC expansion substrates.

Pioneering work from Hook and Alexander led to the discovery of a new class of (bio)materials with broad spectrum resistance to bacterial attachment that would have not been predicted using the current

understanding of material-bacteria interactions.<sup>179</sup> In particular, Hook et al. generated a vast combinatorial polymer microarray from 22 commercially available acrylate monomers. These were combined in varying ratios to create 496 unique polymers incubated with fluorescent bacteria for three days and the resulting attachment or resistance to bacteria was quantified from the fluorescent signal on each polymer surface.<sup>179</sup> In an attempt to rationalise the mechanism involved, it was noted that all the polymers bearing a hydrophilic ester groups and a hydrophobic cyclic hydrocarbon group, in the polymer backbone, were resistant to bacteria attachment. This suggests that a weakly amphiphilic structure might be the cause of the anti-attachment properties.<sup>184</sup>

## 1.7 Microfluidic Processing

The term microfluidics indicates all the devices and methods which control and manipulate fluids in the nano- and micro length scale.<sup>185–189</sup> In the last decades, such technology has experienced an improved interest mainly because of its versatility and applicability in different fields spanning from drug formulation,<sup>190,191</sup> food products,<sup>192</sup> drug delivery system,<sup>193,194</sup> biosensors<sup>195,196</sup> and microreactors.<sup>197–200</sup> Among all the microfluidics systems, those intended for the generation of microdroplets have inspired many researchers and led to various innovations.<sup>201,202</sup> Droplets of one fluid homogeneously dispersed in a second immiscible fluid are useful in a wide range of applications, particularly when the droplets size and size distribution can be highly controlled (coefficient of variation, CV, lower than

5%). In fact, 'droplet microfluidics' can produce highly monodispersed droplets which allow to transport, mix and analyse each droplet individually.<sup>187,203</sup> In addition, it has been demonstrated how the droplet-based microfluidics method has shown high reproducibility, low batch-to-batch variation and easy scalability.<sup>204–206</sup> Thanks to all of these advantages, in the last 20 years, 'droplet microfluidics' has seen a growing interest. Whitesides' group has shown how it is possible to produce polymeric MPs with different shapes by using this system.<sup>207</sup> They described a new strategy for producing monodisperse solid particles with sizes from 20 to 1000  $\mu\text{m}$ . Their method involved the formation of monodisperse liquid droplets by shaping the droplets in a microchannel. These drops were, then, solidified in situ either by polymerizing a liquid monomer or by lowering the temperature of a liquid that sets thermally. Similarly, Nie et al. produced a library of polymeric microparticles with different shapes using a droplet microfluidics device.<sup>208</sup> Different dimethacrylate monomers were used using SPAN 80 as stabiliser. Thanks to the use of this technology, they had precise control over the size of liquid cores, the thickness of shells, and the overall size of the particles. More recently, Xu et al. reported a novel microfluidic method to produce Janus droplets with controlled morphology, and enhanced stability against coalescence suitable for the fabrication of polymeric microlenses.<sup>209</sup> They generated biphasic droplets comprised of a photocurable acrylate monomer and a silicon oil containing a surfactant in the aqueous poly(vinyl alcohol) (PVA) solution. Janus droplets in the aqueous PVA solution are highly stable against coalescence after off-chip

collection, unlike those dispersed in aqueous SDS solution. Finally, bioconvex, planar-convex, and concave-convex polymer microlenses can be synthesized via photopolymerization from Janus droplets carrying surfactants at different concentrations.

From the Whitesides' group, another interesting example shows as MPs produced *via* microfluidics have an impact in the drug delivery.<sup>210</sup> This work described the fabrication of monodisperse and biodegradable MPs made of poly(lactide-co-glycolide) (PLGA), and drug-loaded with model amphiphilic drug (bupivacaine). Interestingly, the kinetic analysis showed that the release of the drug from these monodisperse particles is slower than that from conventional methods of the same average size but a broader distribution of sizes. Finally, they exhibited a significantly lower initial burst than that observed with conventional particles.

Weitz's group, also showed, that thermo-responsive polymer microgels can be produced easily *via* 'droplet microfluidics'.<sup>211</sup> Microgels have an important role in many applications (such as support for cells, drug delivery etc.)<sup>212–215</sup> Weitz's produced monodisperse poly(N-isopropylacrylamide) microgels using a polymer-analogous crosslinking reaction. By developing this method, they showed that gels with higher crosslinking, with nano- and microscale homogeneity, was obtained when compared to the classical free-radical crosslinking copolymerization technique.

Similarly, to the literature examples reported, in the present work, the 'droplet microfluidics' will be exploited as an important tool for producing a library of functionalised polymeric microparticles (MPs). However, all these

examples showed the use of commercial surfactants (PVA, SPAN 80, etc.) as stabilisers. Differently, in the present project a novel method was proposed in which custom-made surfactants were used, not only, to stabilise the emulsion, but also, to decorate the surface with active molecules.

### 1.7.1 Physics of Droplets Production

During an emulsification process different factors are identified which significantly impact upon the formation mechanism of droplets: laminar/turbulent flow, surface tension, capillary and viscous forces.<sup>186,188</sup> For microfluidics system the Reynolds number ( $Re$ ) is an indication of the flow profile.<sup>216</sup> This dimensionless quantity is inversely proportional to the fluid viscosity and direct proportional to the characteristic velocity of the fluid and the dimension of the system where the fluid is involved (Equation 1.2).

$$Re = \frac{\rho V D}{\eta}$$

*Equation 1.2 Reynolds number.  $\rho$  and  $\eta$  are respectively the fluids density and viscosity,  $V$  is the mean fluids velocity and  $D$  is the characteristic dimension of the flow (usually the channel width).*

For microfluidics system the flow is almost always in the laminar regime ( $Re < 2300$ ) which is characterised by flat paths organised in layers with each layer moving past each other independently generating little or no mixing. Thanks to this profile, laminar flow provides highly predictable fluid dynamics and allows predictable diffusion kinetics.<sup>216</sup>

Surface/interfacial tension forces play an important role in the length working scale of the microfluidics system (micro-, nano-). In fact, in the

emulsification process of two immiscible liquids, droplets are forming when the interfacial tension between the two phases is low or negligible. In this respect, the usage of surfactants is a central aspect of the droplets-based microfluidic technology. Surfactants allow for stable emulsification by adsorbing at the liquid-liquid interface and reducing its free energy.

Another important dimensionless number is the capillary number ( $Ca$ ) which role is in determining droplets dynamics.<sup>217,218</sup> This is defined as the effect of viscous forces, related to surface tension, acting across an interface (Equation 1.3):

$$Ca = \frac{\eta V}{\gamma}$$

*Equation 1.3 Capillary number.  $\eta$  is the viscosity of the continuous phase (water in oil-in-water emulsions or oils in water-in-oil emulsions),  $V$  is the velocity of the continuous phase and  $\gamma$  is the interfacial tension between the two immiscible liquids.*

Experimental observations showed that with the increasing of  $Ca$  values, different flow regimes can be defined, within the microfluidics, as the squeezing, dripping and jetting regimes (Figure 1.9).<sup>217–220</sup>

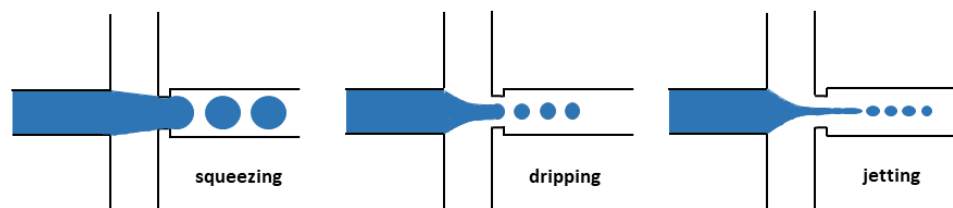


*Figure 1.9 squeezing, dripping and jetting regimes into the microfluidics channel are affected by capillary number.*

The squeezing mechanism is driven mainly by the build-up of a pressure generated by an emerging droplet and both the dynamics of breakup and the scaling of the sizes of droplets are mainly affected by the flow rate ratios

of the continuous/dispersed phase. In fact, in this flow regime  $Ca$  values are negligible; thus, they do not contribute to the dynamics of droplets. In the dripping regime, droplet breakup and size are shear-dominated with a lower pressure coming from the meeting of the two immiscible fluids. The yield droplets tend to be smaller with the increasing of  $Ca$ , with a reduced dependence on the flow rate ratio. Whilst, the jetting regime forms only at very high flow rates, i.e. higher values of the capillary number.

Finally, the viscosity of the continuous phase is helping the formation of droplets. Selection of more viscous continuous phases is one of the first details in the stabilisation of the emulsion. For instance, a common method for improving the viscosity properties of the aqueous phase, in oil-in-water system, is the addition of viscous water-miscible fluids such glycerol or PEG.<sup>203</sup>

### 1.7.2 Droplets Generation

Microfluidics chip can be defined as the device where a set of microchannels are moulded in different geometries.<sup>221</sup> Fluids can reach this network of microchannels by tubes connected, commonly, to either syringe or automatic pumps. The manufacturing technology of these micro devices has had an evolution in the past two decades, reflecting two major trends: microscale platform and low-cost reliable portable analysis. The first generation of microchips has been produced by using either silicon or glass.<sup>221–223</sup> The properties of these materials such as inertness, optical transparency, electrically insulating, organic solvent resistance have

allowed to widen the applications of these devices especially, in the manufacturing of droplets, *in situ* reaction and solvent extraction. The low permeability of these materials and the high fabrication cost, however, make these materials not suitable for cell culture, and thus, biological applications.<sup>188,224</sup> Cheaper and more accessible materials have been extensively developed, dividing the materials to organise microfluidics chip in three mainstreams<sup>186,221,222</sup> (Figure 1.10):

- Inorganic materials (i.e. silicon and glass)
- Elastomers and plastic (i.e. polydimethylsiloxane (PDMS), polymethyl methacrylate, polycarbonates, etc.)
- Hydrogels and paper

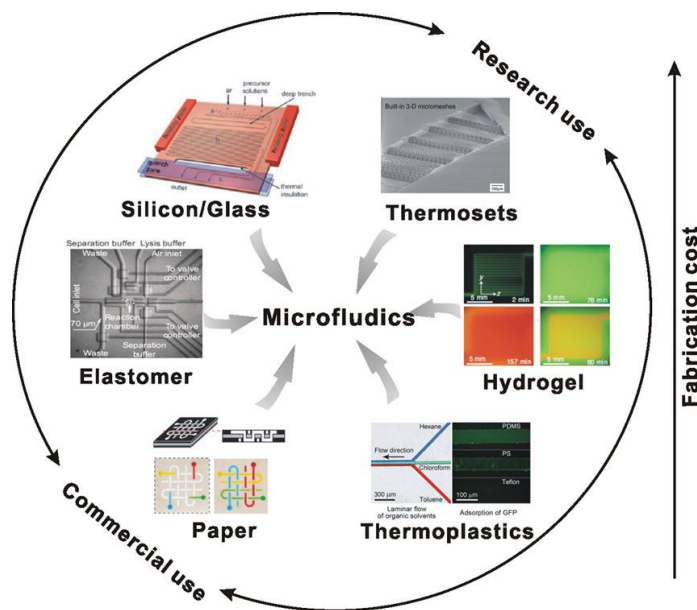


Figure 1.10 Summary of materials adopted for the fabrication of microfluidics chip. Image adapted with permission from Ren et al.<sup>221</sup> Copyright 2013 American Chemical Society.

Another important feature of microfluidics chip is the geometry conformation of the microchannels. Two principal geometries (Figure 1.11) are used for droplet formation:

- T-shaped junction, at which viscous shear stresses from the continuous phase overcome the surface tension at the liquid–liquid interface, generating droplets of a second immiscible stream. The first application of a T-junction device has been presented by Nisisako et al.<sup>225</sup> In this study, polymer beads were successfully synthesised using 1,6-hexanediol diacrylate.
- Flow-focusing junction, in which the dispersed and continuous phases are forced through a narrow region (orifice) and strong elongation and symmetric shearing of the continuous stream enables a stable generation of droplets. Stone and collaborators have been amongst the first groups who developed Flow-focusing device (FFD).<sup>206</sup> Few years after the first development of the FFD, Kumacheva et al. successfully showed the production of polymer particles based on different di- and mono- (meth)acrylates.<sup>226</sup> In particular, once the droplets were formed, the dispersed phase was UV polymerised thanks to the presence of photoinitiator in the droplet phase. This method showed that microfluidics can be an efficient strategy for the production and synthesis of highly monodisperse microparticles. Similarly, Lu et al. have fabricated pH-responsive anionic microgels using the FFD.<sup>227</sup> Droplets based on the hydrophilic acrylic acid, hydrophobic crosslinker, EGDMA, and a free

radical initiator were formed in the microfluidic device and, subsequently, synthesised *via* photopolymerisation. The use of microfluidics enabled the systematic variation of the crosslinking density and the synthesis of microgels with narrower size distributions.

For the interest of this thesis, FFD was exploited for the production of the library of particles.

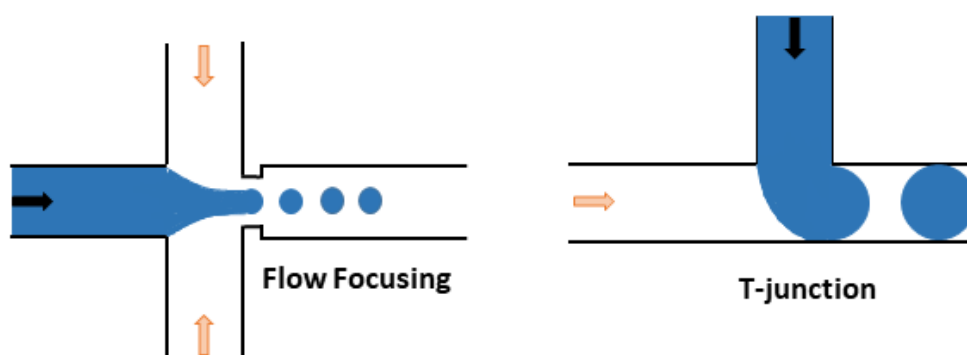


Figure 1.11 Two principle microfluidic geometries for 'droplets microfluidics'.

### 1.7.3 Surfactants in Droplet-based Microfluidics

Surfactants have been extensively exploited in the microfluidic technology. In fact, as mentioned above, they play a key role in the stabilisation of the emulsion for the droplets production preventing droplets coalescence. The amphiphilic structure drives these molecules to the interface of two immiscible liquids, so that the surface tension between the two phases decreases. The Gibbs equation (Equation 1.4) explains how the surface tension decreases with the increasing of the number of molecules at the interface:

$$\Gamma = -\frac{c}{RT} \frac{d\gamma}{dc}$$

Equation 1.4 The Gibbs equation.  $c$  is the surfactant bulk concentration,  $\gamma$  is the surface tension,  $T$  is the temperature and  $R$  is the gas constant.

The mechanism which hinders the droplets coalescence is based on two steps:

- Droplets become stable as a result of steric repulsion of the surfactant molecules.
- Surfactant gradients at the droplets interface is induced by a force acting against the drainage of the continuous phase between two droplets, according to the Marangoni effect.<sup>228,229</sup> The Marangoni effect shows how the surfactant molecules distribution is not uniform when the droplet is moving. The non-uniform distribution is concentrated mainly at the rear of the droplet creating a gradient in surface tension which generates a force against the flow.

For droplets-microfluidic, a surfactant is generally added to the continuous phase in order to provide a dynamic coating that controls the wetting of the channel walls, but also prevents droplet coalescence. In oil-in-water (O/W) emulsion, the most common surfactants usually adopted are the commercially available ones, e.g. poly(vinyl alcohol) (PVA), PEG-based Tween and Tritons. Hüsler et al. have shown how the use of common surfactants such as PVA hides the particular surface features of the MPs core.<sup>230</sup> In particular, they fabricated polymeric microparticles with materials that should prevent *P.aeruginosa* attachment, however, the presence of PVA on the surface, due to the manufacturing process, has revealed greater reduction in bacterial attachment for particles with

increased amount of retained surfactant at particle surfaces. This work has emphasised how the investigation and rationalisation of the role of these amphiphilic species in the emulsion-based methods are still open. In this regard, Wagner et al. synthesised a new class of fluorosurfactants for a water-in-oil (W/O) droplets microfluidics system.<sup>231</sup> Fluorosurfactants are extensively used especially when fluorinated oil is utilised as the continuous phase for single gene, cell, or organism isolation and analysis. The most biocompatible fluorosurfactants employed are polyethylene glycol (PEG) based, however, they offer limited opportunity of chemical modifications. In the work presented by Wagners and collaborators, a novel, non-ionic, polyglycerol based fluorosurfactants was developed. This new amphiphilic moiety, based on poly(methyl glycerol)–perfluoropolyether triblock, showed high stabilisation of W/O emulsions and supported the in vitro expression of GFP inside droplets and proved to be biocompatible with mammalian cell lines.

To the best of the author's knowledge, examples of new functionalised surfactants for O/W microfluidics system are not reported in literature. The present work can open a new chapter for the applications of new functionalised surfactant molecules in this technology.

#### 1.7.4 Microfluidics vs Conventional Methods

The growing interest on microfluidics has started when the traditional methods to produce MPs, e.g. spray drying and emulsion polymerisation, have revealed imprecise control of the process conditions resulting in

polydisperse and irregular particle sizes and shapes.<sup>232,233</sup> The control over shape, size distribution, topography and chemical nature of the surface are key upon final particles performance and bulk properties.<sup>234</sup> In particular, topography and surface chemistry can critically impact on particles stability in biologically relevant environments as well as fundamental in driving cells responses (for example cell adhesion, mobility and morphology).<sup>53,235,236</sup> Moreover, the ability to tailor the shape enables to understand the role of geometric parameters for particles functioning in a wide field of applications. Consequently, because of the importance to control these parameters, researchers have introduced filters/sieves, among others, to narrow the particle size distribution in these traditional methods.<sup>53</sup> The proposed microfluidics methodology adopted in this thesis project appears to be promising in overcoming the issues related to the particle size and shape in controlled the chemical nature of surfaces. Additionally, microfluidics shows potential to readily access a library of materials and to fabricate particles in a high throughput manner. This is required for practical and large-scale application in industry.

## 2 Materials and Methods

### 2.1 Chemical Synthesis

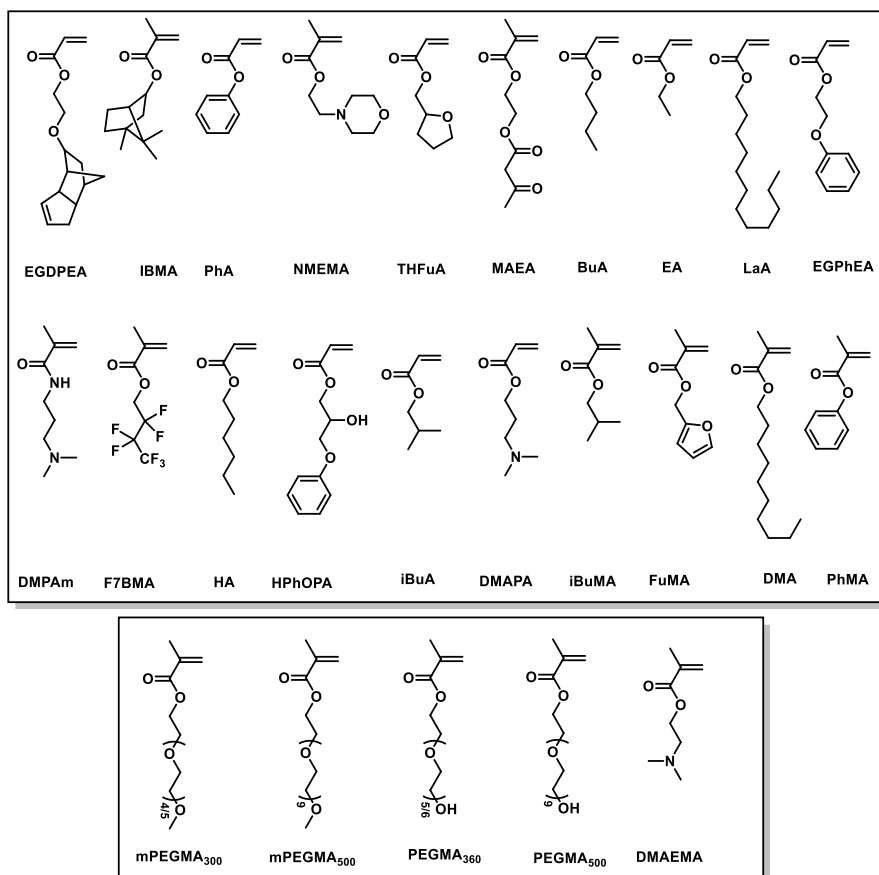
#### 2.1.1 Materials

##### 2.1.1.1 Free Radical Polymerisation Controlled by CTA

All the materials were used as received unless stated otherwise. The monomeric species used to build the library of hydrophobic monomers (Table 2.1) were purchased from the following companies Sigma-Aldrich, Combi-blocks and Polysciences. Poly(ethylene glycol) methyl ether methacrylate (mPEGMA) ( $M_n = 300$  g/mol; 500 g/mol), poly(ethylene glycol) methacrylate (PEGMA) ( $M_n = 360$  g/mol; 500 g/mol), 2, 2'-azobis (2-methylpropionitrile) (AIBN, 98%) and the benzyl mercaptan (BzSH, 99%) were, also, purchased from Sigma Aldrich. The catalytic CTA, Bis[(difluoroboryl)diphenylglyoximato] cobalt (II) (PhCoBF), was supplied from DuPont. The cyclohexanone and heptane used as solvents for the synthesis and precipitations, respectively, were used as received and supplied by Fisher Scientific. The name, acronyms, and vendors of all the monomers used for the CCTP and Thiol-mediated Free Radical Polymerisation are showed in the Table 2.1, while their chemical structures are showed in the Scheme 2.2.

Table 2.1 Monomers used for the synthesis of surfactants using a CTA for the control of the polymerisation.

<i>Monomers</i>	<i>Acronyms</i>	<i>Supplier</i>	<i>Purity</i>
Ethylene glycol dicyclopentenyl ether acrylate	EGDPEA	S-Aldrich	≥90%
Isobornyl methacrylate	iBMA	S-Aldrich	≥80%
Phenyl acrylate	PhA	Polysciences	95%
2-N-Morpholinoethyl methacrylate	NMEMA	S-Aldrich	95%
Tetrahydrofurfuryl acrylate	THFuA	S-Aldrich	≥90%
2-(Methacryloyloxy)ethyl acetoacetate	MAEA	S-Aldrich	95%
<i>n</i> -butyl acrylate	BuA	S-Aldrich	≥99%
Ethyl acrylate	EA	S-Aldrich	99%
Lauryl acetate	LaA	S-Aldrich	≥90%
N-3(Dimethylamino)propyl]methacrylamide	DMPAm	S-Aldrich	99%
Heptafluorobutyl methacrylate	F7BMA	Combi-block	95%
<i>n</i> -Hexyl acrylate	HA	S-Aldrich	98%
Hydroxy-3-phenoxypropyl acrylate	HPhOPA	S-Aldrich	≥80%
Ethylene glycol phenyl ether acrylate	EGPhEA	S-Aldrich	≥82%
3-(Dimethylamino)propyl acrylate	DMAPA	S-Aldrich	95%
Isobutyl methacrylate	iBuMA	S-Aldrich	97%
Furfuryl methacrylate	FuMA	S-Aldrich	97%
<i>n</i> -decyl methacrylate	DMA	Polysciences	99%
Phenyl methacrylate	PhMA	S-Aldrich	90%
Isobutyl acrylate	iBuA	S-Aldrich	≥99%
2-(dimethylamino)ethyl methacrylate	DMAEMA	S-Aldrich	99%

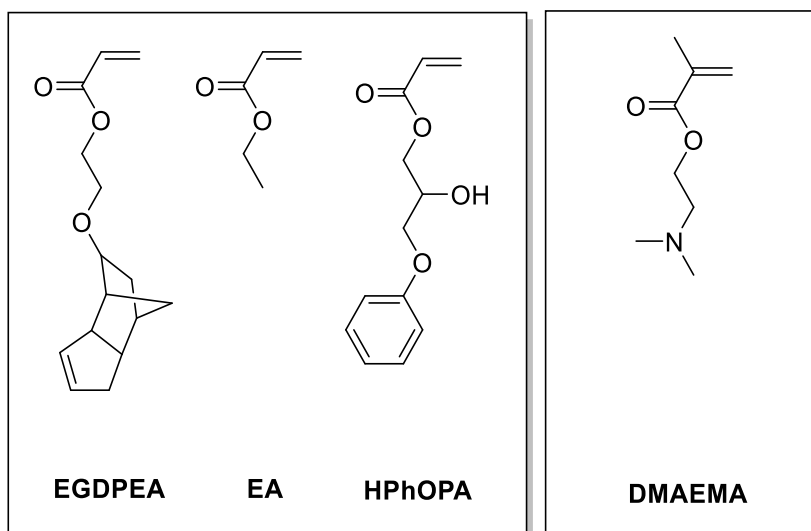


Scheme 2.1 Chemical Structures of monomers used for the FRP controlled by CTA.

### 2.1.1.2 Polymerisation via ATRP

In a typical ATRP experiment monomers, reagents and solvents were used without any further purifications unless stated otherwise. 2-(dimethylamino)ethyl methacrylate (DMAEMA) (98%), ethyl acrylate (EA) (99%), ethylene glycol dicyclopentenyl ether acrylate (EGDPEA) (99%) and hydroxy-3-phenoxypropyl acrylate (HPhOPA) (99%) were purchased from Sigma-Aldrich (Scheme 2.2). Copper(I)Bromide (98%) and copper (II) Bromide were purchased from Strem Chemicals UK LTD and VWR International LTD, respectively. Copper (I) chloride (99.99%) and copper (II) chloride (97%) were procured from Puratrem and Sigma-Aldrich, respectively. 1,1,4,7,10,10-Hexamethyltriethylenetetramine (HMTETA)

(97%), ethyl  $\alpha$ -bromoisobutyrate (EBriBru) (99%), N,N,N',N'',N''-pentamethyldiethylenetriamine (PMDETA) (99%) and tris[2-(dimethylamino)ethyl]amine (Me<sub>6</sub>TREN) (99+%) were obtained from VWR International LTD. Acetone, acetonitrile, methanol, cyclohexanone and heptane were supplied by Fisher Scientific whilst DMSO from Sigma-Aldrich. Aluminium oxide (Al<sub>2</sub>O<sub>3</sub>) was obtained from Fisher Scientific.



Scheme 2.2 Chemical structures of monomers used in the ATRP.

### 2.1.2 Nuclear Magnetic Resonance Spectroscopy

Nuclear Magnetic Resonance (NMR) spectroscopy is a common technique used for the structural and conformational analysis of organic molecules and for the quantitative analysis of reaction mixtures.<sup>237</sup> This analytical technique exploits an external magnetic field ( $B_0$ ) to observe nuclei resonance. In the resonance the nuclei split in a lower energy spin state ( $m=+1/2$ ) and in a higher energy spin state ( $m=-1/2$ ) ( $\Delta E$ ).<sup>238</sup> The entity of the  $\Delta E$  is proportional to the strength of the applied magnetic field, and as a consequence, the stronger the field, the greater is the difference between

the two nuclei populations, and the stronger is the signal.<sup>239</sup> The nuclei that respond to the  $B_0$  are the atomic nuclei of stable isotopes such as  $^1\text{H}$ ,  $^{13}\text{C}$ ,  $^{19}\text{F}$  and  $^{15}\text{N}$ . For each of these atomic nuclei there is only a single resonant frequency, however, in bulk, nuclei are not isolated but surrounded by electronic clouds.<sup>237</sup> The electronic clouds form a second magnetic field which is opposing the  $B_0$  causing a shielding effect. The degree to which a magnetic nucleus is shielded by the resultant magnetic field, due to the electron cloud, determines its precessional frequency ( $\nu$ ); the denser is the electron cloud (increased shielding), the lower is the precessional frequency.<sup>237</sup> The precessional frequency is related to a parameter called the 'chemical shift', in order to normalise the signal to a suitable reference compound and to be independent of the spectrometer's field strength. Chemical shift is the fundamental information used in the characterisation of the structure of molecules and polymers.

The inter-relationship between protons in the same molecule or polymer can also be elucidated based on the principle of 'spin-spin coupling'. Spin-spin coupling describes the effect that nuclei, close to each other (i.e., 3 or fewer bond lengths apart), have on each other's opposing magnetic field.<sup>239</sup> Throughout this project,  $^1\text{H}$ -NMR has been used to calculate conversion of the monomer in polymer and the final composition of the copolymers, i.e. the actual monomer ratio (Figure 2.1)

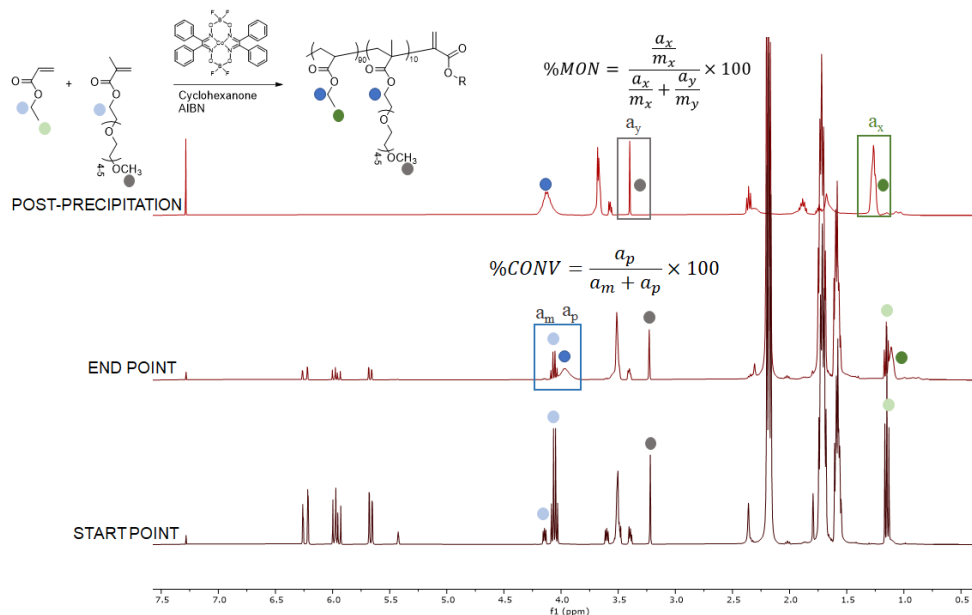


Figure 2.1 Spectroscopic analysis via  $^1\text{H-NMR}$  to calculate the conversion of monomer in polymer and the molar ratio of one component in the copolymer contents. EA-co-mPEGMA<sub>300</sub> was used as example.

In a typical experiment, the conversion has been calculated using the following equation (Equation 2.1):

$$\%CONV = \frac{a_p}{a_m + a_p} \times 100$$

Equation 2.1 Formula used for calculating the %CONV of monomer in polymer.

where  $a_m$  and  $a_p$  are the values of the peaks area related to monomer and polymer, relatively.

The formula applied for the determination of the polymer composition (i.e % MON) was that detailed as Equation 2.2<sup>240</sup>:

$$\%MON = \frac{\frac{a_x}{m_x}}{\frac{a_x}{m_x} + \frac{a_y}{m_y}} \times 100$$

Equation 2.2 Formula used for calculating the final composition of the copolymers.

where  $a_x$  and  $a_y$  are the values of the peaks area related to both the monomers, while  $m_x$  and  $m_y$  are the number of protons that are related to each of these resonances. The  $\text{OCH}_3$  resonance of the mPEGMA

macromonomer and the NC<sub>2</sub>H<sub>6</sub> of DAMEMA which occur at around  $\delta$  3.4 ppm and  $\delta$  2.3 ppm, respectively, were used in the calculation of the actual monomer ratio as they remained unaltered in the hydrophilic component for all the copolymers produced.

In case of EGDPEA-*co*-mPEGMA/PEGMA copolymers the calculation of the ratio has been performed using a different method, because of the multiple peaks overlapping between the two monomers. In Figure 2.2, an example of <sup>1</sup>H-NMR spectra of EGDPEA-*co*-PEGMA is showed to demonstrate the procedure to calculate the actual monomer ratio.

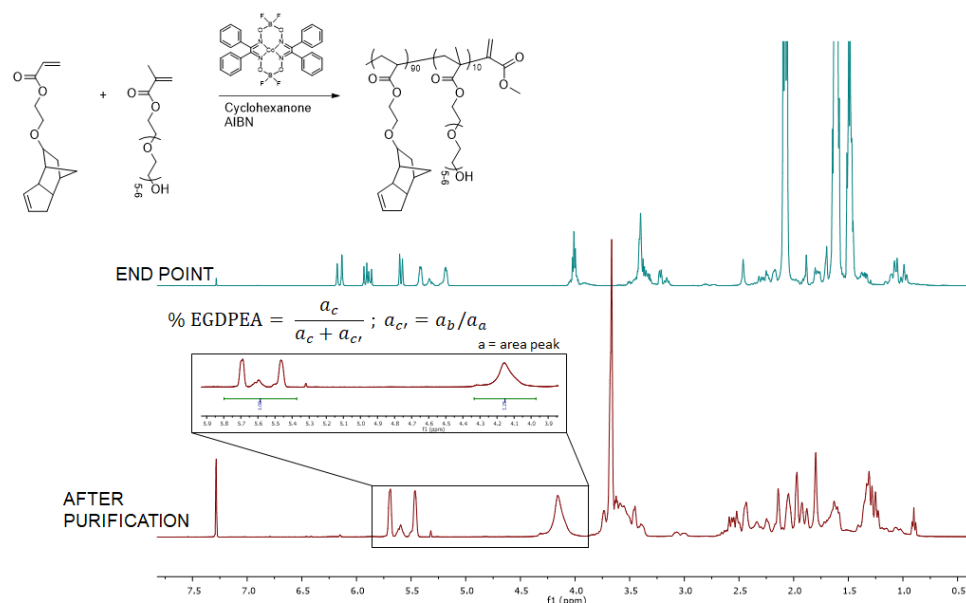


Figure 2.2 Spectroscopic analysis via <sup>1</sup>H-NMR to calculate EGDPEA-*co*-mPEGMA/PEGMA comonomer ratio.

The multiplet centred at 5.6 ppm was assigned to the protons of the double bond inside the EGDPEA pentenyl cycle (*a*, *b*). The peak at 4.15 ppm represents the two protons of the methylene group (C=OCH<sub>2</sub>) of the ester chain of the polymeric backbone of both the monomers (*c*+*c'*). In the range from 3.70 ppm to 3.45 ppm there are peaks overlapping related to the EGDPEA and mPEGMA/PEGMA methylene groups in the polymer backbone,

in particular the two ethers protons, and the methine group in the EGDPEA pentenyl cycle. Finally, in the high fields area (2.6 ppm to 0.9 ppm) different peaks were associated to the EGDPEA pentenyl structure. To calculate the actual monomer ratio, the multiplet at 5.6 ppm (*green dots*) was considered as the relative reference in the spectra. The integral of these peaks was used to assess the EGDPEA contribution on the methylene ester group in the (*blue dots*) peak related to the rest of the polymer. This assumption was made as *a*, *b* and *c* have the same number of protons in the EGDPEA structure (two protons). As a result, as shown in the Equation 2.3 the assessed value was subsequently divided by the total integral value at 4.15 ppm to evaluate the real influence of this monomer in the copolymer.

$$\% \text{ EGDPEA} = \frac{\int a_{c'}}{\int a_c + a_{c'}} ; \int a_{c'} = \int a_a ; a_b$$

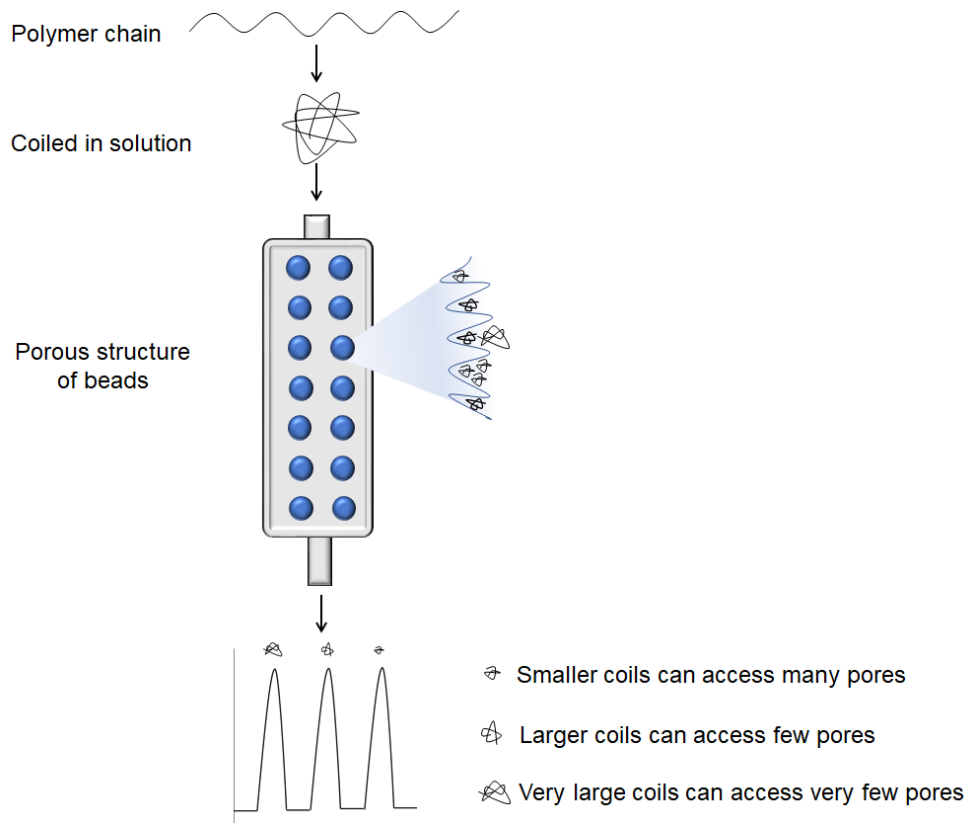
*Equation 2.3 Equation used for the calculation of the % mol of EGDPEA in the copolymer molar content.*

<sup>1</sup>H NMR spectra were recorded at 25°C using a Bruker DPX-300 spectrometer (400 MHz). Chemical shifts were recorded in δH (ppm). Samples were dissolved in deuterated chloroform (CDCl<sub>3</sub>) to which chemical shifts are referenced (residual chloroform at 7.26 ppm).

### 2.1.3 Gel Permeation Chromatography

Gel Permeation Chromatography (GPC), also referred to as Size Exclusion Chromatography (SEC), is a high-pressure liquid chromatography in which the components of a mixture are separated on the basis of size. In fact, GPC is an analytical technique used to determine MWt and its distribution (Đ) of

macromolecules. Polymers in solutions in a good solvent assume a coil conformation and behave like spheres with size dependent on their hydrodynamic volume. Utilising a column packed with porous materials (stationary phase), the separation process happens based on size and, thus, depends on both the porosity of the stationary phase and the coil size. In this regard, when the polymer molecules go through the pores are diffused and permeated differently based on their sizes: smaller coils easily diffuse in and out the pores, penetrating deeper than larger coils and, hence, eluted as last (Figure 2.3). The primary separation is according on the elution volume, this is converted in time for ease of measurements. The time it takes for the molecules, with different sizes, to emerge from the column is



called retention time.

Figure 2.3 How GPC separates molecules of different sizes.

The GPC detector used in this thesis is a differential refractive index (RI) detector. Detection by this method relies on the concentration of the polymeric sample eluting from the column, compared to the reference of pure solvent, as a function of the retention time. This is converted to MWt by the use of a calibration curve, that shows the elution behaviours of standards samples of which the MWt and the distribution (usually very narrow) are known. The MWt data obtained from the GPC are usually in terms of molecular weight averages which describes the polymer at different points of the peak showed in the chromatogram. The most important averages are  $M_n$  and  $M_w$  and they can be calculated as follow (Equation 2.4 Formula of the number average molecular weight ( $M_n$ ) and of the weight average molecular weight ( $M_w$ ).  $N_i$  is the total number of the molecules with the molecular weight  $i$  and  $M_i$  is the molecular weight of the molecule  $i$ ):

$$\text{Number average molecular weight: } M_n = \frac{\sum N_i M_i}{\sum N_i}$$

$$\text{Weight average molecular weight: } M_w = \frac{\sum N_i M_i^2}{\sum N_i M_i}$$

*Equation 2.4 Formula of the number average molecular weight ( $M_n$ ) and of the weight average molecular weight ( $M_w$ ).  $N_i$  is the total number of the molecules with the molecular weight  $i$  and  $M_i$  is the molecular weight of the molecule  $i$ .*

GPC analysis, in this project, has been performed by using an Agilent 1260 Infinity instrument equipped with a double detector with the light scattering and RI configuration. 2 mixed C columns at 25 °C were employed, using THF as the mobile phase with a flow rate of 1 ml/min. GPC samples were prepared in HPLC grade THF and filtered previous injection. Analysis was carried out using Astra software. The number average molecular weight

( $M_n$ ) and polydispersity ( $\mathcal{D}$ ) were calculated using PMMA for the calibration curve.

#### 2.1.4 Automated Synthesiser: Chemspeed Swing Robot

A Chemspeed Swing robot equipped with an isynth reactor containing 48 individual reactors was used for all the polymerisations (Figure 2.4).



Figure 2.4 Chemspeed Swing robot used in this thesis work.

The isynth reactor was fitted with 8 mL disposable glass vials obtained from Chemspeed Technologies Pty Ltd. The enclosed Chemspeed robotic deck was made inert via constant Nitrogen flow over 50 L/min to remove all oxygen with the extraction ports closed. Nitrogen purged reagent vials were passed into the robot immediately after the completion of degassing using a transfer chamber with a vacuum set to 200 mbar to minimise any exposure to oxygen. All reagent vials were degassed with nitrogen for a minimum of one hour prior to transferring into the deck of the robot.

For all aspirations and dispensing of reagent solutions, a 4-Needle Head tool equipped with 2 x 1 mL and 2 x 10 mL syringes was used which was fitted

with stainless steel septa piercing needles. All solvent lines were primed with degassed cyclohexanone which was used for each rinsing step. Typical aspiration and dispense rates of the reagents were 2 ml/min and 5 ml/min, respectively, for the 1 mL syringes and 10 ml/min and 5 ml/min, respectively, for the 10 mL syringes. An airgap of 50  $\mu$ L and an extra volume of 50  $\mu$ L were used for all aspirations using the 4-Needle Head tool. The needles were rinsed after each reagent dispense step with a 3 mL inside and outside volume for the 1 mL syringes and a 5 mL inside and outside volume for the 10 mL syringes. All reagents were added to the reactors including monomers, CTA, initiator, and solvent prior to heating the isynth reactor under reflux conditions to obtain a temperature of 75 °C inside the reactors for 18 hours. The isynth lid was set to close independently from the polymerisations while being actively cooled to 4 degrees Celsius under reflux. The isynth reactor was set to shake at 400 rpm for the duration of the polymerisations to ensure adequate mixing, subsequently, it was then cooled to 20 °C in order to cease the polymerisations.

The scale up of a small range of copolymers was performed on a Chemspeed SLT2 robot equipped with an isynth reactor block containing 12 individual reactors. The isynth reactor was fitted with 100 mL disposable glass vials obtained from Chemspeed Technologies Pty Ltd. A 250 ml reagent bottle of cyclohexanone was placed into the robot with continuous nitrogen bubbling throughout the experiment (minimum 2 hours before use). Septa-capped, nitrogen purged reagent vials were placed into the robot immediately after the completion of degassing (minimum 1 hour), and the enclosed

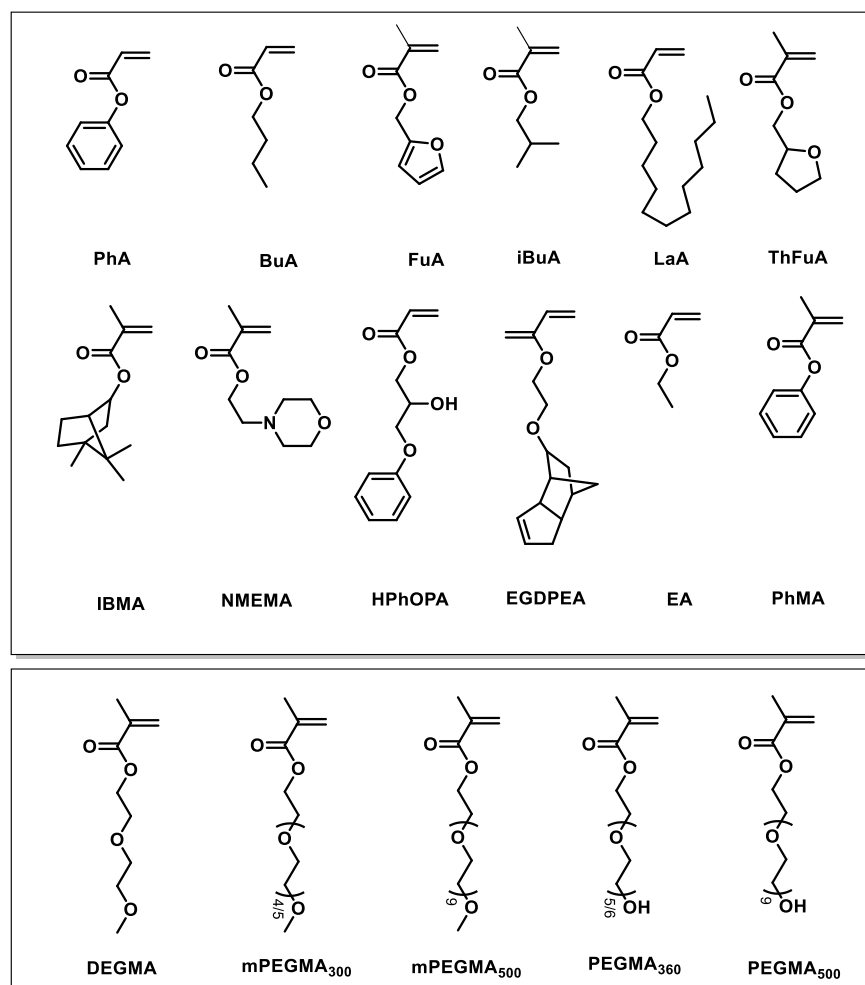
Chemspeed robotic deck was made inert via constant Nitrogen flow over 50 L/min to remove all oxygen with the extraction ports closed. The internal atmosphere was reduced to 0.1% oxygen within 90 minutes. For all aspirations and dispensing of reagent solutions, a 4-Needle Head tool equipped with 2 x 1 mL and 2 x 10 mL syringes was used which was fitted with stainless steel septa piercing needles. All solvent lines were primed with degassed cyclohexanone, which was used for each rinsing step. Typical aspiration and dispense rates of the reagents were 20 and 40 ml/min (respectively) for the 10 mL syringes (the 1 mL needles were not used for dispensing). An airgap of 50 uL and an extra volume of 50 uL was used for all aspirations using the 4-Needle Head tool. The needles were rinsed after each reagent dispense step with a 20 mL inside and outside volumes. Prior to heating the Isynth, reactors were agitated for 4 minutes, and a 250 uL sample was taken from each reactor and automatically dispensed into NMR tubes for later analysis. This was accomplished using 2 x 1 mL needles on the 4-Needle head tool, with 2 mL inside and outside volume rinse following each sample.

## 2.2 Polymer Microarray

### 2.2.1 Materials

12 commercially available monomers (Scheme 2.3) and poly(2-hydroxyethyl methacrylate) (polyHEMA), used for the microarray substrate, and 2,2 dimethoxy-2-phenylacetophenone (photoinitiator) were purchased from Sigma-Aldrich. DMF and ethanol were obtained from Fisher scientific and

used without any further purifications. The commercial epoxy-coated glass slides and the 384 polypropylene well-plates, used as stages for the different 'inks', were obtained from Genetix and Corning, respectively.



Scheme 2.3 Chemical structure of the monomers used for building the polymer microarray.

### 2.2.2 Printing Substrate Preparation

When printing a polymer microarray, the quality of the substrate is crucial to prevent the spreading of monomer spots, in order to distinguish the different polymer spots after the UV-polymerisation. Poly(2-hydroxy ethyl) methacrylate were chosen as a substrate because it avoids the spot to spread and it shows antifouling properties itself.<sup>241</sup> The epoxy-functional

glass slides are dip-coated with a 4% (w/v) poly(HEMA) solution using a solvent mixture of 95% v/v ethanol/water. The epoxy groups present on the surface of the glass slide will ring open by the nucleophilic addition of the hydroxy group present in the side chain of HEMA. The dip-coating was performed using a 48 automated dip coater (Holmarc, India) to maintain insertion and extraction speeds.

### 2.2.3 Microarray Printing

As mentioned in 1.6.2, polymer microarray can be obtained by means of contact and non-contact printing methodologies. Non-contact printers are discussed in more details in Section 2.3.1.1. Contact printing technology, which was used for the microarray preparation, utilised metal pins to transfer material from a source plate onto a printing substrate. An advantage of using quilled metal pins, over metal pins, is the ability to store material within the pin to print multiple microarray slides in a single iteration, however, a disadvantage is that these quills can block easily if a material is too viscous.<sup>242</sup> The general procedure for the polymer microarray formation contemplates different steps as shown in Figure 2.5.<sup>242</sup>

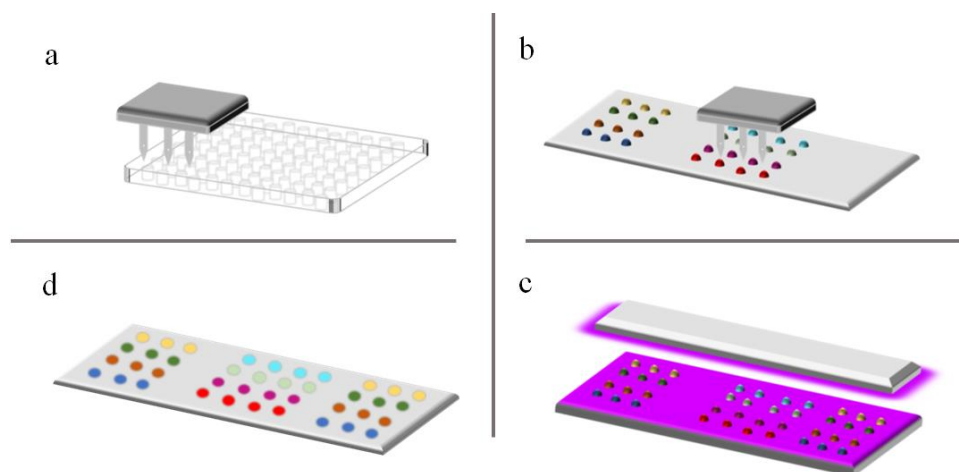


Figure 2.5 Schematic steps process of printing polymer microarray which consist in (a) withdrawing monomer solution from a source plate using 946MP6B Arrayit quilled metal pins (b) transferring monomer solution to pHEMA substrate (c) photopolymerisation of the monomer spots by UV-light and (d) completed polymer microarray with polymer spots.

Firstly, the microarrays were prepared using a contact robot (Bidot) with a XYZ stage and a pin of 220  $\mu\text{m}$  of diameter (946MP6B, Arrayit). All the pins should be cleaned by sonication in dichloromethane for 10 mins before each printing likewise the pin holder. Pins were loaded into the holder and array slides were loaded inside the chamber. This latter was filled with argon to reduce the oxygen level to avoid quenching of the polymerisation radicals by oxygen. The pins were lowered into the solutions at a speed of 25 mm/s, held in solution for 2.5 s and then withdrawn at a speed of 25 mm/s (Figure 2.5a). Pins were blotted before printing to remove monomer solution from the outside of the pin. Subsequently monomer delivery occurred from the quilled part of the pin to achieve consistent spot formation. One contact is made per spot at a pin movement of 175 mm/s and contact time of 10 ms, which depending on the viscosity and surface energy of the monomer solution gives an average spot diameter of 400  $\mu\text{m}$  (Figure 2.5b). Typically, 3 replicate arrays were printed onto each glass slide and a total of 10 slides

are printed on a single run. This equates to 30 spots per cycle. The freshly printed slides were irradiated with a short-wave UV (365 nm) source at a density of 30 mV/cm<sup>2</sup> for 10 min so as to allow the monomers to polymerise (Figure 2.5c). The humidity was maintained fixed at 30%-40%, since, it allows the pHEMA to swell so that the formed polymer can interpenetrates into the pHEMA layer becoming physically entrapped to the surface.<sup>243</sup> The freshly printed arrays were kept at low pressure (<50 mTorr) for 1 week to remove unpolymerised monomer and solvent (Figure 2.5d).

## 2.3 Self-assembling Characterisation

### 2.3.1 Nanoprecipitation Method

In this work, the self-assembling characterisation has been performed by evaluation of the CAC of nano-suspension/emulsion of the synthesised surfactants. In particular, the emulsions/suspensions were produced by nanoprecipitation method, also called solvent displacement method. The nanoprecipitation method has been chosen as model nano-formulation technique due to its simplicity, reproducibility and the low cost,<sup>244–246</sup> but above all, due to the possibility to screen the nano-aggregates in a HT fashion.<sup>247</sup>

The basic principle of this technique is based on using a system containing three basics 'ingredients': the polymer, a good solvent for the polymer and a non-solvent for the polymer. The good solvent is chosen among organic solvents which needs to be miscible with water and presents a relatively low

boiling point. For this reason, acetone and THF are the most frequently used organic solvents for this method<sup>246</sup>

Nanoparticles (NPs) are produced when the polymer solution is added in the non-solvent, which is usually water/aqueous phase. The rapid diffusion of the good solvent into the aqueous phase leads to the formation or nucleation of aggregates, which is followed by aggregation of these nuclei. The aggregation stops as soon as the colloidal stability is reached.<sup>244</sup> The resulting colloidal suspension contains polymer particles with well-defined size characterised by a narrow distribution.<sup>245</sup>

In this project, the nanoprecipitation method has been exploited to produce nano aggregates and also to measure the achieved colloidal stability namely, the detection of critical aggregation concentration (CAC).

#### *2.3.1.1 Ink-jet Printer*

As mentioned in Section 2.2.3, ink-jet printer is part of the non-contact printing processes. This technology is well-known for depositing small droplets (ink) onto substrate and it enables the use of precise quantity of ink with a resolution of picolitres. This high resolution resides in the piezoelectric conformation of the nozzle. In fact, thanks to the generation of electric pulses at a specific frequency, applied to the piezoelectric nozzle, droplets are formed thanks to the impulse pressure.

In this thesis, the use of an ink-jet piezoelectric printer allowed to analyse a large number of samples and to access precise conditions and

concentrations. The test materials were dispensed via a piezoelectric inkjet printer (Sciflexarray S5, Scienion) using a 90  $\mu\text{m}$  orifice nozzle. The droplet size was controlled by the values of the voltage and electrical pulse and were visually observed by a microcam. To do this, firstly the location of the target wells had to be programmed into the system controller.<sup>247</sup> The number of drops delivered per well were selected in such way that the volume aspirated for delivery by the nozzle (max 10  $\mu\text{L}$ ) at the beginning of a run was sufficient to print the whole print pattern.

### 2.3.2 Dynamic Light Scattering

Dynamic Light Scattering (DLS) is a common technique to determine particle size in colloidal dispersions by using the irradiation of particles by a coherent and monochromatic light generally a laser beam. In the current project, DLS has been used to determine sizes and CACs of the nano aggregates of the amphiphilic random and block copolymers. In particular, for the CACs, the variation of the intensity of the light scattering was plotted against the concentration of the suspensions to determine the point of which a changing of trend is evident as the aggregates reach the colloidal stability.

The principle behind this technique is based on the Brownian motion and relates this motion to the size of the particles. In fact, the Brownian motion is the random movement of particles in a liquid (solvent).<sup>248</sup> Larger are the particles and slower the motion will be, consequently, smaller are the particles and more rapidly they will move further from solvent molecules. When the light is scattered off the particles in suspension, the Brownian

motion causes time-dependant fluctuation of the local concentration of the particles resulting in fluctuations in intensity of the scattered light. The rate at which these intensity fluctuations occur will depend on the hydrodynamic size of the particles.<sup>249</sup>

A typical DLS system comprises of 4 components: laser, cell (where the samples are located), detector used to measure the scattered light and the attenuator. the attenuator is important because it helps the detector to measure the intensity of the scattered light. For instance, when too much light is detected, the detector might be saturated, when too low the detector is measuring a small amount of light. To overcome this, the attenuator either reduce or increase laser light through the sample. For the CAC measurements, it is important to maintain the attenuator to a fixed value of the laser intensity (usually at the highest suspension concentration) to avoid that the system gives any artefact at high and low concentration of the nanosuspension.

The HT CAC were performed with a Wyatt DynaPro Plate Reader II DLS instrument, which has a laser wavelength of 817.28 nm and a scattering angle of 158°. The experimental procedures for the intensity measurements were conducted with the temperature fixed at 25 °C and 10 acquisitions lasting 10 seconds, for each sample, were conducted, and the average values were plotted. DYNAMICS software implementing the Dynals algorithm was used for the data analysis. CAC obtained using a traditional

method were obtained Particle size was measured on with Malvern Zetasizer Nano ZS with a laser wavelength of 830 nm at 20 °C.

### 2.3.3 Zeta Potential

Zeta potential ( $\zeta$ ) is a physical property which is exhibited by particles in suspension or material surfaces. It can be used for different reason, to study the stability of the suspension/emulsion or to predict interactions with surfaces. Throughout the project, this technique has been used to study the external outlayer charges of the surfactant nano aggregates as it may reflect the interaction between particular biological response with the surface of microparticles.

Zeta potential is the electric potential difference between electric double layer of particles and the layer of dispersant around them. In fact, most particles in aqueous media is surrounded by a surface charge.<sup>250</sup> There are many origins of this surface charge depending upon the nature of the particle and its surrounding medium (e.g. ionisation of surface groups, adsorption of charged species, etc.). This electric charge can be also referred as electric double layer and it is composed by an inner layer (Stern layer) which consists of ions with opposite charge to that of the particle stronger bound and an outer layer (diffuse layer) with a less electrostatic effect of the same ions.<sup>251</sup> When an electric field is applied to such dispersion, the charged particles move towards the opposite electrode (electrophoresis). Within this diffuse layer there is a hypothetical plane which acts as the interface between the moving particles and the layer of dispersant around

it while electrophoresis. This plane is the characteristic slipping/shear plane and zeta potentials is the potential at this particle-fluid interface.<sup>250</sup>

Zeta potential measurements were taken with Malvern Zetasizer Nano ZS at 25 °C (scattering angle 173°, laser of 633 nm). All measurements were performed in triplicate.

## 2.4 Microparticles Production and Characterisation

### 2.4.1 Materials

1,6-Hexanediol diacrylate (HMDA) (80%), Polyvinyl alcohol (PVA) (25 kDa) and 2,2 dimethoxy-2-phenylacetone (photoinitiator) were purchased from Sigma-Aldrich. Ethyl Acetate, IPA and DCM were obtained by Fisher Scientific.

### 2.4.2 Microfluidics

Droplet microfluidics was utilised as method for the production of monodisperse microparticles (MPs) in this project. The underlying theory, conformation and field of application of microfluidics have been largely discussed in the paragraph 1.7, for this reason in the present section will be reported only a brief technical description.

The experimental setup consisted of a commercially available hydrophilic 3D glass chip with a channel depth of 100 µm (Dolomite), which was assembled in a stainless holder. The geometry chosen to generate the library of microparticles was the flow-focusing junction (Figure 1.11) and

the organic and aqueous phase were pumped with 2 syringe pumps (Havard Instrument) and connected to the device *via* polytetrafluoroethylene (PTFE) tubes (0.25 mm internal diameter). A high-speed video camera (Fastcam-1024PCI, Photron Limited), which was mounted on an upright microscope (Olympus, BX-51), was applied to observe the droplet formation. The droplets were collected in a glass vessel with water and shine by UV-light (wavelength of 365 nm, HAYASHI LA-410UV).

The microchannels were cleaned in between employing different organic phases by introducing and flushing with DCM, ethyl acetate, IPA and distilled water.

### 2.4.3 Scanning Electron Microscopy

Scanning Electron Microscopy (SEM) was used to determine topography and size of the MPs. In SEM analysis, a high-energy electron beam scans over a surface to create an image. The electrons present in the beam interact with the sample, producing various signals (secondary electrons, back scattered electrons and characteristic X-rays) that can be used to obtain information about the surface topography and composition.<sup>252</sup>

SEM imaging was performed using a JEOL JSM-6060LV, the dried microfluidic produced particles were sprinkled, using a spatula, onto a double-sided adhesive carbon tape. Prior to SEM analysis, the samples were sputter-coated for 4-5 minutes at 25 mA with a thin gold layer in an argon

atmosphere utilising a Leica EM SCD005 sputter coater (Leica Microsystems GmbH, Wetzlar, Germany) to give approximately a 25 nm thick coating.

#### 2.4.3.1 Size Characterisation

The sizes of the MPs were determined by processing SEM images at the 130X magnification. The processing of the SEM images was performed by using the Hough Circle Transform plugin within the ImageJ (Fiji software) (Figure 2.6).

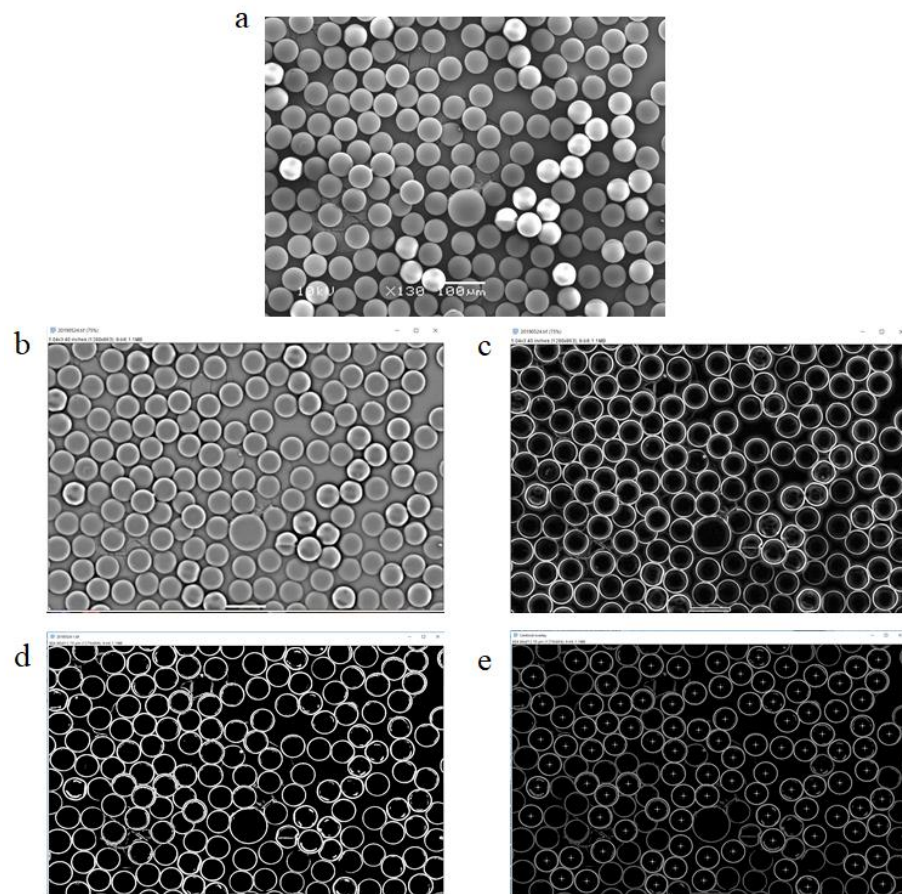


Figure 2.6 Schematic of particle size characterisation from the SEM images (a). Bandpass filter (FFT) (b) find edges (c) and threshold (d) commands was used in order to enable the Hough Circle Transform plugin within the ImageJ (Fiji software) (e).

In order to make readable the images for the plugin, the bandpass filter and find edges commands were applied with the intention of remove eventual

high and low spatial frequencies (blurring images) and to transform the particle in circles, respectively. In addition, with the threshold function, the pixels of the image was replaced with black pixel in order to minimise the background noise.

#### 2.4.4 Time of Flight Secondary Ion Mass Spectrometry

Time of Flight Secondary Ion Mass Spectrometry (ToF-Sims) is a surface analysis technique which gives information about the molecular composition of the uppermost layer of a sample. ToF-SIMS provides a powerful approach to material surface analysis and it is categorised among the widely used ultra-high vacuum (UHV) surface analysis techniques for materials science.<sup>253</sup> In particular, in the analysis of the microparticles, this technique was an important tool for the analysis of the MPs surface composition in order to confirm the presence of the target chemistry of interest.

In this technique, ions from a pulsed primary beam are impinged upon sample with high energy. This results in extensive fragmentation and bond breaking, near the collision site, producing emission of molecular fragments as neutral atoms and molecules, electrons and ions.<sup>254</sup> Only a small fraction of these segments is charged, and their positive or negative state depends on their electron configuration. Species fragmented in the uppermost layer (one or two monolayers of the target sample) have enough energy to overcome the surface binding energy and are ejected from the specimen (secondary ions and molecules).<sup>255</sup> Consequently, the TOF analyser

separates secondary ions according to  $m/z$  (*mass/charge*). The mass,  $m$ , of the ions is determined according to the time it takes them to travel from the sample to the detector, after they have been accelerated in an extraction field to a common energy. The instrument collects both negative and positive mode to obtain all possible data from the samples.<sup>253</sup>

In the present work, MPs were placed onto a poly(hydroxyethyl) methacrylate (Sigma-Aldrich) substrate and subjected to mass-spectrometry using a ToF-SIMS IV (IONTOF GmbH, Münster, Germany) instrument. 500  $\mu\text{m}$  x 500  $\mu\text{m}$  scans were taken with a  $\text{Bi}^{3+}$  primary ion source. Data were calibrated and analysed using IonToF software.

## 3 Synthesis and Characterisation of Amphiphilic Random Copolymers *via* Traditional and High-throughput Methods

### 3.1 Introduction

The overall aim of this chapter was to design, synthesise and characterise a library of novel amphiphilic materials, bearing biological active moieties, which act as surfactants in a microfluidics device. Surfactants are an essential part for the microfluidics technology.<sup>188</sup> The recent progress in microfluidics applications has been made possible by the development of new amphiphilic molecules and their characterisation.<sup>256</sup> In fact, as mentioned in the Introduction, surfactants are an indispensable tool in this technology as they play a key role in the stabilisation of the droplet interface, in the enhancement of the biocompatibility of the system and in the process of molecular exchange between droplets.<sup>257</sup> Lately, the technology related to surfactants manufacturing has seen a renewed interest thanks to the continuous development of new synthetic pathways focused on new designed/engineered amphiphiles and the need for new functional materials with biological features.<sup>258,259</sup> Among these, graft copolymers represents a promising class of amphiphile thanks to the grafting density and distributions which determine their peculiar physical properties (i.e. chain entanglements, rheological behaviour, etc.).<sup>260</sup>

In the present work the design of graft copolymers was focused upon the *grafting through* methodology by using macromonomers with a sufficiently

long hydrophilic side chain (from 4 to 9 units), i.e. PEGMA<sub>360</sub>/PEGMA<sub>500</sub> and mPEGMA<sub>300</sub>/mPEGMA<sub>500</sub>. Consequently, they were copolymerised with more than 20 different biological active hydrophobic (HyB) comonomers by using two general procedures to control radical polymerisation, namely thiol-mediated free radical polymerisation and CCTP. These two synthetic methodologies were selected because they are robust and versatile polymerisation routes that can be readily upscaled to a full industrial manufacture. In addition, they were already used as an efficient method for the synthesis of short polymeric chains in the 10,000 – 20,000 g mol<sup>-1</sup> range, that is the target of this work. With specific relevance to the present study, Adlington et al. reported the successfully copolymerisation of a selection of five “hit” hydrophobic (meth)acrylic monomers, with diethylene glycol ethyl ether methacrylate (classified as DEGMA or mPEGMA<sub>164</sub>).<sup>261</sup> The authors conducted this work in order to optimise the mechanical properties of a range of resultant short copolymers intended as coatings, upon silicone-based urinary catheters.<sup>261</sup> These modifications were required because, in a previous study, the homopolymers of the ‘hit’ monomers had been shown to exhibit significant bacterial attachment resistance *via* high-throughput polymer microarray screening.<sup>184</sup> However, the final homopolymers suffered from a series of limitations, such as poor processability and brittleness. Thus, the resultant homopolymer coatings tended to crack as the catheters were flexed.

The structural alteration introduced, by including the hydrophilic DEGMA/mPEGMA<sub>164</sub> moiety within these copolymers, has been shown to

have a promising impact in some mechanical features of the resulting materials, maintaining the biological properties of the coating. For example, they could now match the flexibility exhibited by the catheter in the body.<sup>261</sup> However, whilst these new materials performed well as coating, the authors concluded that, in order to adopt these active macromolecules as surfactants, the DEGMA/mPEGMA<sub>164</sub> comonomer needed to be replaced with a monomer containing a longer hydrophilic chain. This modification would increase the amphiphilic character of the polymers and the level of steric stabilisation that can be delivered by the molecule as well as promote the self-assembling properties in a non-solvent.

As part of the novelty of this study is focused on the biomaterials discovery, the work detailed by Aldington et al. was extended to apply the CCTP and Thiol-mediated Free Radical Polymerisation approaches to conduct these grafting copolymerisations in an automated synthesiser, in order to adopt a high-throughput synthesis methodology. By employing a synthetic robot, it has been possible to rapidly identify the best polymerisation technique to apply to specific monomer types, and, to screen the optimum CTA and solvent concentration conditions for a specific 'hit' graft copolymerisation. In this study, the end use for these materials was their subsequent application to the production of surface functionalised MPs using the microfluidic techniques.

Finally, to continue the high degree of automation, a HT pilot screening procedure for the assessment of the CACs was performed in order to assess the various copolymers' ability to self-assemble and hence produce stable

emulsions in water within the microfluidics system. This data was mined to develop a proof-of-concept model that can predicted the CAC characteristics of large number of comb-graft copolymers and using four key molecular drivers that underpinned this behaviour.

### 3.1.1 Aims and Objectives

The aim of this chapter was to develop new strategies to synthesise and to physically characterise bespoke amphiphilic copolymers, which possess 3D *comb-graft* molecular structures. One of the features of these polymeric surfactants is the contents of monomeric materials that are known to have impact on both human and microorganism cell attachment properties (both pro- and anti-). In this regard, the design of the synthetic strategy had to ensure that the characteristic biological properties, exhibited by these monomeric species, were preserved in the copolymer.

This was achieved by completing the following objectives:

- Applying a 2D microarray screening, using *P. aeruginosa* as microbial model, to investigate the hydrophilic and hydrophobic monomers ratio ranges that preserved the biological properties of the 'hit' HyB monomers.
- Optimising the synthesis protocol with a small selection of hydrophobic and hydrophilic monomers.
- Utilising the optimised methods to develop a surfactant library by HT parallel and automated polymerisations.

- Expanding the high-throughput pipeline by developing a HT-CAC assay to investigate the self-assembling properties.
- Developing a computational model to understand the correlation between molecular structures and self-assembling

## 3.2 Methods

### 3.2.1 Polymer Microarray Production and 2D Biological Assay

Acknowledgement are made to Dr. Olutoba Sanni, who performed the printing of the polymer microarray, bacterial culture experiments on polymer microarrays and fluorescence imaging.

*Polymer microarray preparation:* the microarray slides were prepared by dip-coating epoxy-coated glass slides into a 4 % (w/v) poly(hydroxyethyl methacrylate). The slides were then left overnight at ambient conditions before being placed into a vacuum oven (room temperature (RT)) for 7 days before printing. The polymer microarrays were then prepared by depositing monomer solutions (with 1 % w/v photoinitiator (2,2 dimethoxy-2-phenylacetophenone) and a mixture of 50:50 % v/v monomer:DMF ) onto the preformed pHEMA-coated slides at 25 °C, with 30-40 % humidity and less than 0.2 % O<sub>2</sub> levels and, finally, irradiated with UV light. A total of 17 commercially available monomers were used for the printing, leading to 17 homopolymers and 150 copolymers. From these latter, 70 copolymers were obtained by mixing EGDPEA and HPhOPA with DEGMA, mPEGMA<sub>300/500</sub> and PEGMA<sub>360</sub> at the volume ratio of (90:10, 85:15, 80:20, 75:25, 70:30, 60:40 and 50:50 only. LaA, FuMA, EA, BuA, PhA, PhMA, iBuA, THFuA iBMA and

NMEMA were mixed with mPEGMA<sub>300</sub> at the same volume ratio. In total 180 spots with a diameter of around 400 µm were printed in one slide in 3 replicates.

The microarray slides were allowed to dry for a week under vacuum before being used for bacterial screening.

*Bacterial strains and growth conditions:* *P. aeruginosa* strain (mCherry tagged *Pseudomonas aeruginosa* PAO1-Washington sub-line, Nottingham collection, 587/610 excitation/emission) was streaked onto LB agar plates for the formation of colonies for bacterial culture experiments. The overnight culture was prepared by adding a single colony of bacteria using a sterile plastic loop to 10 ml of LB media, which was then placed in an incubator at 37 °C at 200 rpm overnight for approximately 18 hours. After the overnight culture, the culture was centrifuged at 10,000 rpm for 10 minutes and this was then resuspended in 10 ml of RPMI-1640 media, and this process was repeated to ensure all LB media had been removed from the culture. The optical density (OD) at 600 nm of the bacterial culture was determined by measuring 1 ml of pure RPMI-1640 as a blank against 100 µL of bacterial culture in 900 µL of RPMI-1640 media. The amount of bacterial culture to include in the polymer microarray incubation was determined by the optical density such that the concentration in a total of 15 ml of RPMI-1640 media was an OD<sub>600</sub> of 0.01.

*Polymer Microarray 2D Biological Assay:* Before the microarrays were incubated with *P. aeruginosa*, the slides were UV sterilised for 10 min. After sterilisation, slides were placed in 15 mL of RPMI-1640 medium in a petri

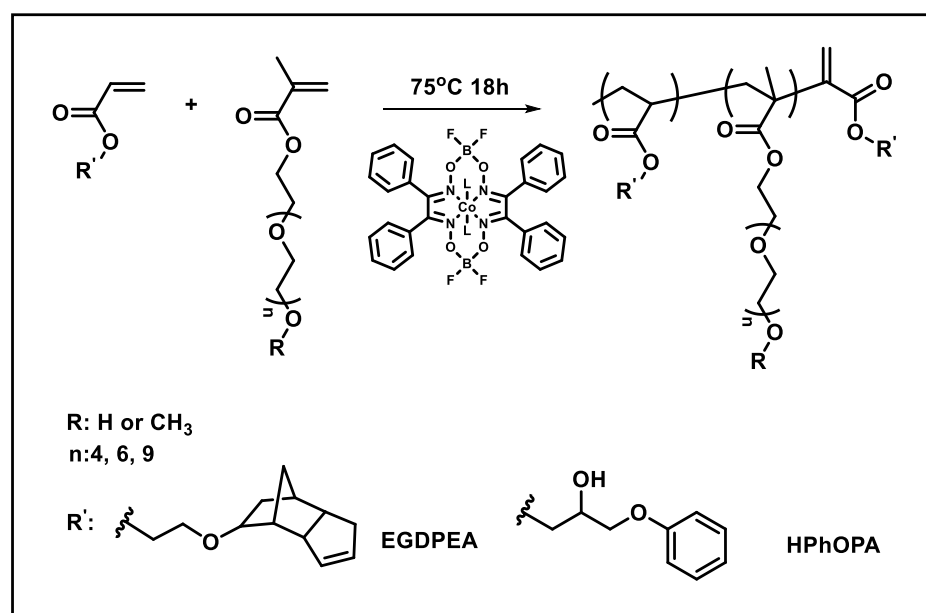
dish which was inoculated ( $OD_{600} = 0.01$ ) with m-cherry tagged *P. aeruginosa* and left for 24 h at 37 °C at 60 rpm shaking. These conditions result in a continuous flow over the surface. After incubation, the polymer microarrays were removed from the incubator and rinsed to remove any non-attached bacteria from the surface and to remove salts that may be deposited on the surface. The polymer microarrays were first placed into individual petri dishes with 15 ml of water and placed on a rocker platform at 30 rpm for 5 minutes. This was repeated a further time with distilled water and then a final time with Phosphate buffered saline (PBS). Both the control slide and the bacteria-incubated slide were washed with the same protocol for consistency. After the final rinse the slides were blotted on a piece of blue roll to remove as much moisture from the slide surface as possible. Fluorescence images were taken of both the control slide (with no incubated bacteria) and bacteria-probed slide using a GenePix Autoloader 4200AL (Molecular Devices, US) scanner. For the mcherry tagged *P. aeruginosa*, a 594 nm laser was used for exciting the fluorophore such that bacterial attachment could be measured. Once an image had been acquired, the data could be extracted using the Genepix Pro 6 software and analysed in Microsoft Excel. The fluorescence value, which correlates biofilm formation on the polymer surface, was obtained by subtracting the fluorescence signal acquired from the directly attached bacteria polymer spots and the fluorescence of the control slide.

### 3.2.2 Synthesis and Characterisation

#### 3.2.2.1 CCTP Performed via Conventional Thermal Polymerisation Method

PhCoBF stock solution was freshly prepared to avoid any catalyst degradation. Typically, 5 mg of PhCoBF were dissolved in 1 mL of cyclohexanone and left in mechanic agitation at 60 rpm for 1 hr to obtain a final clear orange solution.

A typical protocol (Scheme 3.1) used for the CCTP of both EGDPEA-co-PEGMA<sub>360/500</sub>, EGDPEA-co-mPEGMA<sub>300/500</sub> and HPhOPA-co-mPEGMA<sub>300</sub> copolymers is described below and shown in Scheme 3.1.



Scheme 3.1 Reaction scheme of CCTP conducted in a lab traditional method.

The appropriate quantities of the monomers required to reach the targeted molar ratios were dissolved in cyclohexanone in a 1:3 v/v ratio and added to a flask containing a magnetic stirrer. Initiator and chain transfer agent were added in the reaction vessel with monomers and solvent in the follow order. A fresh PhCoBF stock solution of 5 mg/mL was prepared in

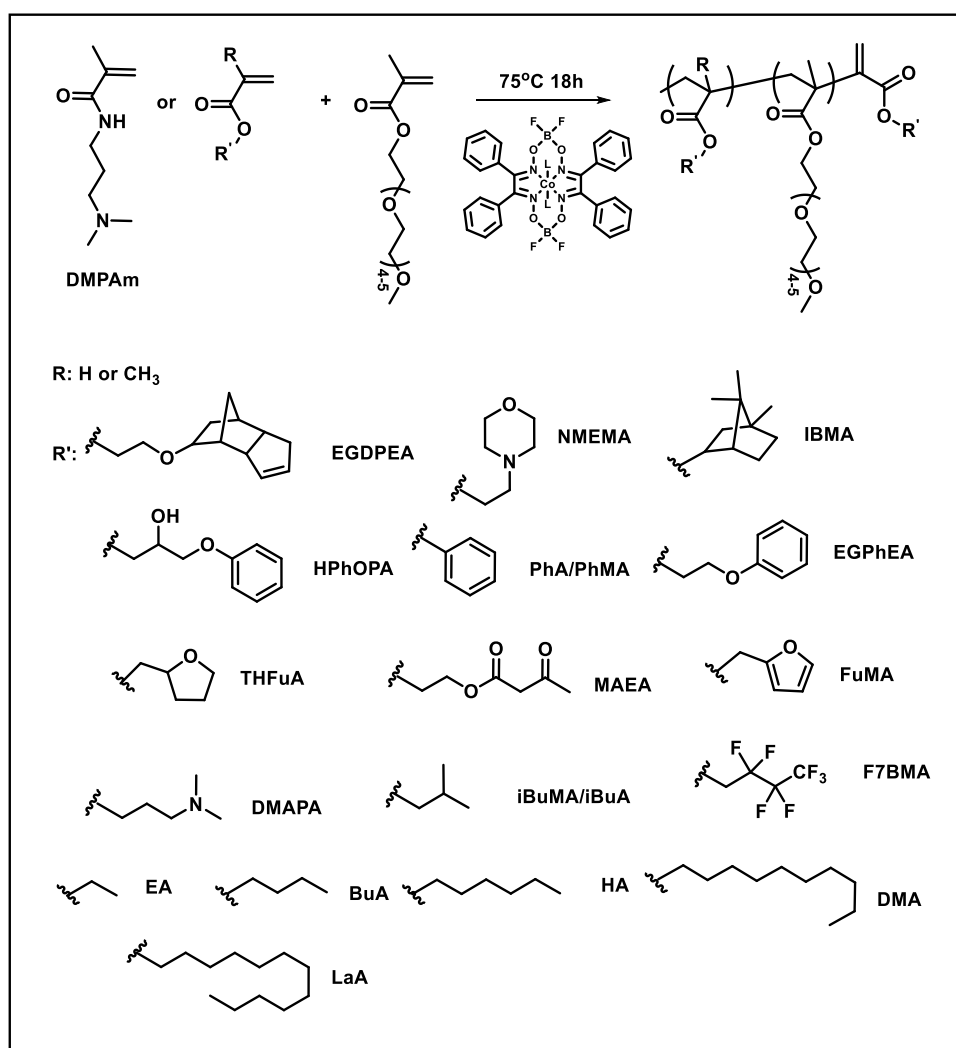
cyclohexanone from which aliquot was taken to achieve the range of final concentration within the vessel. The concentrations were of 1000 ppm (1.05 mg/mL), 850 ppm (0.89 mg/mL), 700 ppm (0.74 mg/mL) and 500 ppm (0.53 mg/mL). Finally, AIBN (0.5% - 1% wt/wt with respect to the total monomer mixture used) was dissolved in cyclohexanone and degassed separately prior to being added to the reaction mixture. Finally, the reaction vessel and the AIBN solution were degassed *via* purging with argon using a standard Schlenk line technique for at least 1 h in ice bath. Subsequently, the AIBN was introduced in the reaction mixture *via* syringe. The temperature of the oil bath was, then, raised to 75°C and, when reached this temperature, the reaction was conducted for 18 h with agitation. The temperature was set at 75°C not only as working temperature for the radical initiator but, to avoid any reverse Diels-Alder side reactions from the cyclopentenyl group of EGDPEA. Polymer purification was conducted *via* precipitation of the crude reaction solution into an excess of heptane. The usual non-solvent:reaction media ratio adopted was 5:1 v/v in order to enhance the precipitation process. Finally, the precipitated materials were collected and left in a vacuum oven at 25°C for at least 24 h.

<sup>1</sup>H-NMR spectroscopic analysis was performed on the crude polymerisation solution to determine polymer conversion and, also, on the precipitate to establish the actual monomer ratio of the final copolymer composition. To evaluate the molecular weight and molecular dispersity of the materials, the purified samples were dissolved in HPLC grade THF for GPC analysis.

### 3.2.2.2 High-Throughput Synthesis of Polymer Libraries via Automated Synthesiser

#### 3.2.2.2.1 Initial Parallel Polymerisation Screen Containing 42 Polymerisations Using CCTP at 1.5 g Scale

The general procedure adopted for the polymerisations, as shown in Scheme 3.2, is detailed below.



Scheme 3.2 Initial Parallel CCTP Screen contemplating a 1.5g scale.

In order to address a series of technicalities intrinsically related to the automated synthesiser, a series of preliminary precautions were put in

place. In particular, dilutions and samplings process needed to be carried out accounting for the differences in molecular weights across the monomer library, the maximum volume of the reaction vessels (4.5 mL) and taking into account for the stoichiometric necessary to maintain the desired monomer:initiator:catalyst:solvent ratios. For responding to these necessities, a series of stock Solutions of the 20 hydrophobic monomers were prepared covering a range of 3 – 4.5 M. The concentrations of stock solutions of mPEGMA<sub>300</sub>, initiator and catalyst (with respect to the monomers) were 1.5 M, 0.1 M and 3 mg/ mL, respectively.

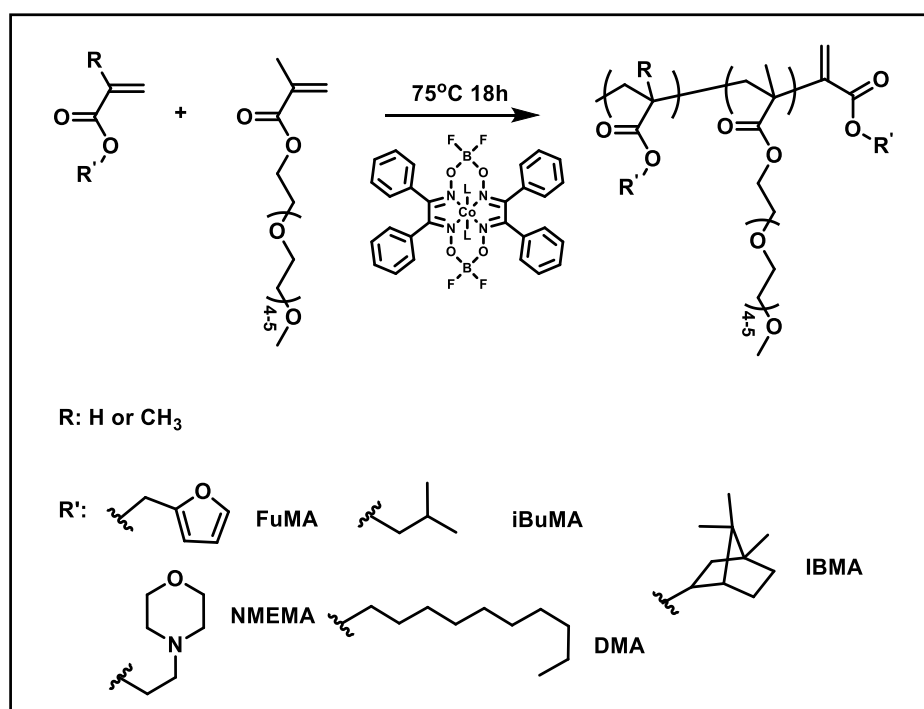
The HyB monomers and mPEGMA<sub>300</sub> were automatically dispensed into each reactor, as defined by the pre-programing of the Chemspeed auto-synthesiser, in the appropriate quantities required to reach the targeted molar ratio of 90:10 (HyB:mPEGMA<sub>300</sub>). The concentrations of the catalyst and initiators adopted for the first screening were fixed for all the copolymerisations at 850 ppm and 0.5% w/w, respectively. The only parameter that varied in this screen was the solvent ratio and the concentration of the reaction media. For the 18 of the tested monomers, the solvent:monomer ratios considered for this study were 1:3 v/v and 1:2 vol/vol (monomers:cyclohexanone). Meanwhile, in the case of the 2-hydroxy-3-phenoxypropyl acrylate (HPhOPA) and ethylene glycol phenyl ether acrylate (EGPhEA) lower concentrations were also explored using the ratios 1:4 vol/vol and 1:5 vol/vol (monomers:cyclohexanone) because of the high viscosity of these monomers.

This sequence was carried out in duplicate in order to confirm the reproducibility of the polymerisation using CCTP for conversion and the control of the molecular weight.

### 3.2.2.2.2 Optimisation of CCTP Parallel Polymerisation for 10 Monomers

*which Exhibited No Conversion in the Initial Screening at 1.5g Scale*

This second CCTP procedure was adopted with the auto-synthesiser to the optimisation of the catalyst concentrations for those monomers that showed either no or low conversion (< 30%) in the first sequence. Monomers and the synthetic procedure applied in this case are shown in Scheme 3.3.



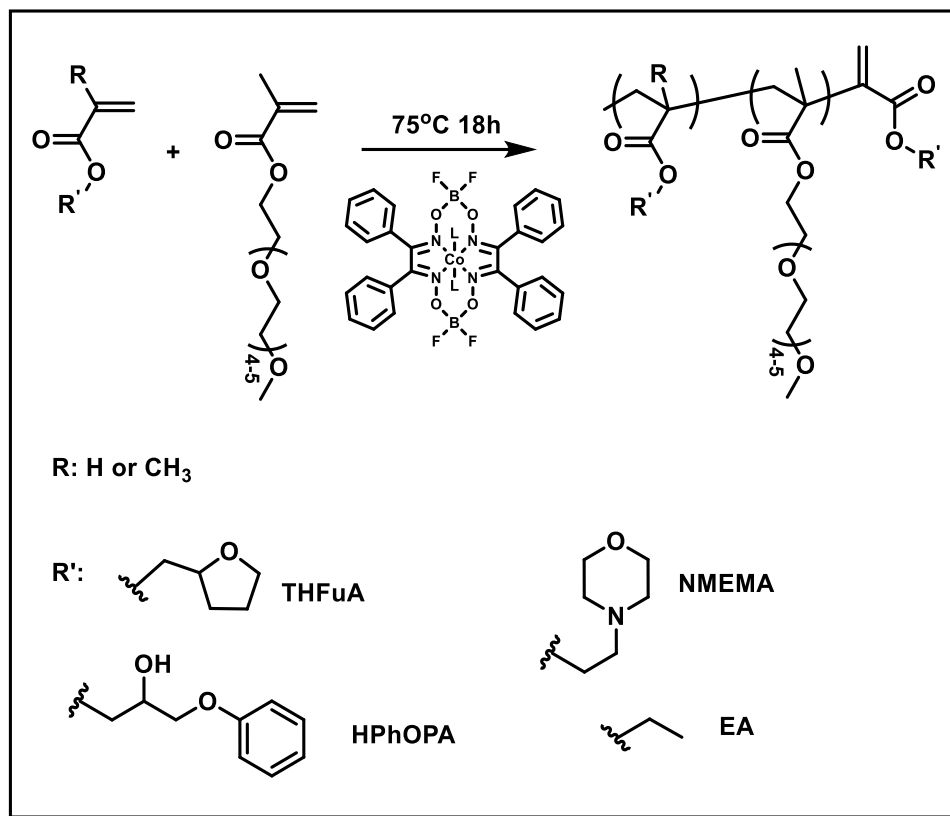
Scheme 3.3 Reaction scheme of the optimisation of CCTP parallel polymerisations at 1.5g scale.

The new concentrations of PhCoBF explored were 650 ppm and 450 ppm relative to the monomers. The same procedure as detailed for the initial screening of 42 parallel polymerisations was utilised with the following

conditions: a) The feed ratio of HyB monomers to mPEGMA<sub>300</sub> was 90:10 % mol/mol (i.e. HyB:mPEGMA<sub>300</sub>), b) Stock solutions of the 5 HyB monomers spanned from 3 M to 4.5 M, c) mPEGMA<sub>300</sub>, AIBN and PhCoBF stock solutions concentrations were 2 M, 0.03 M, 0.5% wt/wt and 2 mg/mL, respectively and d) solvent ratio was 1:3 vol/vol (monomer:cyclohexanone). The latter was chosen as the preferred solvent concentration based on the information gathered from the first screening.

#### *3.2.2.2.3 Scale Up of 4 Selected Parallel Polymerisation Conducted via CCTP from 1.5g to 10 g Scale*

Four copolymers were chosen from the libraries obtained during the initial screening and synthesis optimisation stages to be up scaled to a product volume of 10 g via the Chemspeed auto-synthesiser. Monomers and the synthetic procedure applied are shown in Scheme 3.4.

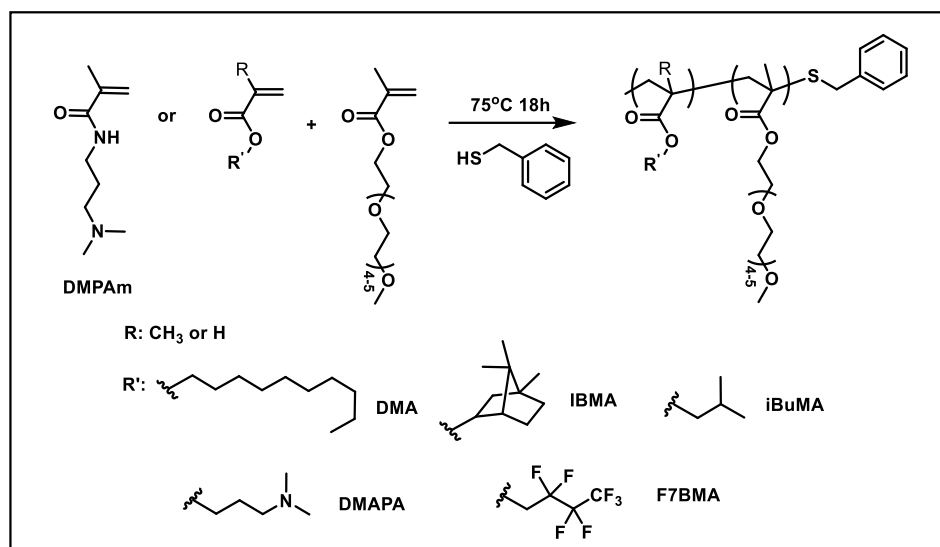


Scheme 3.4 Reaction scheme of the scale up of 4 selected Parallel Polymerisation conducted via CCTP.

These reactions were conducted following the procedure detailed for the initial screening of 42 polymerisations. Using those conditions, it was found to promote both the highest polymer conversion and deliver molecular weights close to the chosen target.

#### 3.2.2.2.4 General Procedure for the Parallel Polymerisation of 12 Auto-synthesiser based Polymerisations Conducted Using a Thiol Control Agents at 1.5 g scale

The same procedure as detailed for the CCTP polymerisations was applied for the Thiol-mediated Free Radical Polymerisation (see Scheme 3.5 for the monomers and synthetic strategy).



Scheme 3.5 Reaction scheme of the Parallel Polymerisations conducted using a Thiol Control Agents at 1.5 g scale.

Stock solutions of all the reagents were prepared, as described above in the 42 parallel CCTP polymerisation procedure. When the solvent ratio applied was 1:3 v/v, the AIBN was introduced at the concentration of 0.5% wt/wt and the comonomers ratio was 90:10 % mol/mol. The thiol species chosen as CTA for these experiments was benzyl mercaptan (BzSH, see Scheme 3.5 for the structural diagram), and two concentrations were applied in the attempt of the control of molecular weight to the target one, 10% mol/mol and 5% mol/mol (with respect to the total monomer concentrations).

### 3.2.2.3 Nuclear Magnetic Resonance Analysis ( $^1\text{H}$ and $^{13}\text{C}$ -NMR)

Due to the large number of the synthesised copolymers,  $^1\text{H}$ -NMR spectra and related structures definitions have been included in the Appendix from Figure Appendix 3-1 to

Figure Appendix 3-25. However, the list of  $^1\text{H}$ -NMR and  $^{13}\text{C}$ -NMR peaks of the main copolymers adopted in the biological characterisation is provided

below as an example of peaks assignment and molecular structure (Figure 3.1 a-k). All the spectra data presented were collected at 400 MHz in CDCl<sub>3</sub> and values are quoted as δH ppm.

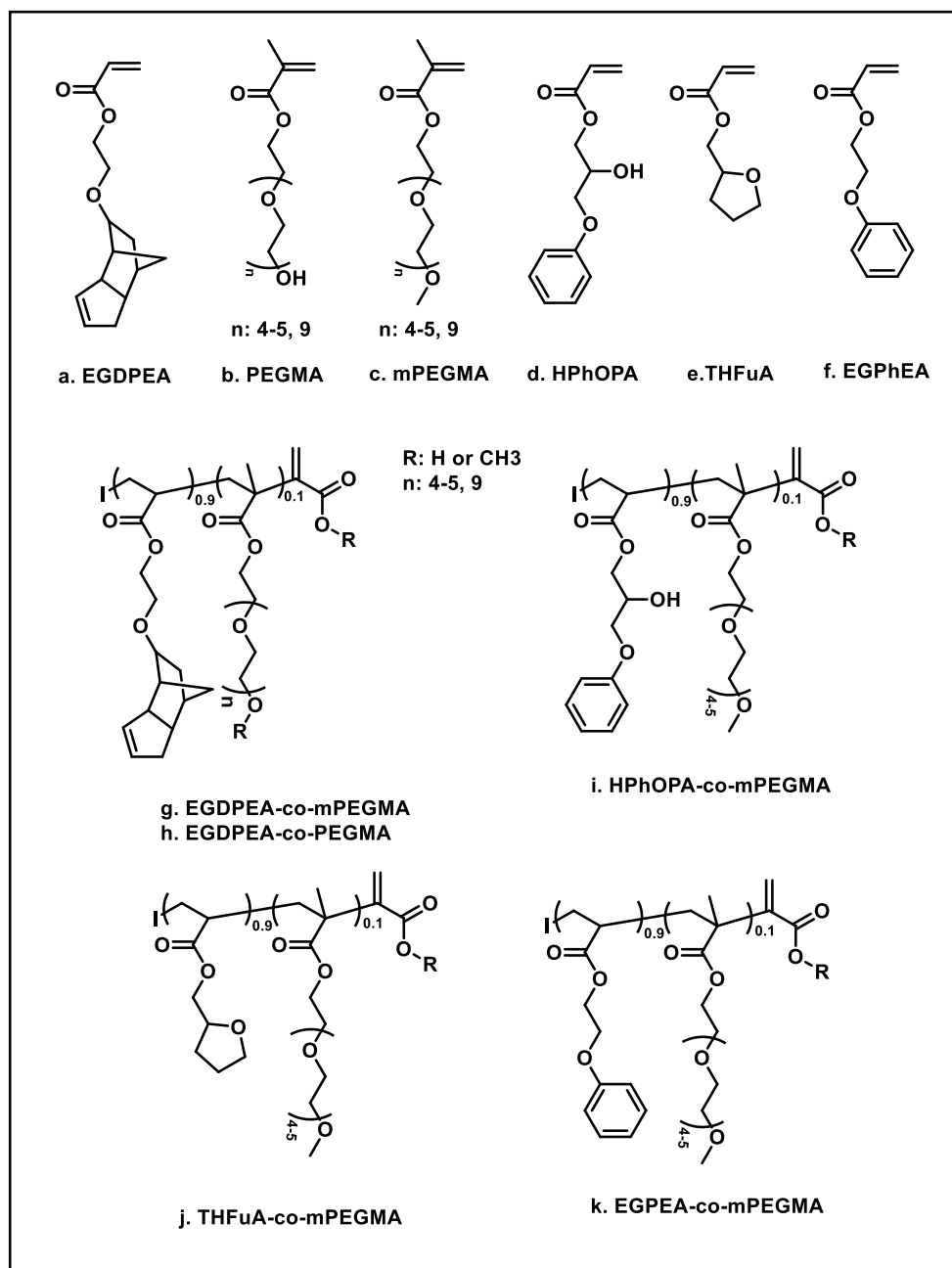


Figure 3.1 Structures of the main monomers (a-g) and copolymers (h-m) adopted in the biological characterisation.

The <sup>1</sup>H-NMR spectra of EGDPEA monomer (Figure 3.1a) (400 MHz, CDCl<sub>3</sub>) δ (ppm): 6.30 (1H, HCH=CH, dd), 6.03 (1H, CH<sub>2</sub>=CH, ddd), 5.70 (1H, HCH=CH,

dt), 5.45 (1H, dicyclopentenyl  $CH=CH$ , m), 4.14 (2H,  $O-CH_2CH_2$ ,m), 3.5 (2H, $CH_2CH_2O$ ,m), 3.34 (1H,  $O-CH-(C_9H_{12})$ ,m), 2.46-2.29 (1H,  $C_7H_{10}$ , m), 2.11-1.72, 1.51-1.09 (10H,  $C_7H_{10}$ , m).

The  $^1H$ -NMR spectra of PEGMA monomers (Figure 3.1b) (400 MHz,  $CDCl_3$ )  $\delta$  (ppm): 5.81 (1H,  $HCH=CH_3$ , s), 5.27 (1H,  $HCH=CH_3$ , s), 3.97 (2H,  $OCH_2CH_2$ , m), 3.33 (2H,  $C=OOCH_2CH_2O$  and  $(OCH_2CH_2O)_5$ , m), 1.71 (3H,  $CH_2=CH_3$ , s).

The  $^1H$ -NMR spectra of mPEGMA monomers (Figure 3.1c) (400 MHz,  $CDCl_3$ )  $\delta$  (ppm): 5.81 (1H,  $HCH=CH_3$ , s), 5.27 (1H,  $HCH=CH_3$ , s), 3.97 (2H,  $OCH_2CH_2$ , m), 3.43 (18H,  $C=OOCH_2CH_2O$  and  $(OCH_2CH_2O)_4$ , m), 3.14(3H,  $OCH_3$ , s), 1.71 (3H,  $CH_2=CH_3$ , s).

The  $^1H$ -NMR spectra of HPhOPA monomer (Figure 3.1d) (400 MHz,  $CDCl_3$ )  $\delta$  (ppm): 7.28-6.91 (5H,  $C_5H_5$ , m), 6.41 (1H,  $HCH=CH_3$ , s), 6.13 ( $^1H$ ,  $HCH=H$ , s), 5.86 (1H,  $HCH=CH_3$ , s),4.61-3.66 ( $^5H$ ,  $OCH_2OHCH_2O$ , m).

The  $^1H$ -NMR spectra of THFuA monomer (Figure 3.1e) (400 MHz,  $CDCl_3$ )  $\delta$  (ppm): 6.29 (1H,  $HCH=CH_3$ , dd), 6.04 (1H,  $CH_2=CH$ , m), 5.73 (1H,  $HCH=CH$ ,dd), 4.12-3.94 (3H,  $OCH_2CHO$ , m), 3.80-3.64 (2H,  $CHOCH_2$ , m), 1.94-1.72 (3H,  $OCH_2CH_2CHH$ , m), 1.51 (1H,  $OCH_2CH_2CHH$ , m).

The  $^1H$ -NMR spectra of EGPhEA monomer (Figure3.1f) (400 MHz,  $CDCl_3$ )  $\delta$  (ppm): 7.28 and 6.91 (5H,  $C_5H_5$ , m), 6.29 (1H,  $HCH=CH_3$ , dd), 6.04 (1H,  $CH_2=CH$ , m), 5.73 (1H,  $HCH=CH$ ,dd), 4.49 (2H,  $C=OOCH_2$ , m), 4.17 (2H,  $OCH_2CH_2$ , m).

The  $^1H$ -NMR of EGDPEA-co-PEGMA<sub>360/500</sub> purified (Figure 3.1g) (400 MHz,  $CDCl_3$ )  $\delta$  (ppm): 5.69-5.47 (2H,  $CH=CH$ , m), 4.36 (4H,  $OCH_2CH_2$ , m), 3.73-3.45

(24H,  $\text{CH}_2\text{CH}_2\text{OCH}_2$ ,  $\text{CH}_2\text{CH}_2\text{O}$  of both the monomers along the ester chain and  $\text{OCHC}_9\text{H}_{12}$ , m), 2.51-0.95 (10H,  $\text{C}_7\text{H}_{10}$ , m).

The  $^1\text{H-NMR}$  of the EGDPEA-co-mPEGMA<sub>300/500</sub> purified (Figure 3.1h) (400 MHz,  $\text{CDCl}_3$ )  $\delta$  (ppm): 5.69-5.47 (2H,  $\text{CH}=\text{CH}$ , m), 4.36 (4H,  $\text{OCH}_2\text{CH}_2$ ), 3.73-3.45 (20H,  $\text{CH}_2\text{CH}_2\text{OCH}_2$ ,  $\text{CH}_2\text{CH}_2\text{O}$  of both the monomers along the ester chain and  $\text{OCHC}_9\text{H}_{12}$ , m), 3.40 (3H,  $\text{OCH}_3$ , m), 2.51-0.95 (10H,  $\text{C}_7\text{H}_{10}$ , m).

The  $^{13}\text{C-NMR}$  of the EGDPEA-co-mPEGMA<sub>300</sub> purified (400 MHz,  $\text{CDCl}_3$ )  $\delta$  (ppm): 174 (C=O), 132-130 ( $\text{CH}=\text{CH}$ ), 82.56 ( $\text{OCHC}_9\text{H}_{12}$ ), 71.74 ( $\text{CH}_2\text{OCH}_3$ ), 70.48 ( $(\text{OCH}_2\text{CH}_2)_{4-5}$ ), 65.70 ( $\text{OCH}_2\text{CH}_2$ ), 63.31 ( $\text{OCH}_2\text{CH}_2$ ), 59.08 ( $\text{OCH}_3$ ), 55.15-28.60 ( $\text{C}_9\text{H}_{12}$ ).

The  $^1\text{H-NMR}$  of HPhOPA-co-mPEGMA<sub>300</sub> purified (Figure 3.1i) (400 MHz,  $\text{CDCl}_3$ )  $\delta$  (ppm): 7.22-6.87 (5H,  $\text{C}_5\text{H}_5$ , m), 4.49-3.71 (7H,  $\text{OCH}_2\text{HOHCH}_2\text{O}$  and  $\text{OCH}_2\text{CH}_2$ , m), 3.50 (18H,  $\text{CH}_2\text{CH}_2\text{O}$   $\text{OCH}_2\text{CH}_2\text{O}$ , m), 3.40 (3H,  $\text{OCH}_3$ , m).

The  $^{13}\text{C-NMR}$  of the HPhOPA-co-mPEGMA<sub>300</sub> purified (400 MHz,  $\text{CDCl}_3$ )  $\delta$  (ppm): 174 (C=O), 129, 121.13 and 114.46 ( $\text{C}_6\text{H}_5$ ), 82.56 ( $\text{OCHC}_9\text{H}_{12}$ ), 71.74 ( $\text{CH}_2\text{OCH}_3$ ), 70.48 ( $(\text{OCH}_2\text{CH}_2)_{4-5}$ ), 68.54 ( $\text{OCH}_2\text{CHOH}$ ), 68.07 ( $\text{OCH}_2\text{CHOH}$ ), 59.08 ( $\text{OCH}_3$ ).

The  $^1\text{H-NMR}$  of THFuA-co-mPEGMA<sub>300</sub> purified (Figure 3.1j) (400 MHz,  $\text{CDCl}_3$ )  $\delta$  (ppm): 3.90-3.66 (3H,  $\text{OCH}_2\text{CHO}$ , m), 3.63-3.45 (4H,  $\text{CHOCH}_2$  and  $\text{C}=\text{OOCH}_2$  (mPEGMA), m), 3.43 (18H,  $\text{C}=\text{OOCH}_2\text{CH}_2\text{O}$  and  $(\text{OCH}_2\text{CH}_2\text{O})_4$ , m), 3.14 (3H,  $\text{OCH}_3$ , s), 1.94-1.72 (3H,  $\text{OCH}_2\text{CH}_2\text{CHH}$ , m), 1.51 (1H,  $\text{OCH}_2\text{CH}_2\text{CHH}$ , m).

The  $^{13}\text{C-NMR}$  of the THFuA-co-mPEGMA<sub>300</sub> copolymer purified (400 MHz,  $\text{CDCl}_3$ )  $\delta$  (ppm): 174 (C=O), 76.22 ( $\text{CHOC}_3\text{H}_6$ ), 71.74 ( $\text{CH}_2\text{OCH}_3$ ), 70.48

$((\text{OCH}_2\text{CH}_2)_{4-5})$ , 68.54 ( $\text{OCH}_2\text{CH}_2$ ,  $\text{OCH}_2\text{CH}$ ), 68.07 ( $\text{OCH}_2\text{CH}_2$ ), 59.08 ( $\text{OCH}_3$ ), 41.95 ( $\text{CHOCH}_2\text{C}_2\text{H}_4$ ), 28.18 ( $\text{CHOCH}_2\text{CH}_2\text{CH}_2$ ), 25.64 ( $\text{CHOCH}_2\text{CH}_2\text{CH}_2$ ).

The  $^1\text{H-NMR}$  of EGPhEA-co-mPEGMA<sub>300</sub> purified (Figure 3.1k) (400 MHz,  $\text{CDCl}_3$ )  $\delta$  (ppm): 7.22 and 6.87 (5H,  $\text{C}_5\text{H}_5$ , m), 4.30 (4H,  $\text{C=OCH}_2$ , m) 4.04 (2H,  $\text{OCH}_2\text{CH}_2$ , m), 3.60 (18H,  $\text{CH}_2\text{CH}_2\text{O}$  and  $(\text{OCH}_2\text{CH}_2)_4\text{O}$ , m), 3.40 (3H,  $\text{OCH}_3$ , m).

The  $^{13}\text{C-NMR}$  of the EGPhEA-co-mPEGMA<sub>300</sub> purified (400 MHz,  $\text{CDCl}_3$ )  $\delta$  (ppm): 174 ( $\text{C=O}$ ), 129, 121.13 and 114.46 ( $\text{C}_6\text{H}_5$ ), 82.56 ( $\text{OCHC}_9\text{H}_{12}$ ), 71.74 ( $\text{CH}_2\text{OCH}_3$ ), 70.48 ( $(\text{OCH}_2\text{CH}_2)_{4-5}$ ), 68.54 ( $\text{OCH}_2\text{CH}_2$ ), 68.07 ( $\text{OCH}_2\text{CH}_2$ ), 59.08 ( $\text{OCH}_3$ ).

### 3.2.3 High-Throughput (HT) Critical Aggregation Concentration Analysis (CAC)

Acknowledgement is made to Dr. Vincenzo Taresco and Dr. Marion Limo. I would thank Dr. Vincenzo Taresco, who helped me to perform the printing process of the suspension/emulsion with the ink-jet printer, and Dr. Marion Limo who performed the HT-DLS *via* plate reader.

Critical Aggregation Concentration (CAC) high-throughput analysis combined three procedures in series. Initially, to ensure the self-assembling of the test surfactants, the nanoaggregates (NA) were prepared by nanoprecipitation method (solvent displacement) at a high concentration using THF as the solvent and water as the non-solvent. The THF polymeric solutions (5 mg in 1 mL) were added dropwise manually *via* a syringe into milliQ water (10 mL) in order to obtain a final stock emulsion/suspension

concentration of 500 µg/mL. Subsequently, the stock emulsion/suspension was dispensed directly into a 96-well plate filled with water (100 µl MilliQ in each well) by means of a piezoelectric ink-jet printer to deliver different concentrations of surfactants in each well of the plate. The concentrations ranged from 100 µg/mL to 0.05 µg/ml (i.e. 12 final concentrations for each material were obtained). To do this, firstly the location of the target wells had to be programmed into the system controller.<sup>247</sup> Water suspension (500 µg/mL) droplets with nominal volumes ranging from 180-220 pL, were dispensed at a 300 Hz jetting frequency by adjusting the voltage and pulse between 98-105 Volt (Voltage) and 45-55 µs (Pulse) respectively. The nozzle was washed with water/DMF, in between each printing cycle, as part of the automated printing-washing loop.

Finally, the last step consisted in the measurement of the intensity (Cnt/s) with an automated DLS plate reader. The experimental procedure for the intensity measurements were conducted by applying a fixed laser power intensity and attenuation in order to determine the scattered light from each sample. By comparison, in the size assessment experiments that were conducted on the same well-plate, auto-attenuation was enabled to determine the optimal laser power and attenuation. In these CAC determinations, each well containing 100 µL of sample, and 10 acquisitions lasting 10 seconds were collected, and the average values plotted. DYNAMICS software implementing the Dynals algorithm was used for the data analysis.

### 3.2.4 Predictive Computational Model Development on Surfactants Self-Assembling Properties

Acknowledgment is made to Leonardo Contreras who performed the machine learning analysis *via* linear multiple regression model.

The RDKit cheminformatics python library was used to extract 200 chemical descriptors from each molecule by feeding it with its SMILES string. Since the logCAC values were obtained from a mixture of monomer and mPEGMA<sub>300</sub> (theoretical % mol/mol ratio of 90:10), descriptors for both the monomer and mPEGMA<sub>300</sub> were obtained for each surfactant and their contributions were weighted by their molar ratios. The initial feature sets were considerably reshaped by multiplying descriptors each other and by themselves: this was done to broaden the feature space and thus to have access to new combined descriptors. The resultant 20,300 descriptors were then pruned to keep only those descriptors not excessively cross-correlated and with a good diversity. As far as concerns the first criterion, Pearson's  $r^2$  of all features was computed to measure the extent of cross-correlation, while the criterion of diversity allows to identify those descriptors whose values do not change significantly across the samples. Ideally, no correlation should be observed between any descriptors, and all of them should assume as many different values as possible with a uniform frequency. Diversity can be expressed in many different ways, but the most common formula is Shannon's entropy. Thus, we decided to compute descriptor diversity as the ratio between the Shannon's entropy of the descriptor vector and the

Shannon’s entropy of the ideal descriptor vector if all its actual values were equally distributed. To compute diversity for a fictitious descriptor:

$$d_{real} = [1,1,0,0,0,0,0,0,0]$$

$$d_{ideal} = [1,1,1,1,1,0,0,0,0]$$

Where  $d_{real}$  is the descriptor vector with all its actual values, and  $d_{ideal}$  is the descriptor vector wherein all its values have the same frequency.

$$\begin{aligned} H_{d_{real}} &= - \sum_{i=1}^n P(x_{real_i}) \ln P(x_{real_i}) = -(0.2 \ln (0.2)) - (0.8 \ln (0.8)) \\ &= 0.321 + 0.178 = 0.499 \end{aligned}$$

$$\begin{aligned} H_{d_{ideal}} &= - \sum_{i=1}^n P(x_{ideal_i}) \ln P(x_{ideal_i}) = -(0.5 \ln(0.5)) - (0.5 \ln(0.5)) \\ &= 2 * 0.347 = 0.694 \end{aligned}$$

$$Diversity = \frac{H_{d_{real}}}{H_{d_{ideal}}} = \frac{0.499}{0.694} = 0.719$$

Where  $P(x)$  is the frequency of the x-th value in the descriptor vector,  $H_{d_{real}}$  is the Shannon’s entropy of the descriptor vector,  $H_{d_{ideal}}$  is the Shannon’s entropy of the ideal descriptor vector, and  $D$  is the diversity associated to the descriptor vector. Diversity can assume any value between 0 and 1 and high values are associated to descriptor vectors with high amount of information.

The multicollinearity and diversity criteria were applied to narrow the feature space down to a more manageable number of descriptors. After setting both maximum tolerated cross-correlation and minimum accepted diversity to 0.9, number of features were reduced to 329. Then, we computed all the  $\binom{329}{k}$  combinations, with  $k=1$  and then  $k=2$ , to obtain a

total number of 53956 different feature subsets, made of either one or two descriptors, which could either be a simple or combined (as described before). Since we had only 18 samples, value of  $k$  was deliberately kept small so that any resultant model could still be simple and interpretable. Once dataset was standardised through mean-centring, a linear regression model was trained on the dataset using one feature subset at a time, and model performance was assessed through the evaluation of Pearson's  $r^2$  and Root Mean Squared Error (RMSE). Then, a Leave-One-Out Cross-Validation (LOOCV) was carried out and its CV RMSE was also computed to validate model robustness. Finally, all models were sorted by the computed geometric mean between training and CV  $r^2$  and first model was chosen. Cross-validation procedure is a common practice to validate results if dataset is such small that it cannot be split into training and test set. Thus, a common way to work around this is to split the dataset, which is made of  $n$  samples, into  $k$  folds so that a model can be trained on  $n-(n/k)$  samples and tested on  $n/k$  samples that were left out of the model. Iteratively repeating the process and computing the mean of the desired performance metrics across all the iterations allows to have a better understanding of whether the model is robust or volatile. In our case, LOOCV is a particular case of  $k$ -fold cross-validation with  $k = n$ . Thus, for 18 times model was trained on 17 samples and RMSE of prediction was computed for the sample that was kept out.

## 3.3 Results and Discussions

### 3.3.1 2D Microarray Screening

In previous studies, *P. aeruginosa* attachment was investigated to a wide library of hydrophobic homopolymers presented in a microarray format.<sup>184,262–264</sup> However, to form a surfactant a hydrophilic partner moiety is required to balance the lipophilicity of these homopolymers and create amphiphilic compounds. In this regard, the work in this thesis reports the use of contact printing technology to produce a polymer microarray screening similar to the studies shown by Alexander group.<sup>184,262–264</sup> The aim is to determine the levels of hydrophilic monomer content that could be introduced into a surfactant composition, whilst retaining the desired level of biological performance from the hydrophobic counterpart.

Polymer microarrays consisting of 70 copolymer spots were produced with two groups of monomers, one hydrophobic and one hydrophilic. The first group contained monomers components to either prevent (ethylene glycol dicyclopentenyl ether acrylate (EGDPEA)) or support (2-hydroxy-3-phenoxypropyl acrylate (HPhOPA)) biofilm development. These monomers were combined with one of the 5 variable chain length hydrophilic monomers that made the second group. This group contained both mPEGMA (-OCH<sub>3</sub> as terminal side chain) and PEGMA (-OH as terminal side group) variants with the following chain lengths PEGMA<sub>360</sub>, PEGMA<sub>500</sub>, mPEGMA<sub>300</sub>, mPEGMA<sub>500</sub> and mPEGMA<sub>164</sub> (also known as diethylene glycol methyl ether methacrylate, DEGMA)). mPEGMA<sub>164</sub> was included as a

comparison with previously published work.<sup>261</sup> HyB:PEG in % v/v ratios of 0:100, 50:50, 60:40, 70:30, 75:25, 80:20, 85:15, 90:10 and 100:0 were prepared. A second screen implemented this investigation to study the effect of mPEGMA<sub>300</sub> concentration on the characteristics of an extended range of biologically active HyB monomers. This HyB set included PhA, PhMA, BuA, EA, FuMA, iBuA, LaA, THFuA, IBMA and NMEMA were combined pairwise with mPEGMA<sub>300</sub>. Figure 3.2a contains the molecular structures of all monomers used while Figure 3.2b-d contain the microarray spots configuration and the HT biological assays of the copolymer spots.

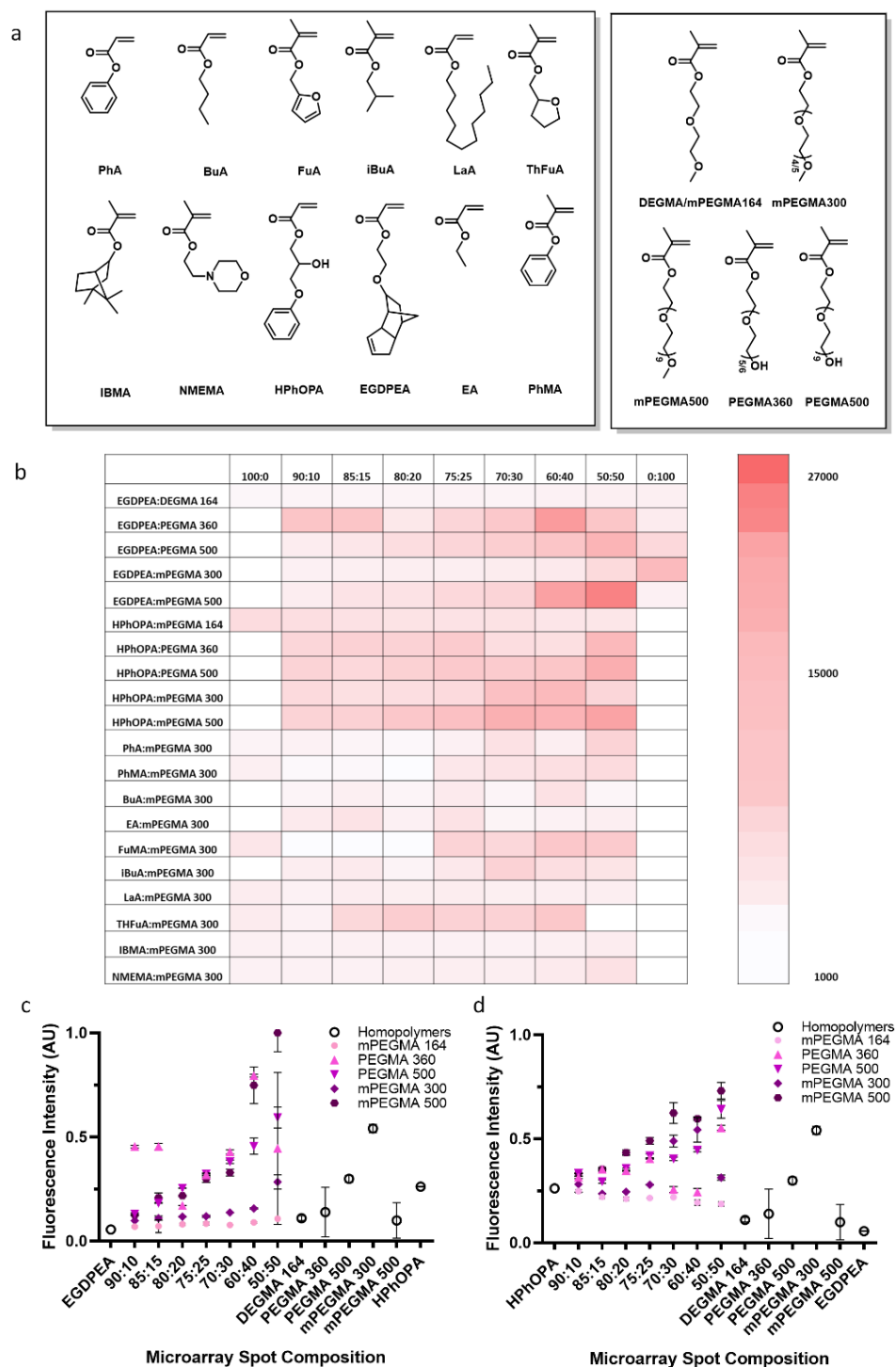


Figure 3.2 (a) Structures of the monomers used for printing polymer microarrays showing major hydrophobic monomers in the blue panel and the minor hydrophilic monomers in the red panel. Chain lengths were either  $n = 6$  or  $9/10$  for PEGMA monomers or  $m = 2, 4/5$  or  $9/10$  for mPEGMA (b) Heat map variation in monomers entity; 1-12 variation in co-monomers concentration) of the polymer microarray showing attachment of mCherry labelled *P. aeruginosa* from high (red) to low (white) showing data from  $n = 6$ ,  $N = 2$  repeats. Narrow columns to the left or right indicate  $\pm 1$  standard deviation. (c) Copolymer data for EGDPEA with a range of different PEG-based hydrophilic chains, showing attachment of *P. aeruginosa* across a sequential copolymer series  $n = 6$  technical repeats and  $N = 2$  biological repeats and (d) Copolymer data for HPhOPA with a range of different PEG-based hydrophilic chains, showing attachment of *P. aeruginosa* across a sequential copolymer series  $n = 6$ ,  $N$

= 2. Data was normalized respect to the highest fluorescence intensity value (EGDPEA-co-mPEGMA<sub>500</sub> 50:50), corresponding to the highest *P. aeruginosa* biofilm spot coverage.

Figures 3.2b, 3.2c and 3.2d show that for all polymer spots investigated, the average bacterial attachment increased with increasing of PEGMA<sub>360/500</sub>/mPEGMA<sub>300/500</sub> concentrations in the copolymer. Statistics have not been performed to investigate the biological relevance of the difference in biofilm formation across homopolymer and copolymer spots. This microarray assay on bacteria attachment was used as an initial and quick method to screen the possible molar ratios, to be employed in the scale up synthesis. On this regard, the data suggested that the introduction of these hydrophilic comonomers compromised the bacteria attachment performance. This was expected, due to the high bacterial attachment exhibited by the PEGMA<sub>360/500</sub>/mPEGMA<sub>300/500</sub> homopolymers during the initial HT screening. When EGDPEA is copolymerised, regardless of the PEG length chain, the materials retain the properties of the EGDPEA homopolymer within a v/v ratio of hydrophobic:hydrophilic 90:10-85:15 (Figure 3.2c). Hydrophilic concentrations beyond this point exhibited *P. aeruginosa* attachment levels significantly higher than that of the homopolymer. However, among all the EGDPEA copolymers, the EGDPEA-co-mPEGMA<sub>300</sub> exhibited attachment levels similar to the EGDPEA homopolymer, at all the ratios investigated. Therefore, it was concluded that a hydrophilic chain length of up to 4-5 ethylene glycol units, when capped with a methoxy terminal group, does not dramatically alter the adhesion of *P. aeruginosa*. Similarly, increasing levels of bacterial

attachment was also typically observed with the copolymers containing HPhOPA, as the concentration of the hydrophilic counterparts increased. The mPEGMA<sub>164</sub> and mPEGMA<sub>300</sub> copolymers were exceptions as they exhibited attachment levels comparable with the control materials (homopolymer of EGDPEA).

Therefore, the 90:10 v/v ratio (hydrophobic:hydrophilic) was selected as the optimum ratio for the surfactant molecular design with respect to the retention of the biological properties of the final material. The bacteria attachment data of the extended range of biologically active HyB monomers included with mPEGMA<sub>300</sub> is not directly discussed in this thesis work as not relevant for the microparticles section. However, the 2D screening results can be found in the Appendix (Figure Appendix 3-26).

### 3.3.2 CCTP Performed *via* Conventional Thermal Polymerisation Method

To achieve the synthesis of polymeric surfactants, exhibiting a target comonomer ratio of 90:10 % mol/mol and a  $M_n$  in the range of 10,000-20,000 g mol<sup>-1</sup>, the catalyst concentration required to be optimised. This  $M_n$  range was chosen to ensure that the viscosity of the subsequent organic/dispersed solutions would be suitable for the use in the chip of the droplets-microfluidic system.

Meanwhile, the 3:1 v/v solvent ratio was selected based on a previous study of EGDPEA-co-mPEGMA<sub>164</sub> copolymerisation, because it was found to deliver the best results relative to achieving the target comonomer ratio and

controlling  $M_n$ /polydispersity.<sup>261</sup> However, for the HPhOPA based surfactant, a higher solvent:comonomer ratio (5:1 v/v) was used because of the high viscosity exhibited by this monomer.

A reaction temperature of 75°C was selected based on the industrial-based AIBN polymerisations that are typically operated between 75 and 85°C. The catalyst optimisation was focused on two copolymers model 90:10 % mol/mol EGDPEA-co-PEGMA<sub>360</sub> and EGDPEA-co-mPEGMA<sub>300</sub>, employing different PhCoBF concentrations (1000 ppm, 850 ppm, 700 ppm and 500 ppm) (Table 3.1).

Table 3.1 Percentage conversions, calculated ratios and  $M_n$  for synthesised polymer surfactants based on EGDPEA-co-PEGMA<sub>360</sub> ((EGDPEA:PEGMA<sub>360</sub>):cyclohexanone 1:3 v/v at 75°C for 18h using 0.5% wt/wt of AIBN (EGDPEA:PEGMA<sub>360</sub>)).

Entry	PhCoBF (ppm)	Conversion <sup>a</sup> (%)	$M_n^b$ ( $g\ mol^{-1}$ )	$\mathcal{D}^b$
1	1000	23%	11,540	2.57
2	850	20%	24,600	2.90
3	700	28%	26,030	2.89
4	500	50%	N/A	N/A

<sup>a</sup> Conversion was calculated by <sup>1</sup>H-NMR (Figure 2.1 and Figure 2.2); <sup>b</sup>  $M_n$  and  $\mathcal{D}$  were calculated by GPC. GPC chromatograms are shown in Appendix, in Figure Appendix 3-27.

The results in Table 3.1 show a consistent trend for  $M_n$  with PhCoBF concentrations with the expected decrease in  $M_n$  with the increasing of catalyst loading. However, broadening of the molecular weight distribution was observed which may indicate relatively poor control of the polymerisation. Additionally, entries 1, 2 and 3 suggest low polymer conversion varying from 20% to 28%, whilst entry 4 shows a higher conversion (50%). The higher conversion and the unreliable  $M_n$  might be related to the performance of the catalyst which may lose activity due to its low concentration.<sup>39</sup> Alternatively, an interesting study performed by

Biasutti et al. have demonstrated that the presence of nucleophilic substituents, such as free -OH or free amino groups, in the monomer structure can inhibit the catalytic activity.<sup>265</sup> This leads to low values of  $C_s$  not allowing the release of the cobalt complex from the transition state. Another interesting study performed by Haddleton et al. reported that when monomers bearing free -OH are polymerised with PhCoBF in bulk, low conversion is obtained after 3 days. In this study, it was noted that when PhCoBF was used with acidic monomers, the low pH causes deactivation of the catalyst. Thus, the additional catalyst needs to be fed in to maintain active the catalyst concentration.<sup>266</sup>

In this work, it was hypothesised that the negative results in terms of conversion (20%-28%) and the lost in control in entry 4, could be attributed to an undesirable interaction between the CCTP catalyst and the hydroxy end-group of PEGMA(-OH). This hypothesis was supported by the catalyst optimisation experiments of the second copolymer model in which the hydrophilic comonomer was replaced with mPEGMA<sub>300</sub> (which contains a methoxy group rather than a free -OH as in PEGMA<sub>360</sub>). These reactions showed improvements in terms of conversion,  $M_n$  and polydispersity such that they aligned with typical FRP values (Table 3.2).

Table 3.2 Percentage conversions, calculated ratios and  $M_n$  for synthesised polymer surfactants based on EGDPEA-co-mPEGMA<sub>300</sub> ((EGDPEA:mPEGMA<sub>300</sub>):cyclohexanone 1:3 v/v at 75°C for 18h using 0.5% wt/wt of AIBN (EGDPEA:mPEGMA<sub>300</sub>)).

Entry	PhCoBF (ppm)	%Conversion <sup>a</sup> (%)	$M_n^b$ (g mol <sup>-1</sup> )	$\mathcal{D}^b$
1	1000	37	2,800	1.93
2	850	43	16,000	1.69
3	700	47	24,000	2.22
4	500	70	59,200	4.10

<sup>a</sup> Conversion was calculated by <sup>1</sup>H-NMR (Figure 2.1 and Figure 2.2); <sup>b</sup>  $M_n$  and  $\mathcal{D}$  were calculated by GPC. GPC chromatograms are showed in Appendix, Figure Appendix 3-28.

This set of copolymers, bearing the -OCH<sub>3</sub> functionality, (Table 3.2 entries 1-4) demonstrated that the  $M_n$  values also showed the expected trend aligned with PhCoBF concentration. Acceptable polydispersity were recorded (Table 3.2 entries 1-3), indicating a significant improvement in the chain transfer mechanism of the catalyst. In addition, conversions also improved, being more than double, when compared to the respective PEGMA<sub>360</sub> based surfactants. Furthermore, better efficiency of chain transfer was observed for all the concentrations for Table 3.2 with Entry 1 (i.e. 1000 ppm catalyst) exhibiting a four-fold smaller  $M_n$  compared to the equivalent EGDPEA-co-PEGMA<sub>360</sub> (Entry 1 Table 3.1). These improvements using methyl end-capped PEG macromonomer highlighted that the end-chain played a role in the deactivation of the catalyst leading in some cases to a FRP-like mechanism without the aid of a CTA. Accordingly, when the concentration of the catalyst was 500 ppm, a dramatic increasing in conversion,  $M_n$  and  $\mathcal{D}$  was depicted (Table 3.1 and Table 3.2 entries 4). This was attributed to this concentration being insufficient to control a polymerisation for monomer types with bulky pendant groups leading the catalyst to fail in the chain transfer step over the polymeric radicals which might react each other

through a traditional FRP mechanism. Furthermore, it has been extensively demonstrated that acrylate monomers in thermal polymerisations might undergo different intermolecular and intramolecular chain transfer reactions like backbiting and  $\beta$ -scission reactions at high temperature.<sup>104</sup> In fact, the chain transfer reactions involve the abstraction of a hydrogen atom from a tertiary carbon atom on the polymer backbone by a propagating radical to form a mid-chain radical. This tertiary radical can then undertake different transformations like propagation,  $\beta$ -scission, or termination.<sup>267</sup> An example of these possible side reactions for polyEGDPEA is shown in Figure 3.3.

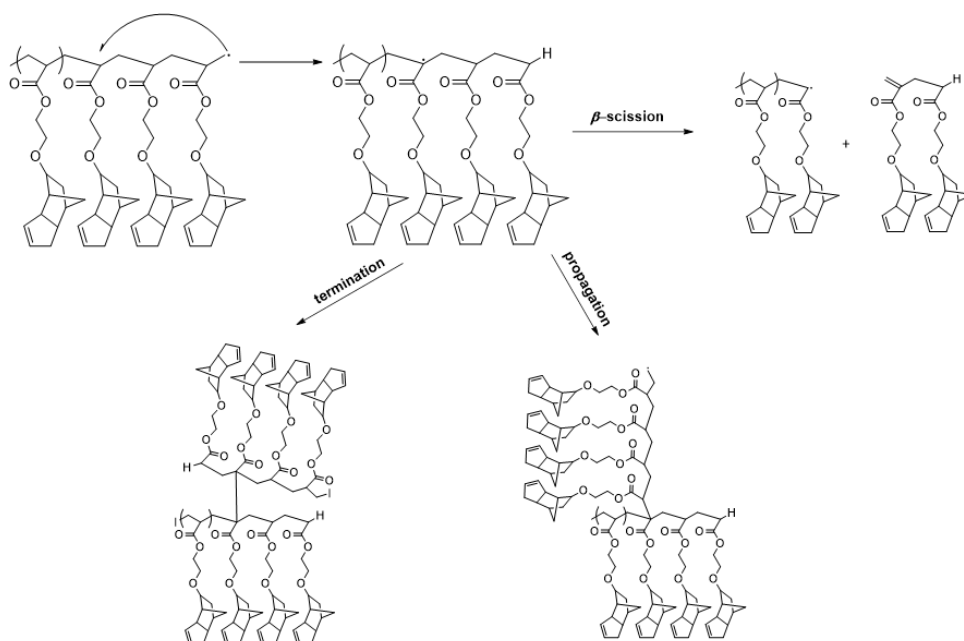


Figure 3.3 Possible intermolecular hydrogen transfer reactions in the FRP of EGDPEA.

Thus, the fact that the acrylate monomer EGDPEA represents around 90% mol of the monomer feedstock in the reaction mixture might be critical for the control over the molecular weight and polydispersity. The highlighted side reactions may compete with the lower activity of PhCoBF

due to the presence of a monomer without  $\alpha$ -methyl group near the double bond C=C, such as EGDPEA.<sup>30,268</sup>

A further study was performed to maximise the conversion of the target surfactant EGDPEA-co-mPEGMA<sub>300</sub>. The catalyst concentration selected from the first set of reactions was 850 ppm, as it gave copolymer with a  $M_n$  of 16,000 g mol<sup>-1</sup> which was within our aim. In the attempt to increase the conversion above 43%, the AIBN concentration was raised from 0.5% w/w to 1% w/w with the intention of increasing the number of radical species and so raise the likelihood of chain initiation. In standard FRP, increasing the initiator concentration would be expected to result in a reduction in MWT as the Degree of Polymerisation (DP) is inversely proportional to the square root of the initiator concentration.<sup>269</sup> However, this reduction would not make an impact to our target. The reactions in this series were monitored at three different reaction times (18 h, 40 h, 70 h) to verify whether initial possible side reactions can interfere in the polymerisation, slowing the process. This doubling of the AIBN concentration was observed to deliver no important changes in conversion as is shown in Figure 3.4.

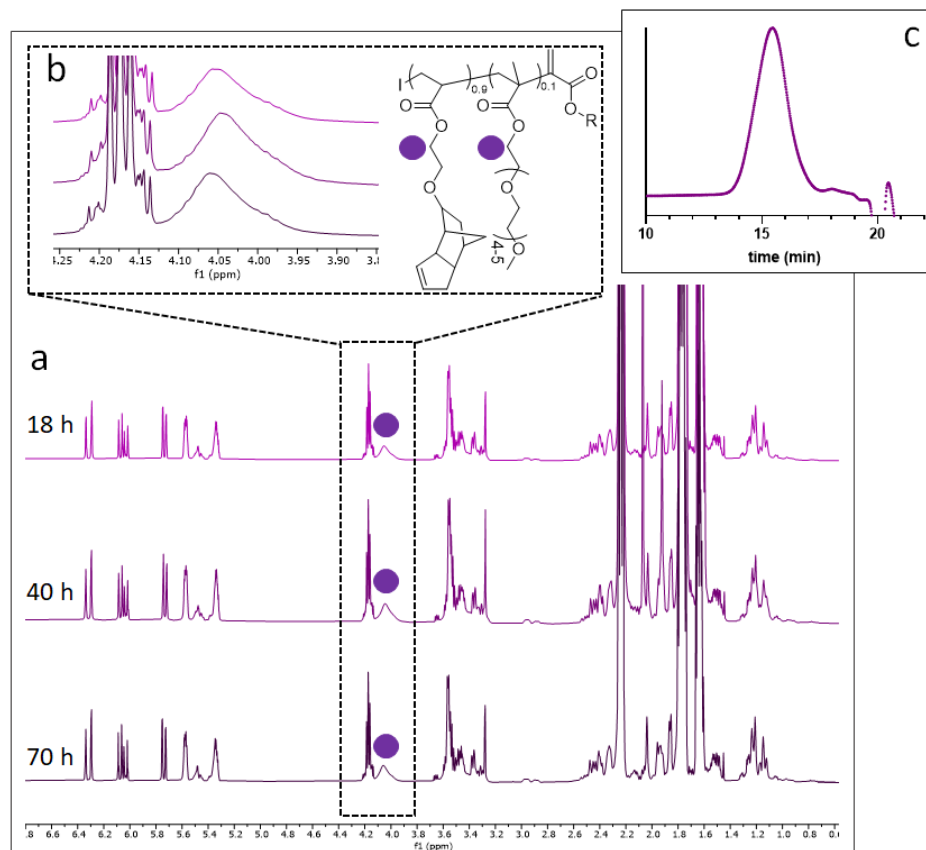


Figure 3.4 Study of the monomer conversion in the EGDPEA-co-mPEGMA<sub>300</sub> copolymer by NMR (a-b) and (c) GPC chromatogram of the final pure copolymer after 70h. ((EGDPEA:mPEGMA<sub>300</sub>):cyclohexanone 1:3 v/v at 75°C for 18h, 40h and 70h using 1% wt/wt of AIBN (EGDPEA:mPEGMA<sub>300</sub>)).

Overall, the final conversion (end point at 70 h) has been of 44% giving a copolymer with a  $M_n$  of 17,000 g mol<sup>-1</sup> ( $\bar{D}$  1.62) (Figure 3.4c). The aliquots of the reaction mixture withdrawn at 16 h demonstrated that the conversion reached the 44 % with no further variations at 40 h and 70 h (Figure 3.4a-b). Potential reasons for the lack of improved conversion with EGDPEA, as the prevalent monomeric species, are: a) the EGPEA bulky pendant group may prevent the chain end radicals accessing the next monomers double bond C=C and b) the double bond presented in the EGDPEA cyclopentenyl side chain might be a competitive radical centre. However, since the reaction is performed in a very diluted environment, i.e. a solvent:monomer

ratio of 3:1 v/v, these side reactions might be limited. However, examples of thiol-ene click chemistry performed on C=C double bond in the pendant of cycloalkenyl functional group have extensively shown in literature.<sup>270–272</sup>

From these initial screenings, it was decided to go forward into the next phase of experimentation and creating a broader library of surfactants using the automated synthesiser, with the following conditions, a PhCoBF concentrations of 850 ppm and a 0.5% wt/wt loading of AIBN.

Before using the automated synthesiser, a small palette of comb-like graft amphiphilic copolymers were synthesised use traditional laboratory techniques to evaluate the robustness of the CCTP using different materials (Table 3.3).

*Table 3.3 Percentage conversions and calculated ratios for synthesised polymer surfactants showing a range of different hydrophilic chains (PEGMA360, PEGMA500, mPEGMA300 and mPEGMA500) and also different major comonomer materials (EGDPEA + HPhOPA) (comonomers:cyclohexanone 1:3 v/v at 75°C for 18h using 0.5% wt/wt of AIBN).*

Entry	Monomer content	Conv <sup>a</sup> (%)	Feed Ratio (% mol/mol)	Final Copolymer Ratio <sup>a</sup> (% mol/mol)	M <sub>n</sub> <sup>b</sup> (Kg mol <sup>-1</sup> )	Đ <sup>b</sup>
1	EGDPEA:PEGMA <sub>360</sub>	20%	90:10	74:26	24.60	2.90
2	EGDPEA:PEGMA <sub>500</sub>	50%	90:10	84:16	304.00	3.50
3	EGDPEA:mPEGMA <sub>300</sub>	43%	90:10	87:13	16.00	1.69
4	EGDPEA:mPEGMA <sub>500</sub>	55%	90:10	80:20	20.60	1.90
5	HPhOPA:mPEGMA <sub>300</sub>	80%	90:10	88:12	26.90	1.86
6	HPhOPA	70%	100:0	-	70.00	1.76

<sup>a</sup>Conversion and Final Copolymer Ratio were calculated by <sup>1</sup>H-NMR (Figure 2.1 and Figure 2.2); <sup>b</sup>M<sub>n</sub> and Đ were calculated by GPC. GPC chromatograms are shown in the Appendix, Figure Appendix 3-29.

In Table 3.3, entry 1 and 3 have been already shown in the optimisation of the catalyst concentration (Table 3.1 and Table 3.2) and are included here for comparison only.

Despite the similar conversion between EGDPEA-co-mPEGMA<sub>500</sub> and EGDPEA-co-PEGMA<sub>500</sub>, the proposed selection of the methoxy alternative, due to its compatibility with CCTP mechanism, was confirmed with a decrease in both of the  $M_n$  from 304,000 g mol<sup>-1</sup> to 20,000 g mol<sup>-1</sup>, and polydispersity, from 3.50 to 1.90. Therefore, the presence of a methoxy end-group on the side chain of the hydrophilic PEG-based comonomer resulted in greater chain transfer control from the adopted catalyst as CTA.

Adopting HPhOPA, as an alternative hydrophobic monomer, using the same conditions applied with EGDPEA (Table 3.3, entry 5), a copolymer with the correct comonomer ratio and good Đ with a  $M_n$  slightly higher than the targeted range (26,900 g mol<sup>-1</sup>) was produced. The conversion achieved was ~80% and the higher  $M_n$  was attributed to the presence of a hydroxy group in the HPhOPA side chain which may interfere in part with the catalyst action as in the case of PEGMA. This conclusion was supported by the much higher  $M_n$  achieved for the CCTP-produced HPhOPA homopolymer (Table 3.3, entry 6) .

The comonomer ratio achieved within the polymer backbone was determined by <sup>1</sup>H-NMR analysis of the purified copolymers. The results in Table 3.3 show that the final monomer composition of all the surfactants was closed to the target feed ratio of 90:10 % mol/mol. All the monomers copolymerised with mPEGMA showed comonomer ratios % mol/mol within a range from 80:20 to 87:13 underlining how the use of this comonomer is important to control the polymerisation.

### 3.3.3 Synthesis of a Library of Surfactants via HT Method

The use of an automated synthesiser to perform the polymerisations in a HT fashion was aimed at building a library of amphiphilic polymeric surfactants adopting a FRP, controlled by CTAs, in a fast, reliable and reproducible way. The HyB monomers were selected by considering: (a) their chemical molecular structure, in order to have a variety of functional groups (e.g. benzyl, alkyl, fluorine, amine, etc.); (b) their hydrophobic character, based on their calculated log P values; (c) their specific biological properties (Figure 3.5).

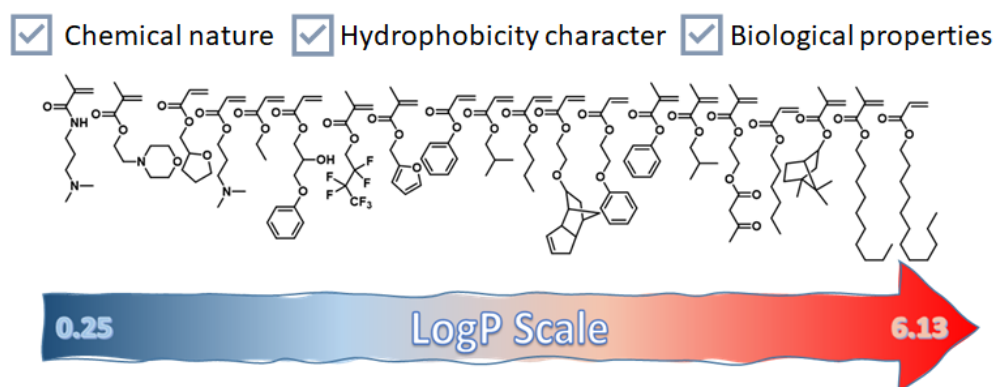


Figure 3.5 Structures of the monomers and the scale of  $clogP$  used to assess the hydrophobicity level of each monomer.

$LogP$ , is a common exploited parameter used to measure the lipophilicity of molecules, indicating the likely partition coefficient of a molecule between an aqueous phase and lipophilic liquids. Thus, is critical for materials aimed at producing surfactants.<sup>273,274</sup> As in prior literature examples, ALOGPS 2.1<sup>®</sup> online open access software has been used for the calculation of the estimate  $LogP$  (i.e.  $cLogP$ ) values of the hydrophobicity of monomers.<sup>273,275,276</sup>

Finally, the target biological properties were based on the 2D microarray screening of the homopolymers ability to either delivery (a) bacteria anti-attachment coatings,<sup>277</sup> (b) enhance of the activity of growth factors during tissue healing on medical devices (e.g. urinary catheters, prosthesis, etc.)<sup>179</sup> and (c) to promote cell attachment on surfaces.<sup>183,278</sup>

### 3.3.3.1 High-Throughput Synthesis of Polymer Libraries via Automated Synthesiser

Once the library of monomers was selected, the first sequence of HT copolymerisation *via* CCTP, consisting of 54 Parallel Polymerisations, was planned. Its aim was to continue the molecular structure optimisation by studying how the monomer library responded to the CCTP catalytic control. This evaluation involved varying the solvent ratios from 1:2 to 1:3 v/v (mon/solvent) to determine if the concentration of the reaction mixture affected the final composition of the polymers, especially in terms of molecular weight. Moreover, in the case of the HPhOPA-*co*-mPEGMA<sub>300</sub> and EPhEA-*co*-mPEGMA<sub>300</sub> copolymers, additional monomer:solvent ratios (1:4 and 1:5 vol/vol) were explored because of the high viscosity exhibited by the starting materials. The concentration of the PhCoBF applied for this first sequence was fixed at 850 ppm, following the results from the lab optimisation. In fact, this concentration should allow a control over the  $M_n$  and result in the production of short (meth)acrylate polymer chains of the order of 15,000 – 20,000 g mol<sup>-1</sup>, that was the target of this study. This MWt range was established to keep the viscosity of the polymers low in the

microfluidics apparatus. In addition, EGDPEA-*co*-mPEGMA<sub>300</sub> and HPhOPA-*co*-mPEGMA<sub>300</sub> were added in the selection as control to verify the robustness of the CCTP can be translated in an automated system from a traditional lab chemistry system.

These first reactions screening experiments resulted in the generation of a library of amphiphilic macromolecules from the 20 HyB monomers being copolymerised with mPEGMA<sub>300</sub> (with replicates) to give materials that exhibited the desired target molecular structure (Figure 3.6).

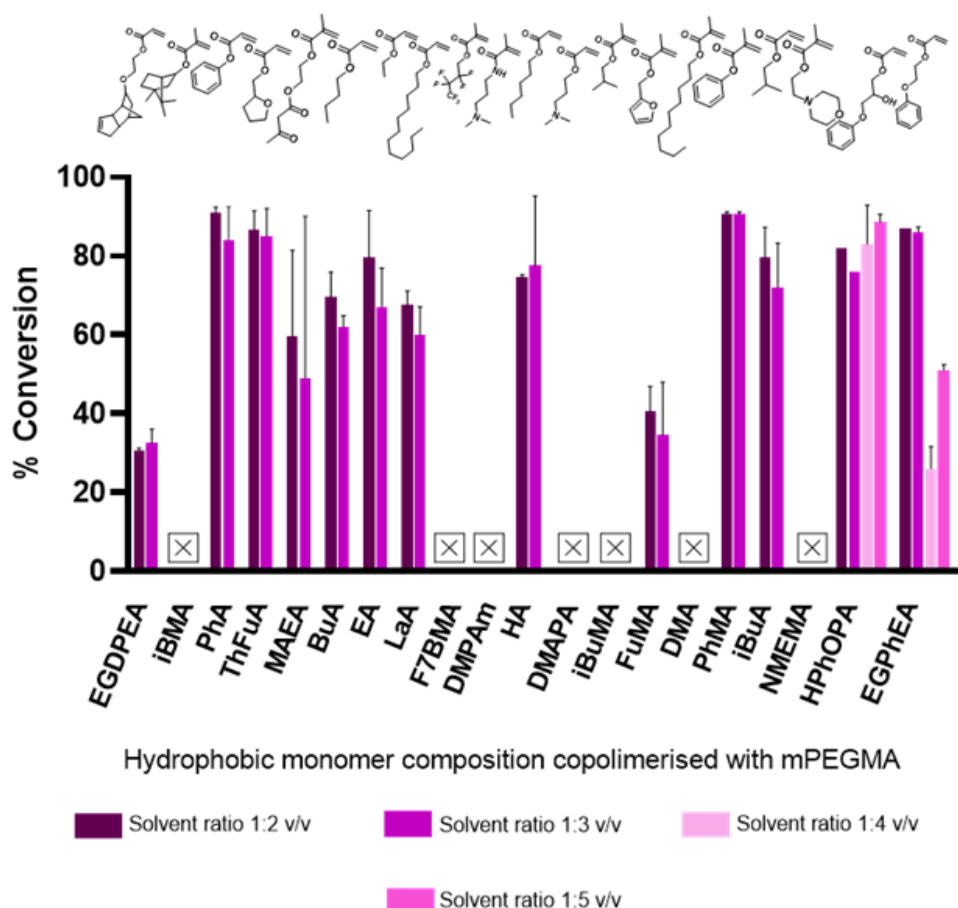


Figure 3.6 Conversion of polymerisation determined by means of <sup>1</sup>H-NMR spectroscopy varying the solvent/monomer ratio.

Figure 3.6 shows that the conversion achieved was 50% or greater for the majority of the copolymers. This meant that the catalytic mechanism was

operating as expected from the previous optimisation studies and sufficient material was obtained to allow further analysis and testing. In addition, the set of copolymers used as control (EGDPEA-co-mPEGMA<sub>300</sub> and HPhOPA-co-mPEGMA<sub>300</sub>) showed comparable results to the optimisation performed using a Schlenk traditional type of chemistry (Section 3.3.2, Table 3.3).

However, eight of the HyB monomers (DMPAm, DMAPA, F7BMA, DMA, iBMA, iBuMA, NMEMA and FuMA) did not form any copolymers or produced a yield less than 30% under these initial conditions. Three potential causes were identified for this disruption of the CCTP reaction: a) the presence of electronic substituents in the monomer structure might deactivate the catalyst activity by not allowing the release of the cobalt complex from the transition state (similar behaviour was observed using PEGMA as comonomer)<sup>254,255</sup> b) the reactivity of the monomer to the radical is so low that the PhCoBF interacts with the newly generated radical prior to being involved in initiation and/or c) the presence of methacrylate moieties in the structure, as it is well known that CCTP works more efficiently with methacrylates than acrylates.<sup>104</sup> Thus, as a consequence of selecting a relatively high concentration of PhCoBF, to reflect the greater number of acrylate monomers present in the test series, it may cause the chain transfer events to dominate before propagation could take place, when methacrylates are involved. In light of this hypothesis, a second series of copolymerisations were conducted with a subset of these methacrylate monomers (i.e. NMEMA, iBMA, iBuMA and DMA) at two lower concentrations of the CTA, at 650 and 450 ppm. In addition to these four

monomers, FuMA was also integrated into this second reaction sequence, as in the previous experiment it had shown poor conversion (<30%), hence, it was considered a failure in the polymerisation. In Figure 3.7 it is reported the conversion results obtained from this second series of copolymerisations.

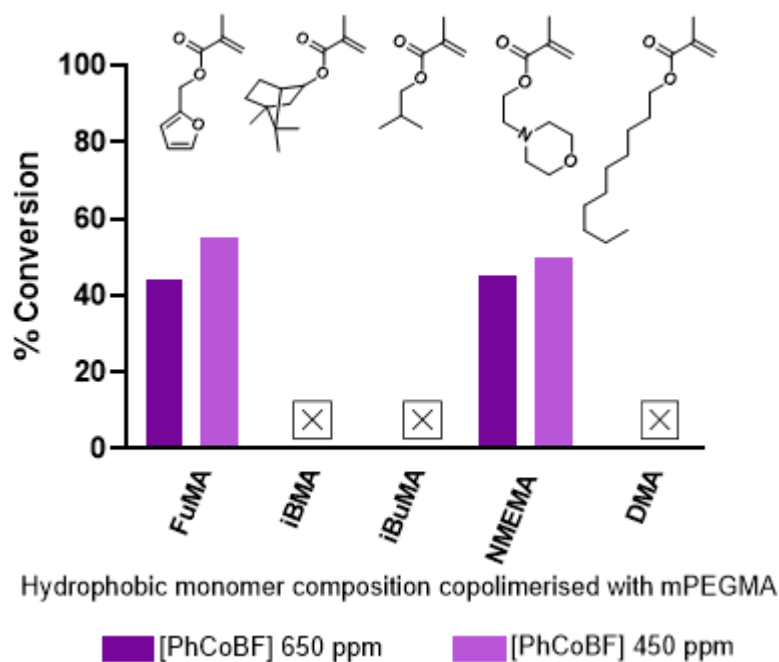


Figure 3.7 Resulted conversions, determined by means of  $^1\text{H-NMR}$  spectroscopy, from a further screening related to the decreasing the catalyst concentrations (i.e. 650 ppm and 450 ppm).

The results reported in Figure 3.7 show that these copolymerisations can be separated into two groups. FuMA-co-mPEGMA<sub>300</sub> and NMEMA-co-mPEGMA<sub>300</sub> showed a net improvement in the yield achieved by varying the amount of catalyst from 850 ppm, in the first run, to 650/450 ppm. The former increased its yield from 30% with 850 ppm to ~ 60% at 450 ppm of catalyst, whilst the conversion of the latter reached ~ 50% with 450 ppm. Thus, it was concluded that these reactions were retarded due to the monomer reactivity. By comparison, the iBMA-, iBuMA- and DMA-co-mPEGMA<sub>300</sub> copolymerisation still did not form any polymer under these

reduced CTA regimes. Their lack of reactivity has been attributed to a level of steric hindrance due to the large pendant groups that are directly attached to the chain with no flexible spacer group present. This is likely due to reduced chain end reactivity with the CTA complex, thereby encouraging the PhCoBF to interact directly with the initiator ligand prior to initiation.<sup>104</sup>

### 3.3.3.2 Copolymer Characterisation Results

The  $M_n$ , polydispersity and final copolymer ratio are shown in Table 3.4 for the 54 CCT polymerisations, performed as first screening, and in Table 3.5 for the further CCTP optimisation, reducing PhCoBF concentration.

Table 3.4  $M_n$ ,  $\bar{D}$  and final copolymer ratios of the initial screening reactions with CCTP with target feed ratio of 90:10 mol/mol.

Entry	Monomer content	Solvent:Monomer Ratio (v/v)	$M_n^a$ (Kg mol <sup>-1</sup> )	$\bar{D}^a$	Final copolymer ratio <sup>b</sup> (% mol/mol)
1	EGDPEA:mPEGMA <sub>300</sub>	2:1	7.26	2.27	91:9
2	EGDPEA:mPEGMA <sub>300</sub>	3:1	4.40	2.19	87:13
3	PhA:mPEGMA <sub>300</sub>	2:1	16.71	2.47	89:11
4	PhA:mPEGMA <sub>300</sub>	3:1	12.88	2.56	88:12
5	THFuA:mPEGMA <sub>300</sub>	2:1	14.69	2.18	94:6
6	THFuA:mPEGMA <sub>300</sub>	3:1	10.64	2.45	91:9
7	MAEA:mPEGMA <sub>300</sub>	2:1	1.50	1.21	68:32
8	MAEA:mPEGMA <sub>300</sub>	3:1	1.20	1.16	63:37
9	BuA:mPEGMA <sub>300</sub>	2:1	10.7	2.16	88:12
10	BuA:mPEGMA <sub>300</sub>	3:1	14.34	2.24	89:11
11	LaA:mPEGMA <sub>300</sub>	2:1	18.54	2.29	96:4
12	LaA:mPEGMA <sub>300</sub>	3:1	13.50	2.80	87:13
13	EA:mPEGMA <sub>300</sub>	2:1	18.21	2.23	90:10
14	EA:mPEGMA <sub>300</sub>	3:1	13.04	2.46	88:12
15	HA:mPEGMA <sub>300</sub>	2:1	20.66	2.90	93:7
16	HA:mPEGMA <sub>300</sub>	3:1	15.42	1.90	93:7
17	FuMA:mPEGMA <sub>300</sub>	2:1	0.94	1.19	87:13
18	FuMA:mPEGMA <sub>300</sub>	3:1	0.99	1.20	87:13
19	PhMA:mPEGMA <sub>300</sub>	2:1	3.00	2.48	94:6
20	PhMA:mPEGMA <sub>300</sub>	3:1	2.50	2.54	92:8
21	iBuA:mPEGMA <sub>300</sub>	2:1	17.82	2.64	89:11
22	iBuA:mPEGMA <sub>300</sub>	3:1	15.00	2.71	89:11
23	HPhOPA:mPEGMA <sub>300</sub>	2:1	25.3	3.58	89:11
24	HPhOPA:mPEGMA <sub>300</sub>	3:1	15.31	3.76	91:9
25	HPhOPA:mPEGMA <sub>300</sub>	4:1	13.13	2.84	90:10
26	HPhOPA:mPEGMA <sub>300</sub>	5:1	15.00	3.61	91:9
27	EGPhEA:mPEGMA <sub>300</sub>	2:1	29.3	3.70	93:7
28	EGPhEA:mPEGMA <sub>300</sub>	3:1	14.50	3.73	88:12
29	EGPhEA:mPEGMA <sub>300</sub>	4:1	6.46	2.24	87:13
30	EGPhEA:mPEGMA <sub>300</sub>	5:1	9.32	2.19	89:11

<sup>a</sup> $M_n$  and  $\bar{D}$  were calculated by GPC; <sup>b</sup>Final copolymer ratios were calculated by <sup>1</sup>H-NMR (Figure 2.1).

Table 3.5  $M_n$ ,  $\bar{D}$  and Copolymer Ratio of the reactions with the altered CCTP catalyst concentrations.

Entry	Monomer content	Catalyst (ppm)	$M_n^a$ (kg mol <sup>-1</sup> )	$\bar{D}^a$	Final copolymer ratio <sup>b</sup> (% mol/mol)
1	FuMA:mPEGMA <sub>300</sub>	650	1.20	1.89	89:11
2	FuMA:mPEGMA <sub>300</sub>	450	1.13	2.30	92:8
3	NMEMA:mPEGMA <sub>300</sub>	650	1.77	1.50	88:12
4	NMEMA:mPEGMA <sub>300</sub>	450	2.55	1.77	93:7

<sup>a</sup> $M_n$  and  $\bar{D}$  were calculated by GPC; <sup>b</sup>Final copolymer ratios were calculated by <sup>1</sup>H-NMR (Figure 2.1).

In Table 3.4, the  $M_n$  obtained for all the majority of the copolymers varied between our target range of 10,000 g mol<sup>-1</sup> and 20,000 g mol<sup>-1</sup>. In addition to the HyB monomers side chain chemistry, the initial screening, also, investigated the effect of monomer concentration, when varying the solvent ratio from 1:3 to 1:2 vol/vol. It has been noted that the variation of the solvent ratio, it affects the  $M_n$  with the most concentrated conditions producing an increase in the  $M_n$  of up to 30%. This may be due to a higher rate of chain transfer to solvent or that the CTA is less likely to meet a chain-end in the dilute conditions. Alternatively, as the degree of polymerisation directly dependent to the monomer concentration (Equation 3.1), in diluted conditions, the  $M_n$  is most likely to be lower when compared to the values in more concentrated conditions.<sup>40</sup>

$$\frac{1}{DP_n} = C_s \frac{[Co(II)]}{[M]}$$

*Equation 3.1 The Mayo equation. Where  $DP_n$  is the degree of polymerisation;  $C_s$  is the general chain transfer constant;  $[M]$  and  $[Co(II)]$  are the concentration of the monomer species and the CTA, respectively.*

By comparison, the variation of the solvent:monomer ratio did not dramatically alter the final values of  $\bar{D}$  of the product surfactants.

Typically, the copolymers bearing a hydrophobic methacrylic comonomer (PhMA, NMEMA, FuMA) showed lower  $M_n$  of around 2,000 g mol<sup>-1</sup> even with the lower levels of CTAs applied, confirming that the catalyst was working more efficiently with these monomers. In Table 3.5, the set FuMA-*co*-mPEGMA<sub>300</sub> and NMEMA-*co*-mPEGMA<sub>300</sub> showed that the  $M_n$  of the polymers decreases as the total amount of catalyst is increased relative to

the monomer. This trend is the correct consequence of the presence of a CTA in the reaction mixture, which allow the control over the  $M_n$ . Also, the polydispersity seems to be affected by the quantity of PhCoBF, in fact, when 650 ppm was applied to the polymerisation, it has resulted in narrower polydispersity.

Table 3.4 and Table 3.5, also, contain the final molar composition of these materials that defines the balance between the hydrophilic and hydrophobic part, which will determine the ability of the surfactant to self-assemble. The actual monomer ratios, i.e. the final relative monomer composition inside the polymer backbone, were determined from the  $^1\text{H-NMR}$  spectra of the purified copolymers. They showed that all the surfactants were within the feed ratio target range of % mol/mol 80:20 to 95:5 with the exception of MAEA-co-mPEGMA<sub>300</sub>. This particular surfactant exhibited a HyB:mPEGMA<sub>300</sub> molar ratio of around 68:32. This was attributed to the fact that the reactivity of the two monomers are significantly different leading to a comonomer ratio out of the target. The characterisation data, in both the Table 3.4 and Table 3.5 demonstrated that when the correct CTA level was used for both acrylates and methacrylates, these HT polymerisations were a robust and broadly applicable process to generate polymer libraries with varied composition.

### *3.3.3.3 HT Polymerisation Scalability – from 1.5g to 10 g*

With the consideration of the potential end industrial applications of CCTP, a design of a HT scalability screening was developed. The scale up of the

CCTP based HyB-copolymerisations from 1 to 10 mL was investigated on a sub-set of 4 polymers as a proof of concept. The four polymers were selected as a result of their chemical functionalities and the range of different experimental conditions that were required for their synthesis, as highlighted in the small-scale reactions. THFuA-co-mPEGMA<sub>300</sub> and EA-co-mPEGMA<sub>300</sub> were chosen because they contained an acrylate group. HPhOPA-co-mPEGMA<sub>300</sub>, whilst also an acrylate, was chosen due to its high viscosity and thus the need for the monomer:solvent ratio used for the reaction to be 1:5 vol/vol. Finally, NMEMA-co-mPEGMA<sub>300</sub> was included both as a representative methacrylate containing functionality and because of the amine pendant group. This scale up experiment was conducted employing the same reaction conditions, previously adopted during small-scale screening, without further optimisation. These results obtained from the scale up are reported in Table 3.6 and compared to the equivalent small-scale results in Figure 3.8.

Table 3.6 Conversion,  $M_n$ ,  $\bar{D}$  and final copolymer ratio of the scale up reactions with CCTP with a target feed ratio of 90:10 % mol/mol.

Entry	Monomer content	Conversion (%)	$M_n^a$ (kg mol <sup>-1</sup> )	$\bar{D}^a$	Final copolymer ratio <sup>b</sup> (% mol/mol)
1	THFuA:mPEGMA <sub>300</sub>	60	11.2	2.44	94:6
2	EA:mPEGMA <sub>300</sub>	63	9.3	2.34	91:9
3	HPhOPA:mPEGMA <sub>300</sub>	77	20.0	1.86	95:5
4	NMEMA:mPEGMA <sub>300</sub>	42	7.0	1.46	94:6

<sup>a</sup>Conversion and final copolymer ratios were calculated by <sup>1</sup>H-NMR (); <sup>b</sup> $M_n$  and  $\bar{D}$  were calculated by GPC.

Table 3.6 shows that conversions, as expected, were between 40-70% for all the entries. In addition, the  $M_n$  are in the range of 10,000 – 20,000 g mol<sup>-1</sup> as for the catalyst concentration applied for the synthesis.

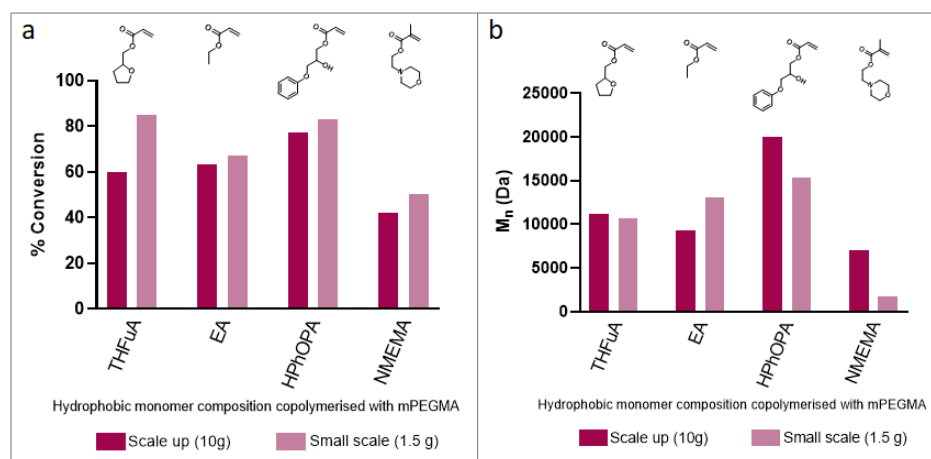


Figure 3.8 (a) Comparison of the % conversion of CCT polymerisations in small scale (1.5g) and large scale (10g) determined by means of <sup>1</sup>H-NMR spectroscopy. (b) Comparison of  $M_n$  of the copolymers obtained in small scale (1.5g) and large scale obtained.

The data in Figure 3.8 confirmed the robustness of CCTP in this initial proof-of-concept scale up because, without any specific alterations in reaction conditions, acceptable  $M_n$  values and comonomer ratios were obtained, whilst high conversion to the final product was retained.

### 3.3.3.4 Thiol-mediated Free Radical Polymerisation via High-Throughput Synthesis

A second industrial-exploited CTA, benzyl mercaptan, has been employed to further investigate the hypothesis that the ‘failure’ of some CCT based HT polymerisation is due to intrinsic limitations of the control method rather than a flaw with the automated process. The model thiol CTA adopted was added at two different concentrations: 5% and 10% % mol relative to the monomers. The HyB monomers used for this sequence of experiments were

DMPAm, DMAPA, DMA, F7BMA, iBMA, iBuMA, i.e. the ones that failed in the previous CCTP screening and the solvent:monomer ratio adopted was 1:3 vol/vol.

Table 3.7 Conversion,  $M_n$ ,  $\bar{D}$  and final copolymer ratio for iBMA, iBuMA, DMA, DMAPA, DMPAm and F7BMA based mPEGMA<sub>300</sub> copolymers with a target feed ratio of 90:10 % mol/mol.

	Monomer content	BzSH (% mol)	Conv <sup>a</sup> (%)	Final Copolymer Ratio <sup>a</sup> (% mol/mol)	$M_n^b$ (Kg mol <sup>-1</sup> )	$\bar{D}^b$
1	iBMA:mPEGMA <sub>300</sub>	5%	87%	92:8	7.10	1.44
2	iBMA:mPEGMA <sub>300</sub>	10%	85%	93:7	3.60	1.43
3	iBuMA:mPEGMA <sub>300</sub>	5%	90%	N/A	6.88	1.67
4	iBuMA:mPEGMA <sub>300</sub>	10%	88%	N/A	4.92	1.43
5	DMA:mPEGMA <sub>300</sub>	5%	80%	93:7	5.40	1.43
6	DMA:mPEGMA <sub>300</sub>	10%	86%	92:8	3.00	1.39
7	DMAPA:mPEGMA <sub>300</sub>	5%	90%	95:5	8.70	1.48
8	DMAPA:mPEGMA <sub>300</sub>	10%	84%	93:7	7.22	1.45
9	DMPAm:mPEGMA <sub>300</sub>	5%	90%	86:14	6.50	2.40
10	DMPAm:mPEGMA <sub>300</sub>	10%	92%	89:11	4.11	2.65
11	F7BMA:mPEGMA <sub>300</sub>	5%	90%	92:8	6.31	1.20
12	F7BMA:mPEGMA <sub>300</sub>	10%	88%	93:7	5.21	1.20

<sup>a</sup>Conversion and final copolymer ratios were calculated by <sup>1</sup>H-NMR (Figure 2.1); <sup>b</sup> $M_n$  and  $\bar{D}$  were calculated by GPC.

In Table 3.7, the thiol mediated polymerisation produced HyB-co-mPEGMA<sub>300</sub> copolymers at high conversion of approximately 80-85% at both BzSH feed concentration. The exception was the DMPAm-co-mPEGMA copolymer that only achieved ~55% conversion, which was still above the targeted level set. This may be related to poor reactivity between the HyB monomer and the thiol due to the presence of the amine group. The  $M_n$  achieved ranged between 3,000 g mol<sup>-1</sup> and 13,400 g mol<sup>-1</sup> and their value depended on the amount of BzSH present in the reaction mixture. As it would be expected, the higher the CTA concentration the lower the  $M_n$ . Unfortunately, the purification of iBuMA-co-mPEGMA was not possible to

via non-solvent precipitation, so further characterisation was not performed on this material.

Despite this CTA exhibits the necessary control, it should be noted that the final molecular structure will be different from that of the CCTP, in fact a portion of the product will contain a thio-ether end-group (BzS-). Furthermore, the terminal groups will all be fully saturated, therefore, no opportunity for post-functionalisation/chain transfer with these materials will exist.

### 3.3.4 HT Evaluation of Critical Aggregation Concentration

To evaluate the threshold at which the amphiphilic copolymers transition between existing as single chains in solution to becoming nanoaggregates, an assessment of their CAC has been conducted. As discussed in the 1.2 Surfactant paragraph, this concentration represents the point where the interface is saturated by amphiphilic molecules (i.e. surfactants) and aggregates are formed. Also, the CAC can be considered as one of the indicators for micelle stability which is an important factor when amphiphilic polymers are used as surfactants.<sup>280</sup>

To experimentally determine this value, firstly, stock emulsions/suspensions at the fixed concentration of 500 µg/mL were prepared by adopting the traditional nanoprecipitation method for all the synthesised surfactants. However, the manual method mentioned above is very time consuming, so by successfully adopting the developed HT method, we are simply moving the bottleneck in the process to the CAC evaluation

in the pipeline of surfactant design and validation. In fact, if conventional manual methodologies were to be adopted, i.e. the preparation of stock emulsions/suspensions at the fixed concentration of 500  $\mu\text{g}/\text{mL}$  and the subsequent 12 serial dilutions (up to 0.05  $\mu\text{g}/\text{mL}$ ), this would become a pinch point in any HT pipeline of surfactant design and validation. Thus, in order to maintain HT methodologies not only for the synthesis but also for the characterisation of these materials, an automated method to assess the self-assembling properties was developed. To achieve this aim, a 2D-picolitre-ink-jet printer was employed to produce a miniaturised, automated serial dilution system. This utilised a manually pre-prepared stock solution, obtained as described in the experimental section. The advantage of this method dwells in the precise and limited amount of material that can be delivered by the ink-jet head. Thus, very low concentration solutions can be prepared without intermediate dilutions. Furthermore, the entire set of the 228 dilution samples could be achieved in just three 96 well-plates. A DLS plate reader was then used to measure the count rate of each well, which was the result of an average of 10 measurements at a fixed laser power which was set fixing the attenuator function. Finally, the CAC was determined from the change in the trend of the data obtained from plotting the Intensity values at the explored concentrations as a function of the log values of concentration ( $\mu\text{g}/\text{mL}$ ) (Example in Figure 3.9).<sup>280,281</sup>

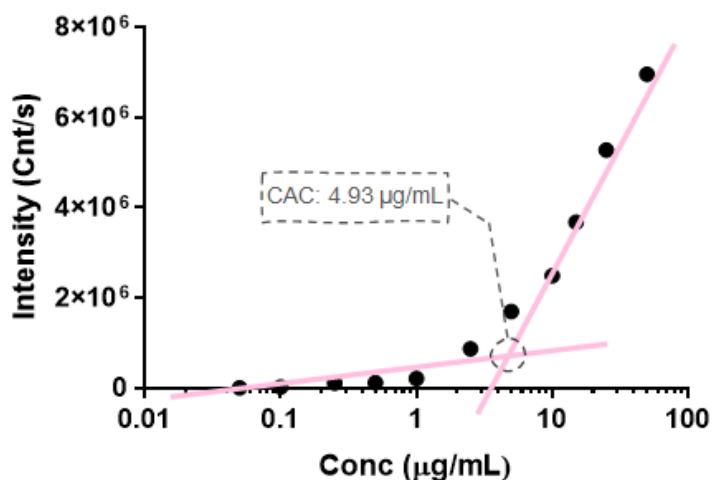


Figure 3.9 CAC of *iBMA-co-mPEGMA*<sub>300</sub>, an example of plot of the intensity of scattered light (kilo counts per second) as a function of concentration ( $\mu\text{g/mL}$ ). The data showed that the scattering detected for the surfactant concentrations below the CAC is similar to deionised water. After the CAC was reached, the scattering intensity shows a linear increase with concentration. The intersection between the 2 lines, at  $4.93 \mu\text{g/mL}$ , corresponds to the CAC.

In Figure 3.9, the change in the plot observed is due to the change of intensity of the scattered light before the micelle/aggregates are formed (before the CAC) and after the presence of micelles. The CAC value was taken from the intersection of the best fit lines as shown in Figure 3.9 and in Figure Appendix 3-30. In Table 3.8, the CAC values obtained for all the surfactants synthesised and their copolymer ratios.

Table 3.8 HT-CAC and final copolymer ratios of the surfactants produced in high-throughput method using either CCTP or thiol mediated free radical polymerisation.

Entry	Copolymer	CAC ( $\mu\text{g}/\text{mL}$ )	Final Copolymer Ratio (%mol/mol)
1	(EGDPEA-co-mPEGMA) <sub>CCTP</sub>	8.4	87:13
2	(iBMA-co-mPEGMA) <sub>BzSH</sub>	4.9	92:8
3	(PhA-co-mPEGMA) <sub>CCTP</sub>	10.3	88:12
4	(THFuA-co-mPEGMA) <sub>CCTP</sub>	11.1	91:9
5	(MAEA-co-mPEGMA) <sub>CCTP</sub>	20	63:37
6	(BuA-co-mPEGMA) <sub>CCTP</sub>	9.5	89:11
7	(EA-co-mPEGMA) <sub>CCTP</sub>	13.0	88:12
8	(LaA-co-mPEGMA) <sub>CCTP</sub>	4.0	87:13
9	(F7BMA-co-mPEGMA) <sub>BzSH</sub>	18.0	93:7
10	(DMPAm-co-mPEGMA) <sub>BzSH</sub>	16.1	86:14
11	(HA-co-mPEGMA) <sub>CCTP</sub>	8.2	93:7
12	(DMAPA-co-mPEGMA) <sub>BzSH</sub>	22.0	95:5
13	(FUМА-co-mPEGMA) <sub>CCTP</sub>	9.5	92:8
14	(DMA-co-mPEGMA) <sub>BzSH</sub>	4.5	93:7
15	(PhMA-co-mPEGMA) <sub>CCTP</sub>	9.0	92:8
16	(iBuA-co-mPEGMA) <sub>CCTP</sub>	4.5	89:11
17	(NMEMA-co-mPEGMA) <sub>CCTP</sub>	13.0	93:7
18	(HPhOPA-co-mPEGMA) <sub>CCTP</sub>	3.5	91:9
19	(EGPhEA-co-mPEGMA) <sub>CCTP</sub>	6.5	87:13

<sup>a</sup>As the (MAEA-co-mPEGMA<sub>300</sub>)<sub>CCTP</sub> copolymerisation ratio was outside an acceptable range limit of between 80:20 and 95:5 it was excluded from the data comparison.

The copolymers data from both polymerisation techniques in Table 3.8 shows a broad range of CAC values. However, the order in magnitude of the CACs is suggesting that the copolymer end-group did not greatly influence micelle formation. Overall, when the hydrophobic:hydrophilic ratio was well-balanced, and so, the copolymer ratio was similar to the target 90:10 mol:mol (HyB:mPEGMA<sub>300</sub>), the CAC values are between 3.5  $\mu\text{g}/\text{mL}$  and 22  $\mu\text{g}/\text{mL}$ , although, this was not observed for MAEA-co-mPEGMA<sub>300</sub>. The highest values of CAC, ascribed to DMAPA-co-mPEGMA<sub>300</sub> and DMPAm-co-mPEGMA<sub>300</sub>, might be attributed to the similar cLogP values between the HyB monomers and mPEGMA<sub>300</sub>, which does not allow the copolymers to self-assemble properly leading to the backbone being the hydrophobic

driving force in the self-assembly process. Comparison with literature tabulated Critical Micelle Concentration (CMC) values of well-known, commercially available surfactants showed that these values were comparable to those of a range of commercial surfactants, e.g. Tween80 (CMC = 12.0  $\mu\text{g}/\text{mL}$ ), Brij 30 (4.8  $\mu\text{g}/\text{mL}$ ), Brij 56 (2.4  $\mu\text{g}/\text{mL}$ ), Brij 58 (8.4  $\mu\text{g}/\text{mL}$ ), Brij 76 (3.6  $\mu\text{g}/\text{mL}$ ), Brij 78 (6.8  $\mu\text{g}/\text{mL}$ ) and Brij 721 (4.7  $\mu\text{g}/\text{mL}$ ).<sup>282,283</sup> These CAC values are comparable to those reported for other amphiphilic methacrylate block copolymers and for the Pluronics.<sup>284–286</sup> This suggests that the self-assembling behaviour and stability of the resultant micelles could be compared to these commercially available surfactants.

A review of the data highlighted the expected trend in the LogCAC vs cLogP for the HyB monomers (Figure 3.10).

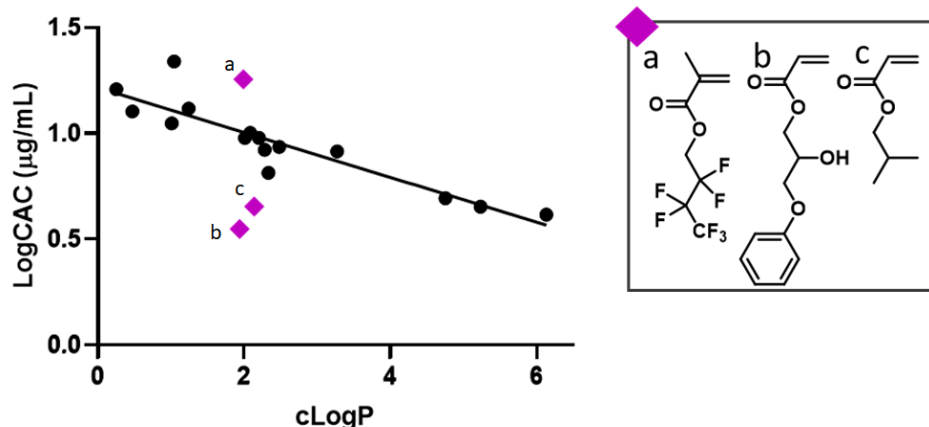


Figure 3.10 the logarithmic values of the calculated CACs were plotted against the value of the LogP of 14 HB monomers. CACs of 4 surfactants with HB monomers in the rectangle (a, b, c and d) were excluded from the trend.

Figure 3.10 shows that the general linear downward trend ( $R^2$ : 0.8304) with the increasing of cLogP values confirmed that the bulkier monomers led to lower LogCACs. The only exceptions to this trend are 3 surfactants: iBuA-co-mPEGMA<sub>300</sub>, F7BMA-co-mPEGMA<sub>300</sub> and HPhOPA-co-mPEGMA<sub>300</sub>. In

particular, F7BMA-*co*-mPEGMA<sub>300</sub> exhibited an overestimation of its CACs when compared to the cLogP values, showing one of the highest CAC. For instance, F7BMA-*co*-mPEGMA<sub>300</sub>, despite the presence of multiple hetero-fluoro atoms conferring hydrophobicity, -(CF<sub>2</sub>) and -CF<sub>3</sub> groups still result bulky and sterically hindrance, in particular in bond rotations, which it may lead to a different packing and so higher CAC. In addition, it has been shown in literature that CF<sub>3</sub> groups interact through-space with CH and OCH<sub>3</sub> groups which are presented in the ether polymer backbone and the hydrophilic side chain of mPEGMA, respectively. These interactions might hamper the self-assembling along the amphiphile.<sup>287</sup>

On the other hand, HPhOPA-*co*-mPEGMA<sub>300</sub> and iBuA-*co*-mPEGMA<sub>300</sub> showed an underestimation compared to the clogP of the HB monomers, with HPhOPA based surfactant having the lowest CAC value of the series. This might be attributed to the presence of the aromatic ring and the -OH group in the side chain of the HB monomer. These two different functionalities might lead to a high packing due to the inter- and intra-  $\pi$ - $\pi$  stacking between the benzyl moieties, and, as well as the hydrogen bond through-space interactions between the hydroxyl groups. Further experimental work and understandings will be required to define the root cause of the deviation of the iBuA copolymer.

To confirm that these copolymers could self-assemble and form aggregates, the sizes of the colloidal mixture particles were measured when the system was below, at and above the CAC (Table 3.9).

Table 3.9 size of the surfactants, produced in high-throughput method using either CCTP or thiol mediated free radical polymerisation, at the CAC of each single copolymers and above the CAC using 100 µg/mL as fixed concentration. Each experiment was conducted using a DLS-plate reader at 25°C and preparing the emulsion/suspension in DI water (as described in Section 3.2.3).

	Copolymer	CAC (µg/mL)	Size (nm) at CAC	Size (nm) above CAC
1	(EGDPEA-co-mPEGMA) <sub>CCTP</sub>	8.36	121	110
2	(iBMA-co-mPEGMA) <sub>BzSH</sub>	4.93	102	103
3	(PhA-co-mPEGMA) <sub>CCTP</sub>	10.3	180	183
4	(THFuA-co-mPEGMA) <sub>CCTP</sub>	11.14	248	246
5	(MAEA-co-mPEGMA) <sub>CCTP</sub>	19.82	157	146
6	(BuA-co-mPEGMA) <sub>CCTP</sub>	9.50	161	168
7	(EA-co-mPEGMA) <sub>CCTP</sub>	13.08	156	149
8	(LaA-co-mPEGMA) <sub>CCTP</sub>	4.13	199	196
9	(F7BMA-co-mPEGMA) <sub>BzSH</sub>	18.00	98	70
10	(DMPAm-co-mPEGMA) <sub>BzSH</sub>	16.15	123	135
11	(HA-co-mPEGMA) <sub>CCTP</sub>	8.20	87	96
12	(DMAPA-co-mPEGMA) <sub>BzSH</sub>	21.82	103	101
13	(FUMA-co-mPEGMA) <sub>CCTP</sub>	9.50	216	231
14	(DMA-co-mPEGMA) <sub>BzSH</sub>	4.50	169	163
15	(PhMA-co-mPEGMA) <sub>CCTP</sub>	8.63	274	365
16	(iBuA-co-mPEGMA) <sub>CCTP</sub>	4.52	109	102
17	(NMEMA-co-mPEGMA) <sub>CCTP</sub>	12.67	217	219
18	(HPhOPA-co-mPEGMA) <sub>CCTP</sub>	3.54	144	144
19	(EGPhEA-co-mPEGMA) <sub>CCTP</sub>	6.50	203	203

At a concentration of 0.05 µg/mL, 40 times below the calculated CAC of the 19 surfactants, no aggregates were observed. However, once the systems were at or above the CAC (100 µg/ml), an increase in the intensity of light scattering was observed, which corresponds to the formation of aggregates and so their hydrodynamic diameters could be detected via the DLS.

It has been previously reported that random copolymers bearing PEG and hydrophobic pendant chains can self-assemble into water producing well-defined micelles-like nanoparticles with size below 10 nm.<sup>288,289</sup> Sizes and assembling behaviours were tuned by varying both the nature of the alkyl chains and PEG/hydrophobic side chain ratio.<sup>288,289</sup> On the other hand, the NPs size observed in this project ranged from *circa* 70 nm to 365 nm, when

above the CAC. Considering these substantial size values and the absence of TEM images (due to the large number of samples and to maintain the concept of HT), to confirm the particles shapes, it has been speculated that the produced NPs are likely to be kinetically trapped nanoaggregates rather than uniform micelles. However, the quality of the nano-objects has been confirmed by plotting both Intensity, Number and Volume distributions of a series of samples (Figure Appendix 3-31 to 3-35). Above the CAC, the three distributions were superimposable with a smooth correlogram, reinforcing the quality of the nanoparticle produced. While, the same samples, when analysed below the calculated CAC showed aggregates and unreliable size distributions (Figure Appendix 3-31 to 3-35).

Thus, whilst the general trends in the data collected were encouraging, it was clear that the correlations to the CAC measured via DLS were not conclusive. For example, three surfactants (iBuA-*co*-mPEGMA<sub>300</sub>, F7BMA-*co*-mPEGMA<sub>300</sub> and HPhOPA-*co*-mPEGMA<sub>300</sub>) appeared to exhibit an overestimation of their CACs when compared to the cLogP values, whereas two (HPhOPA-*co*-mPEGMA<sub>300</sub> and iBuA-*co*-mPEGMA<sub>300</sub>) presented apparent underestimations of the same property. Thus, it was proposed that the hydrophobicity character of the HyB monomers is not the only parameter driving/defining the self-assembling and nano-aggregates stability of these materials.

This conclusion has precedent from similar HT based studies into the definition of the molecular structure characteristics that influence the bioactivity exhibited by these copolymers.<sup>235</sup> These studies demonstrated

that a more complex, computationally derived relationship, defined as the “alpha parameter”, predicted the copolymer behaviour with a much greater degree of accuracy.<sup>184,290</sup> This computational evaluation was conducted by evaluating the contribution of a broad range of structural features, e.g. potential for bond rotation, physical intermolecular interactions between functional groups, pendant group steric bulk etc, to the observed trends in the practical data. Thus, those that might play a key role to understand the complexity of the interactions across these amphiphiles were defined. Thus, a similar computational study was conducted upon this data set to look at the additional factors that may be influencing the CAC behaviour on these copolymers.

### 3.3.5 Predictive Computational Model Development on Surfactants Self-Assembling Properties

In the present study, machine learning analysis was performed by applying a linear multiple regression model using a total number of 20,300 molecular descriptors that considered all of the surfactants possessed the theoretical molar contribution of ~90:10 % mol/mol HyB:mPEGMA<sub>300</sub>. the model performance is summarised in Figure 3.11a and 3.11c.

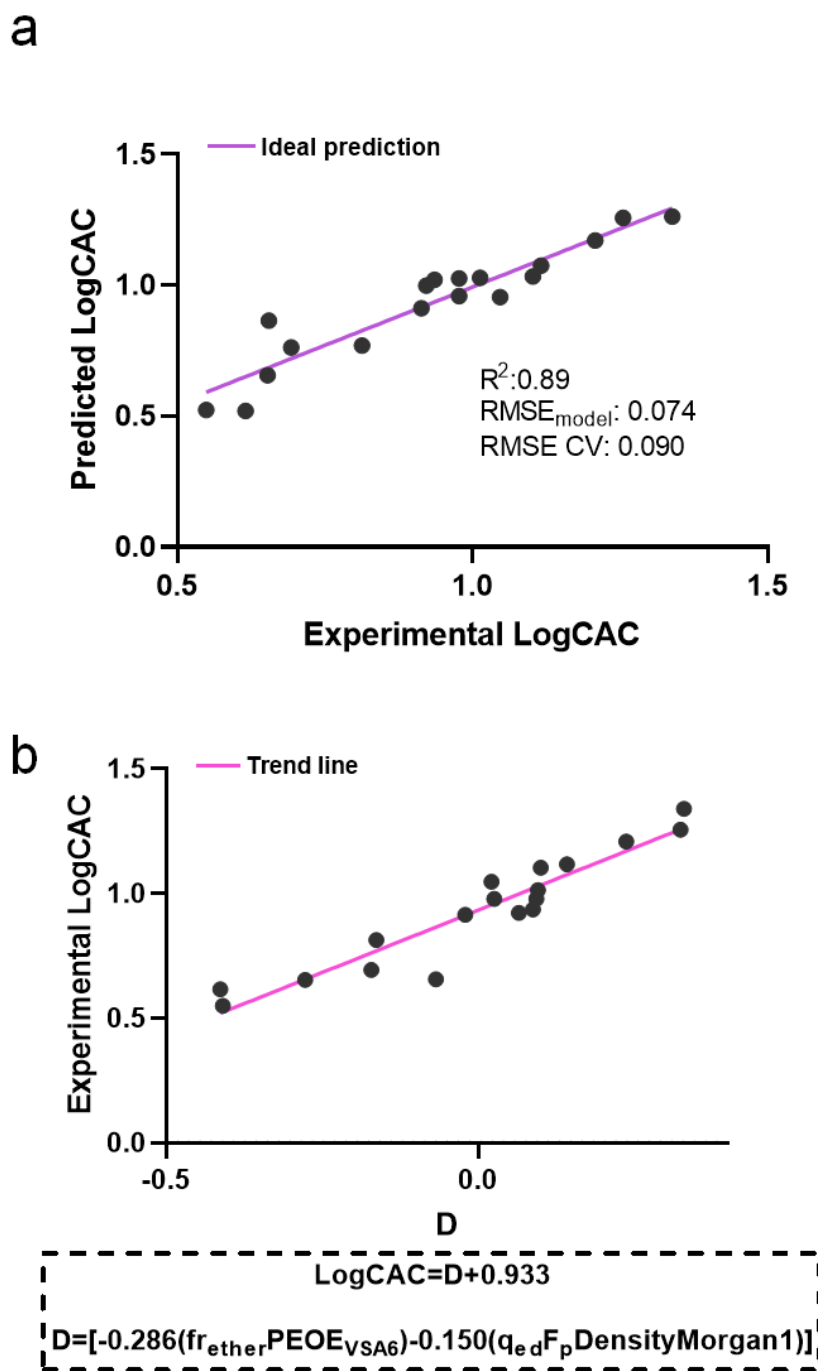


Figure 3.11 a) experimental logCAC values are plotted against the predicted logCAC values, and performance metrics are shown. b) a scatter plot showing how the equation fits the data.

Figure 3.11a contains the results of a modelling exercise conducted using 18 synthesised surfactants, it shows that the best performing model provided a correlation value ( $R^2$ ) of 0.89, a Root Mean Squared Error (RMSE) of 0.074 and a Leave-One-Out Cross-Validation Root Mean Squared Error (LOOCV

RMSE) of 0.090. When compared this new set of data with the  $R^2$  value (0.83) of the direct experimental comparison, depicted in Figure 3.10a, a significant improvement in the fit of the data by using the derived model it was observed. Furthermore, given the LOOCV RMSE value is close to RMSE, it is possible to conclude that the generated computational model is sufficiently robust.

To better understand how well the model performs in terms of a “better-than-random prediction”, the RMSE value has been compared to the standard deviation of the LogCAC value ( $\sigma_{\text{LogCAC}}$ ). This comparison is important in order to establish the quality of the performance of the regression linear model. A bad regression would lead to an RMSE that is equivalent to the standard deviation of LogCAC value. In this study the relationship between these two factors was calculated to be 3.027 (Figure Appendix 3-36). This suggests that the model performs more than 3-fold better than a random model.

The relationship shown in 3.11b is derived the regression model using a linear combination of two factors composed by two physical-chemical descriptors each. The first combined descriptor is  $fr_{ether}PEOE_{VSA6}$  and the second one is  $qedFpDensityMorgan1$ . The original equation generated by the model is shown in Equation 1:

$$\log CAC = -0.286(fr_{ether} * PEOE_{VSA6})0.150(qed * FpDensityMorgan1) + 0.933$$

Equation 3.2 Derived mathematical relationship between LogCAC and the linearly combined descriptors

Consequently, this components of this equation generated by the model can be equated to a linearised relationship (i.e.  $y = mx + c$ ) where:  $m=1$ ;  $x=[-0.286(fr_{ether} * PEO_{VSA6}) - 0.150(qed * FpDensityMorgan1)]$  and  $c = 0.933$ .

These descriptors, shown in the predictive equation above, are poorly/weakly cross correlated. In fact, the  $R^2$  value between the two combined factors ( $qedFpDensityMorgan1$  and  $fr_{ether}PEOE_{VSA6}$ ), is equal to 0.48, whilst the single components of  $qedFpDensityMorgan1$  and  $fr_{ether}PEOE_{VSA6}$ , alone, show an  $R^2$  of 0.01 and 0.05, respectively. The poor correlation is, again, an underlying indication that the prediction performance of the generated model is not affected by feature overlapping or redundancy, thus, its high level of robustness.

In order to give an interpretable molecular meaning to these descriptors, they were associated to tangible physical features/molecular characteristics of the polymer. Examples from literature report define the specific components of the descriptors as follows: a)  $PEOE_{VSA6}$  is a measure of the electrostatic interactions within the molecule,<sup>291</sup> b)  $qed$  quantifies the “drug-likeness” of the molecule,<sup>292</sup> c)  $fr_{ether}$  is the number of ether oxygens in the molecule and d)  $FpDensityMorgan1$  pertains to the influence of steric bulk and the number of heavy atoms present in the structure.<sup>293</sup> In polymer terms this has been hypothesised to relate to a) the potential levels of inter-chain interaction, b) the ability of the HyB monomers to be a hydrogen-bond donator and acceptor, c) the quantity of PEG hydrophile that is in the surfactant and d) the HyB pendant group steric hindrance and molecular mass.<sup>294</sup> Thus, it has been concluded, that the results obtained with this

prediction model are very promising, considering the limited number of materials for which practical results existed. So further expansion of the dataset is planned in order to refine it into a powerful tool for the screening by design of functionalised polymeric surfactants with tuneable self-assembling features.

### 3.4 Conclusions

In this chapter, it was reported for the first time the successful development of a HT pipeline. This was used to design, produce and characterise comb-graft amphiphilic copolymers based on the combination of a library of biologically instructive HyB monomers with the hydrophilic mPEGMA. This was possible thanks to the use in sequence of: a) an automated synthesiser, b) an ink-jet printer, c) a DLS plate-reader and d) a computational study. The strength of applying this HT pipeline successfully demonstrated:

- the conversion of twenty key bioinstructive functional monomers into comb-like graft copolymers suitable for use as a surfactant, at small (1 g) and large (10 g) scale, within a month.
- The development of a novel HT strategy to establish the quality of the surfactants produced at well-plate scale. The CACs obtained were successfully compared with CMCs of common commercially available surfactants (Tween 80, Brij, etc.).
- This data from this property screen was, then, utilised to build a proof-of-concept computational model. This computational model helped to assess the molecular descriptors that identified the four key molecular

drivers that underpin the CAC properties of these types of complexes, comb-graft, architectural polymers.

The development of this HT pipeline might significantly improve the future design of macromolecules used as surfactants. Surfactants are indispensable molecules in many fields. In particular, in the microfluidics the stabilisation of the droplet-interface, delivered by surfactants, allows the fabrication of monodisperse droplets/particles. The possibility of tailoring the specific amphiphilic properties, according to the final application, in a short period of time, can improve the manufacturing process of nano- and microparticles.

### 3.5 Appendix

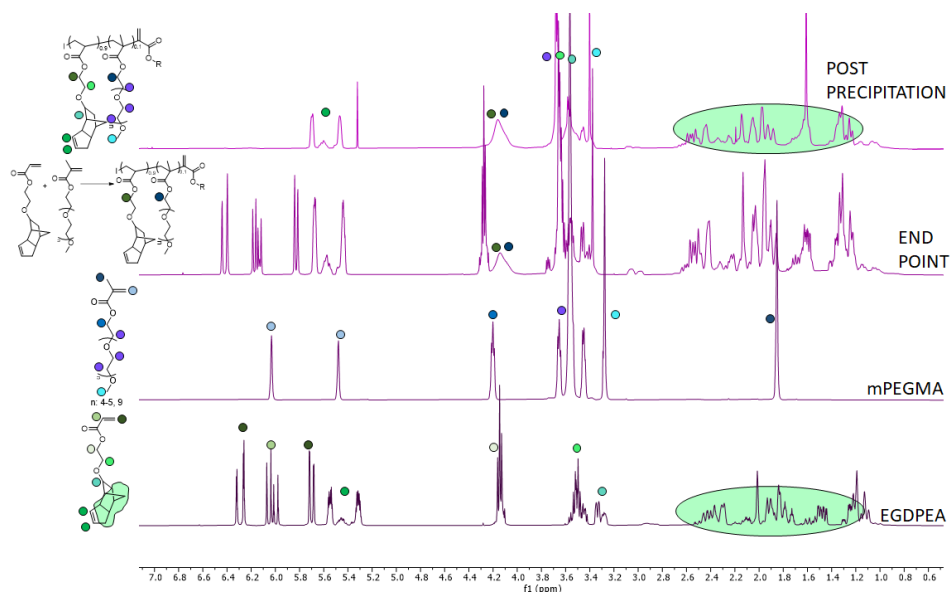


Figure Appendix 3-1 <sup>1</sup>H-NMR of the PEGMA<sub>360</sub>, EGDPEA, end point of the reaction after 18h and the purified copolymer EGDPEA-co-PEGMA<sub>360</sub>, respectively.

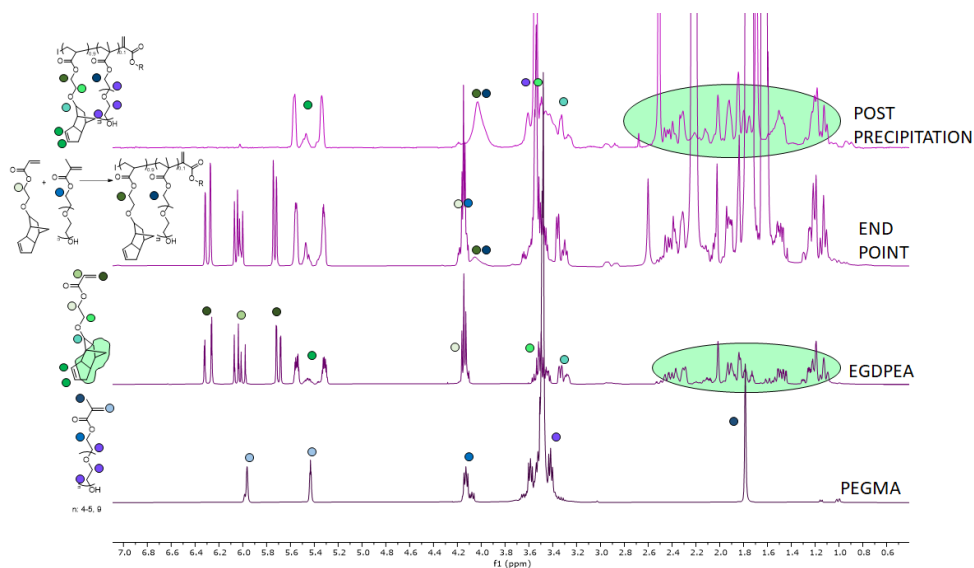


Figure Appendix 3-2 <sup>1</sup>H-NMR of the EGDPEA, mPEGMA<sub>300</sub> end point of the reaction after 18h and the purified copolymer EGDPEA-co-mPEGMA<sub>300</sub>, respectively.

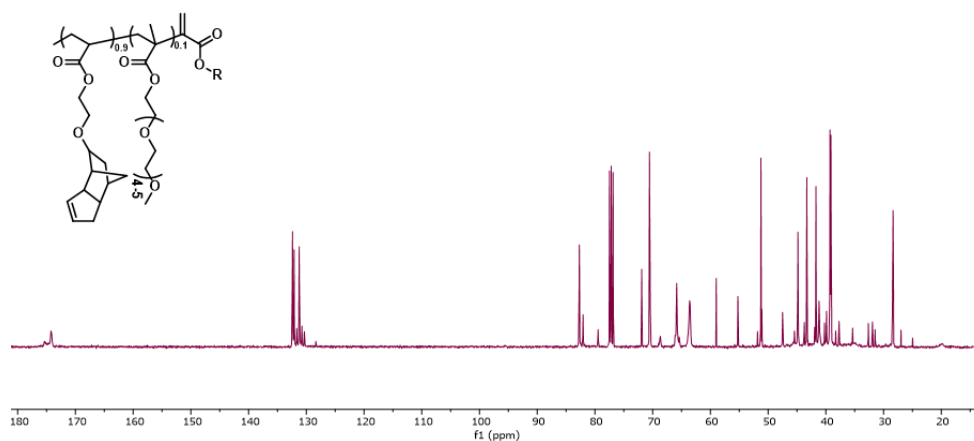


Figure Appendix 3-3 <sup>13</sup>C-NMR of the purified EGDPEA-co-mPEGMA

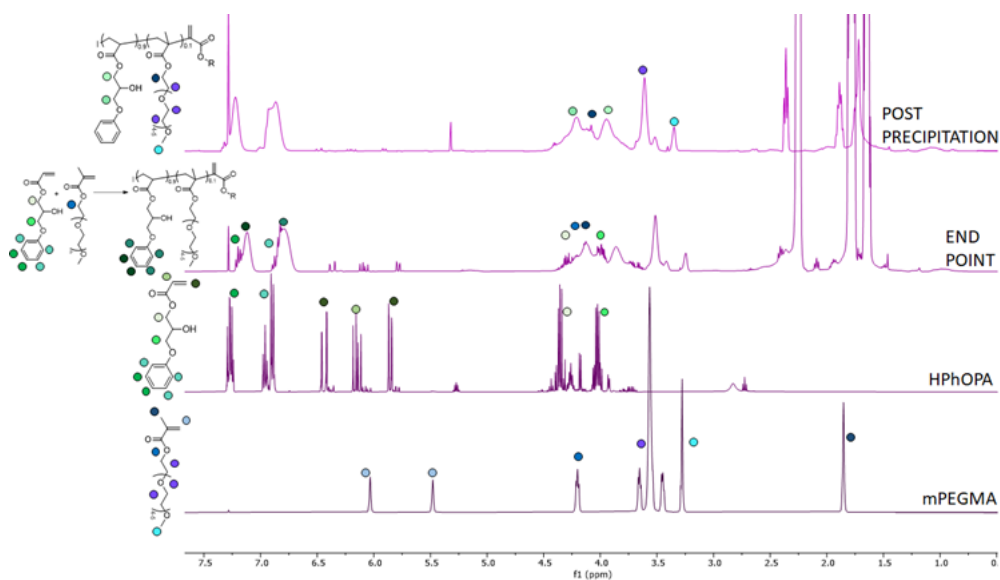


Figure Appendix 3-4 <sup>1</sup>H-NMR of the mPEGMA<sub>300</sub>, HPhOPA, end point of the reaction after 18h and the purified copolymer HPhOPA-co-mPEGMA<sub>300</sub>, respectively.

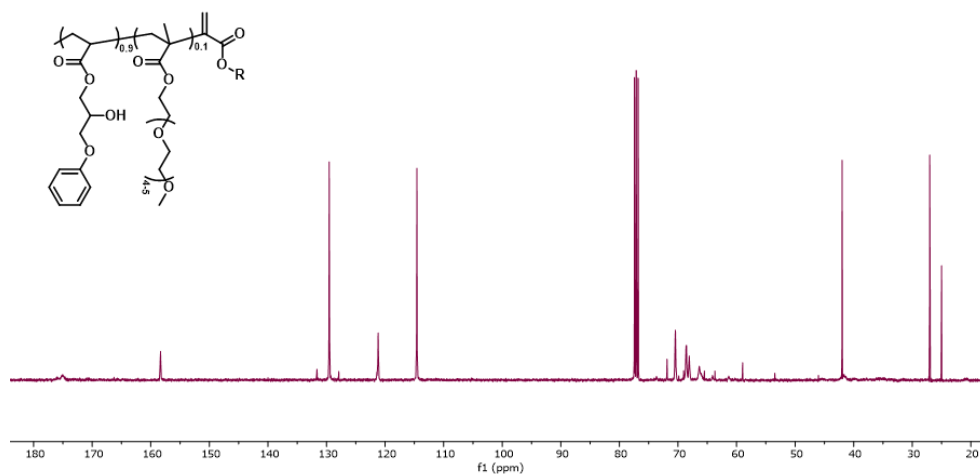


Figure Appendix 3-5 <sup>13</sup>C-NMR of the purified HPhOPA-co-mPEGMA

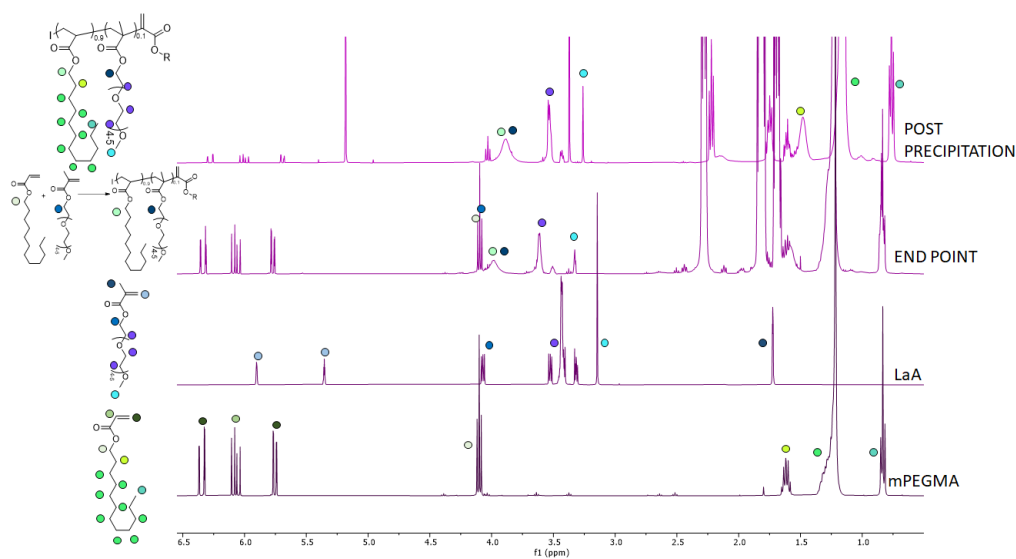


Figure Appendix 3-6 <sup>1</sup>H-NMR of the mPEGMA<sub>300</sub>, LaA, end point of the reaction after 18h and the purified copolymer LaA-co-mPEGMA<sub>300</sub>, respectively.

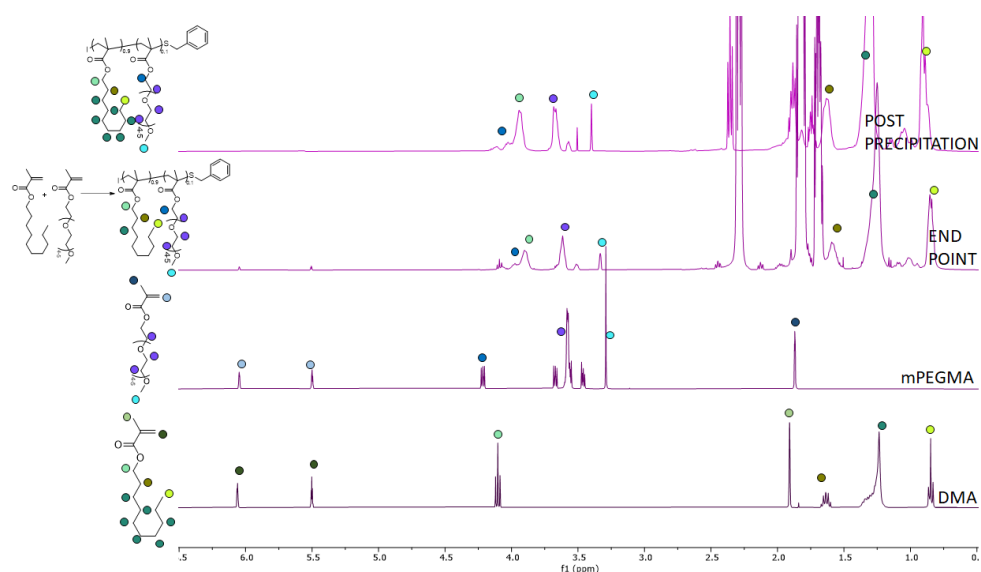


Figure Appendix 3-7 <sup>1</sup>H-NMR of the DMA, mPEGMA<sub>300</sub>, end point of the reaction after 18h and the purified copolymer DMA-co-mPEGMA<sub>300</sub>, respectively.

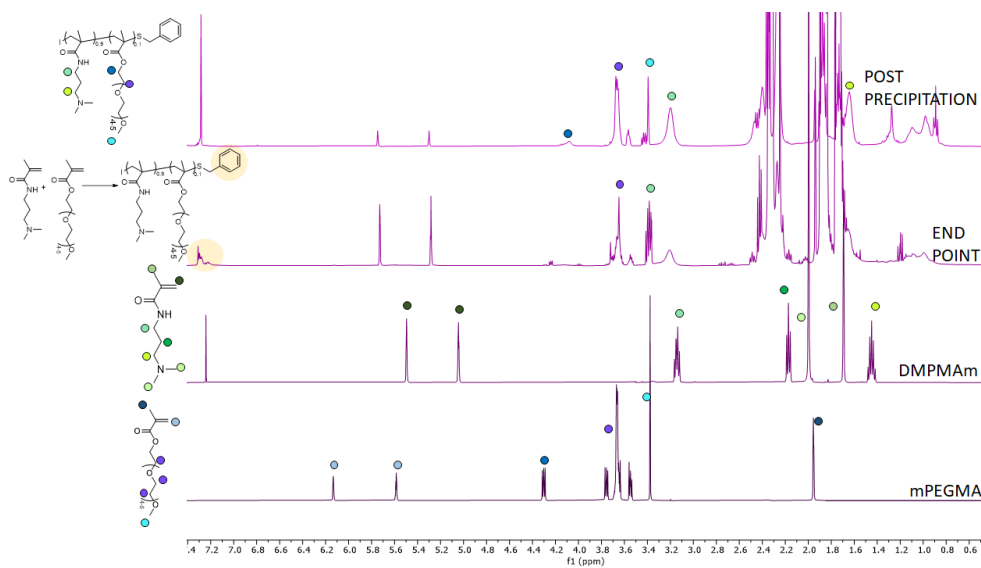


Figure Appendix 3-8 <sup>1</sup>H-NMR of the mPEGMA<sub>300</sub>, DMPMAm, end point of the reaction after 18h and the purified copolymer DMPMAm-co-mPEGMA<sub>300</sub>, respectively.

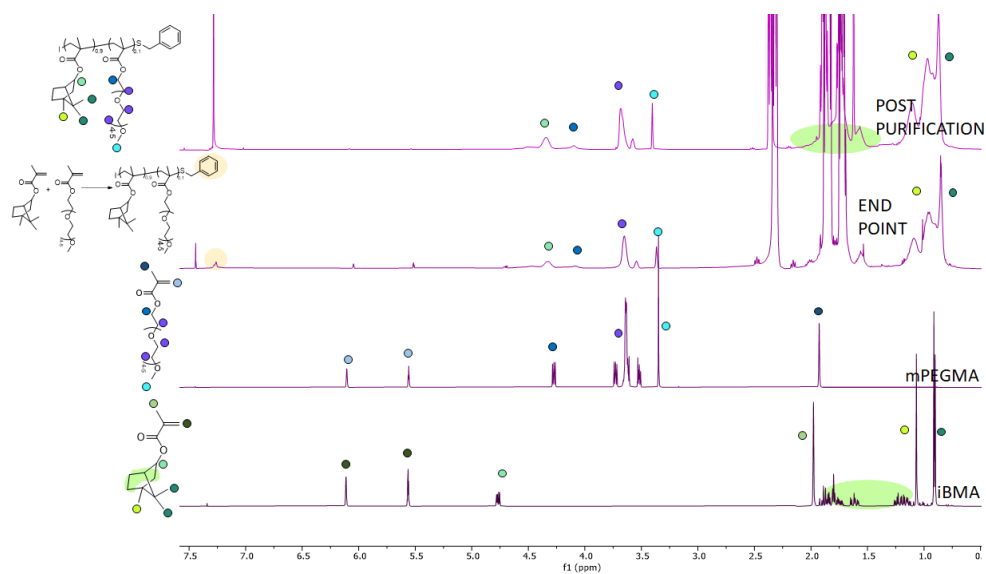


Figure Appendix 3-9 <sup>1</sup>H-NMR of the iBMA, mPEGMA<sub>300</sub>, end point of the reaction after 18h and the purified copolymer iBMA-co-mPEGMA<sub>300</sub>, respectively.

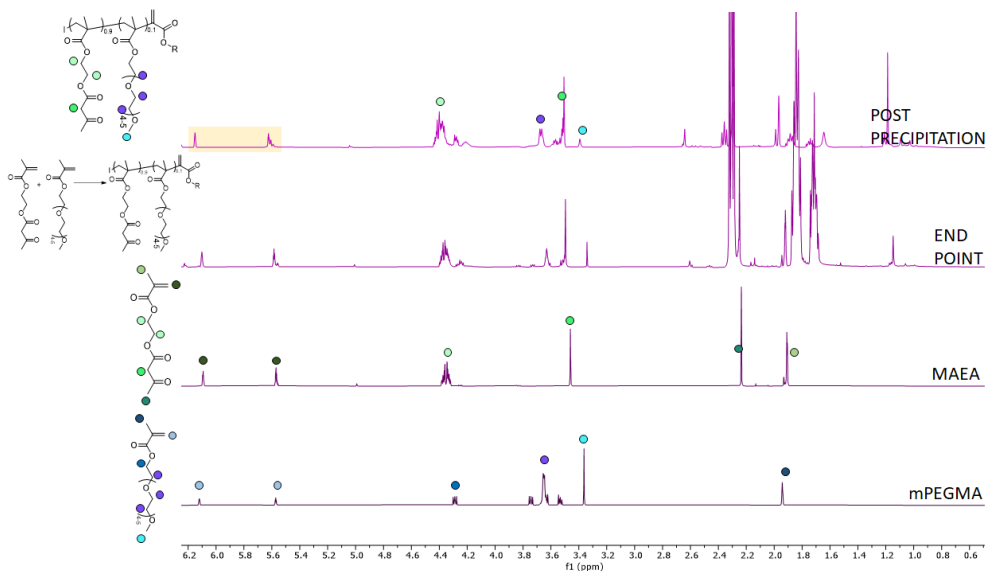


Figure Appendix 3-10 <sup>1</sup>H-NMR of the mPEGMA<sub>300</sub>, MAEA, end point of the reaction after 18h and the purified copolymer MAEA-co-mPEGMA<sub>300</sub>, respectively.

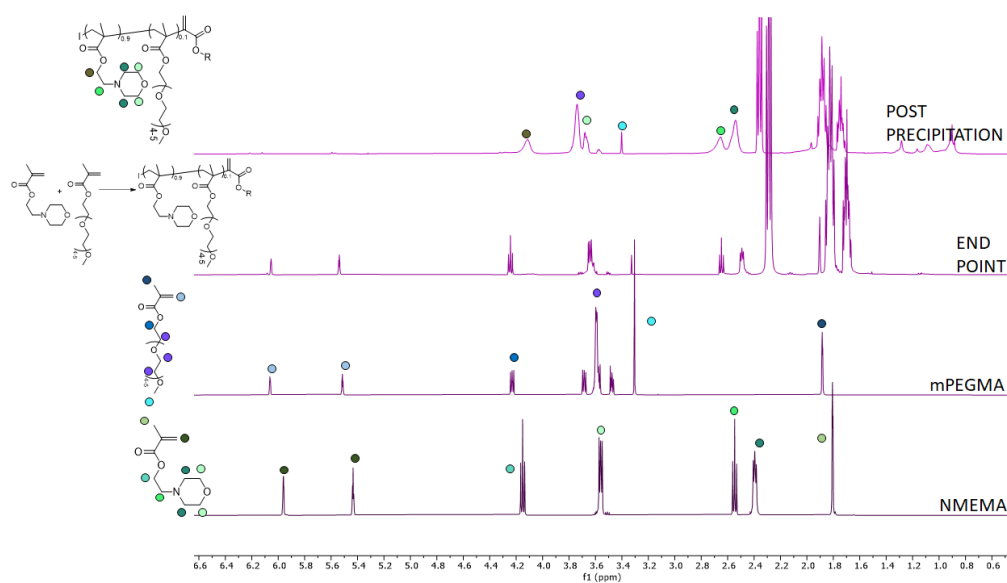


Figure Appendix 3-11  $^1\text{H-NMR}$  of the NMEMA, mPEGMA<sub>300</sub>, end point of the reaction after 18h and the purified copolymer NMEMA-co-mPEGMA<sub>300</sub>, respectively.

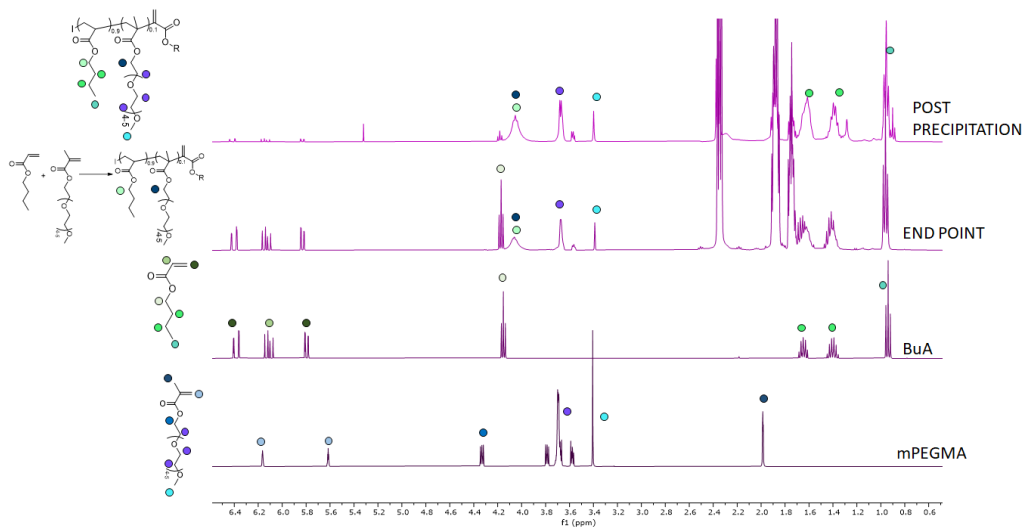


Figure Appendix 3-12  $^1\text{H-NMR}$  of the mPEGMA<sub>300</sub>, BuA, end point of the reaction after 18h and the purified copolymer BuA-co-mPEGMA<sub>300</sub>, respectively.

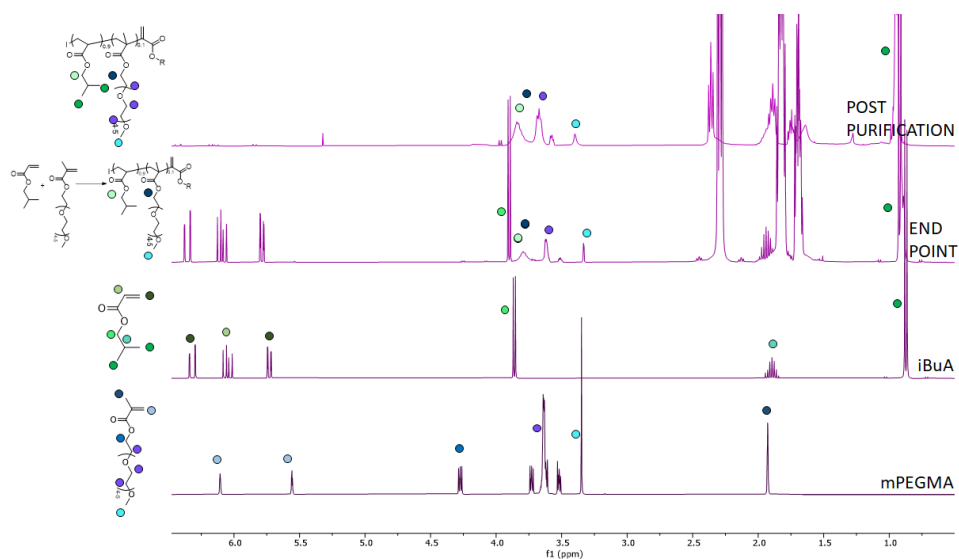


Figure Appendix 3-13  $^1\text{H-NMR}$  of the  $m\text{PEGMA}_{300}$ ,  $i\text{BuA}$ , end point of the reaction after 18h and the purified copolymer  $i\text{BuA-co-}m\text{PEGMA}_{300}$ , respectively.

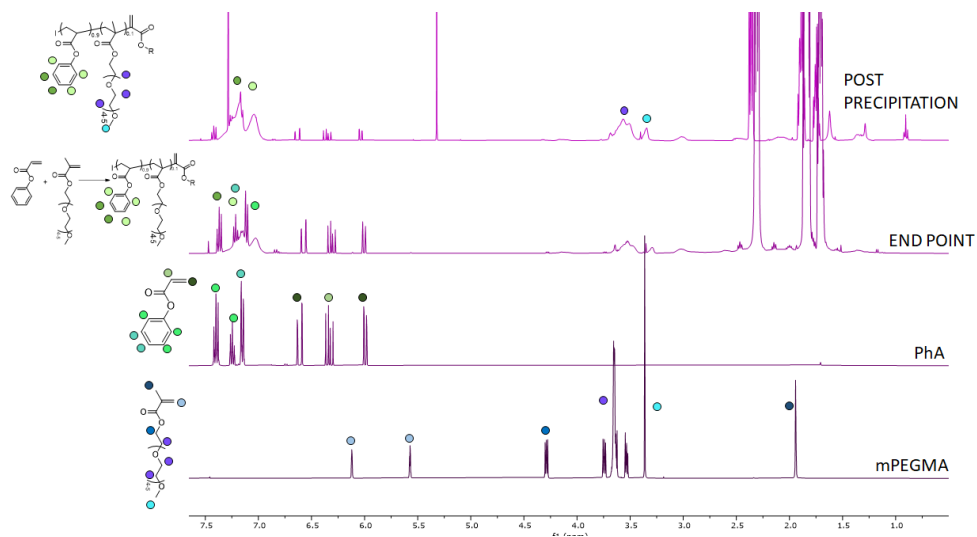


Figure Appendix 3-14  $^1\text{H-NMR}$  of the  $m\text{PEGMA}_{300}$ ,  $\text{PhA}$ , end point of the reaction after 18h and the purified copolymer  $\text{PhA-co-}m\text{PEGMA}_{300}$ , respectively.

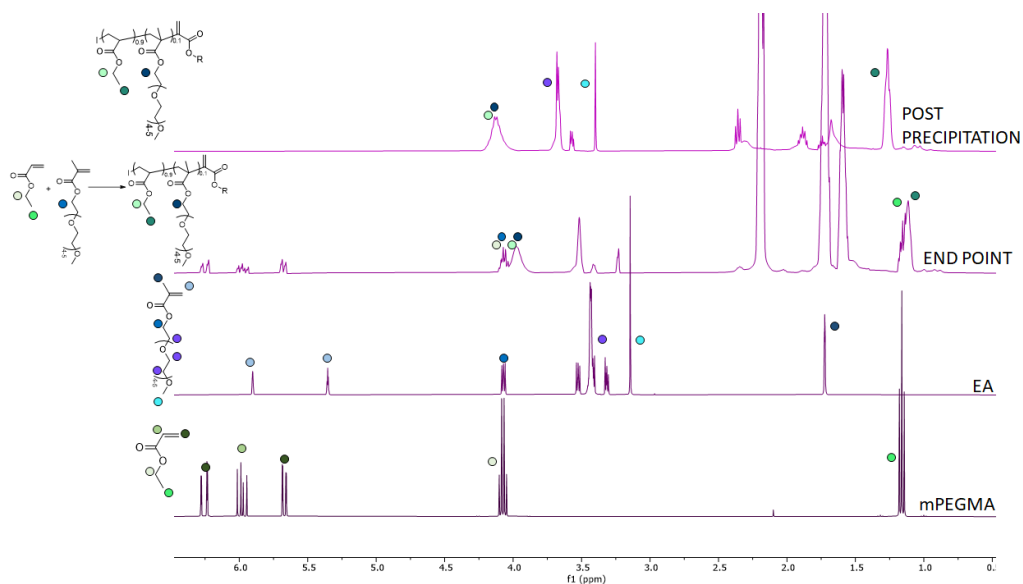


Figure Appendix 3-15 <sup>1</sup>H-NMR of the mPEGMA<sub>300</sub>, EA, end point of the reaction after 18h and the purified copolymer EA-co-mPEGMA<sub>300</sub>, respectively.

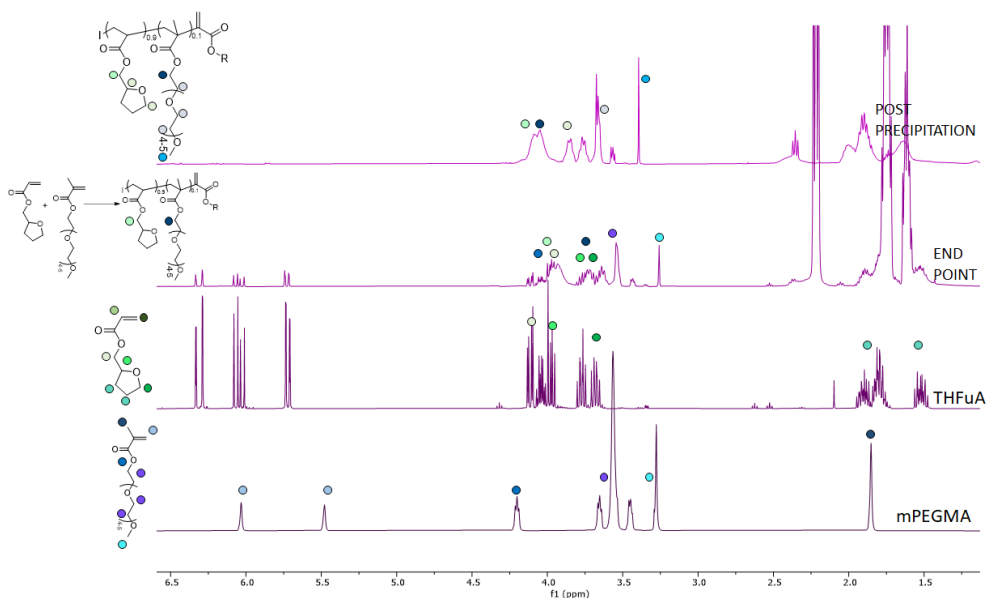


Figure Appendix 3-16 <sup>1</sup>H-NMR of the mPEGMA<sub>300</sub>, THFuA, end point of the reaction after 18h and the purified copolymer THFuA-co-mPEGMA<sub>300</sub>, respectively.

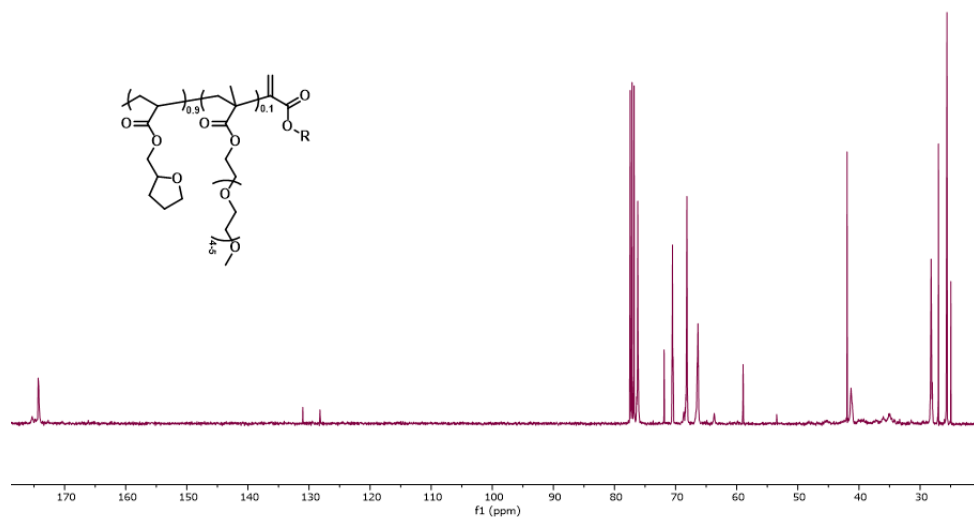


Figure Appendix 3-17  $^{13}\text{C}$ -NMR of the purified THFuA-co-mPEGMA

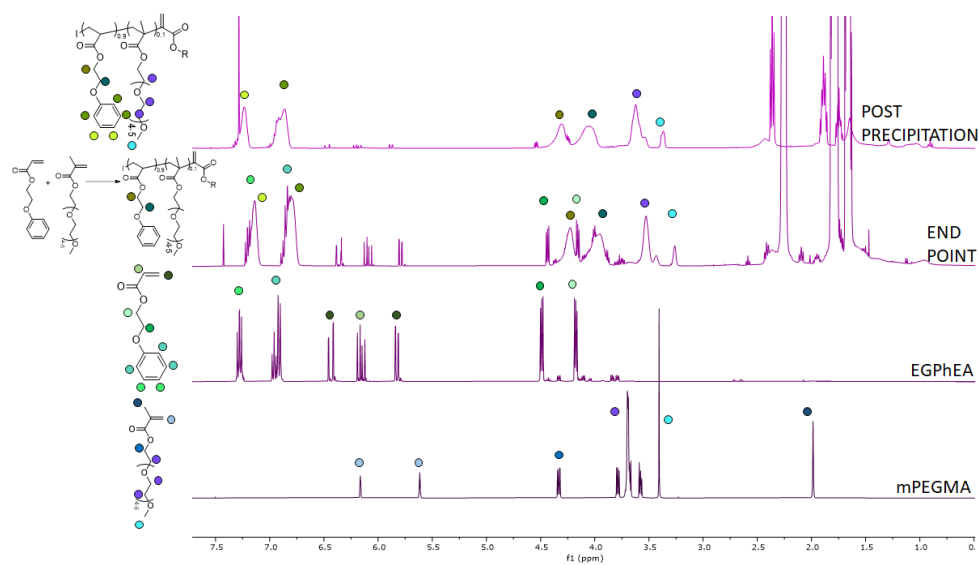


Figure Appendix 3-18  $^1\text{H}$ -NMR of the mPEGMA<sub>300</sub>, EGPhEA, end point of the reaction after 18h and the purified copolymer EGPhEA-co-mPEGMA<sub>300</sub>, respectively.

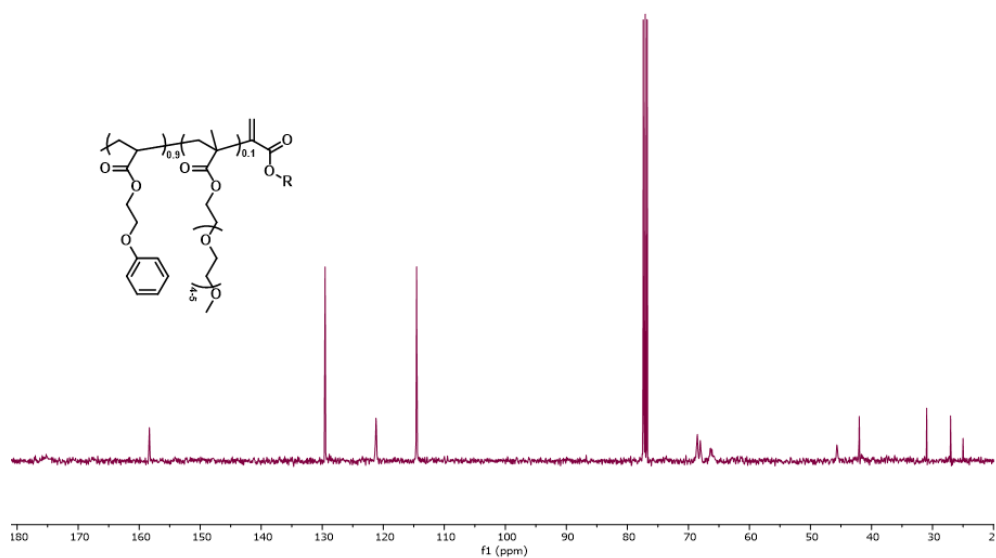


Figure Appendix 3-19  $^{13}\text{C}$ -NMR of the purified EGPhEA-co-mPEGMA

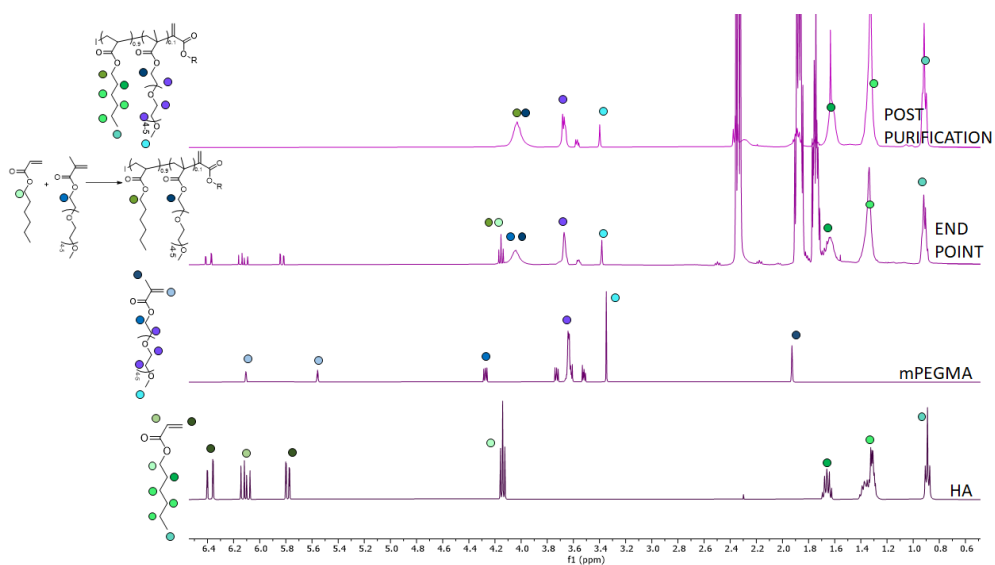


Figure Appendix 3-20  $^1\text{H}$ -NMR of the HA, mPEGMA<sub>300</sub>, end point of the reaction after 18h and the purify copolymer HA-co-mPEGMA<sub>300</sub>, respectively.

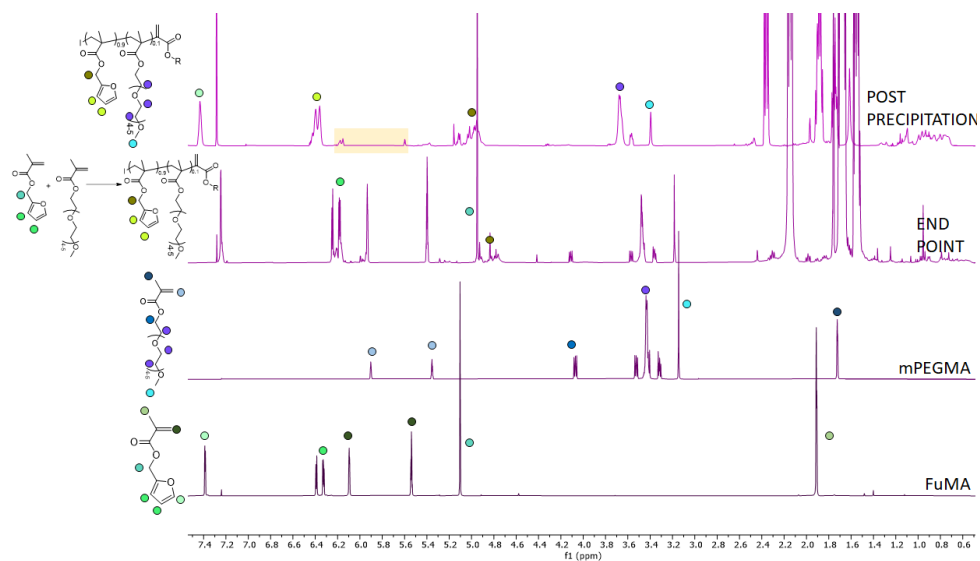


Figure Appendix 3-21 <sup>1</sup>H-NMR of the FuMA, mPEGMA<sub>300</sub>, end point of the reaction after 18h and the purify copolymer FuMA-co-mPEGMA<sub>300</sub>, respectively.

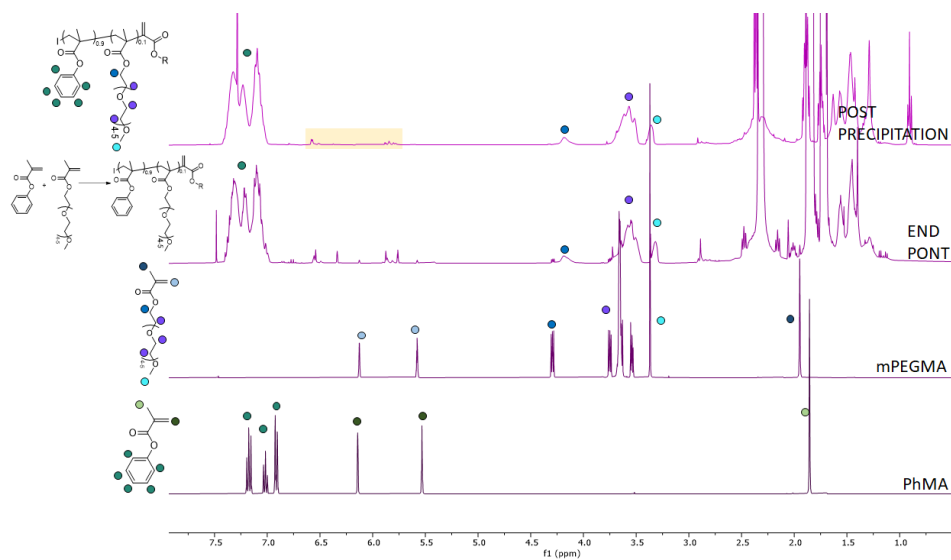


Figure Appendix 3-22 <sup>1</sup>H-NMR of the PhMA, mPEGMA<sub>300</sub>, end point of the reaction after 18h and the purify copolymer PhMA-co-mPEGMA<sub>300</sub>, respectively.

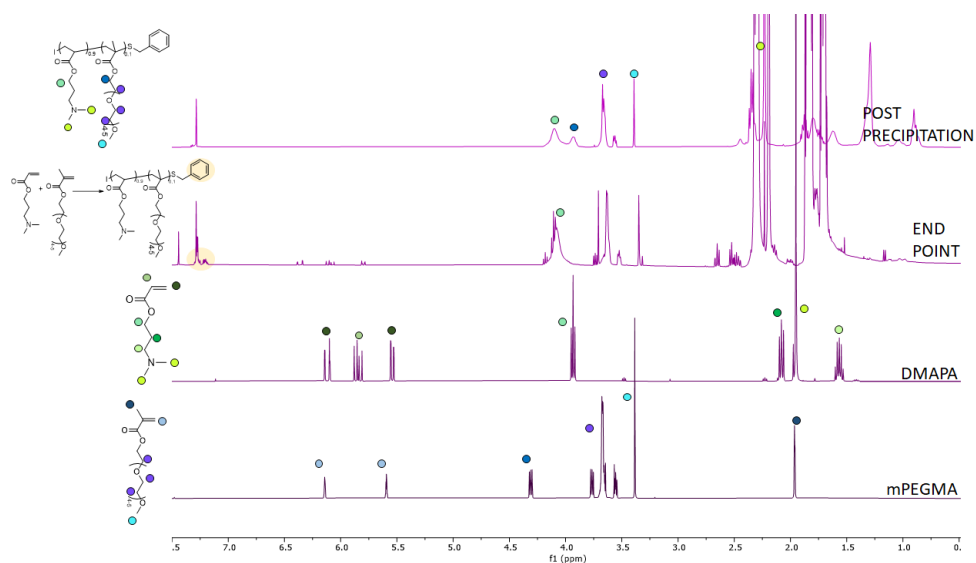


Figure Appendix 3-23 <sup>1</sup>H-NMR of the mPEGMA<sub>300</sub>, DMAPA, end point of the reaction after 18h and the purify copolymer DMAPA-co-mPEGMA<sub>300</sub> respectively.

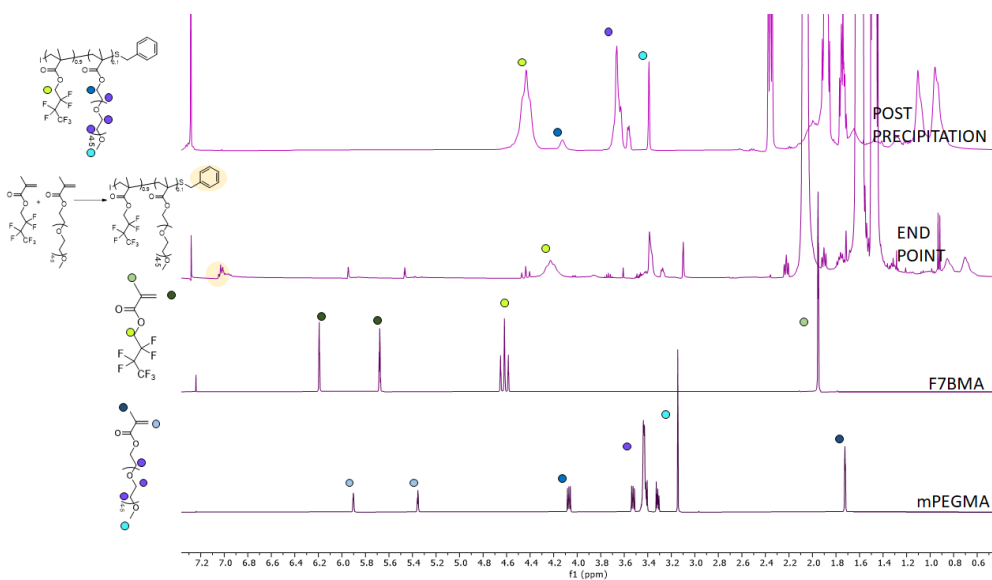


Figure Appendix 3-24 <sup>1</sup>H-NMR of the F7BMA mPEGMA<sub>300</sub>, end point of the reaction after 18h and the purify copolymer F7BMA-co-mPEGMA<sub>300</sub>, respectively.

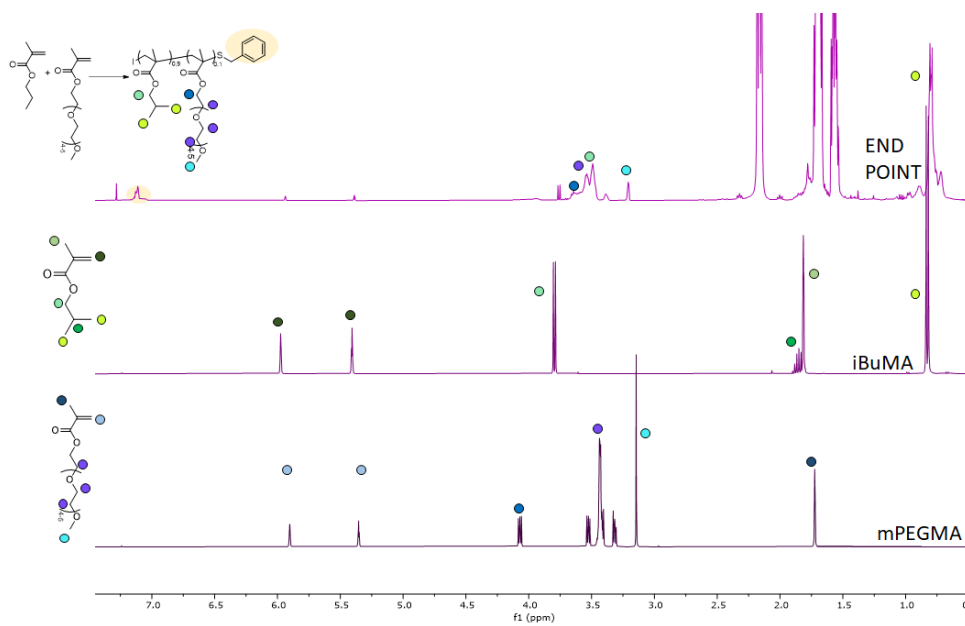


Figure Appendix 3-25 <sup>1</sup>H-NMR of the mPEGMA<sub>300</sub>, iBuMA and end point of the reaction after 18h, respectively.

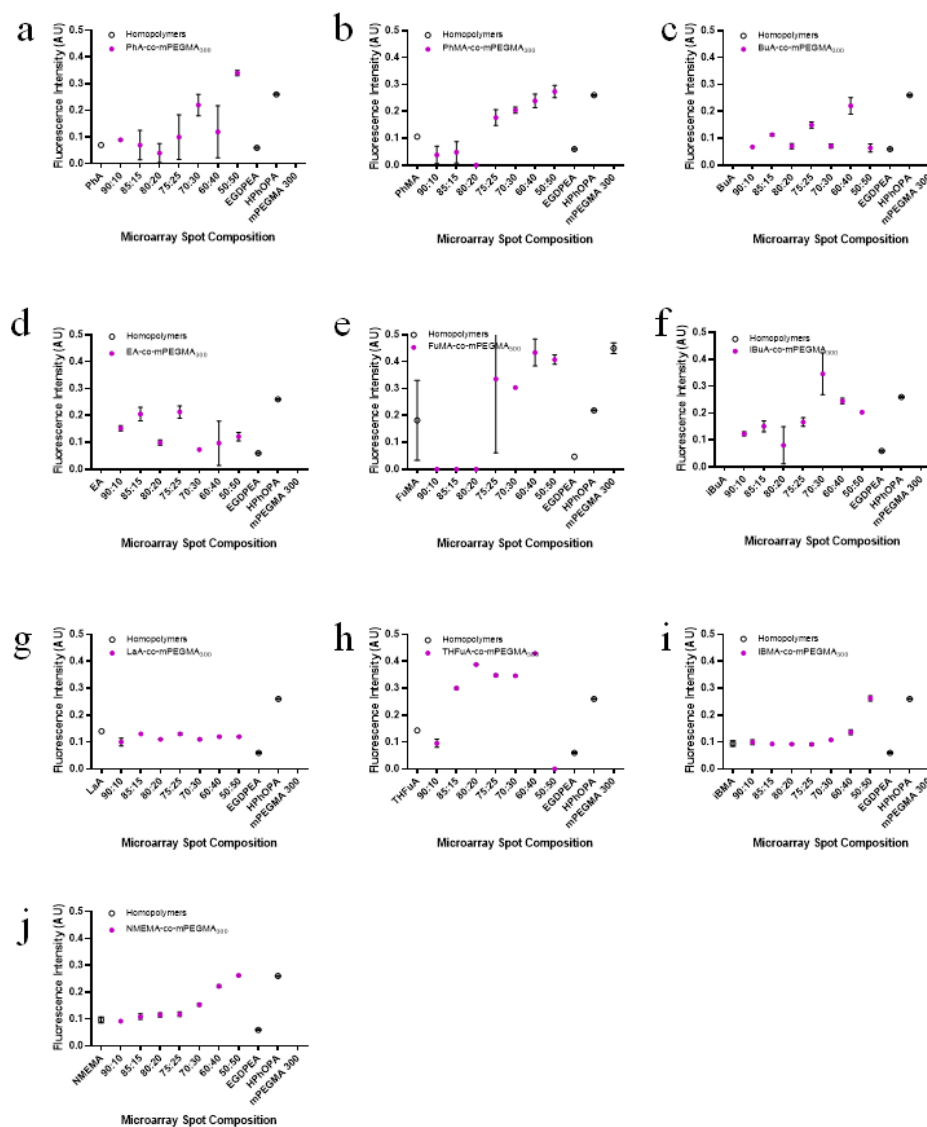


Figure Appendix 3-26 Data showing the attachment of *P. aeruginosa* to copolymers including mPEGMA<sub>300</sub> and (a) phenyl acrylate (PhA) (b) Phenyl methacrylate (PhMA) (c) Butyl acrylate (BuA) (d) Ethyl acrylate (EA) (e) Furfuryl methacrylate (FuMA) (f) Isobutyl acrylate (iBuA) (g) Lauryl acrylate (LaA) (h) Tetrahydrofurfuryl acrylate (ThFuA) (i) Isobornyl metacrylate and (j) 2-N-morpholinoethyl methacrylate (NMEMA). Data points are averaged across  $n = 6$ ,  $N = 2$  data points and the standard deviation plotted as the error.

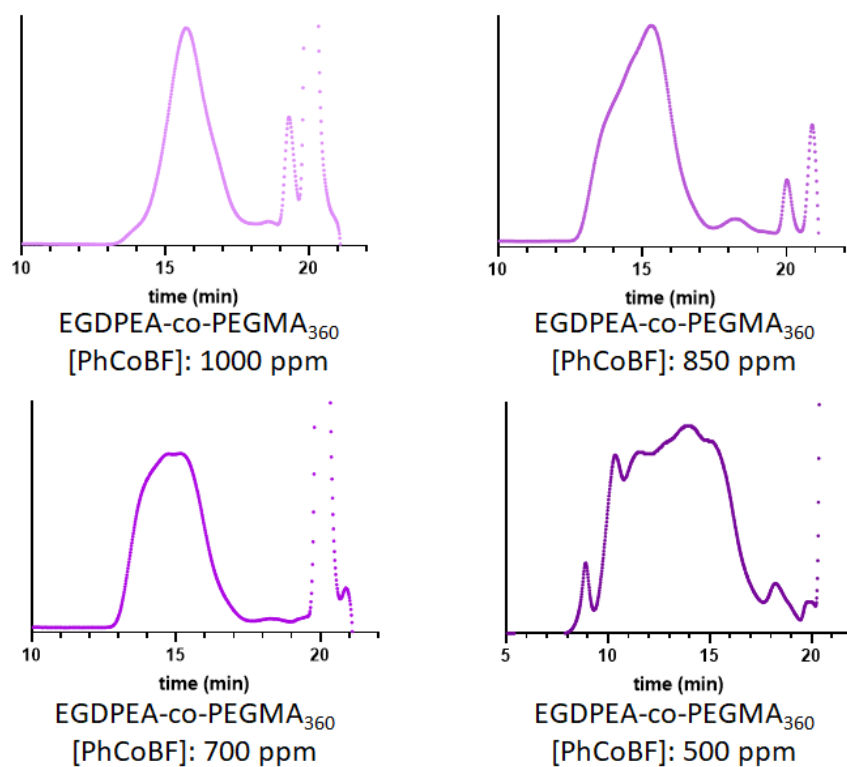


Figure Appendix 3-27 GPC chromatogram of the series of the copolymers EGDPEA-co-PEGMA<sub>360</sub> obtained via CCTP using the follow PhCoBF concentration: 1000ppm, 850 ppm, 700 ppm and 500 ppm.

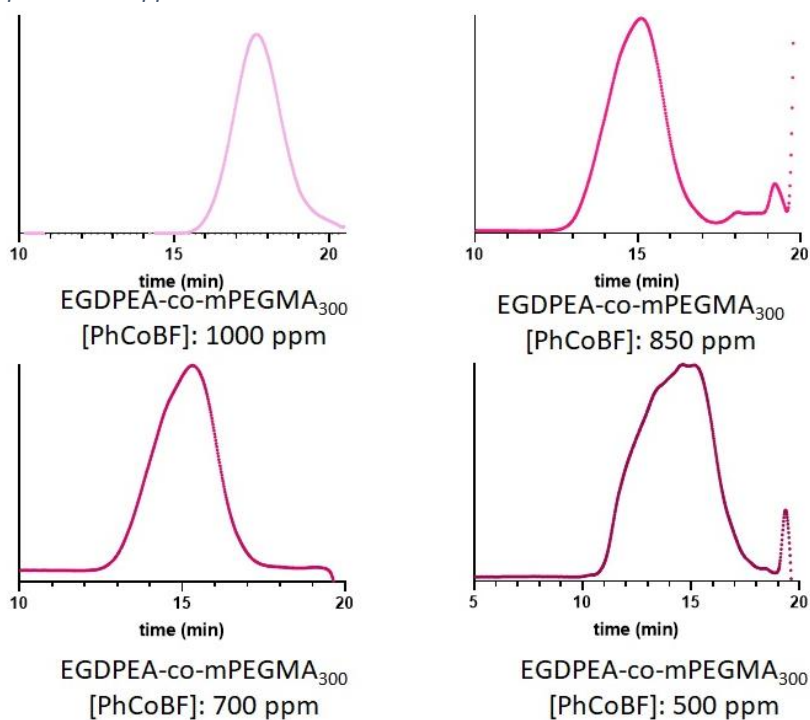


Figure Appendix 3-28 GPC traces of the series of the copolymers EGDPEA-co-mPEGMA<sub>300</sub> obtained via CCTP using the follow PhCoBF concentration: 1000ppm, 850 ppm, 700 ppm and 500 ppm.

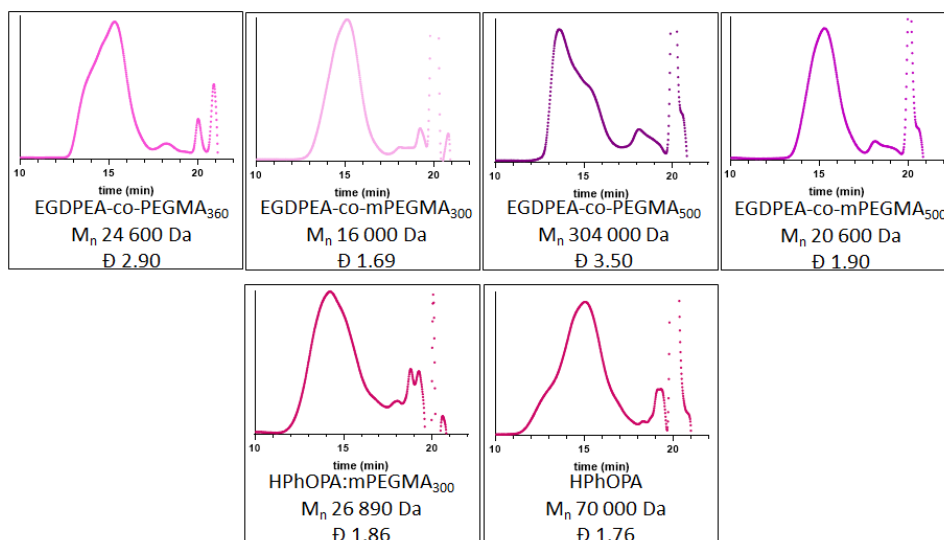


Figure Appendix 3-29 GPC traces of the series of copolymers synthesised via CCTP using the fixed amount of PhCoBF of 850 ppm and a molar ratio of 90:10 % mol/mol. The copolymers presented are: EGDPEA-co-mPEGMA<sub>300/500</sub>, EGDPEA-co-PEGMA<sub>360/500</sub>, HPhOPA-co-mPEGMA<sub>300</sub> and homopolymer HPhOPA

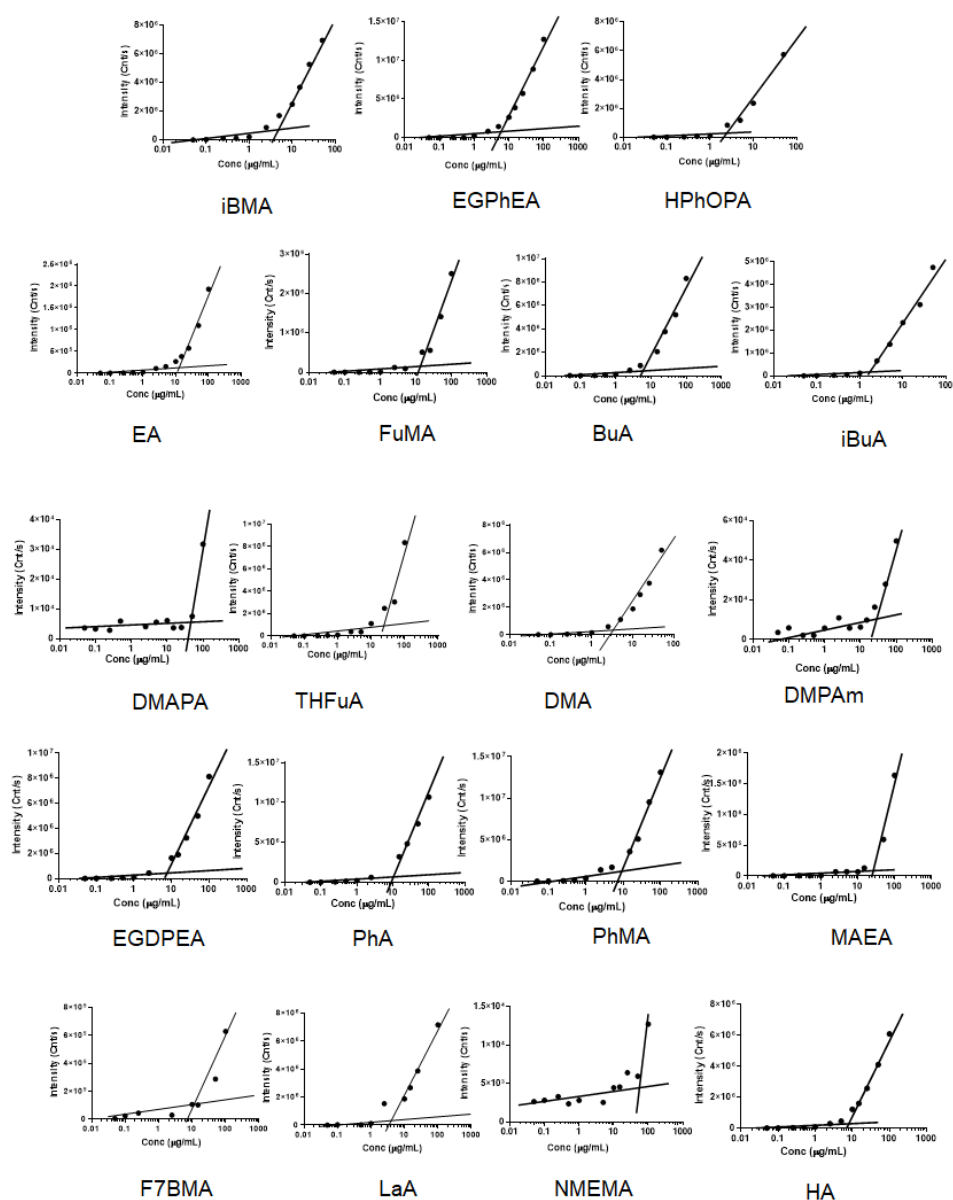


Figure Appendix 3-30 CAC of the 19 surfactants polymerised with  $m\text{PEGMA}_{300}$  ( $\text{HyB-co-}m\text{PEGMA}_{300}$ ). The plots of the intensity of scattered light (kilo counts per second) as a function of concentration ( $\mu\text{g/mL}$ ). The data showed that the scattering detected for the surfactant concentrations below the CAC is similar to deionised water. After the CAC was reached, the scattering intensity shows a linear increase with concentration.

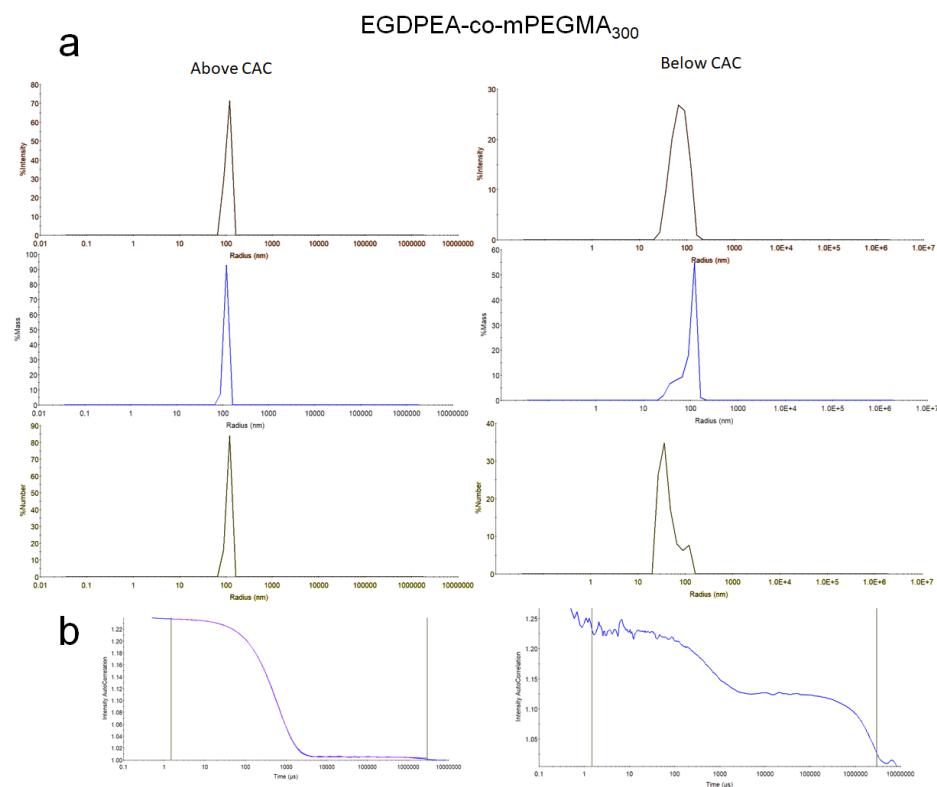


Figure Appendix 3-31 a) Sizes (nm) shown as Intensity, Mass and Number for the copolymers alone: EGDPEA-co-mPEGMA<sub>300</sub>. b) Correlograms related to the signal decay of the sample below and above the CAC.

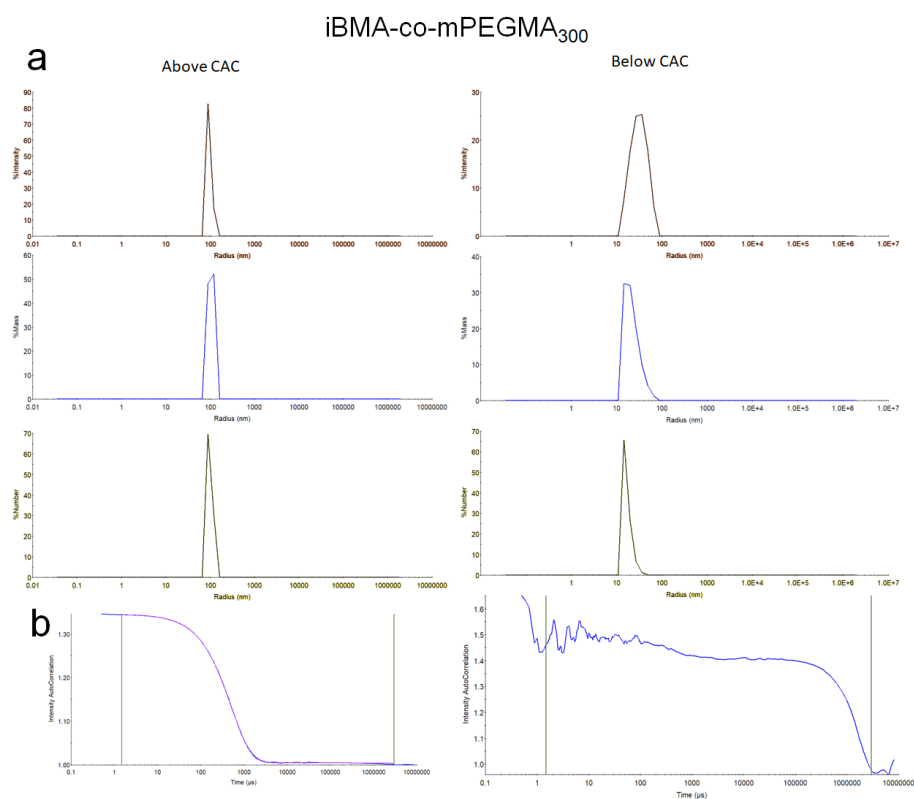


Figure Appendix 3-32 a) Sizes (nm) shown as Intensity, Mass and Number for the copolymers alone: iBMA-co-mPEGMA<sub>300</sub>. b) Correlograms related to the signal decay of the sample below and above the CAC.

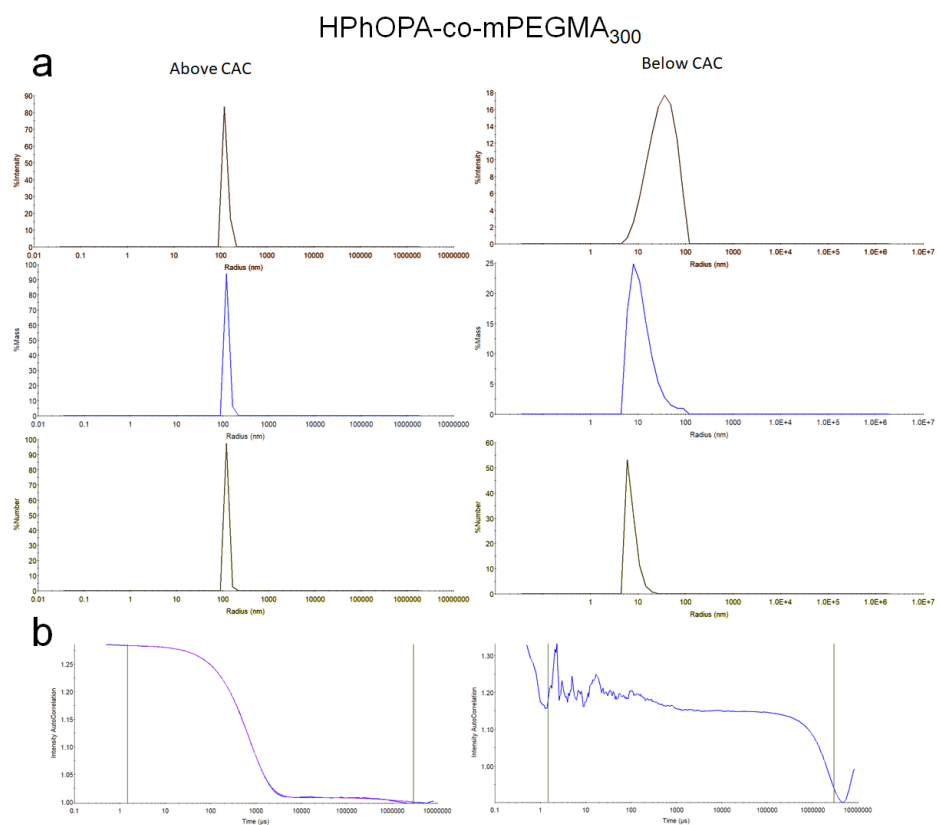


Figure Appendix 3-33 a) Sizes (nm) shown as Intensity, Mass and Number for the copolymers alone: HPhOPA-co-mPEGMA<sub>300</sub>. b) Correlograms related to the signal decay of the sample below and above the CAC.

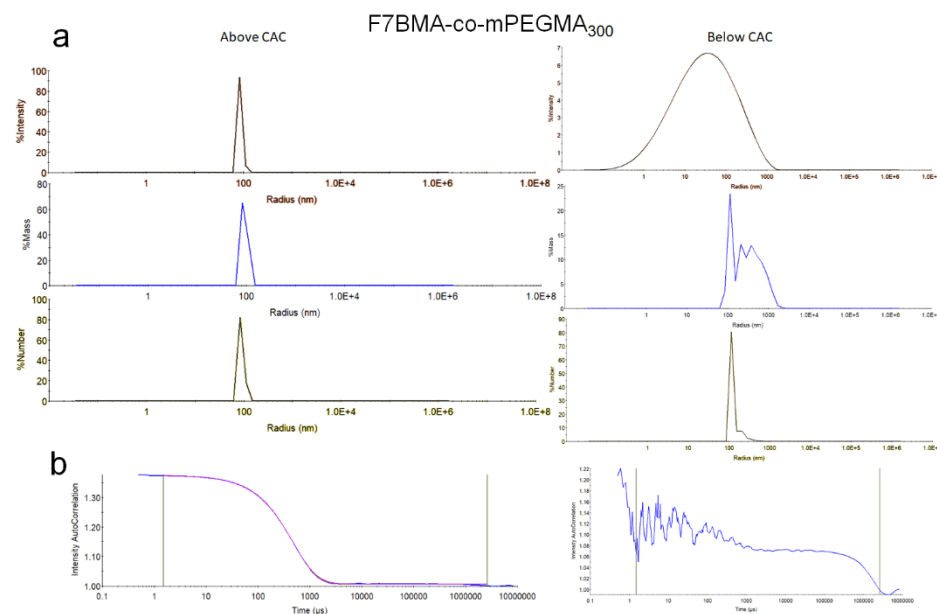


Figure Appendix 3-34 a) Sizes (nm) shown as Intensity, Mass and Number for the copolymers alone: F7BMA-co-mPEGMA<sub>300</sub>. b) Correlograms related to the signal decay of the sample below and above the CAC.

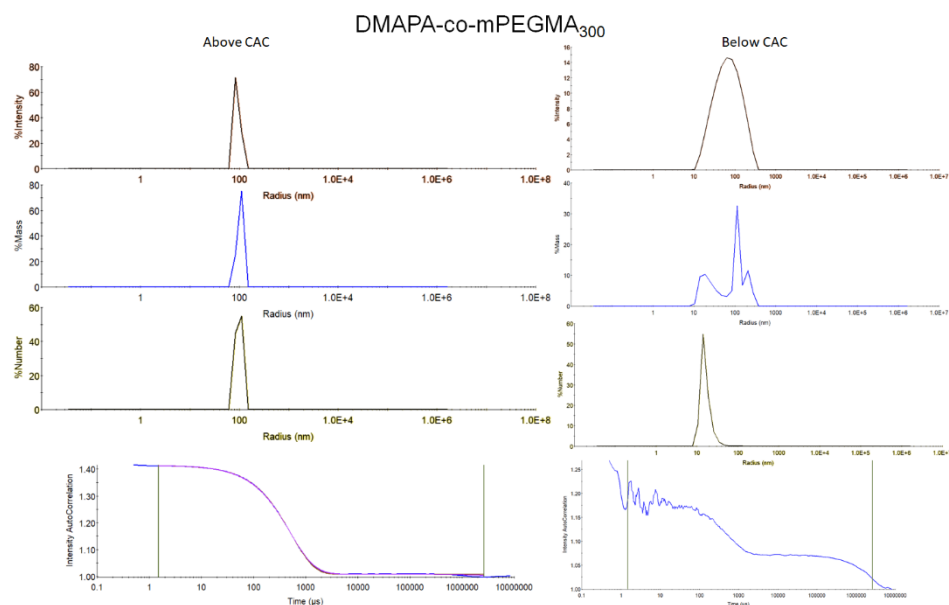


Figure Appendix 3-35 a) Sizes (nm) shown as Intensity, Mass and Number for the copolymers alone: DMAPA-co-mPEGMA<sub>300</sub>. b) Correlograms related to the signal decay of the sample below and above the CAC.

$$\frac{\sigma_{\log CAC}}{RMSE_{model}} = \frac{0.233}{0.074} = 3.027$$

Figure Appendix 3-36 Relationship between the standard deviation of the LogCAC ( $\sigma_{\log CAC}$ ) and the  $RMSE_{model}$

## 4 Fabrication of Microparticles *via* Droplets Microfluidics Processing and their Biological Applications

### 4.1 Introduction

This chapter presents the development and production of a microparticles (MPs) library using a droplet-based microfluidics technology for a manufacturing process. The aim of this work is to exploit the functionalised active surfactants, synthesised and characterised in Chapter 3, to obtain monodispersed MPs with targeted surface chemistries. These targeted functionalities, that are desirable for controlling different biological responses, were built into the surfactants molecular design. The rationale behind the production of these biological functionalised structures is related to the crucial need to develop three dimensional (3D) platforms that can offer an alternative to the biological outcomes that were exhibited by the well-established 2D systems in the screening of biomaterials during *in vitro* tests.<sup>295</sup> This is necessary because, as mentioned in the Introduction, 2D cell culture *in vitro* tests of biomaterials have been shown to be non-representative of their performance when translated in the 3D cell environments, such as the human body.<sup>139,296</sup> 3D models can better mimic *in vivo* cellular behaviour providing more physiologically relevant information on cell growth and responses to a variety of chemical, physical, and immunological stimuli.<sup>297–299</sup> In this regard, the biomedical industry is one of the most relevant field that requires breakthrough in 3D technologies

to fill possible gaps between *in silico* hypotheses/*in vitro* results and the *in vivo* settings. Although high-throughput (HT) technologies offer the possibility to screen large amounts of potential candidate materials, the research and development of physiologically relevant compounds still require *in vivo* test to be completing before progressing towards clinical studies. In this respect, in addition to raising ethical concerns, animal studies can be burdensome with regard time and costs and do not always reproduce human diseases. Thus, alternative or at least complementary pre-clinical tools are needed.<sup>300</sup> This study proposed that MPs can be used as potential 3D microsystems in order to gain deeper understanding of the interactions between materials and biological system at the cellular level with potential effects on target cells.<sup>53</sup> This is made possible due to the high versatility of these structures which allow to tune size, shape and surface functionalisation/topography, all key factors that affect cells behaviour.<sup>301</sup> However, the most common techniques to synthesise MPs with target properties depend on the complex concept of phase separation, and as such are based on the emulsion, dispersion and suspension processes.<sup>302,303</sup> Common problems with the use of these techniques include the use of high amount of solvents, batch-to-batch reproducibility, difficult control in the size/size dispersity and the inclusion of unwanted surfactants which interfere with the surface chemistry.<sup>302</sup> Thus, new approaches are required to produce particles where the process of preparation does not negatively influence the surface chemistry and can be reliably scaled-up or scaled-out in terms of reproducibility and size dispersity. As introduced in Chapter 1,

microfluidics has been attracting more attention as robust and HT alternative for the synthesis of functionalised MPs.

The novel microfluidic approach, proposed in this thesis, allowed the investigation into the development of bio-instructive proof-of-concept 3D platforms with the aid of the aforementioned functionalised surfactants. To demonstrate their ability of interacting a biological environment, subsets of these MPs were used for two biological studies. The first was aimed toward preventing bacterial biofilm formation and the second to enhance fibroblast attachment and proliferation.

Bacterial biofilm is one of the main causes of healthcare-associated infections which are widely recognised as the most frequent adverse events/outcomes in hospitals.<sup>304-306</sup> According to the US National Institutes of Health, biofilms are responsible for more than 80% of microbial infections and more than 60% of all nosocomial infections.<sup>307,308</sup> The US Centres for Disease Control and Prevention has estimated that biofilms is the etiologic agent in 60% of all chronic infections (programme announcements [PA-03-047](#) and [PA-06-537](#)). Individuals at risk of developing biofilm-related infections include those using medical implants/medical devices, and immunocompromised patients, such as those with cystic fibrosis and diabetic neuropathy. In the United States, the annual incidence of biofilm-related infections has been judged to be around 1.96 million cases, causing an estimated of 268,000 deaths, and resulting in a \$US 18 billion in direct costs spend on the treatment of these infections.<sup>309,310</sup> Most strategies for reducing biofilm-associated infections focus on two main approaches: a) the

---

modification of existing materials by the incorporation of antimicrobial agents (i.e. antibiotics, polymerised quaternary ammonium surfactants, antibacterial peptides) that kill bacterial cells that attach onto a material upon contact;<sup>311–313</sup> b) development of new materials which are inherently resistant to bacterial attachment and subsequent biofilm formation (i.e. poly(ethylene glycol)<sup>314,315</sup> brushes, zwitterionic polymers,<sup>316</sup> and weakly amphiphilic poly(meth)acrylates).<sup>184,242,262,290</sup> In the present project the second strategy was adopted, where the bio-instructive focus was on a new class of poly(meth)acrylates, which was screened by a 2D microarray high-throughput method.<sup>277</sup> In fact, avoiding the reversible and/or irreversible attachment of material from the environment, such as macromolecules, microorganisms, or suspended particles, to a surface is very desirable to prevent the spread of infectious diseases, implant rejection, and malfunction of biosensors. So far, the anti-attachment methodology methodologies have seen the used of three strategies: a) fouling resistant (preventing the adhesion of proteins, algae and/or bacteria); b) fouling-release (allowing weak foulant-surface adhesion easily removed by limited shear or mechanical force); and c) Fouling degrading (material from the environment is degraded via oxidizing agents and/or killed by the action of anti-microbial functionalities).<sup>317,318</sup> In the first strategy the new class of poly(meth)acrylates used in this project can be collocated. In the same strategy, also, PEG linear bush polymers have been extensively developed as they have shown to resist the adsorption of numerous protein molecules.<sup>319,320</sup> The reason for its ability to resist foulants has been linked

---

to the extensive hydration layer, rapid conformational changes and steric repulsion. Many groups have tried to find alternatives from PEG. For instance, Wang et al. demonstrated the superior antifouling ability of Polyvinylpyrrolidone (PVP) bottlebrush surfaces over linear PVP brush surfaces, at similar polymer layer thickness and grafting density. The PVP bottlebrushes strongly reduced adsorption of several proteins compared to both bare gold surfaces and linear PVP brush-coated surfaces.<sup>321</sup> Another interesting example of anti-attachment polymers is presented by the group of Benetti. They found that multiple cyclic polymer brushes, mostly based on poly(2-alkyl-2-oxazoline)s, such as PMOXA and poly(2-ethyl-2-oxazoline) (PEOXA) are optimal candidates to prevent bacteria/protein attachment.<sup>322,323</sup> Besides linear, bottle and cyclic polymer brushes, there is another method to develop antifouling brushes, namely by coating surfaces with “hairy” nanoparticles.<sup>317</sup>

Another important challenge faced by biomaterials, when used in the form of medical device/implants, is related to the wound healing process and tissue regeneration when inserted inside the human body.<sup>324</sup> Body response to foreign material can be described as a modified process of wound healing.<sup>325</sup> As the regenerative response is concerned, an implanted material is often processed by the hosts body as a chronic wound, and typically results in the expected deleterious consequences.<sup>324,326,327</sup> Thus, a large focus of biomaterials science is aimed toward developing strategies to integrate the material within the host, while avoiding the scarring and

fibrotic response generated by the recruited fibroblasts during wound healing.<sup>324,328,329</sup> Cell and biochemical events in wound repair can be divided into the following stages: inflammatory reaction, cell proliferation, synthesis of the elements which make up the extracellular matrix, and the posterior period, called remodelling.<sup>330</sup>

Fibroblast cells are key participants in the wound healing and inflammation process. Their correct proliferation and modulation can drive the progression of tissue repair to fully functional tissue. Thus, understanding the fibroblastic response to implanted materials is vital to achieving desirable outcomes, such as long-term implant function or tissue regeneration.<sup>329</sup> Since fibroblasts determine the final outcome of implanted biomaterials, they must be a priority consideration in biomaterial development.

Additionally, when a biomaterial is implanted in the human body, one of the first processes that occurs can be reconducted to the phenomenon of protein adsorption. In fact, as soon as a biomaterial is in contact with the surrounding biological environment (e.g. blood) an interface is usually formed which is stabilised by the adsorption of ions and macromolecules from the medium, such as proteins.<sup>331</sup> These macromolecular layers become fundamental to the promotion of the interaction between the surface of the implants and cells. Thus, the protein layer formed on a biomaterial surface is of paramount importance in determining the fate of an implanted biomaterial.<sup>332</sup> For example, it has been well established that under many natural conditions bacteria do not adhere to bare substratum

surfaces, but rather to adsorbed these deposited macromolecular conditioning films.<sup>333</sup> In the human body, these conditioning films are often composed of adsorbed proteins, like salivary proteins on surfaces exposed to the oral cavity or fibronectin and albumin on surfaces exposed to human serum. Thus, there are many literature reports that have demonstrated hydrophilic, uncharged surfaces, which present a sufficiently uniform density of hydrophilic groups, can deliver resistance to protein adsorption preventing cell adhesion to synthetic substrates.<sup>314</sup> For example, surfaces coated with a series of oligoethylene glycols have been demonstrated to be an ideal 'inert' coating for surfaces in terms of preventing bacteria and fibroblast attachment.<sup>334–336</sup> In particular, it has been found that cell adhesion strength decreases with the increasing of the ethylene glycol units as the hydration of surfaces is increased.

#### 4.1.1 Aim and objectives

The aim of this chapter is focused on the development and optimisation of a method which enable the facile production of MPs using custom designed and synthesised, bio-instructive functionalised, amphiphilic copolymers as surfactants. The method utilised a droplet flow-focusing microfluidics apparatus to produce crosslinked particles using an oil-in-water system. The choice of a low cost diacrylate core material dwells in achieving a polymeric network and a 3D solid, solvent resistant support for the biological assays. Additionally, the higher cure that can be achieved using these functionalised reagents avoids the need of tedious washing steps.

Microfluidics was used to produce initially a broad MPs library of bio-instructive surfactants reported in Chapter 3. Then, from this library two specific sets of particles were selected for their surface chemistry to deliver the development of a proof-of-concept method to study and quantify bacteria attachment, fibroblast attachment/proliferation and BSA attachment. In the light of this, the design and development of the microfluidics process along with the subsequent bioassay were achieved by completing the following objectives:

- Optimisation of the relative flow rates of the aqueous and organic phases using a model surfactant.
- Optimisation of the MPs size to a target range by using the designed bio instructive, amphiphilic copolymers containing different hydrophilic chains (PEGMA<sub>360</sub>, mPEGMA<sub>300/500</sub>) and comparing these results to the use of commercially available surfactants.
- Conducting leaching test to assess if toxic and/or unreacted materials are released from the particles.
- Conducting SEM and ToF-SIMS characterisation to assess morphology, size and surface chemistry.
- Conducting bacteria attachment assay and consequent BSA attachment test
- Conducting a human Skin Fibroblast attachment and proliferation assay.

## 4.2 Methods

### 4.2.1 Microfluidic Microparticle Production

Acknowledgement are made to Dr. Adam Dundas, who performed the microfluidics experiments for the mPEGMA based surfactants library and trained me for the droplet microfluidics instrument.

Polymer microparticles were produced using a 100  $\mu\text{m}$  hydrophilic 3D flow-focusing microfluidic droplet generator. Two syringe pumps were used to deliver the continuous and dispersed flows to the microfluidic generator. The continuous phase used was DI water and was generally set at a flow rate of 5 ml/h if not stated otherwise. The dispersed phase contained the monomer (1,6 hexanediol diacrylate, 96 % w/v) with 2% w/v polymer surfactant and 2% w/v photoinitiator (2,2 dimethoxy-2-phenylacetophenone) and it was set at a flow rate of 0.2 ml/h if not stated otherwise. Once stable generation of the droplets is observed, the droplets were collected in a vial filled with 10 mL of DI water and placed inside the UV protective box. The capillary tube was then placed into the sample vessel, with the tip just slightly submerged in the water to prevent any blockages. The UV fibre optic cable was aligned to the particle collection stream leaving the capillary tube. After the polymeric droplets were undergone their UV cure, the UV was switched off and the polymer beads were filtered in a 40  $\mu\text{m}$  nylon mesh filter.

#### 4.2.2 Microparticles Characterisation

*Microparticles Size and Topography Analysis:* dry samples were characterised using SEM microscopy. Details of samples preparation are described in the Materials and Methods chapter.

*Microparticle Surface Characterisation:* Acknowledgement are made to Dr. Adam Dundas for acquiring and helping to analyse ToF-SIMS data.

Microparticles were placed onto a poly(hydroxyethyl) methacrylate substrate and subjected to mass-spectrometry using a ToF-SIMS IV (IONTOF GmbH, Münster, Germany) instrument. 500µm x 500µm scans were taken with a Bi<sub>3+</sub> primary ion source. Data was calibrated and analysed using IonToF SurfaceLab 7 software.

#### 4.2.3 <sup>1</sup>H-NMR method to Assess Leaching Materials

To identify if any unreacted monomeric species were present, the following method was carried out to qualitatively assess the eventual presence of these species. 40mg of dried sample was weighed into a 1.5 mL centrifuge tube. 1.5 mL of chloroform (400 µL TMS to 100 g of deuterated chloroform) was pipetted into the same centrifuge tube. The tube was closed and sonicated for 15 minutes. This allowed for any monomer to leach into solution. The sonicated solution was then filtered into a clean 10 mL sample vial and the liquid collected was pipetted into an NMR tube for <sup>1</sup>H-NMR testing. If monomer is present in solution, 3 peaks will be observed at around ~5.8, ~6.1 and ~6.4ppm which are indicative of the characteristic

double bond presents in the acrylate functionalities, thus, confirming incomplete or partial photopolymerisation (Figure 4.1).

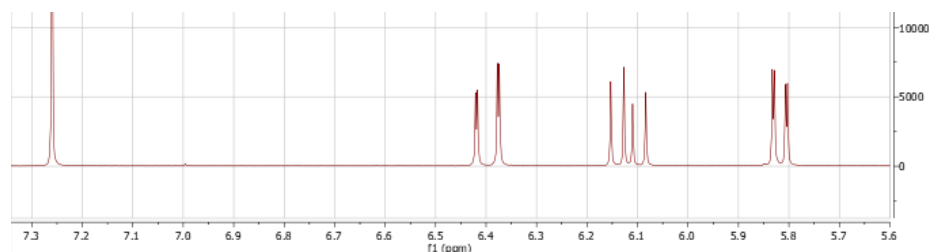


Figure 4.1 Section of the  $^1\text{H-NMR}$  Spectra for HMDA monomer peak which defines the vinyl methacrylate double bond peaks at: 6.4 ppm, 6.1 ppm 5.8 ppm.

#### 4.2.4 Leaching test with Cytotoxicity Assay

Acknowledgement are made to Arsalan Latif who performed the cell viability assay of the EGDPEA-co-mPEGMA based MPs.

*Cell Culture:* The human lung fibroblasts MRC-5 (ATCC CCL171, ATCC) were cultured in MEM Eagles (Sigma) supplemented with fetal bovine serum (10%, Sigma), L-glutamine, non-essential amino acids, penicillin/streptomycin, and sodium pyruvate (1% each, Sigma). The cells were cultured in T75 flasks at 37 °C with 5% supplemental CO<sub>2</sub> until 90% confluent, before passaging.

*Cytotoxicity Assay:* After 24 h of the culture period, a two-colour fluorescence cell viability assay based on simultaneous determination of live and dead cells by calcein-AM and ethidium homodimer-1 was used. The assay was performed by incubating cells in PBS supplemented with 4  $\mu\text{m}$  calcein-AM and 2  $\mu\text{m}$  ethidium homodimer-1 (LIVE/DEAD viability/cytotoxicity kit, Invitrogen) at 37 °C for 20 min. After which, the cells were washed three times with fresh PBS and imaged. The emitted fluorescent signals of calcein-AM and ethidium homodimer were collected

at 517 and 615 nm, respectively. Fibroblasts were considered viable if the cytoplasm was with calcein-AM (green) and if chromatin was not labelled with ethidium homodimer-1 (red).

#### 4.2.5 Bacterial Biofilm Formation

*Bacterial strains and growth conditions:* *P. aeruginosa* strain (mCherry tagged *Pseudomonas aeruginosa* PAO1-Washington sub-line, Nottingham collection, 587/610 excitation/emission) was streaked onto LB agar plates for the formation of colonies for bacterial culture experiments. The overnight culture was prepared by adding a single colony of bacteria using a sterile plastic loop to 10 ml of LB media, which was then placed in an incubator at 37 °C at 200 rpm overnight for approximately 18 hours. After the overnight culture, the culture was centrifuged at 10,000 rpm for 10 minutes and this was then resuspended in 10 ml of RPMI-1640 media, and this process was repeated to ensure all LB media had been removed from the culture. The optical density (OD) at 600 nm of the bacterial culture was determined by measuring 1 ml of pure RPMI-1640 as a blank against 100 µL of bacterial culture in 900 µL of RPMI-1640 media. The amount of bacterial culture to include in the MPs and films incubation was determined by the optical density such that the concentration in a total of 15 ml of RPMI-1640 media was an OD<sub>600</sub> of 0.01.

*Polymeric MPs 3D Biological Assay:* Bacterial attachment and biofilm formation on microparticles and flat films were conducted as previously described.<sup>230</sup> 10 mg of microfluidic produced microparticles were loaded in

triplicate in an UV-sterilised 48 acrylic well-plates. Subsequently, each well was incubated with RPMI medium (1 ml) and inoculated with a *P. aeruginosa* culture (OD<sub>600</sub> of 0.01) for 24 h at 37°C and with shaking at 60 rpm. After 24 hours, planktonic cells were removed from the wells and particles were washed with 500 µl of PBS. Flat films were prepared by UV-polymerising the monomers (EGDPEA and HPhOPA) on coverslips, previously activated by salinisation using 3-(Trimethoxysilyl)propyl methacrylate (Sigma-Aldrich). The films were prepared in three replicates and introduced in UV-sterilised polystyrene petri dishes and incubated with *P. aeruginosa* culture (OD<sub>600</sub> of 0.01) for 24 h at 37°C and with shaking at 60 rpm.

Air-dried samples were examined using a Carl Zeiss LSM 700 laser scanning confocal microscope fitted with 555 nm excitation lasers and a 10x/NA 0.3 objective. Images were acquired using ZEN 2009 imaging software (Carl Zeiss) stacking these optical cross-sections acquired at different depths within a sample, a 3D image was reconstructed. Bacterial surface coverage on microparticles was quantified using a MATLAB (R2016b) script on the fluorescence images (area size 568 x 568 µm, image resolution 512 x 512 pixels at 8-bit colour depth) taken from each well while on flat films with the COMSTAT.<sup>337</sup> However, fluorescence images representing an area of 295 x 295 µm with a resolution of 1024 x 1024 pixels at a 12-bit colour depth were acquired on the MPs, once transferred on glass slides, to observe in depth the bacterial attachment coverage.

#### 4.2.5.1 Statistical Analysis

All data acquisitioned is expressed as mean  $\pm$  standard deviation, with  $n = 6$ ,  $N = 2$ . Statistical significance was calculated using one-way ANOVA and the Tukey's post hoc analysis, whereby  $p \leq 0.05$  was considered as being statistically significant.

#### 4.2.6 Protein attachment Assay *via* Nano ESI-MS/MS.

Acknowledgement are made to Joris Meurs who performed the BSA extraction and quantification analysis.

*Protein culture with MPs:* Bovine Serum Albumine (BSA) stock solution was prepared at fixed concentration of 2 mg/mL, while, the MP stock suspension was prepared at a fixed concentration of 50 mg/mL, regardless the nature of the surface of the particles. From this latter, 4 aliquots of 50  $\mu$ L were withdrawn in order to prepare 4 replicates for each sample and, also, to have a final concentration of 5 mg/mL for each suspension. To the 50  $\mu$ L suspension, 125  $\mu$ L of the BSA stock solution was added to the same test tube in order to obtain a final BSA concentration of 0.5 mg/mL. Finally, 325  $\mu$ L of PBS was used to dilute to this concentrated solution and reach the final volume of 500  $\mu$ L. The MPs in contact with BSA was incubated with BSA at 37°C under agitation of 60 rpm. After 24 h the MPs were washed in PBS for three times by repeated centrifugations steps. The dry particles pellets were stored in fridge prior to BSA extraction.

*BSA Extraction and Quantification:* Proteins were extracted from particles at 37°C by using 250  $\mu$ L of a solubilisation buffer (6 M urea (BioXtra; Sigma-

Aldrich, Gillingham, UK), 150 mM NaCl (BioXtra  $\geq 99.5\%$ ; Sigma-Aldrich, Gillingham, UK), 50 mM Tris (BioXtra  $\geq 99.9\%$ ; Sigma-Aldrich, Gillingham, UK), 0.1% v/v Triton X-100 (BioXtra; Sigma-Aldrich, Gillingham, UK), 0.1% w/v sodium deoxycholate (BioXtra  $\geq 98.0$ ; Sigma-Aldrich, Gillingham, UK), 0.1% w/v SDS (BioXtra  $\geq 99.0\%$ ; Sigma-Aldrich, Gillingham, UK)). The extracted proteins were further reduced by using 12  $\mu\text{L}$  of 100 mM DTT (BioUltra  $\geq 99.5\%$ ; Sigma-Aldrich, Gillingham, UK) for 1 h incubation at 56°C. this was followed by blocking the influence of any free thiols by applying alkylation process using 24  $\mu\text{L}$  100 mM IAA (BioUltra; Sigma-Aldrich, Gillingham, UK) at room temperature in the dark for 30 minutes. The reaction was quenched with 15  $\mu\text{L}$  100 mM DTT. Finally, samples were concentrated and purified by 5 rounds of centrifuging on Amicon 0.5 centrifuge units (Merck Millipore, Gillingham, UK) with 400  $\mu\text{L}$  100 mM  $\text{NH}_4\text{HCO}_3$  (BioUltra  $\geq 99.5\%$ ; Sigma-Aldrich, Gillingham, UK).

The digestion of the proteins in peptides was achieved using sequencing grade trypsin (Promega, Southampton, UK). The working concentration of the trypsin is 0.05  $\mu\text{g}/\mu\text{L}$  in 100 mM  $\text{NH}_4\text{HCO}_3$  and proteins with this latter were incubated overnight at 37 °C with this concentration. The digestion was quenched by adding formic acid (Optima™ LC-MS grade; Fisher Scientific) to a concentration of 1% v/v. The solution was 10-fold diluted using 50% v/v acetonitrile (CHROMASOLV® LC-MS grade; Honeywell, Seelze, Germany) and transferred to a 96-well plate. The digests were analysed using nanoESI-MS/MS on a TriVersa Nanomate (Advion Biosciences, Ithaca, NY) coupled to a Q Exactive plus Orbitrap mass spectrometer (Thermo

Scientific, San Jose, CA). Relative quantification of BSA was done using the summed intensity of identified peptides.

#### 4.2.7 Fibroblast Attachment and Proliferation Assay

Acknowledgement are made to Arsalan Latif who performed the cell viability assay, cell attachment and proliferation assay on the MPs based on these two surfactants THFuA-co-mPEGMA<sub>300</sub> and EGPhEA-co-mPEGMA<sub>300</sub>.

##### 4.2.7.1 Cell Culture

The human skin fibroblasts (CRL-2522, ATCC) were cultured in Minimum Essential Medium Eagles (MEM) supplemented with 10% fetal bovine serum (FBS), 1% L-glutamine, non-essential amino acids, penicillin/streptomycin and sodium pyruvate (Sigma-Aldrich). The cells were cultured in T75 flasks at 37°C with 5% supplemental CO<sub>2</sub> until 90% confluent before passaging.

Fibroblasts were cultured with a MP density of 13mg/cm<sup>2</sup> in a non-TCP well plate. To simulate a pro-fibrotic environment, the pro-fibrotic growth factor TGF-β1 (10 ng/ml) was added after 24 hours of culture. The MPs-fibroblast system was then cultured for the stated time periods.

##### 4.2.7.2 Cytotoxicity

The cell viability of fibroblasts on the microparticles was assessed using the ToxiLight™ non-destructive cytotoxicity bioassay kit (Lonza) at 24 hours of culture. The assay measures the release of adenylate kinase (AK) from cells with compromised cell membranes. The AK catalyses the conversion of ADP to ATP, which was then detected through bioluminescence. The emitted

light intensity is linearly related to the AK concentration, which informs on cell viability.

#### 4.2.7.3 Cell Attachment

Cell attachment of fibroblasts was measured using the CyQuant™ NF assay (ThermoFisher) at 24 hours of culture. This method is based on measurement of cellular DNA content via fluorescent dye binding, where the cellular DNA content is proportional to the number of cells. The DNA content of fibroblasts cultured on MPs was measured and their fluorescence intensity was compared against fluorescence intensity of known cell seeding densities. In summary, this approach identified the number of adherent cells by measuring the cellular DNA of fibroblasts on MPs.

#### 4.2.7.4 Cell Proliferation

Cell proliferation was measured with Click-iT™ Edu microplate assay (Thermofisher). EdU was added to cell medium at 5 $\mu$ M at 72 hours of culture, where it was incorporated into newly synthesised DNA during the G1/S phase of the cell cycle. Cells were fixed after 24 hours, detached from MPs, and stained for EdU following manufacturer's instructions. The relative fluorescence intensity of EdU positive cells resulted a readout for the probability of cells to be in the G1/S phase during the incubation period.

#### 4.2.7.5 Statistical Analysis

All data acquisitioned is expressed as mean  $\pm$  standard deviation, with n = 6, N = 2. Statistical significance was calculated using one-way ANOVA and

the Tukey's post hoc analysis, whereby  $p \leq 0.05$  was considered as being statistically significant.

### 4.3 Results and Discussions

#### 4.3.1 Microparticles Production

An oil-in-water (O/W) droplet flow-focusing system was chosen to determine if the designed amphiphilic copolymers were suitable to act as a surfactant for the microfluidic preparation of microparticles. The developed microfluidics process set up is showed in Figure 4.2.

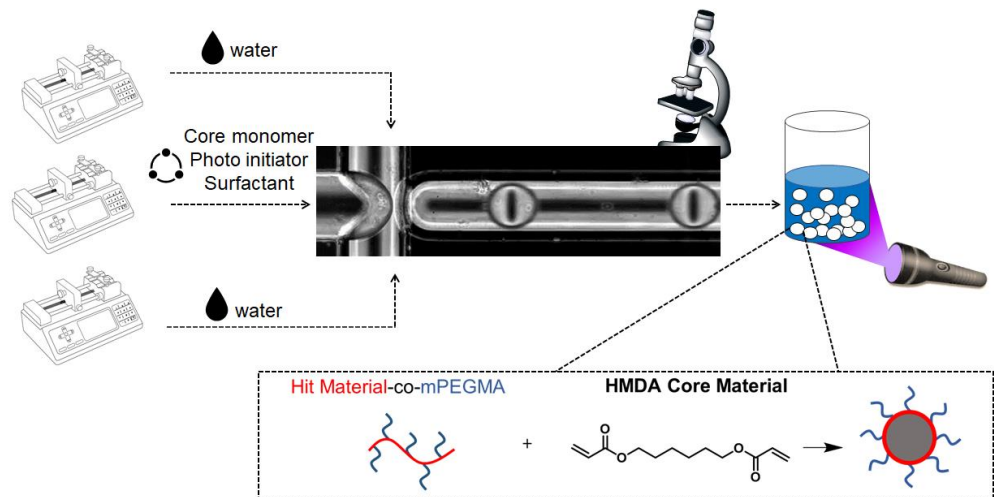


Figure 4.2 Schematic of the experimental microfluidics setup. The organic and aqueous phase were pumped with 3 syringe pumps and connected to the device via polytetrafluoroethylene tubes. A high-speed video camera was applied to observe the droplet formation through the flow focusing microfluidic chip. The droplets were collected in a glass vessel with water and shine by UV-Vis. At the bottom of the picture, it was included a generic schematic of the chemistry used in this set up. The result in the application of the custom-made functionalised surfactants with an inert diacrylate monomer is the formation of cross-linked MPs (60-70  $\mu\text{m}$ ) with a low-density PEG-layer on the surface (around 10 nm).

In Figure 4.2 is shown how the dispersed phase was fed into the central channel and consisted of 96% 1,6 hexanediol diacrylate (HMDA), the particle “core” material, 2% w/v polymer custom-made surfactant and 2% w/v photoinitiator (2,2-Dimethoxy-2-phenylacetophenone (DMPA)). The

continuous phase used was DI water, which has been fed into the two side channels located perpendicularly to the central feed. The emulsion droplets formed by impinging these two phases were collected in a receiver flask where they were simultaneously irradiated with a fibre optic guided 365 nm UV source to form solid cross-linked polymer microparticles.

#### 4.3.1.1 Initial Flow Optimisation

Initially, the microfluidics process was optimised in terms of varying the flow rates of the disperse phase ( $Q_d$ ) and of the continuous phase ( $Q_c$ ). This particular optimisation was performed in order to ensure that stable and monodisperse particles could be produced by achieving a dripping and stable flow of droplets within the channel walls. Others different flow regime profiles were avoided such as wall-wetting events, jetting behaviour, unstable particle satellites formation and squeezing. The presence of these lateral flow regimes would at best lead to a polydisperse MPs population, at worst hamper the long-term stability of the process. When the flow rate of the continuous phase is too low, it was observed that droplets cannot be formed because the viscous shearing force is too weak. This resulted in continuous laminar streams of the dispersed and continuous phase, called wall wetting regime. In contrast, when  $Q_c$  is too high, polydisperse droplets are irregularly formed *via* the dominance of a jetting regime.<sup>338</sup>

Figure 4.3 shows the flow diagram of the system using the EGDPEA-co-mPEGMA<sub>300</sub> as stabiliser at a 2% w/v concentration with 2% w/v of photoinitiator and 96% w/v of HMDA.

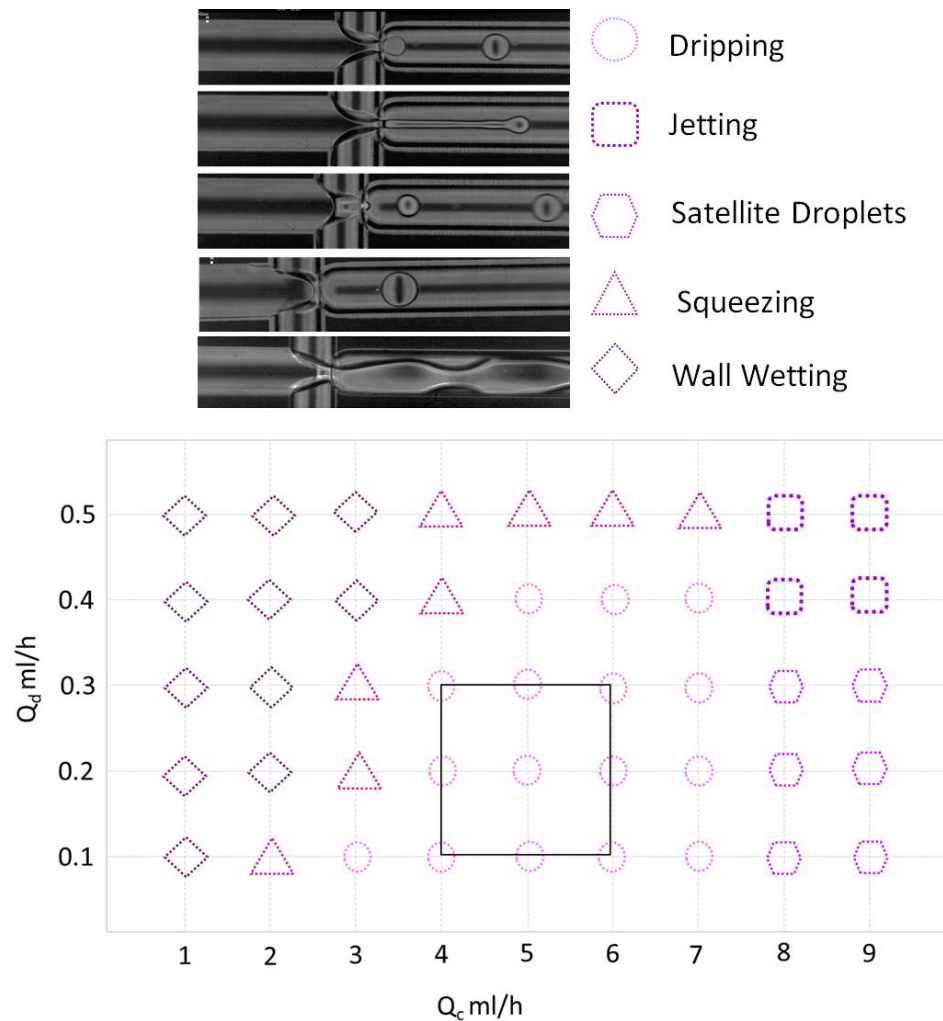


Figure 4.3 Flow diagram of an oil-in-water microfluidics system with HMDA core material and EGDPEA-co-mPEGMA<sub>300</sub>. ○ denotes idealistic dripping behaviour, □ denotes jetting behaviour, ⬡ denotes formation of satellite droplets, ◇ denotes flow rates which caused wall wetting events and △ denotes large dripping. The Black square denotes the region of flow rates that produces monodisperse emulsions. Images show examples of dripping, jetting, satellite droplet formation and wall wetting events, respectively.

In Figure 4.3, the flow diagram has been dynamically built by changing the  $Q_c$  from 1 ml/h to 9 ml/h and  $Q_d$  from 0.05 ml/h to 0.5 ml/h. This allowed for the observation of different regimes and identify the best operational window for the particular surfactant. Finally, this EGDPEA-co-mPEGMA<sub>300</sub> was used as model for the EGDPEA based amphiphilic copolymers series: EGDPEA-co-mPEGMA<sub>500</sub>, EGDPEA-co-PEGMA<sub>360</sub> and EGDPEA-co-PEGMA<sub>500</sub>. This surfactant demonstrated to be sufficiently amphiphilic to produce stable emulsions in the range of  $Q_c$  4-6 ml/h and of  $Q_d$  0.1-0.3 ml/h. In this

range, the droplets were generated by breaking up the monomer thread in or behind the orifice. Thus, the size of the particles produced were similar in the width to the dimension of the orifice. As the flow rates of both  $Q_c$  and  $Q_d$  were increased, the system started to display jetting behaviour, while an increase in  $Q_c$  alone resulted in a halfway situation, where satellites start to appear along with stable droplets. Furthermore, if  $Q_d$  was not large enough, the size of the emulsions formed begins to occupy the majority of the microfluidics junction space and this led to wall-wetting events. Therefore, the conditions of  $Q_c = 5$  ml/h and  $Q_d = 0.2$  ml/h were chosen as flow rates that would ensure the long-term stability of emulsion production within the microfluidics system whilst maximising particle output in terms of yield.

#### 4.3.1.2 Flow Optimisation for HPhOPA Based Surfactant

Following these preliminary results, a second copolymer from the library was used in the microfluidics system. However, prior to collecting particles with the HPhOPA-co-mPEGMA<sub>300</sub> surfactant, a flow diagram was constructed to assess the working conditions that would be required to successfully process this second model molecule. Figure 4.4 shows the flow diagram of the system using the HPhOPA-co-mPEGMA<sub>300</sub> as stabiliser at a 2% w/v concentration with 2% w/v of photoinitiator and 96% w/v of HMDA.

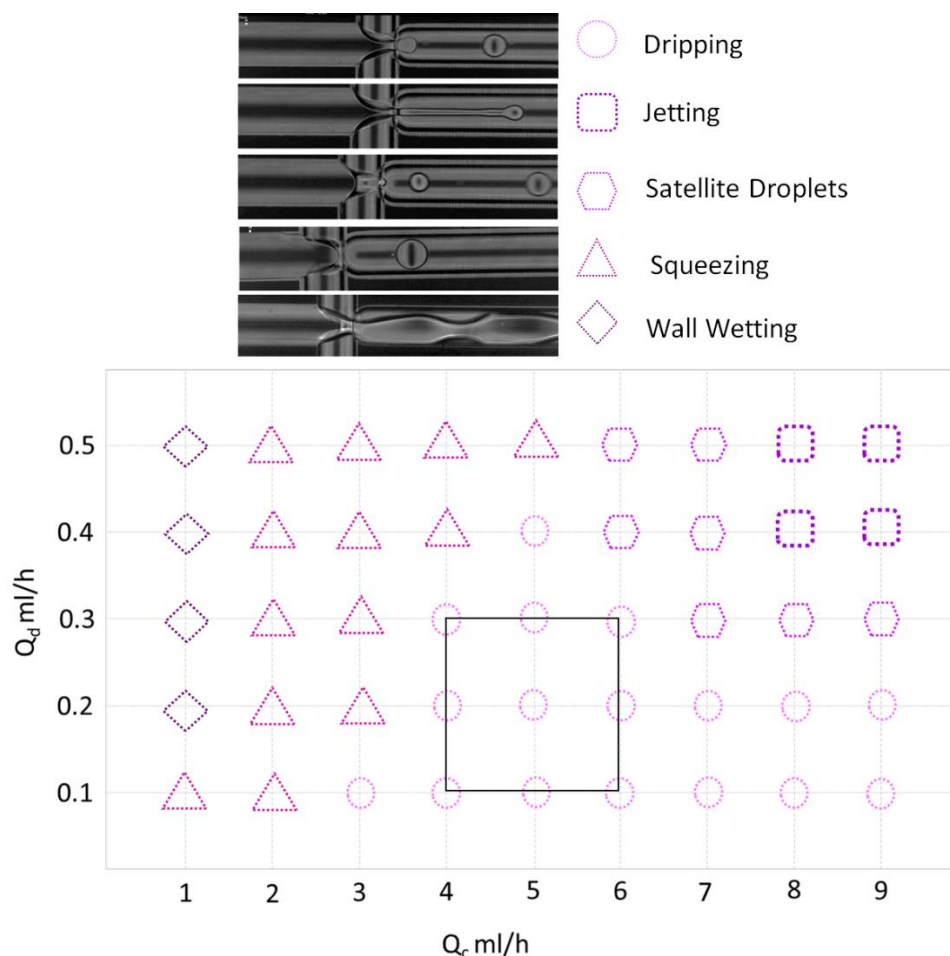


Figure 4.4 Flow diagram of an oil-in-water microfluidics system with HMDA core material and HPhOPA-co-mPEGMA<sub>300</sub>. ○ denotes idealistic dripping behaviour, □ denotes jetting behaviour, ⬡ denotes formation of satellite droplets, ◇ denotes flow rates which caused wall wetting events and △ denotes large dripping. The Black square denotes the region of flow rates that produces monodisperse emulsions. Images show examples of dripping, jetting, satellite droplet formation and wall wetting events, respectively.

From Figure 4.4, it was observed that the  $Q_d$  and  $Q_c$  values that allow stable emulsion are in the similar range to that of EGDPEA-co-mPEGMA<sub>300</sub>. Consequently, monodisperse MPs were also produced by the use of this copolymer to form and stabilise the phase separation interface by adopting the same flow rates values of  $Q_c = 5$  ml/h and  $Q_d = 0.2$  ml/h. This initial outcome hinted that these working conditions do not depend exclusively on the chemical nature of the hydrophobic monomers, but also, by the hydrophilic counterpart, as demonstrated by the computational model (see Chapter 3).

#### 4.3.1.3 SEM Characterisation for MPs Produced by Varying Hydrophilic Chain Length.

A second optimisation experiment was conducted to investigate the effect of the PEGMA/mPEGMA chain length on the emulsion/particle stability (Figure 4.5). 4 different particles were studied in this first SEM analysis and they were produced from the following surfactants: EGDPEA-co-mPEGMA<sub>300</sub>, EGDPEA-co-mPEGMA<sub>500</sub>, EGDPEA-co-mPEGMA<sub>360</sub> and PVA.

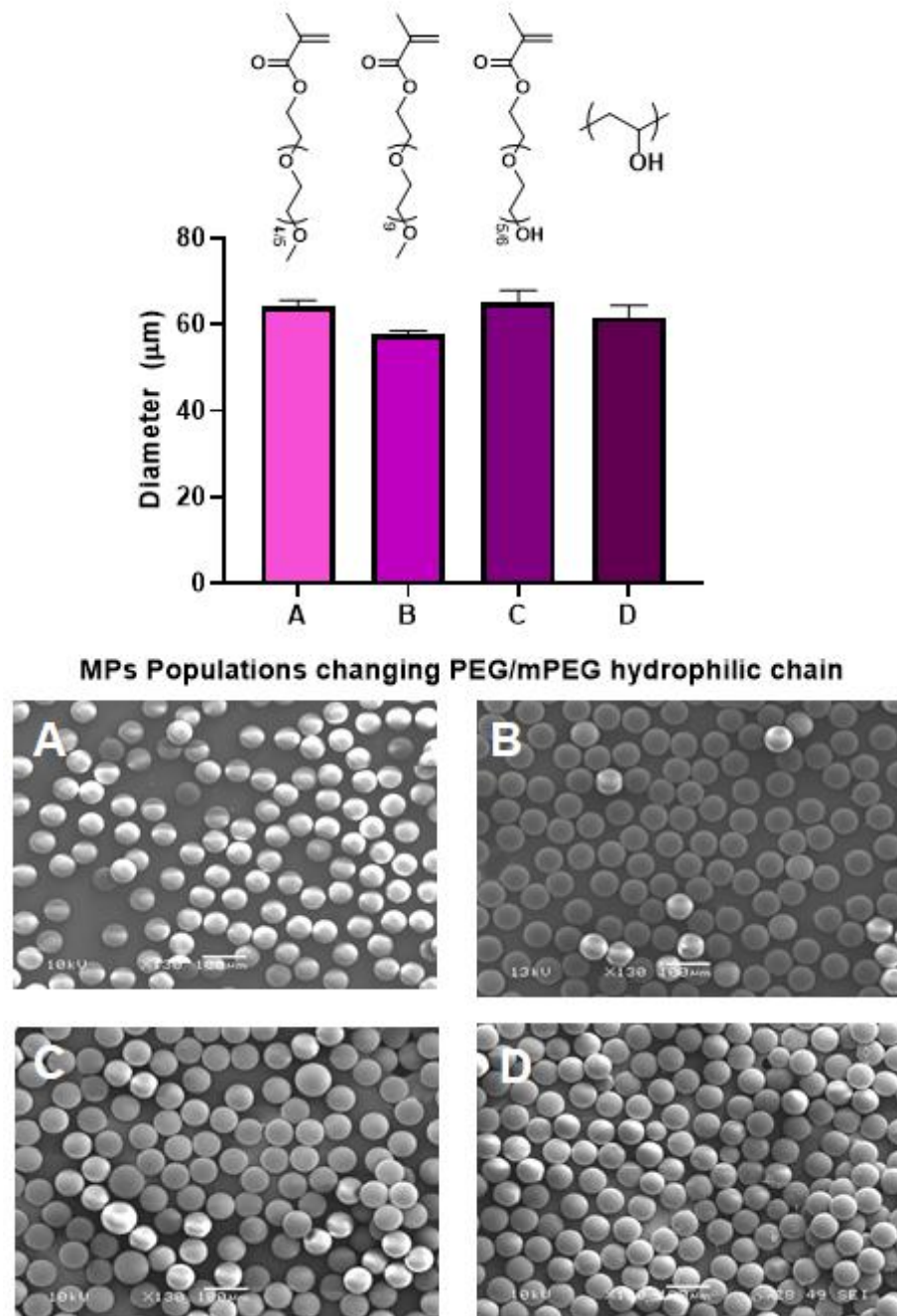


Figure 4.5 SEM of polymer microparticles produced using surfactants with different hydrophilic PEGMA/mPEGMA chains showing graphically the sizes of the images A-D (A) Monodisperse particles made from surfactant EGDPEA-co-mPEGMA<sub>300</sub> and a HMDA core with size  $64.30 \pm 1.33 \mu\text{m}$  (CV = 2.1 %) (B) Monodisperse particles made from surfactant EGDPEA-co-mPEGMA<sub>500</sub> and a HMDA core with size  $57.81 \pm 0.77 \mu\text{m}$  (CV = 1.3 %) (C) Monodisperse particles made from surfactant EGDPEA-co-PEGMA<sub>360</sub> and a HMDA core with size  $65.24 \pm 2.74 \mu\text{m}$  (CV = 4.2 %) (D) Monodisperse particles made from surfactant PVA and a HMDA core with size  $61.60 \pm 2.93 \mu\text{m}$  (CV = 4.8 %)

This investigation was mainly focused on defining the effect of the hydrophilic counterpart on the size and size distribution of the generated MPs library. SEM images in Figure 4.5 show that there was little effect on

the particle size and polydispersity. Therefore, as a result, mPEGMA<sub>300</sub> was chosen to be the hydrophilic component variant for the rest of the library of surfactants, due to the combination of favourable synthetic reaction (as demonstrated in Chapter 3) and microfluidic outcomes. Furthermore, mPEGMA<sub>300</sub> has shown to give both improved conversion as well as higher biological performances without compromising particle stability.

#### 4.3.1.4 SEM Characterisation for MPs Produced with Different Major Chemistry Components

Topography, size and size distribution are key particles properties that need to be assessed when developing a new fabrication method. For this reason, after the optimisation of the combination of  $Q_d$  and  $Q_c$  to determine the flow regime to generate stable droplets, SEM analysis was performed on the particles. SEM analysis has allowed to qualitatively observe the topography providing information on size and the distributions of the different particles populations. Five different MPs were studied in this first SEM analysis and they were produced from the following surfactants: EGDPEA-*co*-mPEGMA<sub>300</sub>, HPhOPA-*co*-mPEGMA<sub>300</sub>, PVA, surfactant free core material only and a mixture of (EGDPEA-*co*-mPEGMA<sub>300</sub>):(HPhOPA-*co*-mPEGMA<sub>300</sub>) (1:1 wt/wt ratio). The mixed system was also used to determine whether the polymer surfactants could be physically blended to create stable MPs with a co-functionalised surface. This process could be particularly useful when wanting to co-functionalise particles with different biological properties for an application. For example, in wound healing it is desirable

to promote an appropriate immune response whilst, simultaneously, preventing bacterial biofilm formation.

Microfluidics particle sizing data obtained are shown in Figure 4.6.

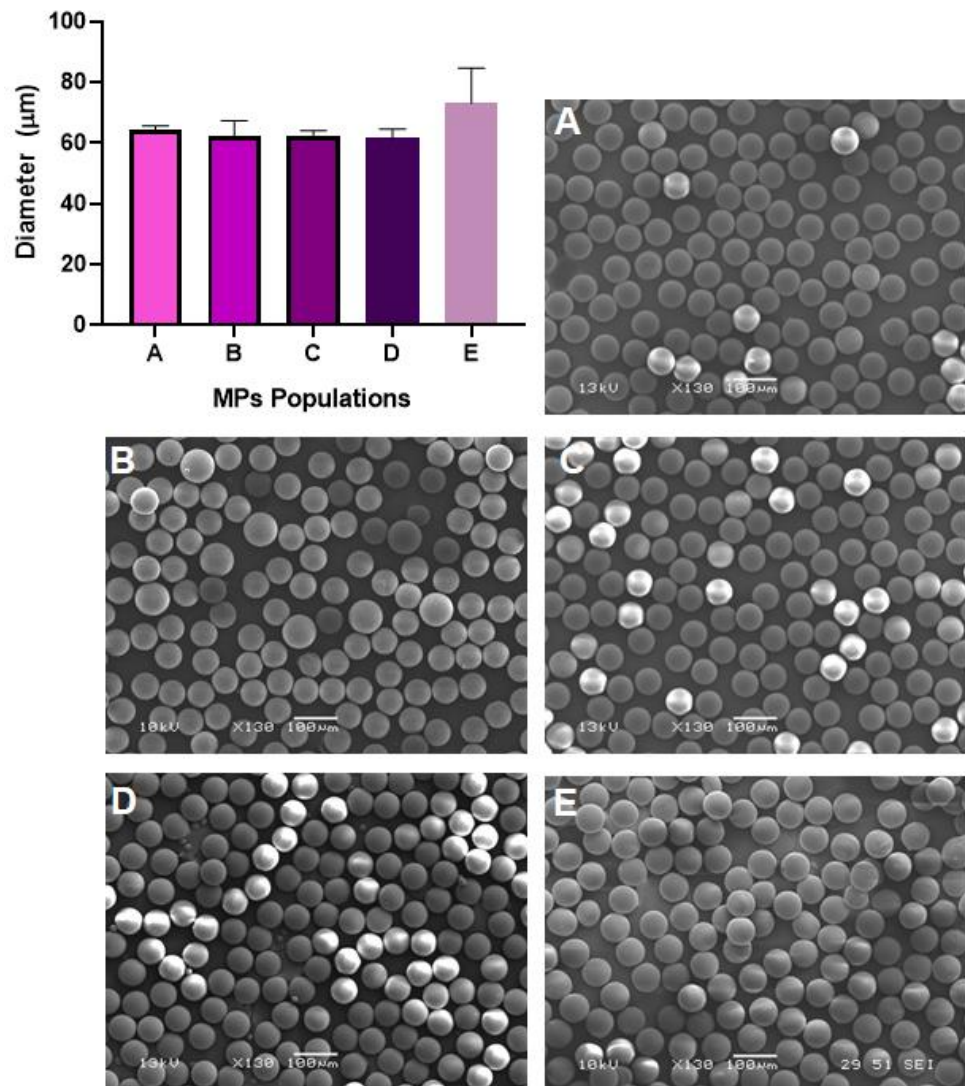


Figure 4.6 SEM images of polymer microparticles produced using a droplets approach showing graphically the sizes of the images A-D size of particles shown in images A-E. (A) Monodisperse particles made with EGDPEA-co-mPEGMA<sub>300</sub> surfactant with a core made from HMDA and a size of  $64.30 \pm 1.33 \mu\text{m}$  (CV = 2.1 %) (B) Particles made with EGDPEA-co-mPEGMA<sub>300</sub> and HPhOPA-co-mPEGMA<sub>300</sub> in a 1:1 ratio with a core made from HMDA and a size of  $62.2 \pm 5.2 \mu\text{m}$  (CV = 8.4 %) (C) Particles produced with HPhOPA-co-mPEGMA<sub>300</sub> with a core made from HMDA with a size of  $62.42 \pm 1.66 \mu\text{m}$  (CV = 2.7 %) (D) Particles made with PVA surfactant with a core made from HMDA with a size of  $61.60 \pm 2.93 \mu\text{m}$  (CV = 4.8 %) (E) Particles made with only HMDA core material with no surfactant with a size of  $73.09 \pm 11.63 \mu\text{m}$  (CV = 15.9 %)

Figure 4.6 depicts that, using the same experimental flow conditions, all the generated MPs are mostly smooth and perfectly spherical with an average

size of around 60  $\mu\text{m}$  and with a coefficient variation (CV) of around 5%, confirming to be monodisperse. The CV is a standardised measure of a distribution and a narrow distribution is considered when this coefficient is lower or around 5%.<sup>235</sup>

The use of the individual surfactants, EGDPEA-co-mPEGMA<sub>300</sub>, HPhOPA-co-mPEGMA<sub>300</sub> and the ratio of 1:1 wt/wt mixed surfactant gave particles of very similar sizes with an overall surfactant concentration of 2% wt/wt. The particles were found to exhibit the following sizes  $64.30 \pm 1.33 \mu\text{m}$  (CV = 2.1%, Figure 4.6a),  $62.42 \pm 1.66 \mu\text{m}$  (CV = 2.7%, Figure 4.6c), and  $62.2 \pm 5.2 \mu\text{m}$  (CV = 8.4%, Figure 4.6b), respectively. This showed that it was possible to produce similar particles when incorporating two different surfactants within the production method. However, the size distribution was slightly larger when compared to that obtained from the single surfactants. The increasing is not dramatically significant, and further optimisation in terms of surfactants concentration and flow rates can be expected to correct this. When no surfactant was added, the HMDA core monomer has been sufficiently amphiphilic to be able to produce polymer microparticles (Figure 4.6e). In this case it was observed that the MPs generated increased in size from 60  $\mu\text{m}$  to 70  $\mu\text{m}$ , and, had a considerably broader size distribution (CV = 15.9 %). This latter result is significant as it demonstrates the importance of using surfactants when controlling the droplets/emulsion formation. Finally, a commercial surfactant, PVA, was used to produce particles, adopting the same core material and flow condition previously applied, as a comparison to the custom-made surfactants (Figure 4.6d). By

using PVA, particles of an analogous size ( $61.60 \pm 2.93 \mu\text{m}$  (CV = 4.8%)) were prepared, demonstrating that the synthesized surfactants were comparative to industrially recognised interfacial agents.

#### 4.3.1.5 Use of the HT produced Surfactants within an MPs Formation Screening Program

Once the initial production of MPs was completed, the library of amphiphilic copolymers (produced *via* the automated synthesiser) was used to the droplets-based microfluidics system to test each member surfactants performance. In Figure 4.7 the bar graph shows the size and size dispersity (% CV) of the MPs obtained using the different members of the surfactant library at a 2% (w/v) concentration, 96% w/v of HMDA as core material and 2% w/v of photoinitiator.

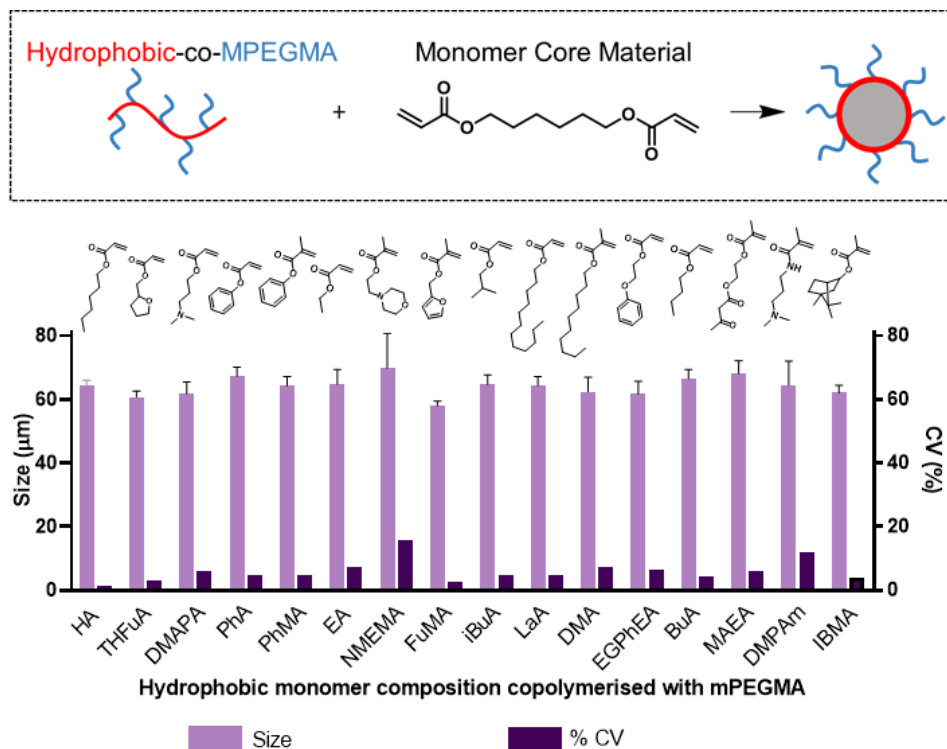


Figure 4.7 Size and % CV of the MPs produced by using surfactants using the automated synthesiser. EGDPEA and HPhOPA were not included as they had already been assessed.

Figure 4.7 shows that by applying the optimised flow conditions described previously with the droplet microfluidics device ( $Q_c = 5$  ml/h and  $Q_d = 0.2$  ml/h), MPs were successfully fabricated with all the surfactants. Furthermore, the size of the particles were comparable to the former produced with HPhOPA-*co*-mPEGMA<sub>300</sub> and EGDPEA-*co*-mPEGMA<sub>300</sub>. In addition, 13 of these experiments resulted in monodisperse populations with calculated CV values for the majority of the particles lying in a range between 2.61% and 7.24%. Two exceptions were found in the library namely, NMEMA-*co*-mPEGMA<sub>300</sub> and DMPAm-*co*-mPEGMA<sub>300</sub>. In fact, these two MPs had CV with values of 15.66 % and 11.80 %, respectively, more than double of 5%. These broader populations might depend on the poor amphiphilic balance between the HyB monomer and mPEGMA<sub>300</sub>. In both cases, NMEMA and DMPAm have a cLogP of 0.47 and 0.25, respectively, lower than the 0.62 of mPEGMA<sub>300</sub>. Similarly, the CAC for both materials is among the highest of the 19 surfactants generated.

The shape and morphology for the 16 MPs were analysed using SEM. Figure 4.8 presents the SEM images of particles produced with HA-*co*-mPEGMA<sub>300</sub> and THFuA-*co*-mPEGMA<sub>300</sub>.

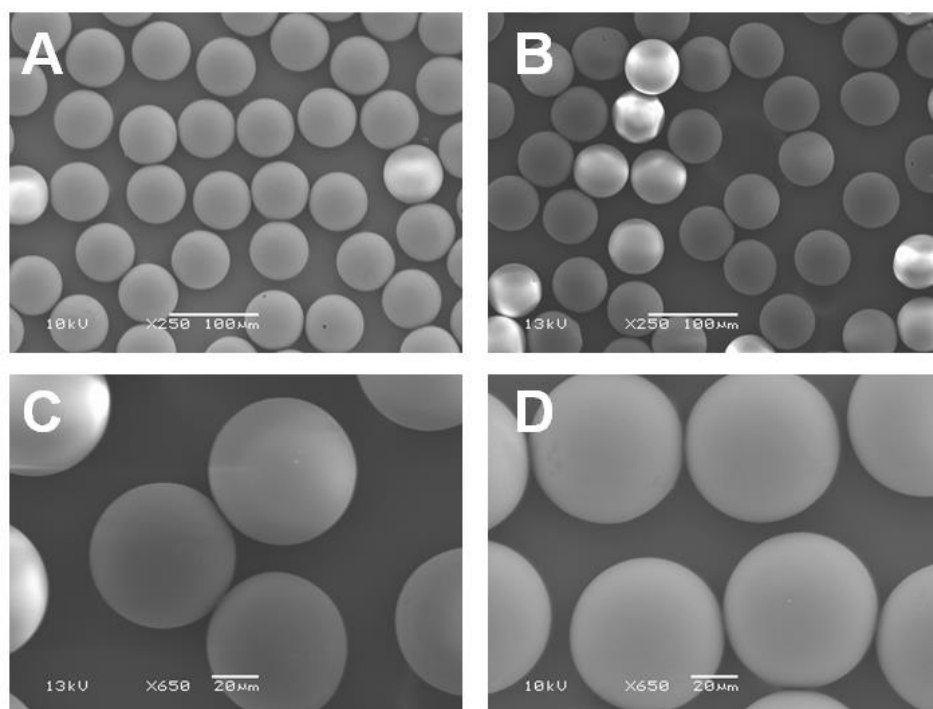


Figure 4.8 SEM pictures at X250 and X650 resolution of the MPs produced with HA-co-mPEGMA<sub>300</sub> (A-C) and with THFuA-co-mPEGMA<sub>300</sub> (B-D)

Figure 4.8 contains an example of the morphology and shape data obtained from two of the surfactants that was typical of the MPs produced from the entire library of particles. The MPs, from the 13 surfactants that produced particles with similar CV values, exhibited smooth surfaces that were generally free from imperfections which may have resulted from the fabrication process. This confirmed that the microfluidics conditions applied, and relative surfactants concentration, were highly suitable for the manufacturing of such 3D systems.

When analysing the exceptions NMEMA-co-mPEGMA<sub>300</sub> (Figure 4.9A-C) and DMPAm-co-mPEGMA<sub>300</sub> (Figure 4.9B-D) particles, irregular surface morphology and imperfections were detected. In Figure 4.9 the surface defects are identified in the SEM images.

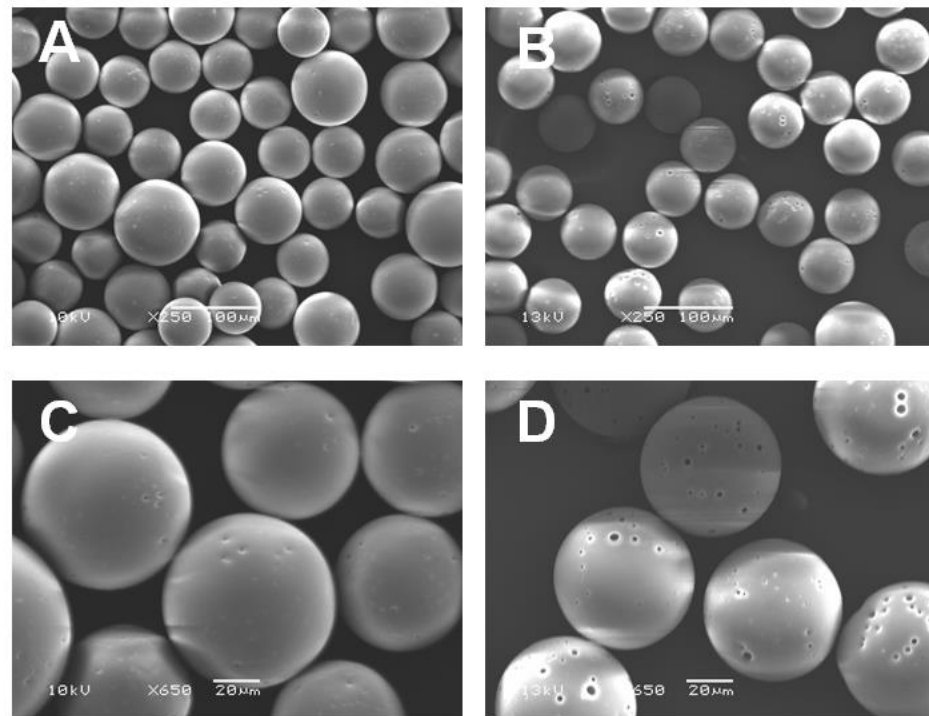


Figure 4.9 SEM pictures at X250 and X650 resolution of the MPs produced with NMEMA-co-mPEGMA<sub>300</sub> (A-C) and with DMPAm-co-mPEGMA<sub>300</sub> (B-D).

Figure 4.9 shows that particles have a high level of surface porosity throughout the populations, making the quality of the overall surface inconsistent. This porosity might be due to air bubbles in the organic solutions, caused by a poor mixing and low chemical affinity between the diacrylate core monomer and the surfactant. Due to this observation, these two particles have not been analysed or used further in this study.

The final exception was the surfactant F7BMA-co-mPEGMA<sub>300</sub> where it was found to be unusable in the production of MPs because of the poor level of solubility within HMDA experienced during the sample preparation making formulation of the dispersed phase impossible.

#### 4.3.1.6 Microparticles leaching

Obtaining a high level of polymer conversion during the curing process of the cross-linked core material is fundamental to avoid leaching of residual monomer during biological assays. A systematic study was conducted by varying the photoinitiator concentration from 1% to 4% w/v to observe the effect of this change on the final cure achieved. To carry out these series of experiments, EGDPEA-co-mPEGMA<sub>300</sub> has been used as model surfactant (2% w/v) and HMDA as core material. <sup>1</sup>H-NMR analysis was performed on the supernatant of a chloroform-based suspension containing 40 mg of MPs (27 mg/mL) to identify qualitatively the presence of any unreacted monomer. An example of <sup>1</sup>H-NMR is showed in Figure 4.10.

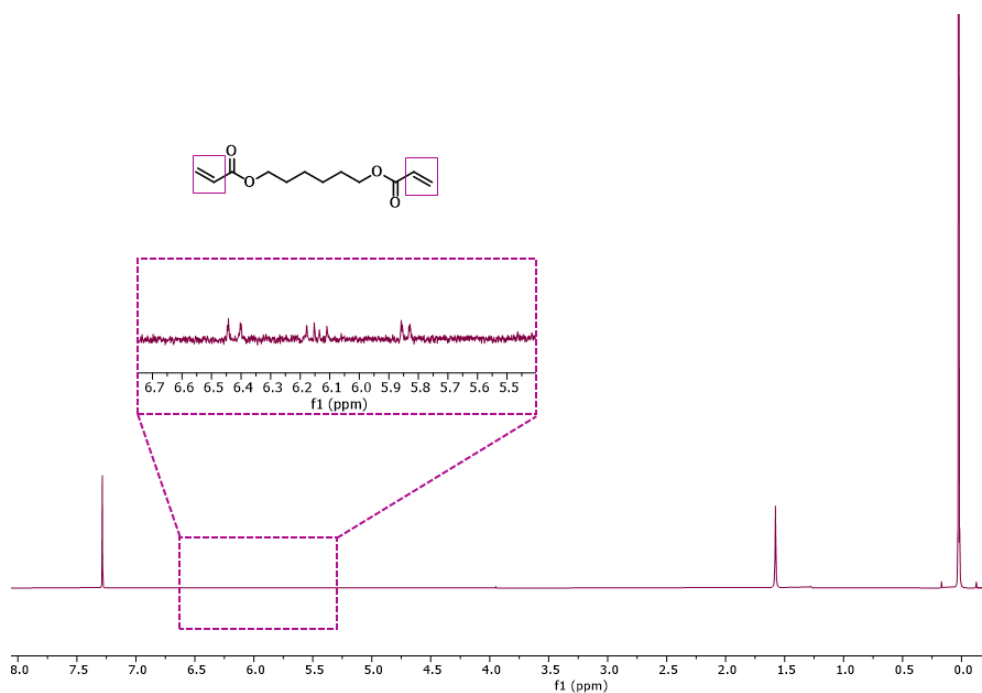


Figure 4.10 <sup>1</sup>H-NMR spectrum showing minimal amount of leaching from particles when exposed to deuterated chloroform. Internal control used is TMS. Peaks in expanded section refer to acrylate bond protons, which facilitated calculation of the concentration of HMDA (0.5 mM).

Figure 4.10 shows that only trace amounts of monomer were detected from the supernatant and, this was experienced for all the photoinitiator

concentrations explored. However, the sensitivity of this analytical technique was felt to not give an accurate analysis of the overall concentration of the unreacted molecule because of its low level in the solution.

As the main goal of this study is to ensure that any toxic residual compounds released from the MPs do not harm the biological environment, during exposure to the particles, cell-viability test has been performed on MRC-5 (ATCC CCL171) human lung fibroblasts. As the chain propagation of a polymer during a photopolymerisation is directly correlated to the initiator concentration, the biological test was carried out adopting different MPs, produced at 1%, 2%, 3%, 4 % and 5 % w/v of initiator. In addition, different suspension concentrations (from 1 mg/mL to 10 mg/L) were prepared to understand the particle packing may have upon cell response. (Figure 4.11).

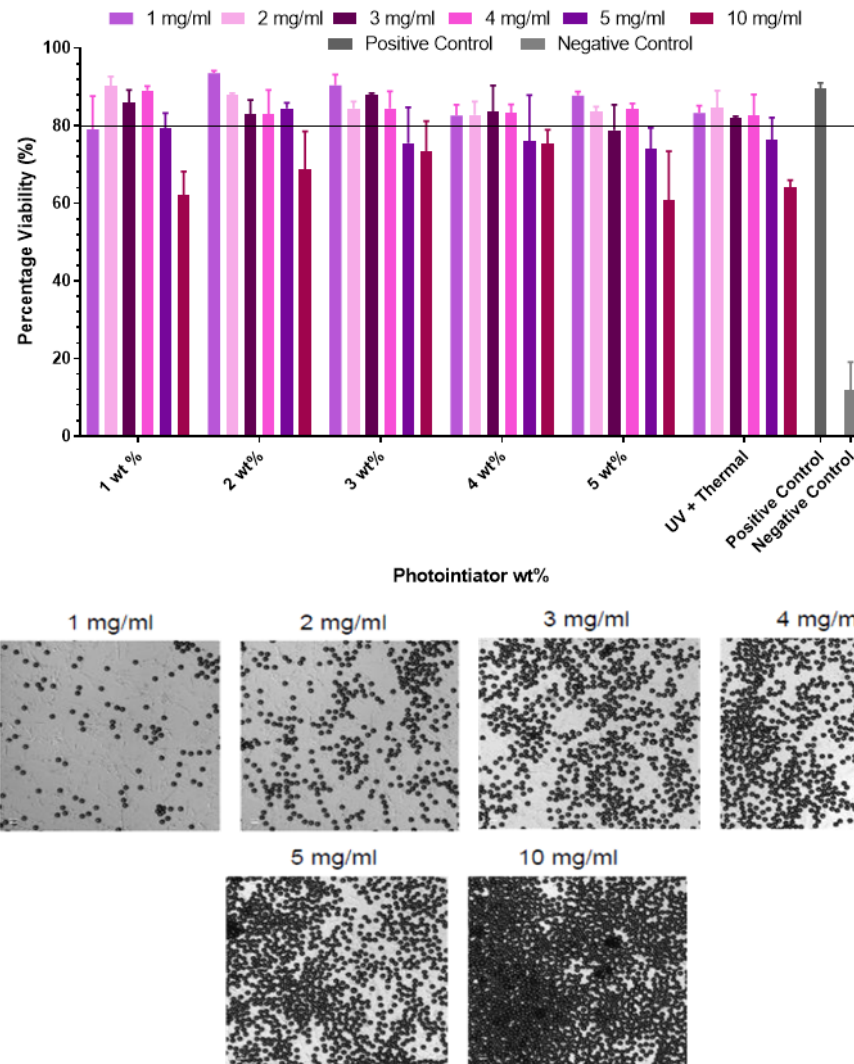


Figure 4.11 LIVE/DEAD cell viability study using MRC-5 (ATCC® CCL171™) human lung fibroblast cells. Particles produced with different photoinitiator content up to 5 wt % were used across a range of different particle concentrations. Cells grown on tissue culture plastic (TCP) and cells treated with Triton-X were used as positive and negative controls respectively. Measurements taken over N = 3 biological repeats.

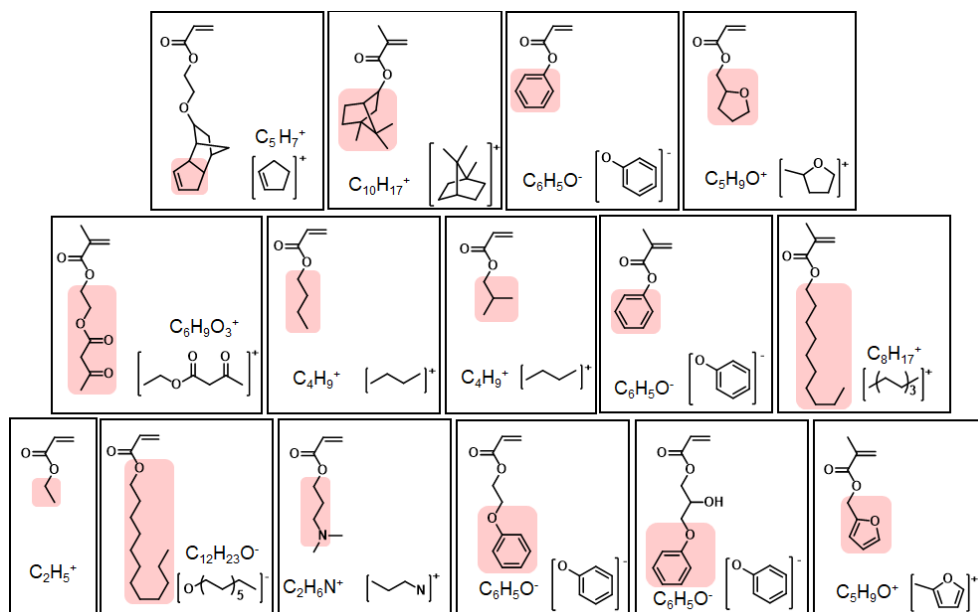
Figure 4.11 shows that regardless of the photoinitiator concentration (1-5 wt/v) used for the UV-curing process, no drop in viability of the cells was observed for MPs concentration ranging from 1 to 4 mg/mL when compared to the positive control. However, for MPs at 5 mg/mL a cell viability issue was observed when the photoinitiator concentration has been increased above 2% wt/v. Finally, 10 mg/mL MPs concentrations resulted in a toxic response being observed for all the initiator concentrations (toxicity was

defined as cell viability less than 60%). This toxicity has been attributed to the high particle density covering the cell layer and blocking the flow of growth medium, preventing the removal of waste products resulting in cell death.

Overall, this proof-of-concept study has confirmed that despite the presence of monomer unreacted observed spectroscopically ( $^1\text{H-NMR}$ ), this level is insufficient to confer unwanted toxicity to the biomaterial 3D model system. However, it also pointed to the fact that including a great quantity of initiator may lead to leaching of initiator/by-products that may also produce a toxic response.

#### *4.3.1.7 Microparticle Surface Characterisation*

Time of flight secondary ion mass spectrometry (ToF-SIMS) analysis was conducted to investigate the surface chemistry of the microparticles produced. The data was collected in both positive and negative secondary ion mode in order to determine unique ions associated with the polymer surfactants. Unique identifiers for the majority of the hydrophobic comonomers were identified for the surfactants and they were presented in the Scheme 4.1.



Scheme 4.1 structures of the monomers and their representative ions (both positive and negative secondary ion mode) emerged during ToF-SIMS analysis.

From Scheme 4.1, 15 identifiers out of the 16 different surface chemistries on MPs were successfully identified from the analysis of the ToF-SIMS spectra. However, for MPs characterised by the surface with HA-co-mPEGMA<sub>300</sub>, it was difficult to find differences from the SIMS spectra of the core HMDA material. The similarity between both spectra, characterised by ions derived from acrylate group and hydrocarbon fragments, is expected due to the similar chemical structure between HA and HMDA. For example, they both have the hydrocarbon chain composed by 6 carbon atoms. For this material, the unique ion considered is the one attributed to mPEGMA fragments ( $C_3H_7O^+$ ), which could also be used as an ion for all surfactants that is unique when compared to the core chemistry.

No characteristic peak could be identified for the HMDA core polymer. However, particles prepared with surfactants were compared with the HMDA core particle prepared without surfactant to demonstrate the

difference between the unfunctionalized and functionalised particles. This was achieved utilising the representative ions of both the hydrophobic monomers and mPEGMA<sub>300</sub>. This data is presented in Figure 4.12.

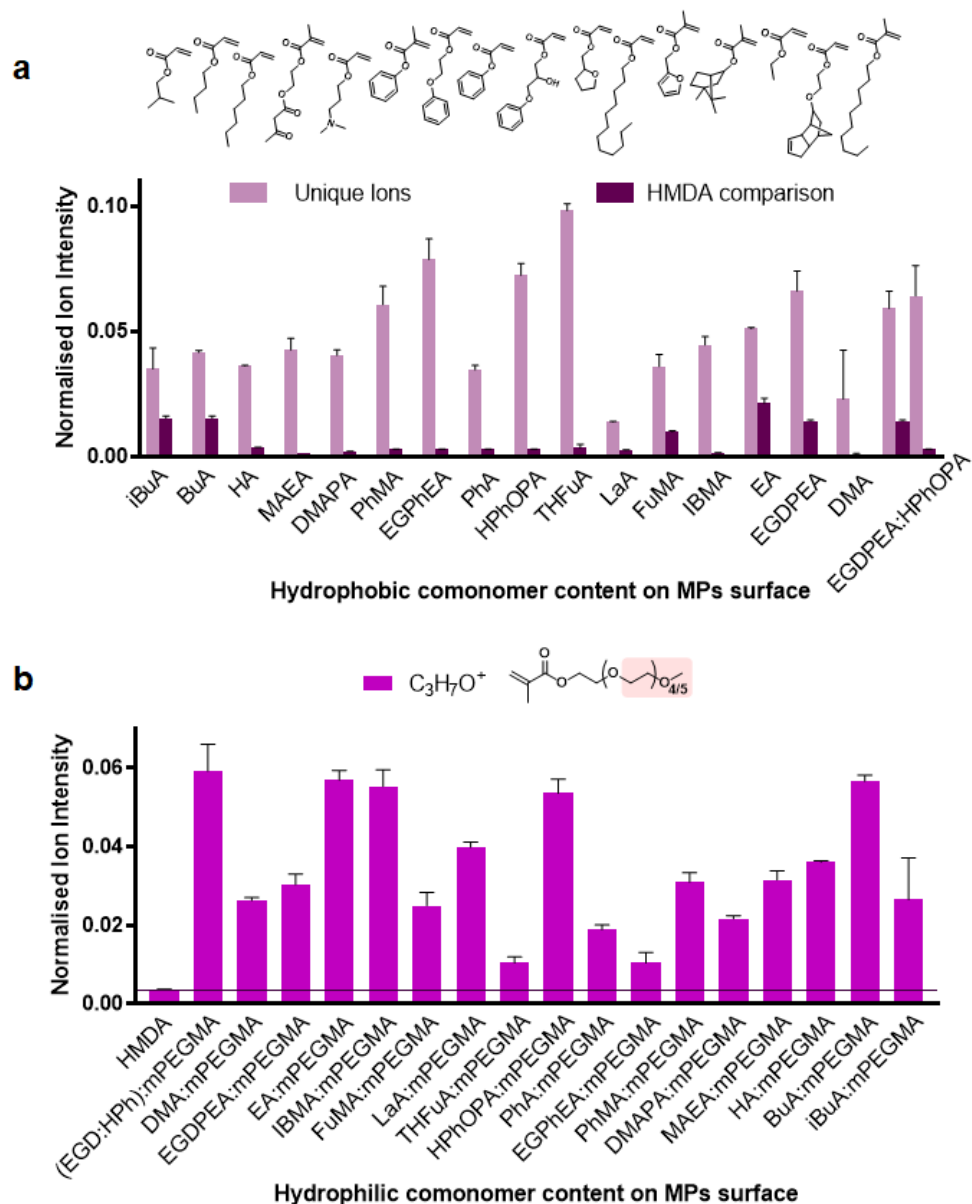


Figure 4.12 ToF-SIMS data showing intensities of: a) the key ions associated to the hydrophobic comonomers within the surfactant structures compared to the intensity of the same ions present in the HMDA spectra and b) the key ion associated to mPEGMA<sub>300</sub> ( $C_3H_7O^+$ ) present on the surface of each MPs. Ion images for each MPs are shown in Figure Appendix 4-1.

In Figure 4.12a and Figure 4.12b, the comparison of the ‘hit’ particles with the plain core HMDA particle clearly demonstrated that the identified ions

are unique to the individual surfactants and, therefore, it showed that the surfactant is located at the surface of the particles. Thus, these observations confirmed that functionalising the surface with the biologically active material of choice has been successfully achieved. Similarly, the indicative ion of the mPEGMA<sub>300</sub> chain ( $C_3H_7O^+$ ) can, also, be found at the surface of the functionalised particles and significantly different when compared to the no surfactant plain HMDA core. It was also demonstrated that the EGDPEA-co-mPEGMA<sub>300</sub> and HPhOPA-co-mPEGMA<sub>300</sub> mixed surfactant microparticles exhibited both the unique ions for both surfactants ( $C_5H_7^+$  and  $C_6H_5O^-$ ) on the particle surface, indicating that surfaces with mixed surfactants was successful produced.

These results establish the concept that, by using bespoke, bio-instructive, functionalised surfactants, polymer microparticles can be manufactured with specific targeted surface chemistry. Therefore, such particles should allow for specific surface chemistry structures to be tested on a 3D scale that was not previously possible.

#### 4.3.2 Biological Performance of Functionalised Polymer Microparticles

After confirmation that the surface chemistry could be tailored by using the synthesised surfactants, a screening experiment was performed to determine whether the presence of a surface-located surfactant layer was enough to modify the biological performance. As previously mentioned in the introduction of this chapter, the interest of this project has been focused

on novel materials that can control bacterial attachment, subsequently biofilm formation, as well as materials that enhance the correct attachment of fibroblasts. The monomers that have been shown to deliver these properties via microarray HT screening (within the Next Generation Biomaterials Programme Grant) were chemically incorporated in the surfactants backbone and then two tailored 3D in-vitro cell (mammalian cells and bacteria) attachment assays were developed as an initial proof of concept of the hypothesis.

#### 4.3.2.1 Bacterial Biofilm Formation Assay

By combining a series of new HT methods along with the combinatorial screening, Hook et al. discovered a new class of Bacteria Attachment Resistant (BAR) (meth)acrylate polymers.<sup>179,263</sup> Among these, EGDPEA and HPhOPA were selected for the purpose of this study within this thesis project as example of bacterial anti-attachment and pro-attachment control polymers, respectively. *P. aeruginosa* was selected as a representative of Gram-negative pathogens because it is frequently found in medical device-associated infections and it has been intensively investigated with respect to biofilm development.<sup>339,340</sup> It is known that *P. aeruginosa* cells, suspended in a liquid environment, can attach/detach on/from a surface and/or stay and explore the surface by ‘walking’ or ‘crawling’ (Figure 4.13 – stage 1). This behaviour can be affected by the type of pilus and pilus motility functions.<sup>341</sup> When irreversible attachment occurs (Figure 4.13 – stage 2-3), the development of a mature biofilms starts. In this step,

aggregated cells embed in a self-generated extracellular matrix, containing exopolysaccharides (EPS, e.g. Psl and Pel in *P. aeruginosa*), proteins, lipids and extracellular DNA (eDNA) and engaging in physical and social interactions distinct from those of free-living bacterial cells (Figure 4.13 – stage 4).<sup>339,342,343</sup> In addition, Lee, Vachier et al. demonstrated that the production of EPS is considered to be the dominant mechanism driving irreversible attachment of *P. aeruginosa* strain PAO1 lineages, used in this project.<sup>344</sup>

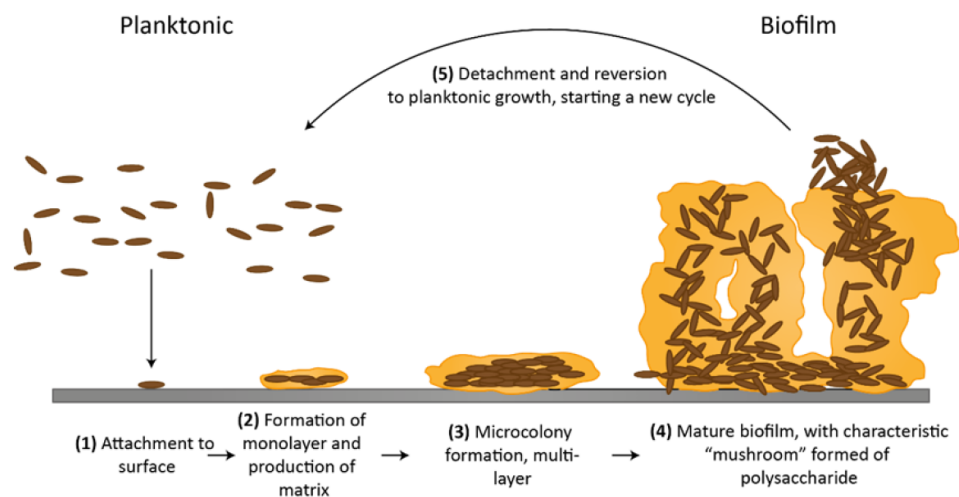


Figure 4.13 Schematic representation of biofilm formation. Biofilm formation can be divided into five stages: Initial reversible attachment (1), irreversible attachment (2-3), maturation (4) and dispersion (5). During later stages, the biofilm is mature, forming characteristic “mushroom” structures due the polysaccharides. Finally, some cells start to detach, and the biofilm (shown in yellow) will disperse.<sup>345</sup>

Crosslinked particles (10 mg in each well) produced with the aid of these two materials, were cultured with fluorescently labelled *P. aeruginosa* (PAO1-N mcherry) in RPMI medium for 24 h under agitation at 60 rpm. Data was acquired using confocal microscopy to measure the fluorescence intensity of the bacteria. The analysis of attachment/biofilm levels was performed using a computer script that discarded any background fluorescence and only measured fluorescence associated with the particles.

This was conducted using both brightfield and fluorescence images. Finally, the data was normalised for particle surface area and compared to the non-surfactant HMDA control. The variation in biological performance related to modifying the surface chemistry *via* the choice of surfactant used is exemplified in the data presented in Figure 4.14a.

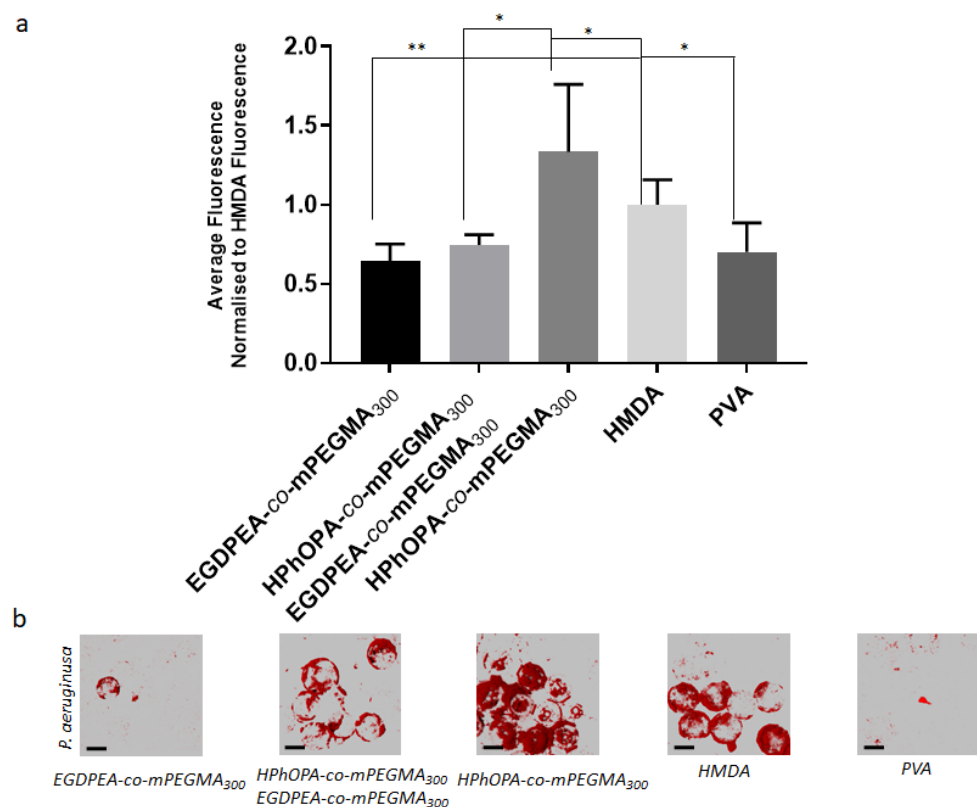


Figure 4.14 a) Surface coverage by single species (*P. aeruginosa*) biofilms quantified after 24 h incubation on particles coated with EGDPEA-co-mPEGMA<sub>300</sub>, HPhOPA-co-mPEGMA<sub>300</sub>:EGDPEA-co-mPEGMA<sub>300</sub>, HPhOPA-co-mPEGMA<sub>300</sub>, none and PVA surfactants respectively in RPMI. Quantification was performed on fluorescence images acquired on the 48 well-plate considering an area of 568 x 568  $\mu\text{m}$ . Error bars equal  $\pm 1$  SD unit,  $n = 3$ . Particle data were normalised for surface area and then to the non-surfactant (HMDA) control for comparison b) confocal microscopy images for mcherry tagged *P. aeruginosa* growing on each polymer surface. Each image is 295 x 295  $\mu\text{m}$ .

The Figure 4.14 shows a number of functionalised MPs performed in a bacteria-attachment assay experiment under agitated culture. In the case of HPhOPA-based surfactant MPs, which homopolymer had been shown to

promote bacterial attachment in the 2D microarray assay, they exhibited the greatest amount of biomass on the surface. Also, when compared to the EGDPEA-based surfactant MPs and no surfactant (HMDA) control sample the level of biofilm was higher than 2.2- and 1.3-folds, respectively. The mixed surfactant surface ((EGDPEA-*co*-mPEGMA<sub>300</sub>):(HPhOPA-*co*-mPEGMA<sub>300</sub> 50:50 wt/wt)) had a similar level of *P. aeruginosa* attachment as the anti-attachment EGDPEA based particles. This bacteria inhibition might be due to the difference in  $M_n$  of the two amphiphilic copolymers (where EGDPEA-*co*-mPEGMA<sub>300</sub> and HPhOPA-*co*-mPEGMA<sub>300</sub> have a  $M_n$  of 16,000 g mol<sup>-1</sup> and 26,890 g mol<sup>-1</sup>, respectively). This has led to a higher concentration of the anti-attachment material on the surface. PVA has also shown to prevent effectively biofilm formation on the surface effectively, and this corresponds with previous literature.<sup>230,346</sup> In fact, surface-located water-soluble PVA has been proposed to induce surface hydration via hydrogen bonding. A tightly bound layer of water molecules near the surface is known to generate a physical and energetic barrier able to prevent stable bacterial attachment.<sup>347,348</sup>

In order to confirm that the variation in biological performance of 3D particles could be directly attributed to the surface chemistry, rather than the 3D topography of the particles, a similar assay was conducted to 2D systems. A series of 2D films of the homopolymers of EGDPEA and HPhOPA were prepared, and a *P. aeruginosa* attachment/biofilm assay was conducted (Figure Appendix 4-2).

When considering bacteria-material surface interactions, the outcome will be determined by a combination of the physicochemical factors in the near-surface environment and bacterial surface sensing.<sup>349</sup> The underlying anti/pro-attachment mechanism involved with this new class of BAR (meth)acrylate materials is still not fully understood and still under investigation. However, for *P. aeruginosa* it is clear that BAR materials inhibit biofilm formation by blocking the transition from reversible to irreversible attachment (Carabelli, A.M. Ph.D Thesis University of Nottingham, 2019).

Generally, attempts to correlate bacterial biofilm formation with surfaces of materials *in-vitro*, the hydrophobic/hydrophilic nature of such surfaces and their wettability is widely studied.<sup>344,350,351</sup> In early biomaterials science, water contact angle (WCA) was the most readily available measurement technique, with the most specific measurement of surface chemistry.<sup>352</sup> Given that, hydrophilic materials are usually thought to be best for resisting bacterial adhesion. In fact, as the hydrophilicity of a surface increases, the displacement of water interphase requires an amount of energy (free energy) that controls the maximum amount of protein that can be adsorbed.<sup>353</sup> Ultimately, this leads to reduced protein adsorption near an adsorbent water wettability.<sup>354</sup> In the lack of this conditioning protein layer, fundamental to the promotion of the interaction between the material surface and cell, the attachment of bacteria is not favoured.

However, in the last decade, with the advance of new surface analytic techniques, as x-ray photoelectron spectroscopy and static secondary ion

mass spectrometry (SIMS), other parameters have been considered besides wettability.<sup>355</sup> In fact, structural parameters like polymer chain density and thickness as well as chain conformation can control the bioactivity of the surface.<sup>356–359</sup> Looking at *P. aeruginosa* attachment and biofilm formation, Sanni et al.<sup>262,360</sup> found that, for these new BAR class of polymers, there was no relationship with water contact angle in the narrow range of materials considered which constituted those found to resist biofilm formation (in the range of 80° – 90°).<sup>262,360</sup> They noted instead that parameters related to the hydrophobicity (clog P) and molecular flexibility (number of rotatable bonds= $nR_oTB$ ) when combined in the alpha parameter ( $\alpha=0.44nR_oTB-c \log P$ ) strongly correlated with resistance to attachment and subsequent biofilm development. Only recently, M. Alexander and co-workers have adopted multilinear regression model to determine the ability of different parameters to describe bacteria attachment propensity on surfaces.<sup>361,362</sup> WCA, ToF-SIMS ions and molecular descriptors have been used to describe the attachment and biofilm formation of *P. aeruginosa*, *Staphylococcus aureus*, and *Escherichia coli* across a large and diverse polymer library. In the multipathogen model, it was seen that WCA, thus, the wettability of surfaces, had an insignificant contribution to the prediction process. On the other hand, it was demonstrated that the richness of TOF-SIMS structural information and the descriptors analysis can clearly control factors for biofilm formation in these large diverse polymer libraries.

In the attempt to rationalise the bacteria attachment results observed in this present work, they were related to literature reports.<sup>363–366</sup> In some cases, the adhesion of proteins to surfaces is highly desired to generate surfaces with enhanced biocompatibility. In other cases, the strong adhesion of proteins and other biomolecules, with the concomitant incorporation of cells, might lead to the formation of thick microorganism biofilms with vary composition depending on the surrounding environment.<sup>366</sup> Recently, many studies have been undertaken to understand the main requirements to make a bioactive and anti-fouling surface. Firstly, the high hydrophilicity, usually provided by polymers like PEG, plays a key role in the resistance of non-specific protein adsorption and cell adhesion.<sup>296,367,368</sup>

An initial proof of concept, to probe the possible event of the connection between the protein and bacteria attachment on these BAR materials, was performed. A novel analytical method was developed to see the difference in protein attachment among the 3D structures used previously in the bacteria attachment assay. Bovine serum albumin (BSA) has been used as the protein model being ubiquitous in different tissue and organs. The BSA extraction was applied following the same methodology previously reported by Meurs et al., in which different ion sequences of different proteins present in urine samples have been detected by Mass Spec after a liquid extraction.<sup>338</sup> In Figure 4.15, it is reported the variation in protein attachment described as % of Sequence Peptide Coverage, which represents the summed length of each peptide peaks divided by the total

protein length expressed as percentage. Each peptide peak has been searched against theoretical peptides using MATLAB software.

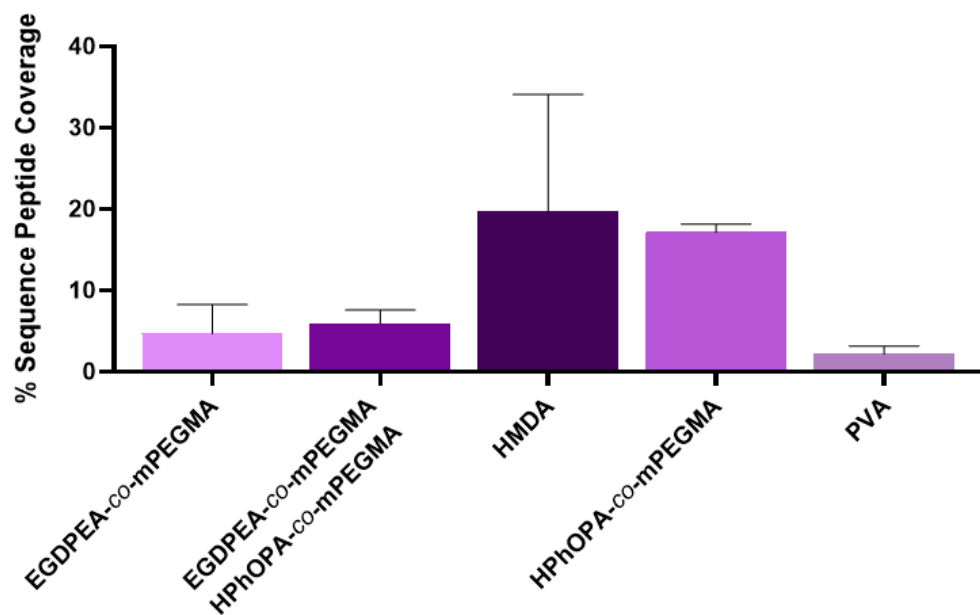


Figure 4.15 % Sequence Peptides Coverage of BSA quantified after overnight protein extraction and digestion from particles coated with EGDPEA-co-mPEGMA<sub>300</sub>, EGDPEA-co-mPEGMA<sub>300</sub>:HPPhOPA-co-mPEGMA<sub>300</sub>, HPPhOPA-co-mPEGMA<sub>300</sub>, none (HMDA core alone) and PVA surfactants. Quantification was performed using nanoESI-MS/MS and ion mass peaks in the mass spectra were confronted with tabled peptides mass ions. Error bars equal  $\pm 1$  SD unit,  $n = 3$ ).

Interestingly, from this attempt to experimentally link the protein attachment to the bacteria attachment results, a similar trend can be observed between the two set of data. In particular, both the anti-attachment model PVA and EGDPEA particles have shown the lowest level of BSA covering compared to the rest of the structures. This means that they have shown the lowest number of peptides sequence in their mass spec. The low presence of BSA conditioning film on PVA has been already reported in many previous literature examples. In fact the high hydrophilicity of this macromolecule tightly bound layer of water molecules near the surface, acting as a physical and energetic barrier, able to prevent stable protein adsorption (Figure Appendix 4-3a).<sup>347,348</sup> Similar mechanistic

effect has been extensively observed for poly(ethylene glycol) (PEG) and oligo(ethylene glycol) (OEG) based materials.<sup>336,369</sup>

At this stage, these results are hinting that there might be a correlation between the two different biological attachments (Figure Appendix 4-3b). However, further investigations will be needed as this method studies the protein concentration as a result of an extraction from a surface and it does not give direct information of the actual surface of the particles. Future work might involve the use of surface analysis (such as ToF-Sims dept profiling and Orbi-Sims) to corroborate or reinterpret this set of data.

#### 4.3.2.2 Human Skin Fibroblasts Attachment and Proliferation

Three-dimensional cell aggregate in vitro culture platforms have been particularly useful for both large-scale expansion and lineage-specific differentiation of stem cells.<sup>370–372</sup> Co-cultures of cells with MPs is a growing field as these latter have shown to increase control over cell phenotype and improve the scalability of cell culture thanks to the higher surface area-to-volume ratios compared to 2D surfaces.<sup>370</sup> The work reported here aimed to further use these chemically functionalised MPs as platform to grow human skin fibroblasts (CRL-2522, ATCC) (HF) *in vitro*.

As for previous literature study on the screening of new (meth)acrylates material for the attachment of bacteria and pluripotent stem-cells,<sup>178,183</sup> a big interest has been to extend the same (meth)acrylate monomer library to different biological responses. In particular, one of the interests has been to target new materials that can support fibroblast attachment,

proliferation and differentiation through the appropriate process of the restoration of functional tissue and prevent unwanted fibrosis. In fact, fibrosis and loss of function of both the host tissue and medical implant can happen when a remodelling fibroblast, known as a myofibroblast: a) continues to receive activation cues, long after it is no longer needed; b) experiences epigenetic alterations, that inhibit its normal programmed apoptosis/dedifferentiation.<sup>326</sup> On this extent two 'hit' materials were selected. These materials showed good human skin fibroblast attachment/proliferation from a 2D microarray screening. However, they promote anti-fibrotic and fibrotic responses. These materials are THFuA (anti-fibrotic) and EGPhEA (pro-fibrotic) which were copolymerised and characterised with mPEGMA<sub>300</sub> (Chapter 3) and were used as surfactant in the microfluidics processing (Chapter 4). The main interest of the present study was to identify only any differences led by the particles surface chemistries, monitored by observing changes in cell attachment and proliferation. Any study focused on the expression of the protein  $\alpha$  Smooth Muscle Actin ( $\alpha$ SMA) was not reported as it is not of interest for this work. The protein  $\alpha$ SMA is usually expressed by an activated myofibroblast, when stimulated with key growth factors, such as TGF- $\beta$ . The presence of  $\alpha$ SMA hints that the process of wound healing is progressing towards pathologic scar and/or fibrosis of the tissue.<sup>324</sup>

Before the cell attachment and proliferation assay, a viability study was conducted on both the particles using human skin fibroblasts (CRL-2522, ATCC) (**Error! Reference source not found.6**).

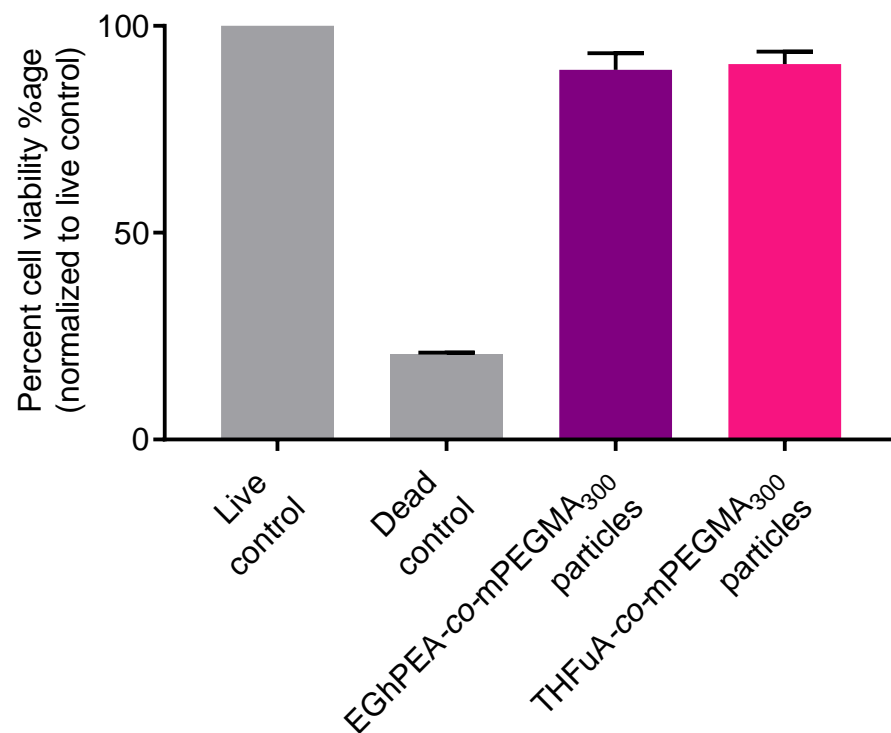


Figure 4.16 ToxiLight™ non-destructive cytotoxicity bioassay study using human skin fibroblasts (CRL-2522, ATCC). The assay measures the release of adenylate kinase (AK) from cells with compromised cell membranes. The AK catalyses conversion from ADP to ATP is detected through bioluminescence and the emitted light intensity is linearly related cell viability.  $n=6$ ; ANOVA;  $p<0.05$ .

**Error! Reference source not found.** shows that when using both chemistries, no dropping in viability of the cells was observed, when compared to the live positive control, as assessed by the Adenylate Kinase Activity Assay. The high viability confirmed that these materials exhibited low toxicity as it was previously proved with EGDPEA-co-mPEGMA<sub>300</sub> based particles. Once the biocompatibility of these materials was confirmed, cell attachment and proliferation studies were performed on the same set of materials (Figure 4.177).

Figure 4.17 Human skin fibroblasts (CRL-2522, ATCC) attachment using CyQuant NF Assay, 24 h post seeding [ $n=6$ ; analysis of variance (ANOVA);  $p \leq 0.05$ ] on polymer MPs in comparison to tissue culture plastic (PS flat). On the bottom confocal images of the human

*skin fibroblasts attachment obtained fixing (with PFA 4%) and staining with Phalloidin 488 and DAPI. b) Human skin fibroblasts (CRL-2522, ATCC) proliferation over 72 h using Click-iT™ Edu microplate assay [n=6; analysis of variance (ANOVA);  $p \leq 0.05$ ] on polymer MPS in comparison to tissue culture plastic (PS flat).*

In Figure 4.177 is possible to observe that the pro-fibrotic particles (i.e. EGPhEA-based surfactant MPs) had significantly lower cell attachment and lower proliferative potential (+TGF- $\beta$ 1) than the anti-fibrotic particles (ie. THFuA-based surfactants MPs). In particular, HFs proliferates readily when cultured with THFuA-co-mPEGMA<sub>300</sub> based particles, showing almost a 2-fold increase in cell proliferation compared to both the tissue culture plastic, the positive control of the assay, and the EGPhEA-co-mPEGMA<sub>300</sub> based MPs. However, there is no statistically significant differences between the cell proliferation of the Polystyrene (PS) flat control and the EGPhEA particles. It has been speculated that the differences in cell proliferation between the two different particles might be due an incorporation/interaction of growth factor (present in the medium) within the pro-fibrotic particles which hindered the proliferation of the cells. These preliminary results demonstrated the role that surface chemistry plays in modulating fibroblasts adhesion/proliferation and how this can be affected through the use of bespoke polymer surfactants with judiciously chosen chemistries.

Due to time limitations related to 19-COVID restriction, ongoing investigations, within the programme grant, are currently performed on the differentiation of fibroblast into myofibroblast on 3D to confirm the ability of these bio-instructed particles to perform as pro- and anti-fibrotic system.

## 4.4 Conclusions

In this chapter, for the first time, custom-made biological active surfactants were employed for the stabilisation of O/W emulsions into a droplet microfluidics device. This is the first example of bespoke surfactants, with target chemistry, applied in a microfluidics device that deliver the fabrication of 3D functionalised crosslinked MPs. Being at the oil/water interface, these surfactants stick to the droplets surface conferring a target biological activity to the manufactured MPs. In fact, as demonstrated in this chapter, the presence of this 'active' surface layer plays a key role in the biological-material interactions with human cells and bacteria.

The microfluidics process adopted revealed to be effective in producing particles in a continuous flow with control over sizes, shapes and chemical nature. In fact, surface morphology studies conducted on these MPs, performed utilising SEM imaging, showed mostly spherical and smooth particles with sizes of around 60  $\mu\text{m}$  and a CV of around 5% for most of them. ToF-SIMS analysis was performed in order to assess the surface chemistry of the particles. SIMS spectra confirmed the presence of unique ions enabling the quantification and the comparison of the same peaks with HMDA core materials only particles. In addition, mPEGMA<sub>300</sub> showed a characteristic ion ( $\text{C}_3\text{H}_7\text{O}^+$ ) and its presence was observed in each surface chemistry. Both SEM and ToF-SIMS analysis successfully showed the presence of the target chemistries on the outermost layer of interest.

Therefore, the ability of the MPs to affect biological response was tested using *P. aeruginosa* as a bacterial model and human skin fibroblast as a human cellular model. From the different biological results, it was shown how (meth)acrylate polymers modify the behaviour of bacteria and cells on surfaces both on individual particle surfaces as well as previously demonstrated coating applications. This also provides evidence that these (meth)acrylate polymers, when incorporated into surfactants, can be used to functionalise surfaces which would be impossible with the original homopolymer.

All this data taken together revealed that the microfluidics process can be used as a powerful technology for the production of surface bio-instructed MPs. The main advantages of the reported approach lied on the use of functionalised bespoke surfactants to enable the biologically on-demand production of smooth and monodisperse particles.

## 4.5 Appendix

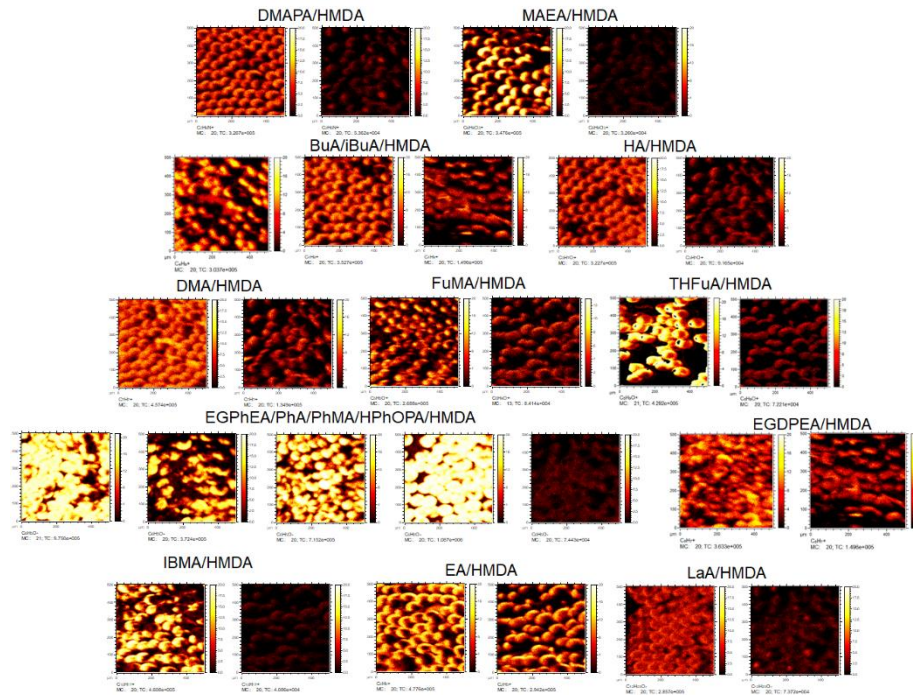


Figure Appendix 4-1 Ion images associated to the unique ions of the ‘hit’ hydrophobic comonomers (HyB-co-mPEGMA<sub>300</sub>) used for the synthesis of the surfactants library.

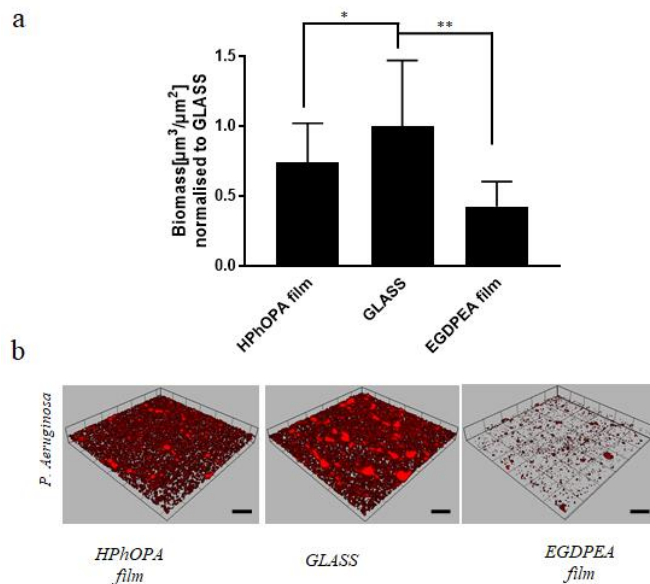


Figure Appendix 4-2 (a) Surface coverage by single species (*P. aeruginosa*) biofilms quantified after 24 h incubation in RPMI on an EGDPEA or HPhOPA homopolymer film respectively or on glass. Error bars equal  $\pm 1$  SD unit,  $n = 3$ . Film data were normalised to a glass control for comparison (b) The corresponding confocal microscopy images for mcherry tagged *P. aeruginosa* growing on each polymer surface and glass control. Each image is  $568 \times 568 \mu\text{m}$ .

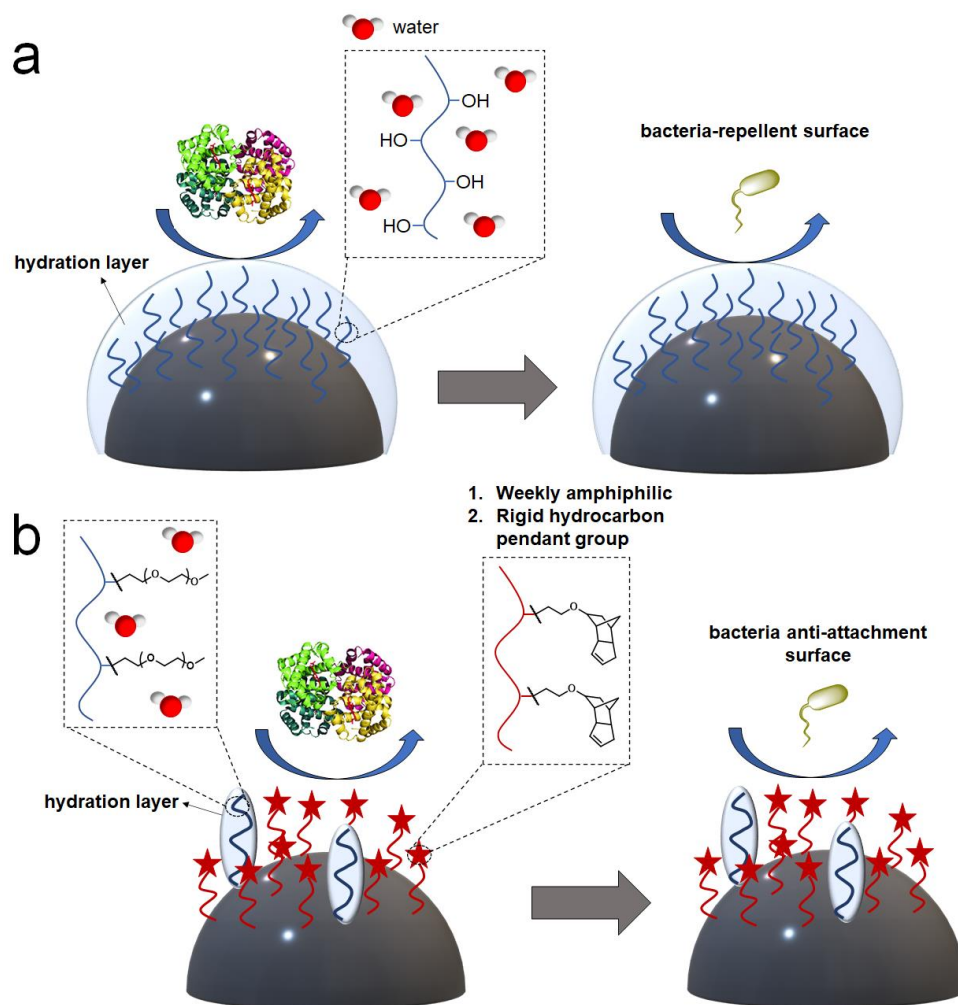


Figure Appendix 4-3 a) Schematic diagram of the protein and bacteria attachment for MPs obtained using PVA as surfactant. The high hydrophilicity of PVA tightly bound layer of water molecules near the surface (hydration layer), acting as a physical and energetic barrier for protein and bacteria. b) Schematic diagram of the bacteria attachment for the MPs obtained using EGDPEA-co-mPEGMA<sub>300</sub> as surfactant.

## 5 Synthesis and Characterisation of Amphiphilic Copolymers Using an Alternative Hydrophilic Monomer: Replacing PEG Side Chain with a Tertiary Amine

### 5.1 Introduction

The focus of this chapter resides in the initial design and synthesis of novel block and random amphiphilic copolymers, in the study of their 3D architectures and in the utilisation of an alternative model hydrophilic comonomer. In this chapter, the neutral graft PEG based hydrophilic monomers, used in the synthesis of the amphiphilic copolymers discussed up to this point, were replaced with a methacrylic monomer with a tertiary amine functionality in the side chain. The latter allowed the polymer backbone to bear a positive charge (when the appropriate external pH is applied). This charge might affect the biological responses of the resultant microfluidic particles surface layer represented by the surfactants. In fact, cationic polymers are extensively used in a variety of biological applications, for example gene and drug delivery, thanks to their ability to form electrostatic complexes with the anionic biomolecules, such as deoxyribonucleic acid and proteins.<sup>373</sup> In addition, the inherent bioactive properties exhibited by cationic polymers, which includes stimuli responsiveness, antimicrobial, antioxidant, antitumor and anti-inflammatory activity increase the promise of being able to deliver

further/additional enhanced therapeutic potential.<sup>374–377</sup> Among cationic polymers, chitosan, poly(ethyleneimine) (PEI), poly-L- (lysine) (PLL) and poly[2-(N,N-dimethylamino)ethyl methacrylate] (PDMAEMA) have been all widely adopted.<sup>378–380</sup> For the purpose of this study, the PEG moieties was replaced with the 2-(N,N-dimethylamino)ethyl methacrylate (DMAEMA) which was copolymerised with three hydrophobic (HyB) monomers selected from the library of monomers used in the previous surfactants synthesis. EGDPEA,<sup>179</sup> HPhOPA<sup>179</sup> and EA<sup>381</sup> were used as biological active model monomers.

In this chapter, the effect of the 3D polymer architecture upon the copolymers ability to the self-assembly was, also, studied in addition to the influence of chemical nature of the hydrophilic comonomer. In the previous chapters, random comb-graft copolymers were synthesised using a *grafting through* strategy, where PEG macromonomers were copolymerised with the bioactive HyB monomer of interest. Here, both random and block copolymers were produced and studied for their performance as surfactants in the microfluidics process. It has been shown that block or statistical (random) cationic copolymers can assume different structures when self-assembling in aqueous media. Block copolymers have been reported to form well-defined core-shell structure promoted by intermolecular interactions, more specifically a core of hydrophobic blocks surrounded by flexible hydrophilic blocks.<sup>382,383</sup> On the contrary, random copolymers form less defined self-assembled structures, since the interactions with the media and the hydrophobic and charged groups can,

in some cases, occur in the same region of the polymer chains in certain areas of the polymer.<sup>384,385</sup>

### 5.1.1 Aim and Objectives

In this chapter, the main aim was the synthesis of random and block amphiphilic copolymers, by using two different radical polymerisation techniques. Then, their ability to self-assemble in water and to act as surfactants into the O/W microfluidics setup, previously reported, was compared. As these copolymers are formed from a biological active hydrophobic monomer and a positively charged hydrophilic counterpart, their ability to bind to proteins, as a first indication on cell and bacteria attachment, was studied. The study of the protein binding properties was performed to assess the formation of a conditioning layer between the polymeric NPs and these biomacromolecules. As mentioned in the previous chapter, this layer becomes fundamental to the promotion of the interaction between the surface of the implants and cells. Bovine serum albumin (BSA) was selected as the protein model being ubiquitous in different tissue and organs. The design and development of the synthesis along with the microfluidics process, as well as the study of proteins interaction was achieved by completing the following objectives:

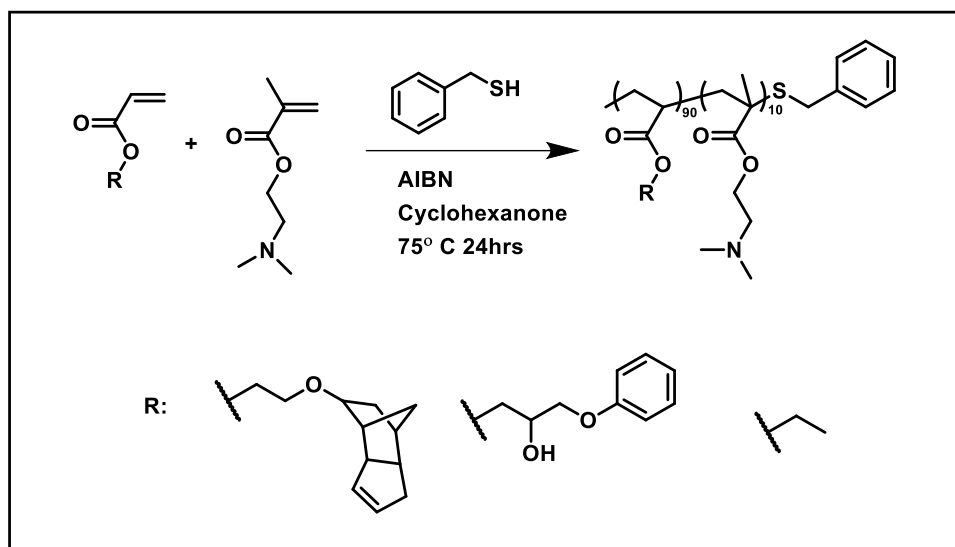
- Thiol-mediated Free Radical Polymerisation was used to synthesise random copolymers in order to maintain the rationale with the design of the synthesis in the previous chapters.

- Atom Transfer Radical Polymerisation (ATRP) was selected for the synthesis of the block copolymers. This technique required the use of 2 steps reaction process: a) the synthesis of the macroinitiator and b) the growth of the second block DMAEMA.
- DLS and Zeta Potential analysis were used to obtain the CAC of the amphiphilic copolymers and the superficial charge, once they had been formulated as nanoaggregates.
- Protein Corona Binding Assay was performed to study the level of interaction of the nanoaggregates with the BSA protein model.
- Optimisation of flow rates of aqueous and organic phase was performed to set the appropriate microfluidics conditions to achieve the production of microparticles (MPs).
- SEM and ToF-SIMS characterisation were assessed to study size, morphology and surface chemistry on the produced MPs.

## 5.2 Methods

### 5.2.1 Thiol-mediated Free Radical Polymerisation

The general procedure adopted for the polymerisations, as shown in Scheme 5.1, is detailed below.



Scheme 5.1 Reaction Scheme of the Thiol-mediated Free Radical Polymerisation

The protocol for the synthesis of the random copolymers, EGDPEA-co-DMAEMA, HPhOPA-co-DMAEMA and EA-co-DMAEMA *via* Thiol-mediated Free Radical Polymerisation was developed as follow. The appropriate quantities of the monomers (EGDPEA:DMAEMA 2.33g:0.16g; HPhOPA:DMAEMA 1.598g:0.157g and EA:DMAEMA 1.71g:0.29g) required to reach the targeted molar ratios, 90:10 % mol/mol, were introduced into a the required volume of cyclohexanone with stirring, such that a 1:3 v/v ratio mixture was achieved. The thiol CTA, benzyl mercaptan (BzSH) was added at the concentration of 3% mol with respect to the monomers. The initiator, AIBN (0.5% wt/wt with respect to the monomers) was, first, dissolved in cyclohexanone and degassed separately prior to being added to the reaction mixture. Finally, the reaction vessel and the AIBN solution were degassed in ice bucket purging argon using a standard Schlenk line for at least 1 h. To commence the reaction, the temperature was raised up to 75°C in an oil bath and was continued stirring for 18 h. Polymer purification was

conducted *via* precipitation into an excess of heptane. The usual non-solvent:reaction media ratio was 5:1 v/v in order to enhance the precipitation process and, finally, the precipitated materials were collected in a vial and left in a vacuum oven at 25°C for at least 24 h.

<sup>1</sup>H-NMR spectroscopic analysis was performed on the crude polymerisation solution to determine polymer conversion and, finally, on the precipitate to establish the actual monomer ratio of the final copolymer composition. To evaluate the MWt of the materials, the purified samples were dissolved in HPLC grade THF for GPC analysis. All the spectra data presented were collected at 400 MHz in CDCl<sub>3</sub> and values are quoted as δH ppm. The <sup>13</sup>C-NMR and the <sup>1</sup>H-NMR spectra of the copolymers are showed from Figure Appendix 5-2 to Figure Appendix 5-7.

<sup>1</sup>H-NMR of the EGDPEA-*co*-DMAEMA purified (400 MHz, CDCl<sub>3</sub>) δ (ppm): 5.69-5.47 (2H, CH=CH, m), 4.15 (4H, OCH<sub>2</sub>CH<sub>2</sub>, m), 3.60-3.16 (24H, CH<sub>2</sub>CH<sub>2</sub>OCHC<sub>9</sub>H<sub>12</sub>), 2.30 (6H, NCH<sub>3</sub>CH<sub>3</sub>) 2.51-0.95 (10H, C<sub>7</sub>H<sub>10</sub>, m).

<sup>13</sup>C-NMR of the EGDPEA-*co*-DMAEMA purified (400 MHz, CDCl<sub>3</sub>) δ (ppm): 174 (C=O), 132-130 (CH=CH), 82.56 (OCHC<sub>9</sub>H<sub>12</sub>), 65.70 (OCH<sub>2</sub>CH<sub>2</sub>), 63.31 (OCH<sub>2</sub>CH<sub>2</sub>), 55.15-28.60 (C<sub>9</sub>H<sub>12</sub>), 45.67 (NCH<sub>3</sub>CH<sub>3</sub>).

<sup>1</sup>H-NMR of HPhOPA-*co*-DMAEMA purified (400 MHz, CDCl<sub>3</sub>) δ (ppm): 7.22-6.87 (5H, C<sub>5</sub>H<sub>5</sub>, m), 4.49-3.71 (7H, OCH<sub>2</sub>HOHCH<sub>2</sub>O and OCH<sub>2</sub>CH<sub>2</sub>, m), 3.50 (18H, CH<sub>2</sub>CH<sub>2</sub>O OCH<sub>2</sub>CH<sub>2</sub>O, m), 3.40 (<sup>3</sup>H, OCH<sub>3</sub>, m).

<sup>13</sup>C-NMR of the HPhOPA-*co*-DMAEMA purified (400 MHz, CDCl<sub>3</sub>) δ (ppm): 174 (C=O), 129, 121.13 and 114.46 (C<sub>6</sub>H<sub>5</sub>), 68.54 (OCH<sub>2</sub>CHOH), 68.07 (OCH<sub>2</sub>CHOH), 59.08 (OCH<sub>3</sub>).

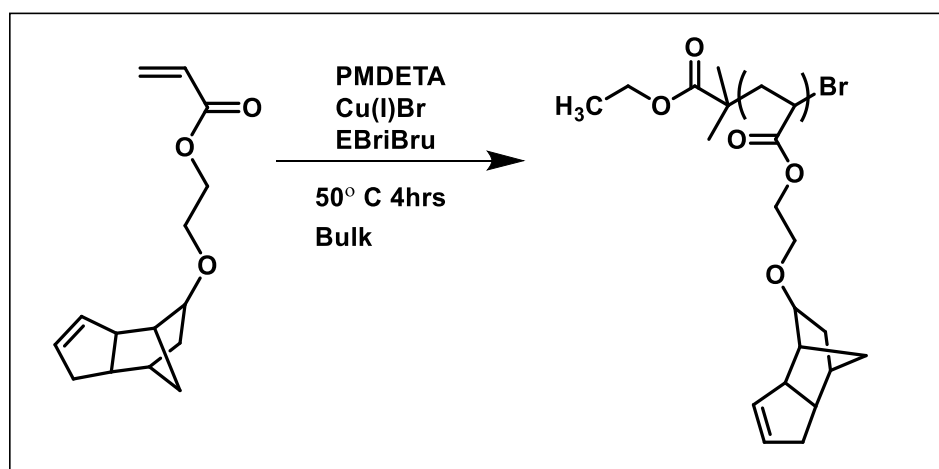
$^1\text{H-NMR}$  of EA-co-DMAEMA purified (400 MHz,  $\text{CDCl}_3$ )  $\delta$  (ppm): 4.12 (4H,  $\text{C}=\text{OOCH}_2$ , m), 2.55 (2H  $\text{CH}_2\text{CH}_2\text{N}$ , s), 2.28 (6H,  $\text{NCH}_3\text{CH}_3$ , s), 1.26 (3H,  $\text{OCH}_2\text{CH}_3$ , m).

$^{13}\text{C-NMR}$  of EA-co-DMAEMA purified (400 MHz,  $\text{CDCl}_3$ )  $\delta$  (ppm): 174 (C=O), 63.09, ( $\text{C}=\text{OCH}_2\text{CH}_2$  DMAEMA), 60.25 ( $\text{C}=\text{OCH}_2\text{CH}_3$ ), 56.77 ( $\text{C}=\text{OCH}_2\text{CH}_2$  DMAEMA), 45.80 ( $\text{NCH}_3\text{CH}_3$ ), 14.077 ( $\text{OCH}_2\text{CH}_3$ ).

## 5.2.2 ATRP of EGDPEA-*b*-DMAEMA

### 5.2.2.1 Synthesis of EGDPEA Macroinitiator

The general procedure adopted for the polymerisation, as shown in Scheme 5.2, is detailed below.



Scheme 5.2 Reaction scheme for the synthesis of poly(EGDPEA)

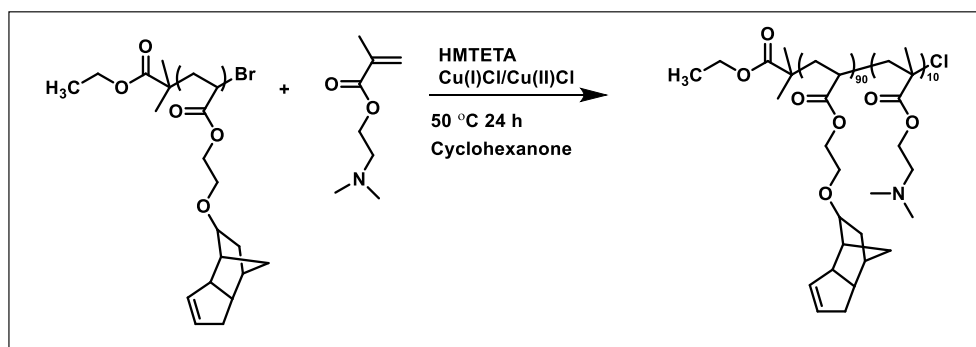
The macromonomer based on EGDPEA was synthesised using the following procedure. The molar ratios were calculated and quoted with respect to the initiator level. The initiator, the ligand, EGDPEA and Cu(I)Br were in molar ratios [EBriBru:Me<sub>6</sub>TREN-PMDETA:EGDPEA:Cu(I)Br] 1:1:60:0.5-1 mol/mol. The chosen ligands to be used in the specific polymerisation, i.e. either

Me<sub>6</sub>TREN or PMDETA (16.5 μL and 35 μL), were added to a Schlenk flask that already contained EBriBru (24.2 μL) and EGDPEA (2.5 g). After three freeze-pump thaw cycles, the mixture was added to Cu(I)Br (11 mg) under argon atmosphere *via* canula. The reaction vessel was left purging in argon for 30 min in the oil bath at the temperature set at 50°C with agitation. Depending on the ligand used, the reaction was conducted for different time-length. When Me<sub>6</sub>TREN was utilised, the reaction was observed to reach the completion after 1 h, whilst, with PMDETA the reaction was terminated after 4 hours. Once the reaction was completed, the reaction mixture was diluted with 10 mL of THF and passed through a small neutral alumina column to remove the catalyst. The final pure product was obtained after a scCO<sub>2</sub> extraction. The scCO<sub>2</sub> extraction was performed using a 20 mL high pressure autoclave built in-house using a pressure of 2500 psi and a temperature of 40°C for 30 min. The optimisation of pressure and temperature, that were adopted for the extraction, had been previously achieved by using a still stainless view cell. The view cell is designed and built in-house, and it is made of 316 stainless steel and is rated for use up to 34.5 MPa. The view cell allowed to observe the solubility point between the scCO<sub>2</sub> with the monomer EGDPEA at a given pressure and temperature. <sup>1</sup>H-NMR spectroscopic analysis was performed on the crude polymerisation solution to determine polymer conversion and, finally, on the precipitate to establish the actual monomer ratio of the final copolymer composition. To evaluate the MWt and polydispersity of the materials, the purified samples were dissolved in HPLC grade THF for GPC analysis.

$^1\text{H-NMR}$  (400 MHz,  $\text{CDCl}_3$ )  $\delta$  (ppm) = 1-2.7 (m,  $\text{OCHC}_7\text{H}_{10}\text{C}_2\text{H}_2$ ); 3.38-3.61 (m,  $\text{OCHC}_7\text{H}_{10}\text{C}_2\text{H}_2$ ); 3.76 (m,  $\text{OCH}_2\text{CH}_2\text{O}$ ); 4.16 (m,  $\text{OCH}_2\text{CH}_2\text{O}$ ); 5.47-5.70 (m,  $\text{OCHC}_7\text{H}_{10}\text{C}_2\text{H}_2$ ).

#### 5.2.2.2 Synthesis of EGDPEA-*b*-DMAEMA

The general procedure adopted for the block copolymerisation, as shown in Scheme 5.3, is detailed below. The procedure for the synthesis of EGDPEA-*b*-DMAEMA was developed following the methodology reported in literature.<sup>386</sup>



Scheme 5.3 Scheme of the synthesis of EGDPEA-*b*-DMAEMA.

In brief, the EGDPEA macromonomer (0.00431 mmol, 500 mg) and DMAEMA (0.065 mmol, 121  $\mu\text{L}$ ) was dissolved in cyclohexanone in a v/v ratio of 1:2.1 (monomers:cyclohexanone). Subsequently, Cu(I)Cl (0.086 mmol, 8.54 mg) and Cu(II)Cl (0.017 mmol, 3.31 mg) was added in the Schlenk flask. The ligand HMTETA (0.052 mmol, 14  $\mu\text{L}$ ) was introduced immediately before starting the three freeze-pump thaw cycles, to minimise the interaction with the inorganic catalyst. The reaction was conducted for 24 h at a temperature of 50°C with stirring, after which the polymerisation was stopped by opening the flask to air and cooling to room temperature. The

reaction mixture was then diluted with 10 mL DCM and passed through a small neutral alumina column to remove the catalyst. The final pure product was obtained after precipitation into an excess of hexanes.  $^1\text{H-NMR}$  spectroscopic analysis was performed on the crude polymerisation solution to determine polymer conversion and, finally, on the precipitate to establish the actual monomer ratio of the final copolymer composition. To evaluate the MWt and polydispersity of the materials, the purified samples were dissolved in HPLC grade THF for GPC analysis.

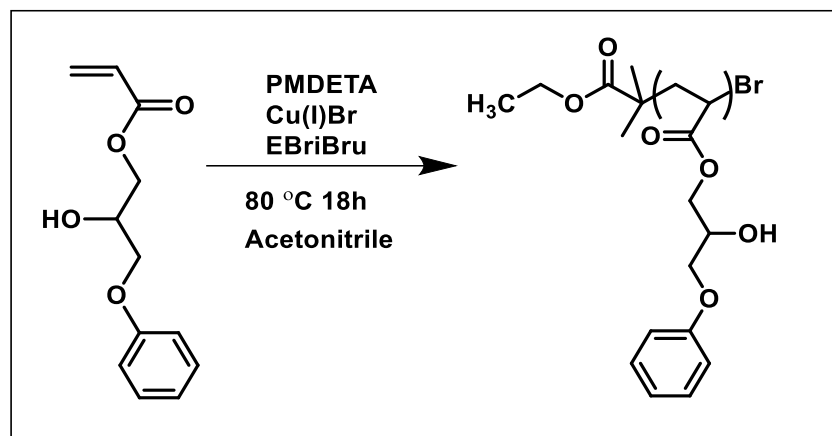
$^1\text{H-NMR}$  (400 MHz,  $\text{CDCl}_3$ )  $\delta$  (ppm) = 0.72-2.5 (m,  $\text{OCHC}_7\text{H}_{10}\text{C}_2\text{H}_2$ ); 2.28 ppm (s,  $\text{NCH}_3\text{CH}_3$ ); 2.56 (m,  $\text{CH}_2\text{CH}_2\text{N}$ ); 3.34-3.63 (m,  $\text{OCHC}_7\text{H}_{10}\text{C}_2\text{H}_2$ ); 4.06-4.14 (m,  $\text{OCH}_2\text{CH}_2\text{O}$ ); 5.47-5.70 (m,  $\text{OCHC}_7\text{H}_{10}\text{C}_2\text{H}_2$ ).

$^{13}\text{C-NMR}$  (400 MHz,  $\text{CDCl}_3$ )  $\delta$  (ppm) = 174 (C=O), 132-130 (CH=CH), 82.56 ( $\text{OCHC}_9\text{H}_{12}$ ), 65.70 ( $\text{OCH}_2\text{CH}_2$ ), 63.31 ( $\text{OCH}_2\text{CH}_2$ ), 55.15-28.60 ( $\text{C}_9\text{H}_{12}$ ), 45.67 ( $\text{NCH}_3\text{CH}_3$ ) (Figure Appendix 5-9).

### 5.2.3 ATRP of HPhOPA-*b*-DMAEMA

#### 5.2.3.1 Synthesis of HPhOPA Macroinitiator

The general procedure adopted for the polymerisations, as shown in Scheme 5.4, is detailed below.



Scheme 5.4 Scheme of the synthesis of poly(HPhOPA).

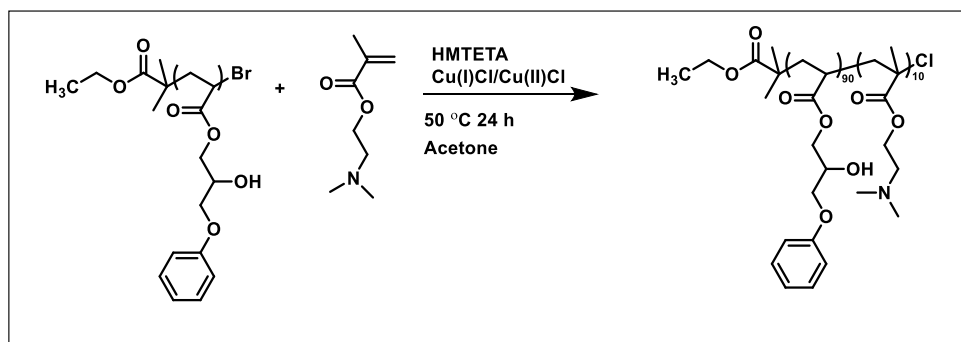
The macroinitiator based on HPhOPA was synthesised using the follow procedure. In a Schlenk flask, HPhOPA (2.5 g, 11.25 mmol) was added to EBriBru (24.2  $\mu$ L, 0.16 mmol), Acetonitrile (400  $\mu$ L) and the ligand. In this study, PMDETA was introduced at two different molar Initiator:Ligand mol/mol ratios, namely 1:1 and 1:2). After three freeze-pump thaw cycles, the mixture was added to Cu(I)Br (I:catalyst 1:0.5, 1:1, 1:1.5, 1:2 mol/mol) under argon atmosphere *via* canula. The reaction vessel was purged with argon for 30 min whilst being stirred in the oil bath with the temperature set at 80°C. The polymerisation was conducted at 80°C for 18 h and stopped by opening the flask to air and cooling at room temperature. The reaction mixture was then diluted with 10 mL DCM and passed through a small neutral alumina column to remove the catalyst. The final pure product was obtained after precipitation into an excess of hexane.  $^1\text{H-NMR}$  spectroscopic analysis was performed on the crude polymerisation solution to determine polymer conversion and, finally, on the precipitate to establish the actual monomer ratio of the final copolymer composition. To evaluate

the MWT and polydispersity of the materials, the purified samples were dissolved in HPLC grade THF for GPC analysis.

$^1\text{H-NMR}$  (400 MHz,  $\text{CDCl}_3$ )  $\delta$  (ppm) = 1-2.6 (m,  $\text{CHCH}_2$ ); 3.90-4.20 (m,  $\text{OCH}_2\text{HOHCH}_2\text{O}$  and  $\text{OCH}_2\text{CH}_2$ ); 3.76 (m,  $\text{OCH}_2\text{CH}_2\text{O}$ ); 4.16 (m,  $\text{OCH}_2\text{CH}_2\text{O}$ ); 5.47-5.70 ppm (m,  $\text{OCHC}_7\text{H}_{10}\text{C}_2\text{H}_2$ ); 7.22-6.87 ppm (m,  $\text{C}_5\text{H}_5$ ).

### 5.2.3.2 Synthesis of HPhOPA-*b*-DMAEMA

The general procedure adopted for the polymerisation, as shown in Scheme 5.5, is detailed below. The procedure for the synthesis of HPhOPA-*b*-DMAEMA was developed following the methodology showed in literature.<sup>386</sup>



Scheme 5.5 Synthesis of HPhOPA-*b*-DMAEMA

In brief, the HPhOPA macromonomer (0.041 mmol, 500 mg) and DMAEMA (0.065 mmol, 245  $\mu\text{L}$ ) were dissolved in acetone in a v/v ratio of 1:2.1. Subsequently,  $\text{Cu(I)Cl}$  (0.083 mmol, 8.27 mg) and  $\text{Cu(II)Cl}$  (0.016 mmol, 2.25 mg) was added in the Schlenk flask. The ligand HMTETA (0.050 mmol, 14  $\mu\text{L}$ ) was introduced immediately before starting the three freeze-pump thaw cycles, to minimise the interaction with the inorganic catalyst during the three cycles. Following this, the reaction was conducted for 24 h at a

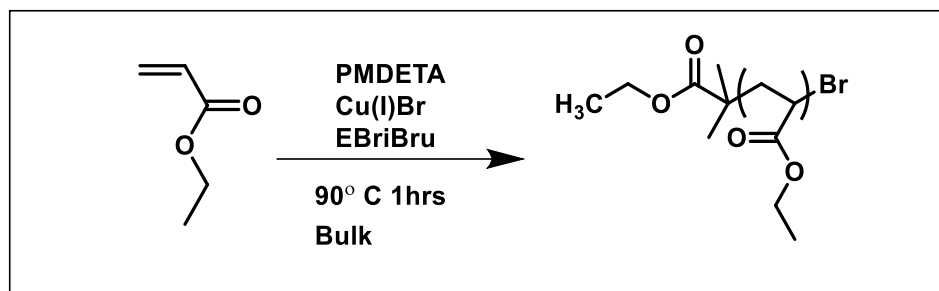
temperature of 50°C. The polymerisation was stopped by opening the flask to air and cooling to room temperature. The reaction mixture was then diluted with 10 mL DCM and passed through a small neutral alumina column to remove the catalyst. The final pure product was obtained after precipitation into an excess of hexane. <sup>1</sup>H-NMR spectroscopic analysis was performed on the crude polymerisation solution to determine polymer conversion and, finally, on the precipitate to establish the actual monomer ratio of the final copolymer composition. To evaluate the MWt and polydispersity of the materials, the purified samples were dissolved in HPLC grade THF for GPC analysis.

<sup>1</sup>H-NMR (400 MHz, CDCl<sub>3</sub>) δ (ppm) = 1-2.6 (m, CHCH<sub>2</sub>); 2.28 (s, NCH<sub>3</sub>CH<sub>3</sub>); 2.56 (m, CH<sub>2</sub>CH<sub>2</sub>N); 3.90-4.20 (m, OCH<sub>2</sub>HOHCH<sub>2</sub>O, OCH<sub>2</sub>CH<sub>2</sub> and OCH<sub>2</sub>CH<sub>2</sub>O); 7.22-6.87 (m, C<sub>5</sub>H<sub>5</sub>,) (Figure Appendix 5-10).

## 5.2.4 ATRP of EA-*b*-DMAEMA

### 5.2.4.1 Synthesis of EA Macroinitiator

The general procedure adopted for the polymerisations, as shown in Scheme 5.6, is detailed below. The procedure for the synthesis of polyEA developed following the methodology showed in literature.<sup>387</sup>



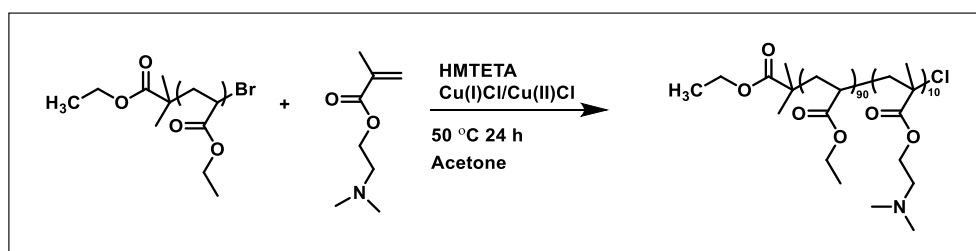
Scheme 5.6 Reaction scheme of poly(EA)

In a Schlenk flask, EA (2.5 g, 25 mmol) was added to EBriBru (37  $\mu$ L, 0.25 mmol) and PMDETA (52.3  $\mu$ L, 0.25 mmol). After three freeze-pump thaw cycles, the mixture was added to Cu(I)Br (0.25 mmol, 35mg) under argon atmosphere *via* canula. The reaction vessel was purged with argon for 30 min while stirring in the oil bath with the temperature set at 90°C. After the reaction was conducted for 1 h at 90°C, it was stopped by opening the flask to air and cooling to room temperature. The reaction mixture was then diluted with 10 mL DCM and passed through a small neutral alumina column to remove the catalyst. The final pure product was obtained after precipitation into an excess of hexane.  $^1\text{H-NMR}$  spectroscopic analysis was performed on the crude polymerisation solution to determine polymer conversion and, finally, on the precipitate to establish the actual monomer ratio of the final copolymer composition. To evaluate the MWt and polydispersity of the materials, the purified samples were dissolved in HPLC grade THF for GPC analysis.

$^1\text{H-NMR}$  (400 MHz,  $\text{CDCl}_3$ )  $\delta$  (ppm) = 1.23 (m,  $\text{CH}_2\text{CH}_3$ ); 4.14 (m,  $\text{OCH}_2\text{CH}_3$ )

#### 5.2.4.2 Synthesis of EA-*b*-DMAEMA

The general procedure adopted for the polymerisations, as shown in Scheme 5.7, is detailed below. The procedure for the synthesis of EA-*b*-DMAEMA was developed following the methodology showed in literature.<sup>386</sup>



Scheme 5.7 Reaction scheme of EA-*b*-DMAEMA

In brief, the EA macroinitiator (0.031 mmol, 500 mg) and DMAEMA (1.1 mmol, 186  $\mu$ L) was dissolved in acetone in a v/v ratio of 1:2.1 (monomers:acetone). Subsequently, Cu(I)Cl (0.063 mmol, 6.23 mg) and Cu(II)Cl (0.014 mmol, 1.7 mg) was added in the Schlenk flask. The ligand HMTETA (0.062 mmol, 11.42  $\mu$ L) was introduced immediately before starting the three freeze-pump thaw cycles, to minimise the interaction with the inorganic catalyst during the three cycles. The reaction was conducted for 24 h at a temperature of 50°C with stirring. The polymerisation was stopped by opening the flask to air and cooling to room temperature. The reaction mixture was then diluted with 10 mL THF and passed through a small neutral alumina column to remove the catalyst. The final pure product was obtained after precipitation into an excess of hexane. <sup>1</sup>H-NMR spectroscopic analysis was performed on the crude polymerisation solution to determine polymer conversion and, finally, on the precipitate to establish

the actual monomer ratio of the final copolymer composition. To evaluate the MWt and polydispersity of the materials, the purified samples were dissolved in HPLC grade THF for GPC analysis.

$^1\text{H-NMR}$  (400 MHz,  $\text{CDCl}_3$ )  $\delta$  (ppm) = 1.23 (m,  $\text{CH}_2\text{CH}_3$ ), 2.28 (s,  $\text{NCH}_3\text{CH}_3$ )  
2.56 (m,  $\text{CH}_2\text{CH}_2\text{N}$ ); 4.14 (m,  $\text{OCH}_2\text{CH}_3$ ).

$^{13}\text{C-NMR}$  (400 MHz,  $\text{CDCl}_3$ )  $\delta$  (ppm) = 174 (C=O), 63.09, (C=OCH<sub>2</sub>CH<sub>2</sub> DMAEMA), 60.25 (C=OCH<sub>2</sub>CH<sub>3</sub>), 56.77 (C=OCH<sub>2</sub>CH<sub>2</sub> DMAEMA), 45.80 ( $\text{NCH}_3\text{CH}_3$ ), 14.077 ( $\text{OCH}_2\text{CH}_3$ ) (Figure Appendix 5-8).

## 5.2.5 Dynamic Light Scattering

### 5.2.5.1 Critical Aggregation Concentration (CAC) Analysis

The Critical Aggregation Concentration (CAC) of the surfactants of both block and random copolymers were determined by DLS analysis. The initial surfactant emulsions/suspensions were prepared by nanoprecipitation method using THF as the solvent and water as the non-solvent. The THF polymeric solutions (5 mg in 1 mL) were added manually via syringe dropwise into milliQ water (5 mL) in order to obtain a final emulsion/suspension concentration of 1000  $\mu\text{g}/\text{mL}$ . Once prepared the stock surfactant emulsions/suspension, 11 dilutions were prepared in order to generate the different concentrations necessary for the analysis. These ranged from 850  $\mu\text{g}/\text{mL}$  to 20  $\mu\text{g}/\text{mL}$  (i.e. 11 final concentrations for each material were obtained).

The intensity (Cnt/s) and size (nm) of the light scattered by the final nanosuspensions were measured using a Zetasizer Nano ZS. The

experimental procedures for the intensity measurements were conducted with a fixed laser power intensity and attenuation were applied in order to determine the scattered light from each sample.

#### 5.2.5.2 Zeta Potential

The Zeta Potential ( $\zeta$ ) of the nano suspension/emulsion at 1 mg/mL (Prepared as described in the CAC section) was evaluated according to the electrophoretic mobility of the particles and calculated by the Helmholtz-Smoluchowsky equation. All measurements were performed in triplicate using a Zetasizer Nano ZS.

#### 5.2.5.3 Protein Corona Binding Assay

To determine protein corona association to the nanoparticles (NPs), binding studies were undertaken using Bovine Serum Albumin (BSA), as the model protein, according to the studies showed from Alexander's group.<sup>388,389</sup> Each specific NPs (1 mg/mL in PBS) and a sample of BSA alone (2 mg/mL in PBS) was sized by DLS at a fixed attenuation. BSA was added (150  $\mu$ L) to NPs (150  $\mu$ L) (final conc. NPs:500  $\mu$ g/mL, BSA: 0.2% wt equivalent to culture media +10% FBS). The samples were incubated at 37°C and size measurements of the samples were taken by DLS on a Zetasizer after 0, 1 and 24 h.

## 5.2.6 Particles Production

### 5.2.6.1 Microfluidics

Polymer microparticles were produced using a 100  $\mu\text{m}$  hydrophilic 3D flow-focusing microfluidic droplet generator. Two syringe pumps were used to deliver the continuous and dispersed flows to the microfluidic generator. The continuous phase used was DI water while, the dispersed phase contained the monomer (1,6 hexanediol diacrylate, 96% w/v) with 2 % w/v polymeric surfactant and 2% w/v photoinitiator (2,2 dimethoxy-2-phenylacetophenone). Once stable generation of the droplets was observed, the droplets were collected in a vial filled with 10 mL of DI water and placed inside the UV protective box. The capillary tube was then placed into the sample vessel, with the tip just slightly submerged in the water. The UV fibre optic cable was aligned to the particle collection stream leaving the capillary tube. The production was continued for up to two hours or until enough sample was collected for post curing. After the polymeric droplets were undergone their UV cure, the UV was switched off and the polymer beads were filtered in a 40  $\mu\text{m}$  nylon mesh filter.

## 5.2.7 Microparticles Characterisation

*Microparticles Size and Topography Analysis:* dry samples were characterised using SEM microscopy. Details of samples preparation are described in the Materials and Methods chapter.

*Microparticle Surface Characterisation:* Microparticles were placed onto a poly(hydroxyethyl) methacrylate substrate and subjected to mass-spectrometry using a ToF-SIMS IV. 500µm x 500µm scans were taken with a Bi<sub>3+</sub> primary ion source. Data were calibrated and analysed using IonToF software.

## 5.3 Results and Discussions

### 5.3.1 Positively Charged Amphiphilic Random Copolymers

Thiol-mediated Free Radical polymerisation was used for the synthesis of relatively low MWt random copolymers. This technique was selected due to the robustness of thiols as CTA in presence of hetero atoms such as amino group which are present in the side chain of DMAEMA. The utilisation of the HT synthesiser (Chapter 3) revealed that CCTP mechanism is negatively affected by the presence of such moieties. For this purpose, benzyl mercaptan (BzSH) was used as thiol model considering the high performance observed in the aforementioned HT synthetic screening. Considering that this last chapter was designed as proof of concept for the initial alteration of nature of the hydrophile as well as the final 3D polymeric architecture, thus, only three hydrophobic monomers were adopted, i.e. EA, EGDPEA and HPhOPA. The chemical properties of the final material along with the related NPs characterisation were reported in Table 5.1.

Table 5.1 Percentage conversions, calculated ratios (HyB:DMAEMA),  $M_n$  and the physical characterisation of the nanoaggregates (size, CAC and zeta potential) for the synthesised polymer surfactants EA-co-DMAEMA, EGDPEA-co-DMAEMA and HPhOPA-co-DMAEMA. The DLS analysis were performed at 25°C and the Intensity (%) values were registered and analysed. The suspension/emulsion were prepared in DI water at pH of around 7. All the obtained conversions<sup>a</sup> were above 90%.

Entry	$M_n^b$ (kg mol <sup>-1</sup> )	$\bar{D}^b$	Final Copolymer Ratio <sup>a</sup> (% mol/mol)	Size (nm)	CAC (µg/mL)	$\zeta$ (mV)
EGDPEA-co-DMAEMA	8.4	1.24	92:8	73±1.4	174	+45±0.8
EA-co-DMAEMA	13.1	1.25	80:20	111±0.8	150	+42±1.3
HPhOPA-co-DMAEMA	5.9	1.77	86:14	205±5.0	160	+44±0.7

<sup>a</sup>Conversion and Actual Copolymer Ratio were calculated by <sup>1</sup>H-NMR (Figure 2.1); <sup>b</sup> $M_n$  and  $\bar{D}$  were calculated by GPC. GPC chromatograms are showed in Figure Appendix 5-1.

The characterisation data for the three different amphiphilic random copolymers generated is shown in Table 5.1. Conversions indicated quantitative reactions with values of greater than 90%. The  $M_n$  of the three polymers ranged between 6,000 and 13,000 g mol<sup>-1</sup> which aligned well with the copolymer synthesised using mPEGMA<sub>300</sub>. The relatively low resultant  $M_n$  confirmed that the amount of CTA employed (3% mol I with respect to the monomers) was sufficient to control the length of the polymer chains. The  $M_n$  of EA-co-DMAEMA was the highest of the three values, which was attributed to its pendant group exhibiting the least hindrance side chain, which may result in a higher reactivity to polymerisation for this monomer. In the case of the three surfactants, <sup>1</sup>H-NMR analysis showed that the actual comonomer molar ratio is closed to the theoretical ratio of 90:10 % mol/mol HyB monomer:DMAEMA. Also, polydispersity were between 1.3 and 1.8, which are values that regarded as being typical for a ‘well-controlled’ FRP. Envisaging the use of these materials as surfactants, the ability to self-

assemble into nanoaggregates, in milliQ water, was studied in terms of aggregates size (at 1000 µg/mL), CAC and surface charge. At 1000 µg/mL, HPhOPA-co-DMAEMA and EA-co-DMAEMA showed sizes above 100 nm, while, EGDPEA-co-DMAEMA has resulted in NPs of around 70 nm. The difference in trend, might be due to the different hydrophobic core interactions and different packing. All the aggregates resulted net positively charged NPs, suggesting that they had successful core-shell self-assembled and, thus, it was concluded that they all presented DMAEMA in the out layer. In addition, the whole set of surfactants showed a good dilution stability with CACs ranging from 150-175 µg/mL, confirming the quality of these materials as surfactants.

### 5.3.1.1 Comparison Random Copolymers

A comparison between the random amphiphilic copolymers obtained with mPEGMA<sub>300</sub> and the DMAEMA is displayed in Table 5.2 and Table 5.3, where Table 5.2 is a subset of the data presented in Table 5.1 for convenience.

Table 5.2 Summary of the physicochemical characterisation data of the amphiphilic copolymers using DMAEMA as the hydrophilic component. The DLS analysis were performed at 25°C and the Intensity (%) values were registered and analysed. The suspension/emulsion were prepared in DI water at pH of around 7.

Entry	Mol Ratio <sup>a</sup> (%) mol/mol)	Size (nm)	CAC <sup>b</sup> (µg/mL)	ζ (mV)
EGDPEA-co-DMAEMA	92:8	73±1.4	174	+45±0.8
EA-co-DMAEMA	80:20	111±0.8	150	+42±1.3
HPhOPA-co-DMAEMA	86:14	205±5.0	160	+44±0.7

<sup>a</sup>Molar Ratio (HyB:DMAEMA) was calculated by <sup>1</sup>H-NMR (Figure 2.1) <sup>b</sup>The CAC values were obtained from the plots of the intensity of the scattered light as a function of the concentration (Figure Appendix 5-11)

Table 5.3 Summary of the physicochemical characterisation data of the amphiphilic copolymers using mPEGMA<sub>300</sub> as the hydrophilic component. The DLS analysis were performed at 25°C and the Intensity (%) values were registered and analysed. The suspension/emulsion were prepared in DI water at pH of around 7.

Entry	Mol Ratio <sup>a</sup> (% mol/mol)	Size (nm)	CAC (µg/mL)	ζ (mV)
EGDPEA-co-mPEGMA <sub>300</sub>	87:13	111	8.5	-8
EA-co-mPEGMA <sub>300</sub>	88:12	150	13	-12
HPhOPA-co-mPEGMA <sub>300</sub>	91:9	145	3.5	-16

<sup>a</sup>Molar ratio (HyB:DMAEMA) was calculated by <sup>1</sup>H-NMR (Figure 2.1).

The collocation of Table 5.2 and Table 5.3 allows the properties of the two set of amphiphilic systems to be compared in terms of their hydrodynamic size distribution (at 1000 µg/mL), CAC and zeta potential to further corroborate that both the chemical nature of the hydrophile (i.e. comb-graft mPEGMA vs linear DMAEMA) and the chain architecture can affect the final particles features. The hydrodynamic diameter of both sets of materials were found to be in the same order of magnitude. However, whilst the size of PEG based polymers was more consistent, a net decreasing trend in hydrodynamic diameter is observed in the DMAEMA-based surfactants when copolymerising this hydrophilic with HPhOPA>EA>EGDPEA. Prior literature has reported that PEG chains grafted on NPs can generate a hydrated cloud with a large excluded volume that sterically might increase the hydrophilic external layer, and, consequently the NPs size.<sup>390</sup> Thus, the presence of this hydrated cloud may lead to a greater homogeneity in the NPs size, as a result. This may dominate over the effect of the hydrophobic monomers chemistry characteristics. Meanwhile, with the DMAEMA set of polymers, the lack of a relatively long graft chain might reduce the surface hydration leading to smaller sizes. However, this event might hamper the

stability under dilution conditions of the aggregates which might explain the CAC being one order of magnitude higher than the PEG polymeric systems (Table 5.2). It may, also, mean that the chemistry characteristics of the HyB monomer may have greater influence over the particle size and, thus, result in the specific trend observed.

A further confirmation of the different hydrophilic surface charge nature is the net charge density observed between the two sets (measured as zeta potential in DI water). The strong positive surface charge densities of the DMAEMA surfactants can be related to the partial protonation of the tertiary amine on the surface functional group. On the contrary, the weak negative charge measured for the PEG systems can be referred to the polarisation of the water molecules interacting with the lone pairs of the oxygen of the ethylene glycol present on the grafted surface chain. On the light of this comparison, a possible different behaviour of the DMAEMA surfactants can be foreseen when applied into the microfluidics device.

### 5.3.2 Positively Charged Block Copolymers

The development of the synthesis of a block copolymer, usually, require the use of two step polymerisation.<sup>116</sup> The first step is related to the synthesis of the macromonomer from which the second block is, subsequently, grown. In the design of the synthesis, the HyB monomers (i.e. EA, EGDPEA and HPhOPA) were designated for the synthesis of the first block. In practise, different conditions were applied for each synthesis as the chemical nature of each hydrophobic monomer is very different.

Meanwhile, the second step, which consists in the growth of DMAEMA block, was achieved by adopting the same conditions for the three different surfactants.

### 5.3.2.1 Synthesis of the Macromonomers

#### 5.3.2.1.1 Synthesis of poly(EA)

The procedure for the synthesis of the poly(EA) was obtained from the work of Datta et al.<sup>387</sup> In particular, they carried out ATRP in bulk using EBriBru as the initiator and a range of different catalysts (e.g. Cu(I)Br and Cu(I)Cl) in combination with different ligands. In this study, during the different screenings/optimisation of the different reaction conditions, the polymerisations were found to be well-controlled with a linear increase of  $M_n$  with conversion and relatively narrow polydispersity observed. However, when the combination of PMDETA/Cu(I)Br was exploited the polymerisation resulted in faster kinetics without any detrimental effects on the quality of the polymer produced being observed. Thus, these latter conditions were applied for the synthesis of the macromonomer. The target theoretical  $M_n$  was  $13,000 \text{ g mol}^{-1}$  in order to maintain the similar molecular weight obtained with the random copolymers throughout the project. Table 5.4 shows the percentage conversion, molecular weight of the final polymer and polydispersity index actually achieved.

Table 5.4 Summary of the polymerisation of EA via ATRP considering a theoretical  $M_n$  of 13,000  $g\ mol^{-1}$ .

Catalytic system	[EA]:[EBriB]: [Cu <sup>I</sup> ]: [PMDETA]	T (°C)	Time (h)	Conv <sup>a</sup> (%)	$M_n^b$ ( $g\ mol^{-1}$ )	$\mathcal{D}^b$
Cu(I)Br/PMDETA	130:1:1:1	90	1	>90	13,190	1.12

<sup>a</sup>Conversion was calculated by <sup>1</sup>H-NMR (Figure 2.1); <sup>b</sup> $M_n$  and  $\mathcal{D}$  were calculated by GPC.

The data from Table 5.4 demonstrates that the EA macromonomer was successfully obtained. In particular, high polymer conversion (>90%) was observed after 1 h with narrow polydispersity index (1.12) suggesting a well-controlled nature of the polymerisation. A confirmation of the well-controlled polymerisation is the experimental  $M_n$  being very close to the theoretical one 13,000  $g\ mol^{-1}$ . In Figure 5.1, a combination of the GPC traces and <sup>1</sup>H-NMR spectra of p(EA) is shown, the former has been included to indicate that a mono-modal trace was observed.

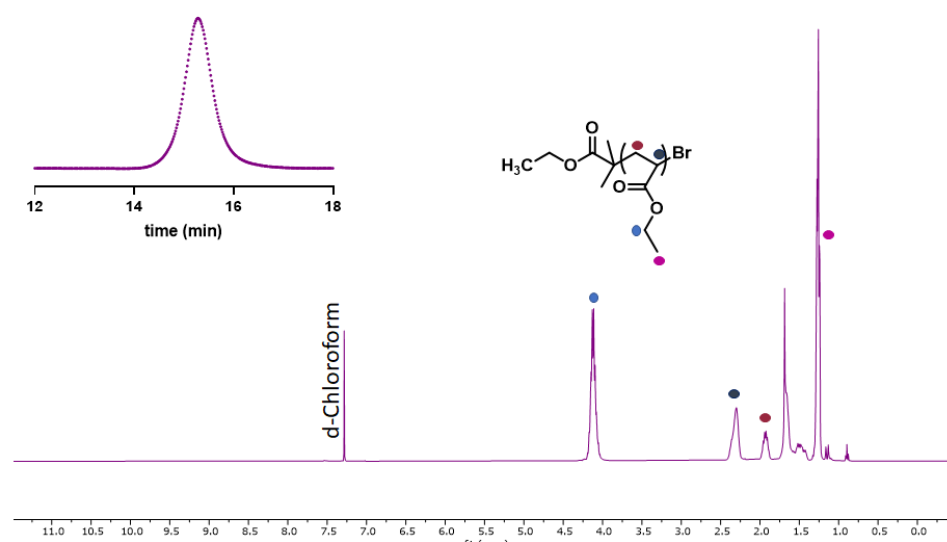


Figure 5.1 GPC chromatogram and <sup>1</sup>H-NMR spectra of poly(Ethyl Acrylate).

Figure 5.1 shows the <sup>1</sup>H-NMR spectra of the macromonomer obtained from EA. From the peak signals system, it was possible to confirm the production of this material. However, because of the overlapping between the peaks

related to EA and the end groups (e.g. [CH(Br)]), these latter have not been indicated in the NMR spectra. In fact, the [CH(Br)] should appear at  $\delta=4.1$  ppm and the peaks relative to the initiator are around  $\delta=4.19$  (OCH<sub>2</sub>), 1.90 (COCH<sub>3</sub>CH<sub>3</sub>) and 1.27 (CH<sub>2</sub>CH<sub>3</sub>).<sup>387</sup>

#### 5.3.2.1.2 Synthesis of poly(EGDPEA)

A few examples of CRP using EGDPEA are present in literature. In particular, Maupu et al. performed NMP of the homo and block copolymer of EGDPEA and EGDPEMA (methacrylated version), while, Mandal et al. performed the ATRP of the homo and triblock of EGDPEMA.<sup>270,271,391</sup> However, it is difficult to prepare well defined block copolymers of either EGDPEA and EGDPEMA, because moieties bearing bicyclo-alkenyl functionality undergo to several side reactions leading to gel formation during the course of polymerisation reaction and a steady increase of the molecular weight distribution.<sup>391</sup> In fact, two important points were considered during the optimisation of the ATRP in this project: a) the prevention of gel formation and b) to maintain high conversion and relatively low polydispersity. Table 5.5 shows a summary of the results of ATRP of EGDPEA using different catalyst systems, solvents, and temperatures.

Table 5.5 Summary of the polymerisation of EGDPEA via ATRP considering a theoretical  $M_n$  of 15,000  $g\ mol^{-1}$ .

Entry	Catalyst system [I]:[Cu]:[Ligand]	Solv	T (°C)	Time (h)	Conv <sup>a</sup> (%)	$M_n^b$ ( $g\ mol^{-1}$ )	$\bar{D}^b$
1	EBriB:Cu(I)Br:Me <sub>6</sub> TREN (1:0.5:1)	Bulk	50	1	-	GEL	GEL
2	EBriB:Cu(I)Br:Me <sub>6</sub> TREN (1:0.5:1)	THF	50	24	20	-	-
3	EBriB:Cu(I)Br:PMDETA (1/0.5/1)	Bulk	90	1	-	GEL	GEL
4	EBriB:Cu(I)Br:PMDETA (1/0.5/1)	THF	50	24	20	-	-
5	EBriB:Cu(I)Br:PMDETA (1:0.5:0.85)	Bulk	50	4	50	10,200	1.4

<sup>a</sup>Conversion was calculated by <sup>1</sup>H-NMR (Figure 2.1); <sup>b</sup> $M_n$  and  $\bar{D}$  were calculated by GPC.

From Table 5.5, it was noted that ATRP of EGDPEA was extremely fast when using bulk conditions regardless the catalyst system used, and with very high conversion. In fact, when THF was employed in a vol/vol ratio of 0.5:1 (THF:EGDPEA) the conversions never reached a value of over 20%. However, using bulk condition resulted problematic in the control of the polymerisation as in both catalyst systems PMDETA/Cu(I)Br and Me<sub>6</sub>TREN/Cu(I)Br a gel point was observed very quickly in less than one hour. Because of the tendency of EGDPEA to gel, it is important to keep low the concentration of the active radicals throughout the polymerisation reaction in order to avoid unwanted side reactions. PMDETA was preferred to Me<sub>6</sub>TREN as this latter is well known to form one of the most active Cu complexes among all the ligands which can push the ATRP equilibrium to the activation process, thus, the generation of radicals.<sup>45</sup> In addition, PMDETA molar ratio (EBriB:L) was reduced from 1 to 0.85 with the same intention of maintain low the radical concentration. In the entry 5, a

macromonomer based on EGDPEA was obtained after 4h with a conversion of around 50% and a  $M_n$  of 10,200 g mol<sup>-1</sup>. The low conversion of the polymerisation hampered the possibility to reach the theoretical molecular weight, however, a  $M_n$  of 10,000 g mol<sup>-1</sup> is in accordance with the  $M_n$  of the surfactants produced previously so no further changes were considered. Polydispersity is relatively high (1.4) for a CRP technique and gel point was observed after 4h. Interestingly, Mandal et al demonstrated through UV-vis spectrometry analysis that EGDPEMA tends to interact with CuBr.<sup>391</sup> The UV-vis spectrometry analysis showed that the UV spectrum of CuBr/EGDPEMA was very broad with a small hump at 280 nm indicating the interaction between CuBr and EGDPEMA, which in turn activates the monomer. The activation of the monomers may lead to interactions among the different EGDPEA polymeric chains, and this might explain the experienced crosslinking and a higher polydispersity.

Due to this propensity to crosslink, the purification of the macromonomer p(EGDPEA), also, required an optimisation. Using the precipitation in a non-solvent (methanol) as main technique for the purification, low final yield was experienced (around 20%) after 2 steps. However, a different approach was considered for the purification which compelled in the use of scCO<sub>2</sub> as the non-solvent. In fact, it is known in literature that many polymers are not soluble in scCO<sub>2</sub> which make this solvent as a green solvent of election for the extraction of monomeric species from the mixture with polymers. Thanks to the facility present in the department of Chemistry, a systematic study was conducted to find the soluble point at which the EGDPEA

monomer is soluble in scCO<sub>2</sub> using a stainless view cell. The soluble point (Figure 5.2) was observed at a pressure of 1550 psi and at a temperature of 40°C.

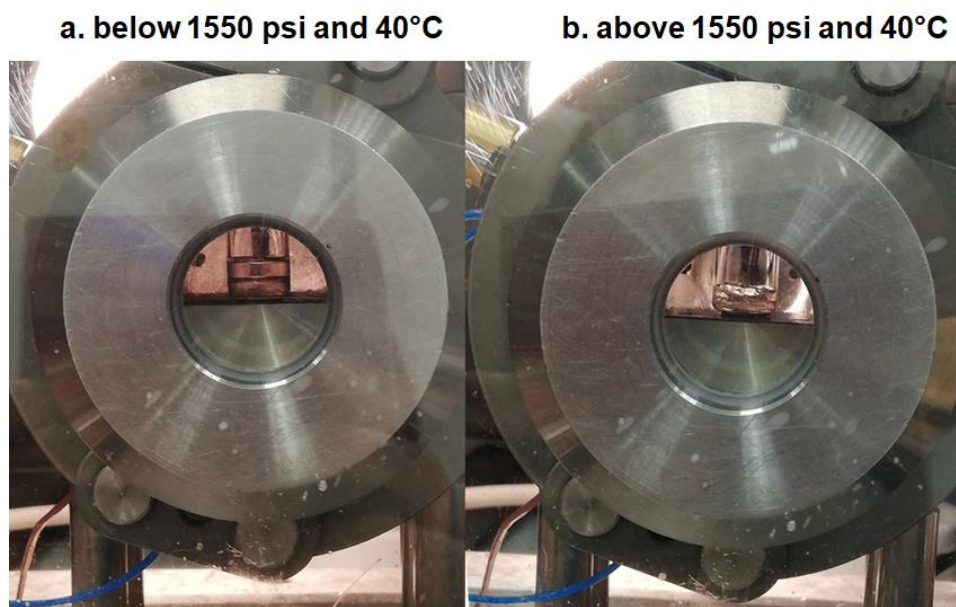


Figure 5.2 Cell view experiments for the solubility study of EGDPEA in scCO<sub>2</sub>. Below 1550 psi and 40°C the monomer is not soluble as it is possible observe from the figure a. Above 1550 psi and 40°C the monomer starts being soluble (figure b) and interacting with solvent.

Once assessed the pressure and temperature conditions for the EGDPEA extraction with the view cell, the reaction mixture was introduced in using a 20 mL high pressure autoclave built in-house using a pressure of 2500 psi and a temperature of 40°C for 30 min. Meanwhile, in Figure 5.3 the comparison of the <sup>1</sup>H-NMR of the two methods of purification.

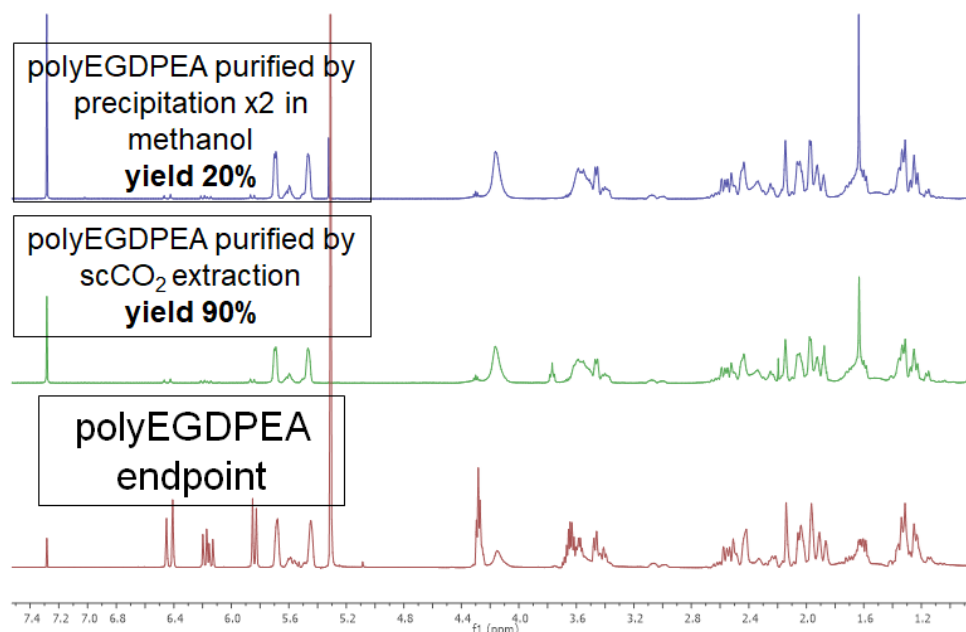


Figure 5.3  $^1\text{H-NMR}$  spectra of the pure poly(EGDPEA) using two different purification methods.

From Figure 5.3 was possible to conclude that with both methods pure poly(EGDPEA) is obtained, however, using  $\text{scCO}_2$  has allowed a purification almost quantitative of this macromonomer with not loss of materials.

#### 5.3.2.1.3 Synthesis of the poly(HPhOPA)

To the best of the author's knowledge, examples of ATRP of HPhOPA have not been found in literature up to this point in time. In the light of this, optimisation experiments were conducted in order to find the optimal condition to have a good compromise between high polymer conversion and good control of the polymerisation. Table 5.6 shows a summary of the results of ATRP of HPhOPA using different catalyst systems, solvents and temperatures.

Table 5.6 Summary of the polymerisation of HPhOPA via ATRP conducted for 24 h and considering a theoretical  $M_n$  of 15,000  $g\ mol^{-1}$ .

Entry	[EBriB]:[Cu <sup>I</sup> ]:[PMDETA]	Solv	HPhOPA: SOLV vol/vol	T (°C)	Conv (%)	$M_n$ ( $g\ mol^{-1}$ )	$\bar{D}$
1	1:1:1	bulk	-	80	GEL	GEL	GEL
2	1:1:1	methanol	1:1	60	GEL	GEL	GEL
3	1:1:1	Acetone	1:1	50	15	N/A	N/A
4	1:1:1	acetonitrile	1:1	80	40	N/A	N/A
5	1:1:1	acetonitrile	1:0.5	80	50	7,400	1.2
6	1:1:1	acetonitrile	1:0.25	80	GEL	GEL	GEL
7	1:0.5:1	acetonitrile	1:0.5	80	70	13,400	1.4

<sup>a</sup>Conversion was calculated by <sup>1</sup>H-NMR (Figure 2.1); <sup>b</sup> $M_n$  and  $\bar{D}$  were calculated by GPC.

As shown in Table 5.6, one of the challenges faced with the optimisation experiments of the ATRP of poly(HPhOPA) was the screening of the solvents and their volume ratio with respect to the monomer. The use of the solvent is important when managing this monomer because it is very viscous and, when the polymerisation is conducted in bulk at 80°C, the reaction mixture is observed to be crosslinked in less than an hour (entry 1). Matyjaszewsky group calculated the rate constants of activation for the reactions of tertiary alkyl halides with Cu(I)Br in 14 different solvents and found that their polarity plays a role in the ATRP equilibrium ( $k_{act}/K_{deact}$ ).<sup>392</sup> For the purpose of this study, methanol, acetonitrile and acetone were employed in the ATRP considering that the polarity of these solvents decreases in the follow order  $CH_3OH > CH_3CN > CH_3COCH_3$ . From the Table 5.6 it is possible to observe that the use of methanol leads the reaction mixture to form a gel (Entry 2), probably the presence of the hydroxyl group in the side chain of HPhOPA forms intra hydrogen bond chain-chain with this solvent. At the same time, by pushing the rate constant of activation, methanol may help the concentration of radicals being too high that the polymerisation goes to

completion too quickly. On the other hand, when acetone was used (entry 3), the resulting reaction was very slow, with only a conversion of 20% after 24 h being achieved. At the same catalyst system concentration, acetonitrile was found to be a good compromise giving rise to conversions of 40% and 50% for the vol/vol ratio 1:1 and 0.5:1, respectively (entry 4 and 5) after 24 h. Also, entry 5 showed a  $M_n$  aligned with what it was expected with a 50% of conversion and a molecular weight distribution of around 1.2. Surprisingly, when the volume ratio is reduced to 0.25:1 vol/vol, it was found that this is not enough to sufficiently reduce the viscosity of the system to give viable reaction. Once both the best solvent and working concentration were identified (acetonitrile and a vol/vol ratio of 0.5:1), the catalyst system conditions were changed to improve the conversion. Table 5.6 Entry 10, shows that when the molar concentration of EBriB:Cu(I):PMDETA were 1:0.5:1, respectively, the conversion successfully reached 70% after 24 h with a relatively controlled polymerisation and a  $M_n$  of around 13,400 g mol<sup>-1</sup>. Reducing the concentration of the Cu(I)Br resulted successful for the increasing of the conversion likely due an improvement with the equilibrium pointing towards the deactivation steps and, thereby, forming a low concentration of radicals to reduce radical-radical termination reactions.

The <sup>1</sup>H-NMR of the pure poly(HPhOPA) and its GPC trace is showed in Figure 5.4.

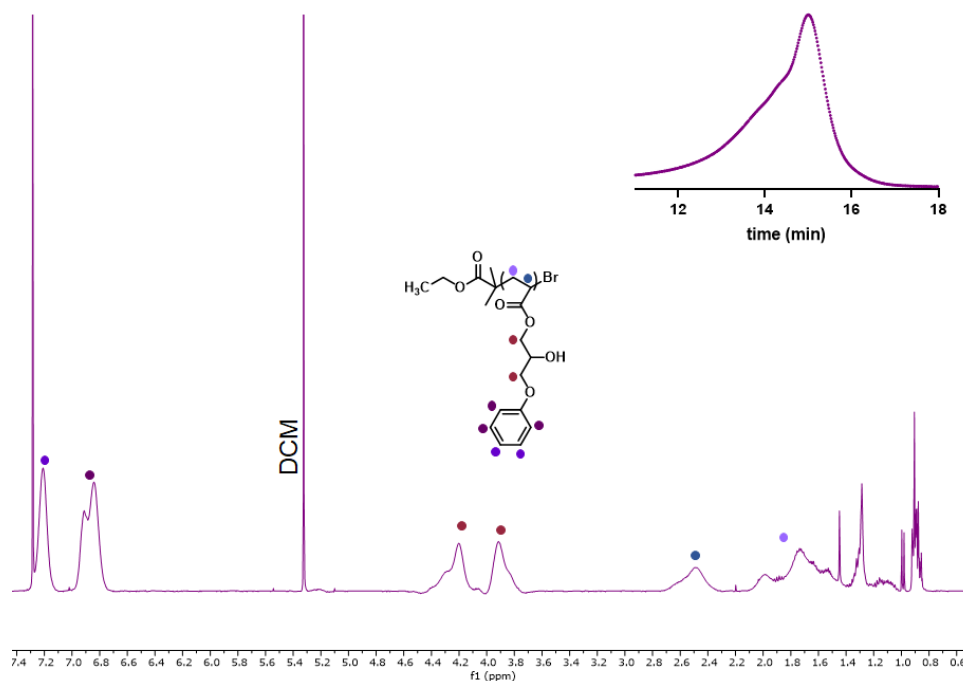


Figure 5.4  $^1\text{H-NMR}$  spectra with peaks assignment and the GPC chromatogram of poly(HPhOPA)

From Figure 5.4 it is possible to see the  $^1\text{H-NMR}$  spectra with the assignment (for full analysis see materials and methods). However, for the same reasons listed for the macromonomer of EA (e.g. peaks signals overlapping between the peaks related to EA and the end groups), peaks assignments of the end groups were not indicated in the p(HPhOPA)  $^1\text{H-NMR}$  spectra.

In addition, the inserted GPC trace showed an asymmetric peak which explain the relatively broader polydispersity. The relatively broad molecular weight distributions suggested that either the deactivation of the growing radical chain ends was slow, or some side reactions, such as coupling of the polymer chains at very high conversion, were occurring.<sup>96</sup> This broadening of the GPC may also indicate to potential onset of branching in the system which will eventually lead to the gel formation.

### 5.3.2.2 Synthesis of the second block DMAEMA

As anticipated in the materials and methods, the procedure for the synthesis of the second block DMAEMA was adopted from a literature established synthetic route. Huang et al. synthesised well-defined copolymers of DMAEMA and benzophenone methacrylate (BPMA) with different compositions via atom transfer radical polymerisation.<sup>386</sup> The ATRP polymerisation of DMAEMA was performed in either acetone or cyclohexanone using a Cu(I)Cl/Cu(II)Cl/HMTETA complex as catalyst at 50°C. These conditions were applied in order to control the polymerisation. For instance, copper(II) chloride (CuBr<sub>2</sub>) was used as deactivator in order to reduce the polymerisation rate. However, some changes were carried due to the different chemical nature of the macromonomers used for this project. In particular, in the case of poly(EGDPEA) the solvent system was switched from acetone to cyclohexanone because of the poor solubility of the macromonomer with acetone. Cyclohexanone was chosen for its similar polarity ( 0.28) to the acetone (0.35).<sup>393</sup> In addition, in order to achieve the target molar ratio of 90:10 % mol/mol (Macroinitiator:DMAEMA), DMAEMA was introduced in a molar excess, usually the double with respect to the required quantity to reach the 10% in mol. In Table 5.7 a summary of the ATRP of EGDPEA-*b*-DMAEMA, HPhOPA-*co*-DMAEMA and EA-*co*-DMAEMA are showed.

Table 5.7 Summary of the ATRP and the physical characterisation of the nanoaggregates (size, CAC and zeta potential) of EA-*b*-DMAEMA, EGDPEA-*b*-DMAEMA and HPhOPA-*b*-DMAEMA. ATRP was conducted using a molar ratio Initiator:Cu(I)Cl:Cu(II)Cl:HMTETA of 1:2:0.4:1.2 and aiming at a molar ratio Macroinitiator:DMAEMA of 90:10 % mol/mol. physical characterisation of the nanoaggregates (size, CAC and zeta potential). The DLS analysis were performed at 25°C and the Intensity (%) values were registered and analysed. The suspension/emulsion were prepared in DI water at pH of around 7.

Entry	Final Copolymer Ratio <sup>a</sup> (% mol/mol)	$M_n^b$ MacroIn (Kg mol <sup>-1</sup> )	$M_n^b$ block (Kg mol <sup>-1</sup> )	$\bar{D}^b$	Size (nm)	CAC (µg/mL)	$\zeta$ (mV)
HPhOPA- <i>b</i> -DMAEMA	93:7	13.4	14.8	1.4	564±28	201	+20.0±0.5
EGDPEA- <i>b</i> -DMAEMA	82:18	10.2	12.3	1.4	86±14	240	+43.0±0.4
EA- <i>b</i> -DMAEMA	91:8	13.2	15.7	1.2	98±1	176	+37.0±2.0

<sup>a</sup>Conversion was calculated by <sup>1</sup>H-NMR (Figure 2.1); <sup>b</sup> $M_n$  and  $\bar{D}$  were calculated by GPC.

<sup>c</sup>The CAC values were obtained from the plots of the intensity of the scattered light as a function of the concentration (Figure Appendix 5-11).

From Table 5.7, using similar condition from literature, it is possible to observe that the second block of DMAEMA successfully grew for all the three polymers. The three entries show a molar ratio close to the target 90:10 % mol/mol and a slightly increase in  $M_n$  due to the addition of the second block. A confirmation of the presence of DMAEMA within the copolymer is obtained from the <sup>1</sup>H-NMR spectra and the GPC in Figure 5.5.

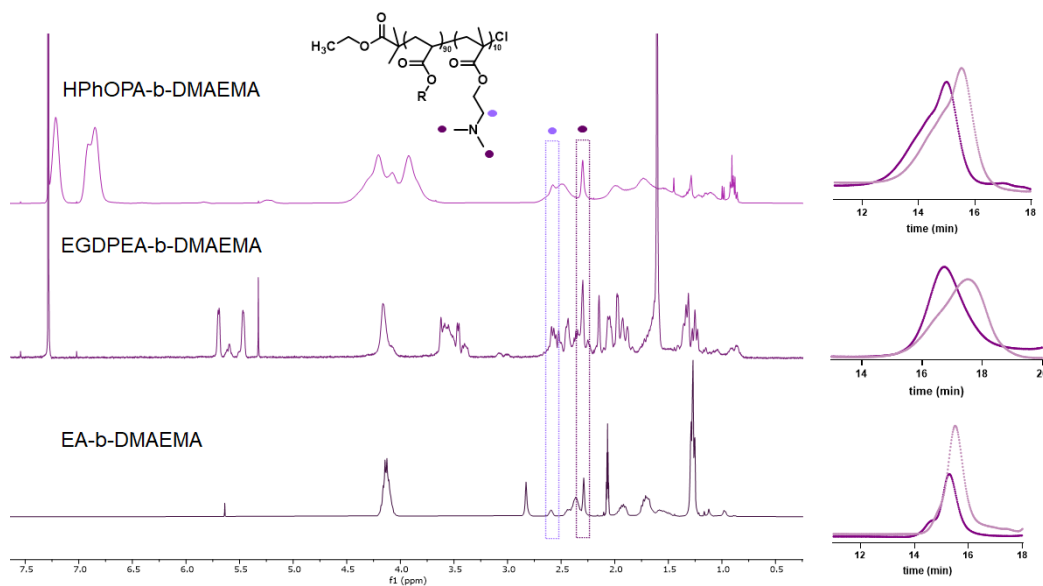


Figure 5.5  $^1\text{H-NMR}$  spectra and the respective GPC chromatogram of the block copolymers HPhOPA-*b*-DMAEMA, EGDPEA-*b*-DMAEMA and EA-*b*-DMAEMA.

The identification peaks for DMAEMA block are highlighted in the  $^1\text{H-NMR}$  spectra in Figure 5.5. The chemical shifts attributed to the DMAEMA side chain, the  $(-\text{CH}_3)_2$  and the  $-\text{CH}_2$  groups, can be observed in the three spectra suggesting the presence of this monomer in the copolymer structure. In addition, the GPC traces show a slightly shift from the macromonomer to the block copolymer hinting at the growing of the second block.

As for the random copolymers, the ability to self-assemble into nanoaggregates was studied in terms of size (at  $1000 \mu\text{g/mL}$ ), CAC and surface charge. At  $1000 \mu\text{g/mL}$ , EGDPEA-*b*-DMAEMA and EA-*b*-DMAEMA showed sizes below  $100 \text{ nm}$ , while, HPhOPA-*b*-DMAEMA has resulted in NPs of around  $500 \text{ nm}$ . The difference in trend, might be due to the different hydrophobic core interactions and different packing. It may also indicate that the potential untargeted species, indicted in the GPC trace, for p(HPhOPA), may be affecting the size data, e.g., this may indicate the likely onset of branching in the polymer it will significantly affect the particle size

produced. All the aggregates resulted net positively charged, indicating that the successful core-shell self-assembling had been achieved and, thus, the presence of DMAEMA in the out layer. In addition, the whole set of surfactants showed CACs ranging from 176-240 µg/mL.

### 5.3.2.3 Comparison Random and Block Architecture

A comparison between the random and block amphiphilic copolymers obtained with DMAEMA in terms of hydrodynamic size distribution (at 1000 µg/mL), CAC and zeta potential is analysed in Table 5.8 and Table 5.9. Where the data in Table 5.9 is a subset of the data shown in Table 5.2 and it was included here for convenience.

Table 5.8 Summary of the physicochemical characterisation data of the amphiphilic block copolymers using DMAEMA as the hydrophilic component. The DLS analysis were performed at 25°C and the Intensity (%) values were registered and analysed. The suspension/emulsion were prepared in DI water at pH of around 7.

Entry	Molar Ratio <sup>a</sup> (% mol/mol)	Size (nm)	CAC <sup>b</sup> (µg/mL)	ζ (mV)
EGDPEA- <i>b</i> -DMAEMA	82:18	86±14	240	+43.0±0.4
EA- <i>b</i> -DMAEMA	91:8	98±1	176	+37.0±2.0
HPhOPA- <i>b</i> -DMAEMA	93:7	564±28	201	+20.0±0.5

<sup>a</sup>Molar Ratio (HyB:DMAEMA) was calculated by <sup>1</sup>H-NMR. <sup>b</sup>The CAC values were obtained from the plots of the intensity of the scattered light as a function of the concentration (Figure Appendix 5-11)

Table 5.9 Summary of the physicochemical characterisation data of the amphiphilic random copolymers using DMAEMA as the hydrophilic component.

Entry	Molar Ratio <sup>a</sup> (% mol/mol)	Size (nm)	CAC <sup>b</sup> (µg/mL)	ζ (mV)
EGDPEA- <i>co</i> -DMAEMA	92:8	73±1.4	174	+45±0.8
EA- <i>co</i> -DMAEMA	80:20	111±0.8	150	+42±1.3
HPhOPA- <i>co</i> -DMAEMA	86:14	205±5.0	160	+44±0.7

<sup>a</sup>Molar Ratio (HyB:DMAEMA) was calculated by <sup>1</sup>H-NMR. <sup>b</sup>The CAC values were obtained from the plots of the intensity of the scattered light as a function of the concentration (Figure Appendix 5-11)

In Table 5.8 and Table 5.9, the properties of the two different amphiphilic systems were compared to initially assess the effect of the architecture upon particles features. Although these preliminary observations need additional measurements and further analysis, they reveal key differences between the block and random series. In fact, the random copolymers generally had smaller sizes, lower CACs and slightly higher surface charges when compared to the block ones.

A more detailed investigation of the data showed that the hydrodynamic diameter follows a similar trend with both types of polymer architecture, with EGDPEA:DMAEMA polymers showing the smallest size (<100 nm) and the highest CAC. However, the most relevant observation is that the copolymers presenting HPhOPA as comonomer, under the specific formulation protocol, have the biggest size. In particular, the block copolymer showed the lowest surface charge hinting to a lower stability, in water, when compared to the other materials.

### 5.3.3 Microfluidics

#### *5.3.3.1 Microparticles Production with DMAEMA Based Random Copolymers*

To determine the suitability of the new functionalised positively charged random copolymers to have utility as surfactant for the preparation of microparticles. A similar microfluidic setting system, used for the random amphiphilic graft copolymers with mPEGMA, was utilised. In detail, an O/W droplet flow-focusing chip was used for the optimisation of these new

amphiphilic copolymers with the same initiator concentration (2% w/v) and core material (HMDA, 96% w/v). Also, for these new materials, the flow rates of the disperse (HMDA/initiator/surfactants) and the continuous phase were optimised to ensure the formation of stable and monodisperse particles. As shown previously when changing the flow rates of  $Q_d$  and  $Q_c$  different regime profiles can be seen within the channels (e.g. dripping wall wetting, jetting, unstable particle satellites formation and squeezing) which can affect the performance of the MPs manufacturing process. Figure 5.6 contains the flow diagrams of the three surfactants (2% w/v) using 2% w/v of photoinitiator and 96% w/v of HMDA. The diagram was built by varying the  $Q_d$  and the  $Q_c$  from 0.1 ml/h to 0.5 ml/h and from 1 ml/h to 9 ml/h, respectively.

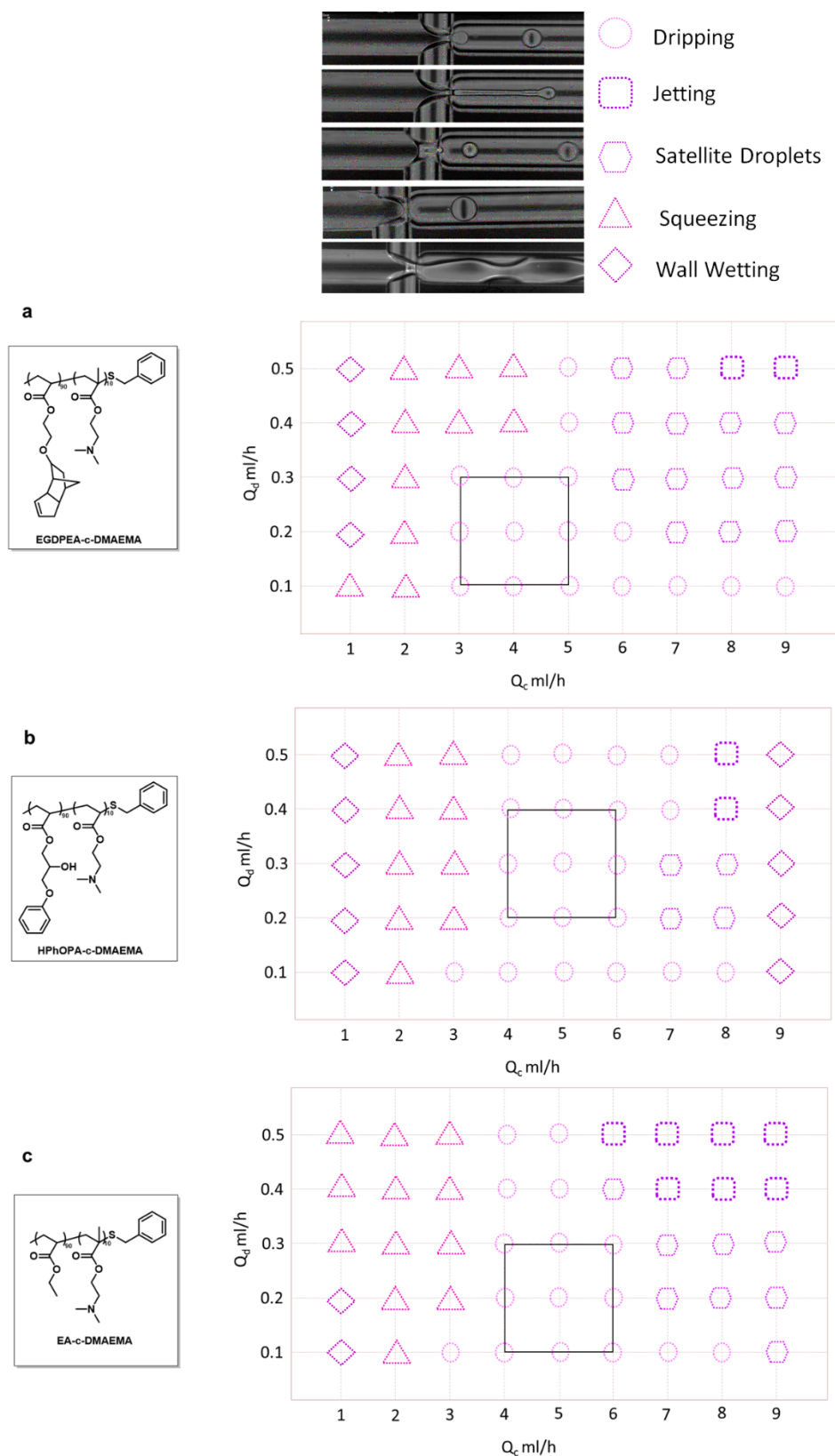


Figure 5.6 Flow diagram of an O/W microfluidics system with HMDA core material and EGDPEA-co-DMAEMA (a), HPhOPA-co-DMAEMA (b) and EA-co-DMAEMA (c). In the diagram: ○ denotes idealistic dripping behaviour, □ denotes jetting behaviour, ◇ denotes formation of satellite droplets, ◇ denotes flow rates which caused wall wetting events and △ denotes large dripping. The Black square denotes the region of flow rates that produces monodisperse emulsions. Images show examples of dripping, jetting, satellite droplet formation and wall wetting events, respectively.

As shown in Figure 5.6, all the amphiphilic copolymers have demonstrated their ability to form stable emulsion and, thus, to behave as surfactants. However, each material exhibited a different range where stable and monodisperse droplets were formed inside the channels of the microfluidic chip. For instance, in the case of EGDPEA-co-DMAEMA (Figure 5.6a) this range is around  $Q_c$  4 ml/h and  $Q_d$  0.2 ml/h. Similarly, EA-co-DMAEMA produced a stable emulsion within the flow window of  $Q_c$  4-6 ml/h and  $Q_d$  0.1-0.3 ml/h (Figure 5.6c). Also, both of these surfactants display a gradually flow regime change, with the increasing of  $Q_d$  and  $Q_c$ , passing through the main four different flow behaviours: wetting, squeezing, dripping and jetting. Meanwhile, HPhOPA-co-DMAEMA data were found to be inconsistent with respect to the previous surfactants. Firstly, this surfactant experienced wall-wetting behaviour at a  $Q_c$  of 1 ml/h and 9ml/h regardless the value of  $Q_d$  (Figure 5.6b). This structureless state is probably related to the low performance of the surfactant which is not forming a stable interface between the oil and water phase. When the oil phase is partially adhering to the channel walls, the emulsification process is clearly in disordered states and the performance of the surfactant plays a key role in the formation of this state.<sup>394,395</sup> In addition, the transition from a structureless system to a structured monodisperse regime is not as gradually as in the other surfactants. The drastic changes among the difference regimes happens when the system works in partial wetting case, as Dreyfus et al. explained, hinting that the surfactant system is not enough controlled.<sup>395</sup> The relative lack of control that was, also, observed in the

development of the copolymerisation of HPhOPA with DMAEMA indicating that further research into the control of this monomers interactions whilst polymerising is required.

The overall flow rates ( $Q_c$  and  $Q_d$ ) conditions employed in the microfluidics apparatus, for of each random amphiphilic copolymer, are briefly summarised in the Table Appendix 5-1. Meanwhile, Figure 5.7 contains the microfluidics particle sizing data and the SEM images of each of the resulting MPs at the resolution of 250X and 650X for EGDPEA-*co*-DMAEMA and EA-*co*-DMAEMA surfactants.

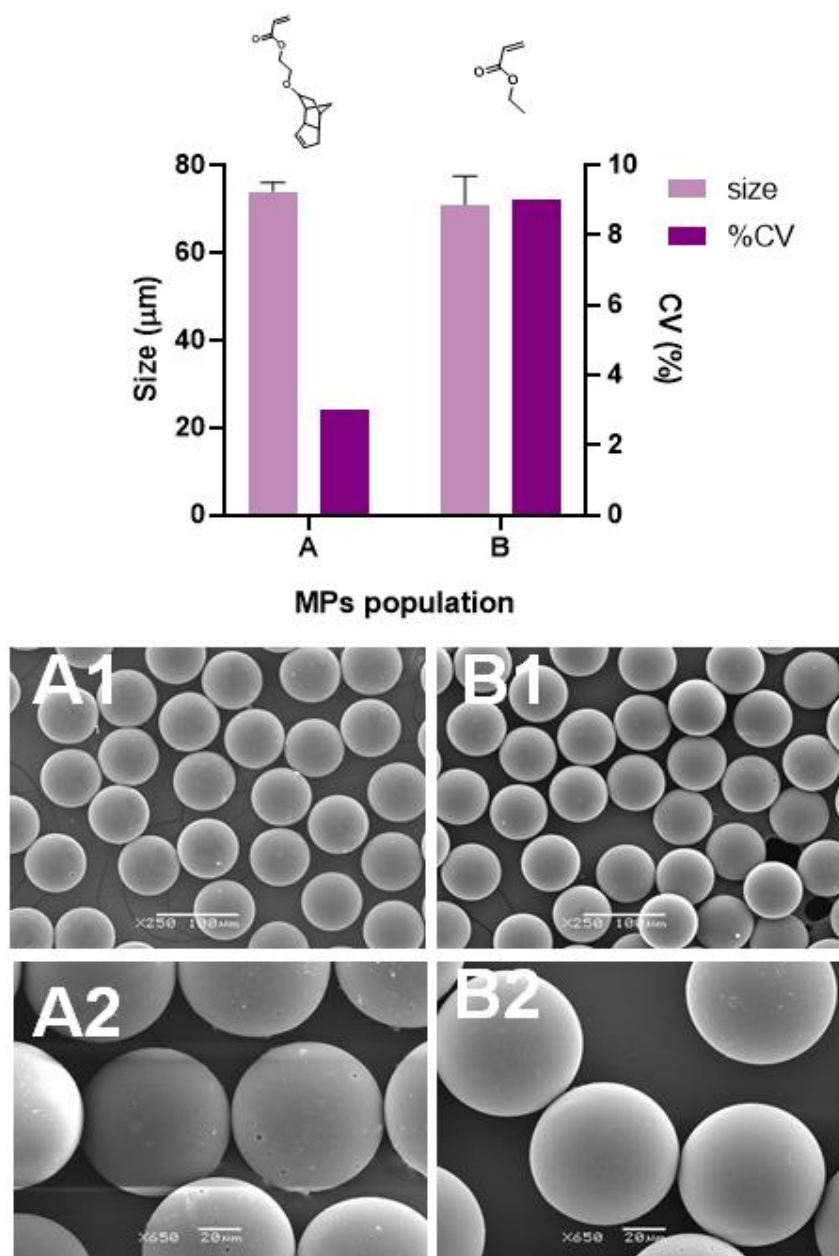


Figure 5.7 Plot with size summary and the Coefficient of Variation (%) for the surfactants EGDPEA-co-DMAEMA and EA-co-DMAEMA produced by analysing the SEM images of the polymer MPs.

Figure 5.7 showed that all the generated MPs, using the O/W droplet microfluidics, are perfectly spherical with a diameter lower than the orifice width (70 µm) highlighting the work of the surfactant in reducing the surface tension between the two phases. When EGDPEA-co-DMAEMA based particles are taken into consideration, the coefficient of variation, CV, resulted lower than 5% (~3%) (CV is a parameter used to measure a

distribution, narrow distribution is considered when this coefficient is less or around 5%) confirming that these particles are monodisperse. The EA-co-DMAEMA seems to be performing less well as surfactant causing an increase in the CV to 9%. However, this increasing is not dramatically high and still acceptable for the application of these MPs as 3D biologically active platforms. The SEM analysis indicated the appearance of pores on the surface of this set of particles. The lack of smoothness of the surface might be caused by a poor mixing between the diacrylate core material and the surfactants which led to the formation of surfactants-rich domains at or near the particles surface. The larger amount of the surfactants adsorbed near the surface may rapidly detach leaving behind this porosity.

Interestingly, the instability detected for HPhOPA-co-DMAEMA from the preliminary self-assembling study *via* DLS to the lack of flow control in the microfluidics chip, was also observed in the manufacturing process. This was because, despite droplets successfully exited from the microfluidics chip, they were to collapse in the outlet channel forming bigger agglomerated emulsified structures and losing their spherical shapes. Because of these phenomena, HPhOPA base droplets were not collected and, consequently, subjected to the photo-polymerisation. Because of this instability, this surfactant has not been further analysed in this study.

### 5.3.3.2 *Microparticles Production with DMAEMA Based Amphiphilic Block Copolymers*

The production process of the MPs by means of the block copolymers required first the optimisation of the flows rates, similarly to the random copolymers described earlier. One of the interests in this optimisation study concerned the role of different architecture in the stabilisation of the emulsion, i.e. the formation of monodisperse droplets occurring at the same flow rates range of the random copolymers. In Figure 5.8 contains the flow diagrams of the EGDPEA-*b*-DMAEMA and EA-*b*-DMAEMA surfactants (2% w/v) using 2% w/v of photoinitiator and 96% w/v of HMDA. The diagram was built by varying the  $Q_d$  and the  $Q_c$  from 0.1 ml/h to 0.5 ml/h and from 1 ml/h to 9 ml/h, respectively.

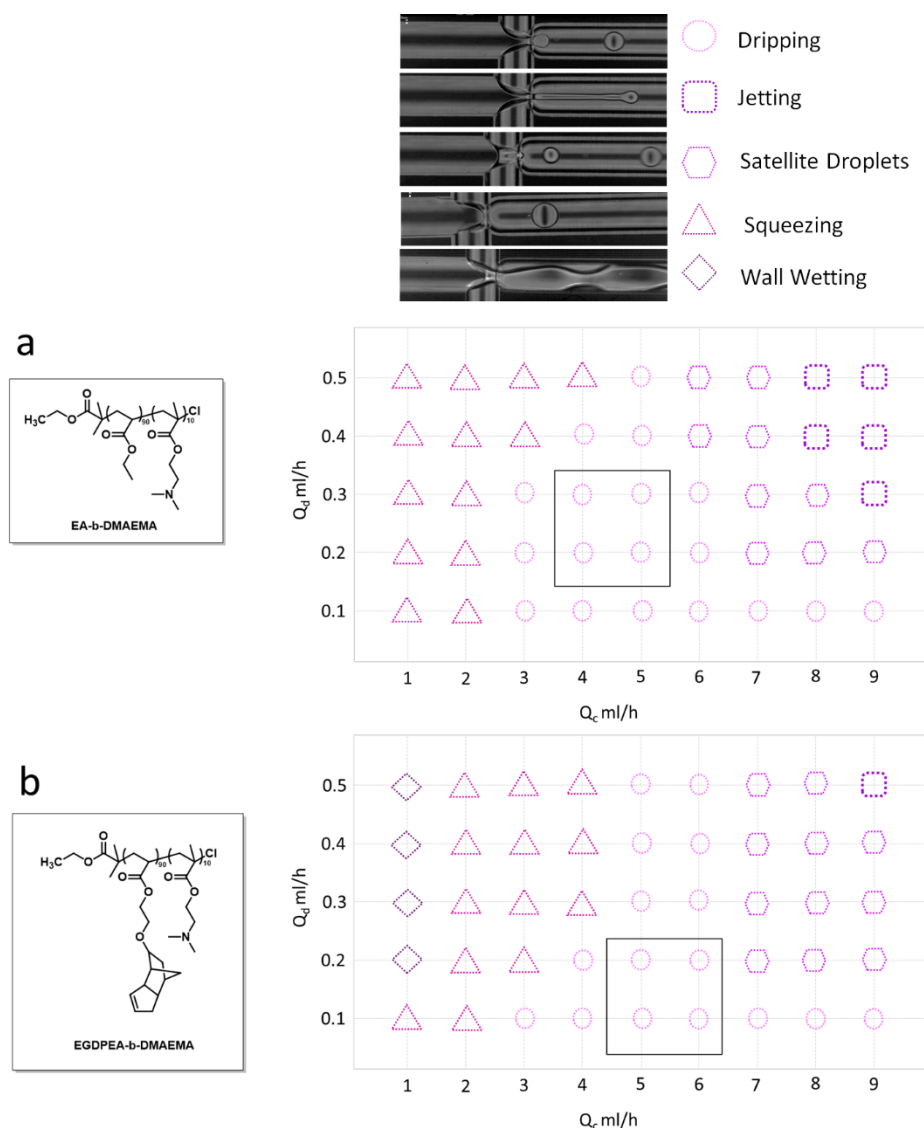


Figure 5.8 Flow diagram of an O/W microfluidics system with HMDA core material and EA-*b*-DMAEMA (a) EGDPEA-*b*-DMAEMA (b) as surfactants. In the diagram:  $\circ$  denotes idealistic dripping behaviour,  $\square$  denotes jetting behaviour,  $\hexagon$  denotes formation of satellite droplets,  $\diamond$  denotes flow rates which caused wall wetting events and  $\triangle$  denotes large dripping. The Black square denotes the region of flow rates that produces monodisperse emulsions. Images show examples of dripping, jetting, satellite droplet formation and wall wetting events, respectively.

From the phase diagram showed in Figure 5.8, it was observed that monodisperse droplets were formed in flow rates ranges slightly different, from the respective random copolymers, in both cases. Interestingly, the phase that varied was, in both studies the water phase. In fact, it appears that in case of EGDPEA-*b*-DMAEMA, the  $Q_c$  needs to be higher to obtain a

stable drippings area (5-6 ml/h). In contrast, EA-*b*-DMAEMA showed a shifting of the working flow region towards lower  $Q_c$ . However, to form stable droplets the followed flow rates, 5.5 mL/h-0.2 mL/h and 4.5 mL/h-0.2 mL/h, were exploited for EGDPEA-*b*-DMAEMA and EA-*b*-DMAEMA, respectively (Table Appendix 5-1 for comparison with the random). Figure 5.9 shows the size and morphology of the MPs obtained *via* the microfluidics technique.

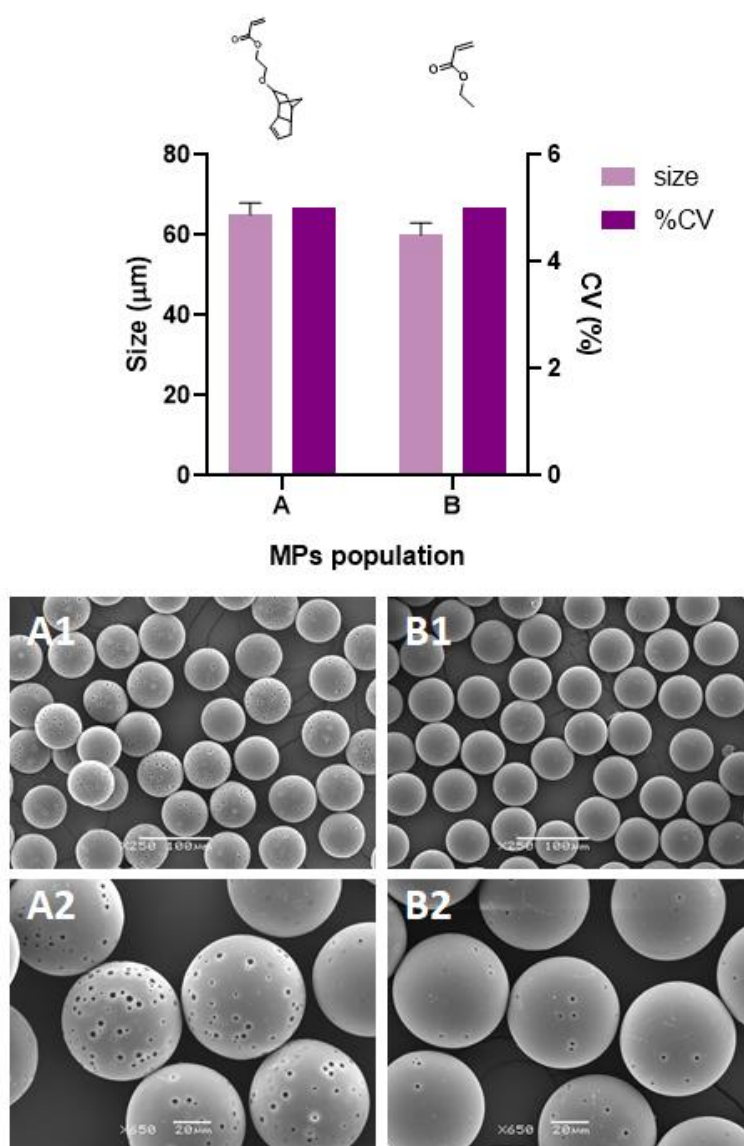


Figure 5.9 Plot with size summary and the Coefficient of Variation (CV %) for the surfactants EGDPEA-*b*-DMAEMA and EA-*b*-DMAEMA produced by analysing the SEM images of the polymer MPs.

From the graph in Figure 5.9, overall, the block copolymers showed a good control in terms of size and achieving a monodisperse particle size distribution. The size of the particles resulted were observed to be around 60  $\mu\text{m}$  for both the surfactant systems. Surprisingly, the size decreased to 10  $\mu\text{m}$  with respect to the size of the MPs controlled by the random surfactants. This highlighted how the stability of the block self-assembly changed in terms of reducing the O/W interface energy and leading to smaller particles. In addition, both produced MPs are monodispersed with a value of CV around of 5%.

However, the morphology was drastically affected with an increase of the porosity throughout the whole surface of the particles. As mentioned previously, the presence of the porosity may be due to a formation of surfactants cluster on the MPs surface causing detachment during the droplets collection. The detachment seems to be higher for these amphiphilic copolymers, likely due to the architecture of the surfactants. The DMAEMA hydrophilic part being more exposed to the aqueous medium, as a consequence of the self-assembling, can result in an easier washing out effect of the surfactant from the surface of the particles. These phenomena need to be studied more in depth to better understand the interplay among the nature of the hydrophile, architecture of the surfactants and nature of the collection media. However, a preliminary study, which aimed at tuning the porosity of the surface of the MPs, was conducted by preparing surfactants mixture system combining the block and the random copolymers in a molar ratio of 50:50 % mol/mol.

Considering that these two architectures have shown different degrees of surface porosity as well as a different control in the size distributions, by mixing the surfactants might overcome the low control in polydispersity for the random polymers (i.e. EA-co-DMAEMA) and the topography defects observed for the blocks (EA-*b*-DMAEMA and EGDPEA-*b*-DMAEMA). In Figure 5.10 a summary of the size and the SEM images at 250X and 650X resolution are shown.

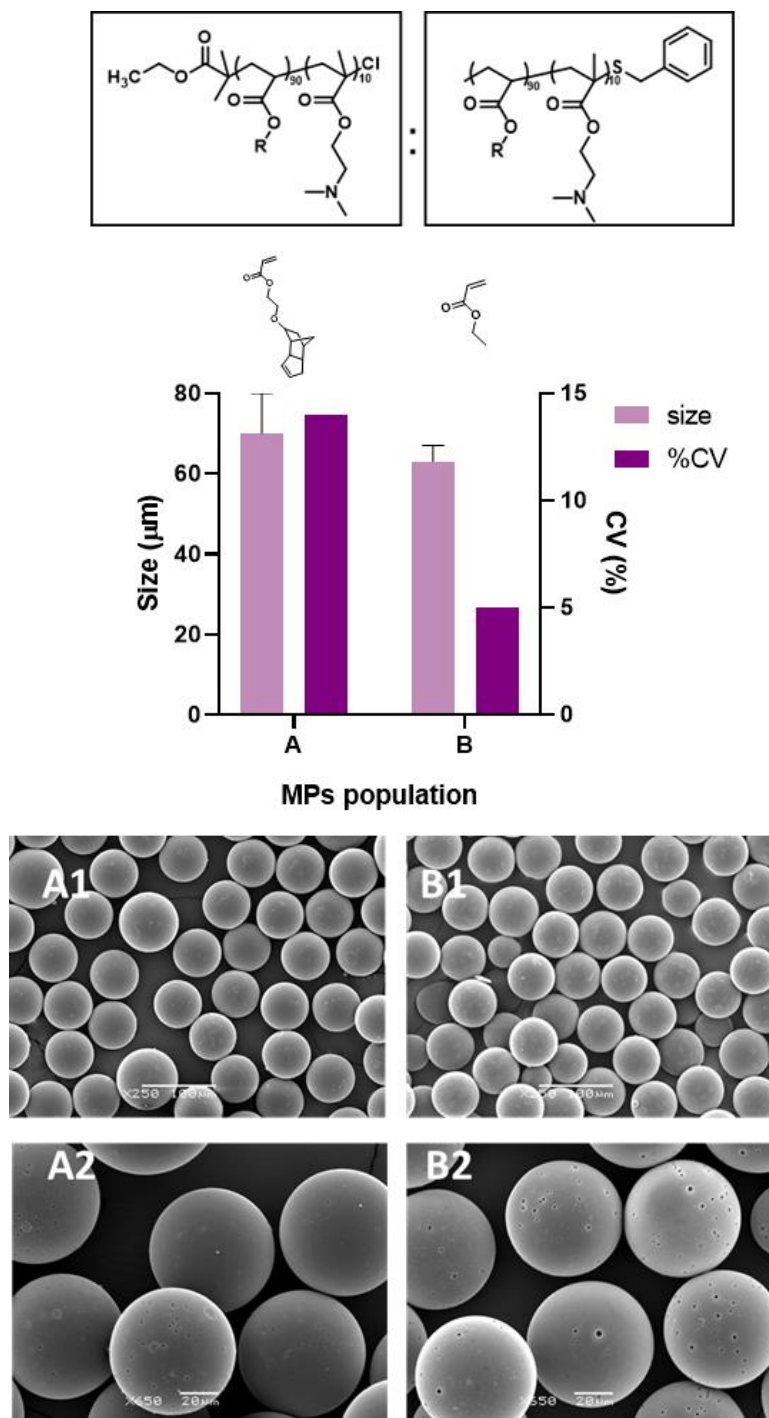


Figure 5.10 Plot with size summary and the Coefficient of Variation (%) for the mixed system formed by the surfactants  $(\text{EGDPEA}-b\text{-DMAEMA}/\text{EGDPEA}-co\text{-DMAEMA})_{50/50}$  and  $(\text{EA}-b\text{-DMAEMA}/\text{EA}-co\text{-DMAEMA})_{50/50}$  produced by analysing the SEM images of the polymer MPs.

From the plot in Figure 5.10, the sizes of these sets of particles present values lower than the width of the chip orifice, more specifically the distributions are around 70  $\mu\text{m}$  for the EGDPEA (CV 14%) and 63  $\mu\text{m}$  (CV 5%)

EA based surfactants. Focusing the attention on the EA/DMAEMA copolymers, the mixed system appears to be a good compromise between the size distribution (similar to the random copolymer) and the improving of the % CV. The topography, also, benefitted from this system as it shows a reduced degree of porosity compared to the block copolymers. Similar improvement in terms of the porosity is observable for the EGDPEA mixed system. However, the control over size and dispersity is lost, for instance, the CV of this particles is around 14%, among the highest in the library of particles produced so far. There may be an anti-synergistic effect between these two materials due to a poor mixing which have hampered their performance in the stabilisation of the emulsion.

Overall, this preliminary screening on the effect of a premixing of the random/block formulations showed a possible and elegant strategy to alter surface properties and size distribution broadening and tailoring the potential final applications of the produced MPs.

#### 5.3.4 Microparticle Surface Characterisation

Time of Flight Secondary Ion Mass Spectrometry (ToF-SIMS) analysis was used to investigate the bio instructive surface, represented by the surfactant, of the produced MPs. The data was collected in both positive and negative ion mode in order to identify the unique ions associated with the hydrophilic and hydrophobic sides of the copolymers.

For the copolymers with DMAEMA, the unique identifiers found were  $C_3H_8N^+$ ,  $C_5H_7^+$  and  $C_2H_5^+$  which were associated with the DMAEMA, EGDPEA

and EA moieties, respectively. In the spectra of the copolymers made of EA it was difficult to find major differences with the SIMS spectra of the core HMDA particles. The similarity between both spectra, characterised by ions derived from acrylate and hydrocarbon fragments, was expected due to analogous chemical structure. However, it was still possible to confirm the presence of the surfactant thanks to the presence of the DMAEMA.

In Figure 5.11 is presented the bar graph with the total ion counts for the particle produced using random, block copolymers and their mixed system. The particles prepared with surfactant were compared with the HMDA core particles prepared without surfactant to demonstrate the difference between the unfunctionalised and functionalised particles.

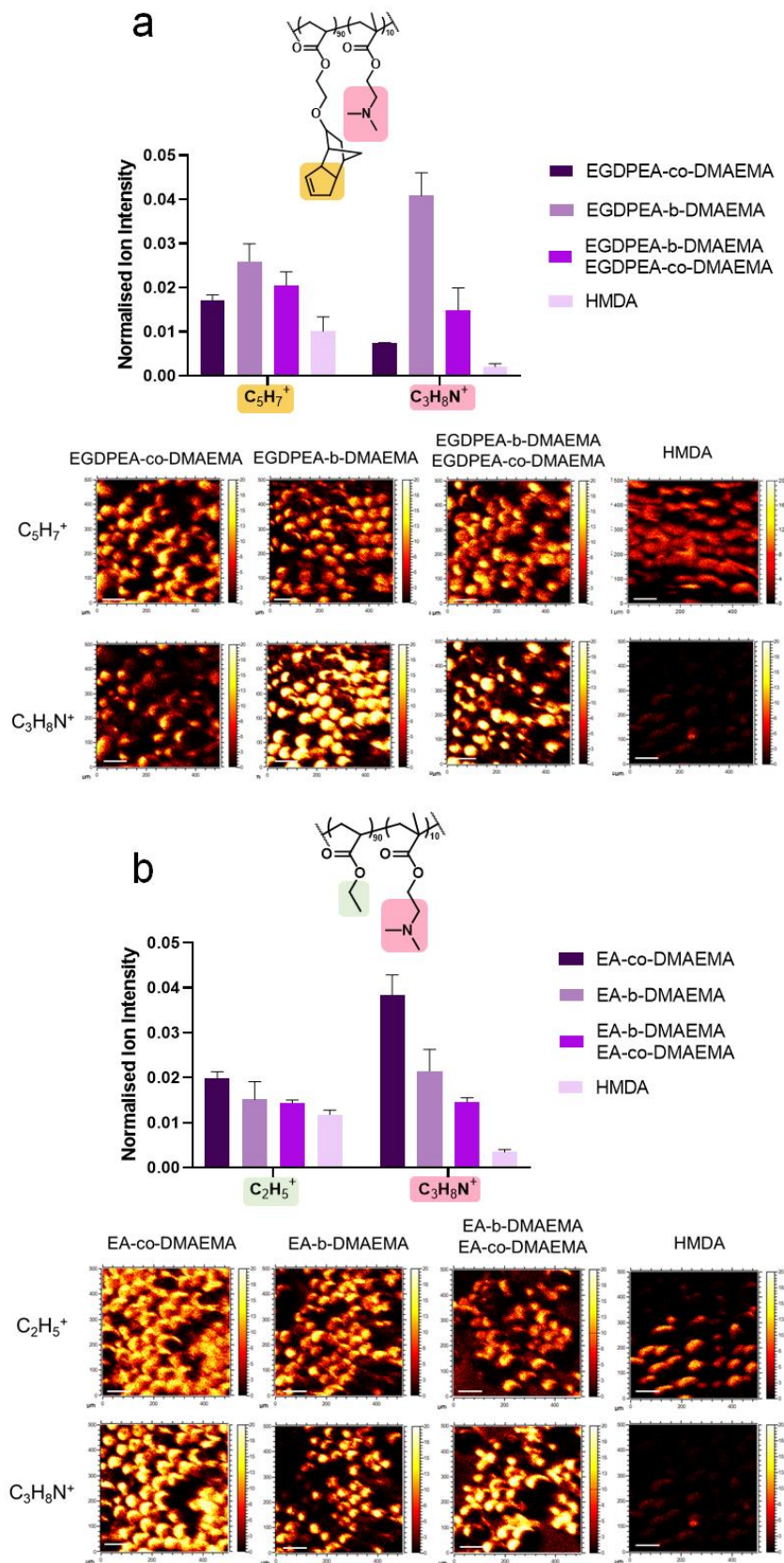


Figure 5.11 ToF-SIMS data showing intensities and the related images of the key ions associated to the (a) EGDPEA:DMAEMA and (b) EA:DMAEMA comonomers within the surfactant structure compared to the intensity of the same ions present in the core HMDA particles spectra.

In both Figure 5.11a and Figure 5.11b, the comparison of the particles with the plain core HMDA clearly demonstrated that the identified ions are unique to the individual surfactants and therefore showed that the surfactant is located at the surface of the particles. The characterisation of the EGDPEA based particles depicts that the surfactants (Figure 5.11a) are on the surface due to the increase of the ions  $C_5H_7^+$  and  $C_3H_8N^+$  with respect to the plain core HMDA particles.

Differences can be seen between the random and the block copolymers. Despite the presence of high porosity throughout the surface of the particles, as shown in the SEM images, EGDPEA-*b*-DMAEMA has the highest intensity for both ions. This indicates that the surface defects do not affect the concentration of the surfactant and so the bio instructive feature. In contrast, Figure 5.11b showed that the particles controlled by EA-*b*-DMAEMA have the highest presence of the unique ions of both comonomers. In addition, the intensity of  $C_2H_5^+$  ion (i.e. EA ion identifier) of the block copolymer and the mixed surfactant is not significantly varying from the HMDA core. It was hypothesised that the hydrophobic block may interact particularly with HMDA, due to the chemical affinity, leading to a further migration of the surfactant towards the inner core. Further surface analysis will be required to better investigate this set of data. Meanwhile, the ion indicative of the DMAEMA chain ( $C_3H_8N^+$ ) can also be found at the surface of the functionalised EA particles, and the intensity for this ion is reduced on the HMDA core particle with no surfactant, which is to be expected as there is no DMAEMA on the sample.

### 5.3.5 Protein Corona Binding Assay

In order to evaluate the stability of the formulated NPs as the effect of surface charge and polymer architecture in biologically relevant conditions, a screening assay was developed using DLS in presence of BSA used as model protein to assess protein-induced aggregation.<sup>396</sup> A DLS-based assay was chosen as the preliminary screening technique due to the fast response time and straightforward possibility to detect macroscopic aggregation within each sample. This intuitive screening was performed as an initial understanding before the more complexed testing of the surface-decorated MPs samples. The assayed concentration of BSA in solution, 0.2 wt%, was chosen as representative of the protein concentration within DMEM culture media with 10% Fetal Bovine Serum. All the samples were incubated at 37°C and sized by DLS after 0, 1 and 24 h. Interestingly, from this preliminary attempt, similarity can be observed between this simple test and the previous BSA test performed on the mPEG-stabilised MPs library (see Chapter 3). Figure 5.12, contains the DLS results comparison of the DMAEMA based amphiphilic random copolymers versus both the mPEGMA<sub>300</sub> variant and the DMAEMA block copolymers. The DLS traces depict the interaction, throughout the time (0 h, 1 h and 24 h), between the surfactants and the model protein BSA.

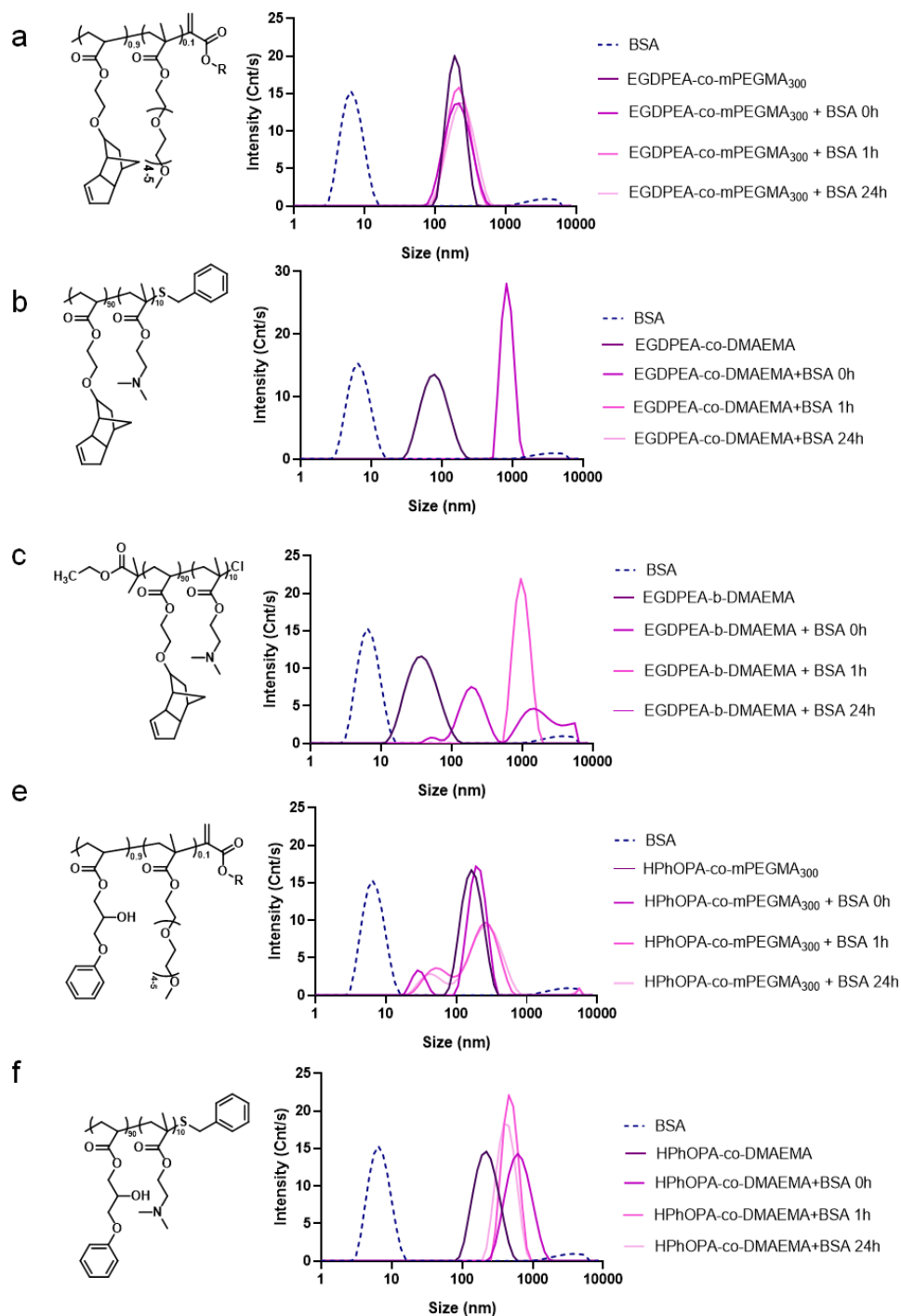


Figure 5.12 Protein corona binding studies of the follow copolymers EGDPEA-co-mPEGMA<sub>300</sub>, EGDPEA-co-DMAEMA, EGDPEA-b-DMAEMA, HPhOPA-co-mPEGMA<sub>300</sub> and HPhOPA-co-DMAEMA with representative DLS traces of each polymer architectures after incubation in 2 wt% of BSA, confirming stability to aggregation in these conditions. Correlograms of the DLS traces and sizes as Intensity, Volume and Number are shown in Figure Appendix 5-12 and 5-13.

This data shows that the NPs produced with the anti-attachment model EGDPEA-co-mPEGMA<sub>300</sub> (Figure 5.12a) showed a monomodal size distribution, throughout the whole incubation time with BSA. This highlights a high stability with no interaction with the protein and this observation mirrored by this sample exhibiting the lowest level of BSA covering observed for the MPs produced with the same surfactants in Chapter 4 Section 4.3.2.1. In contrast to this, the DLS traces of EGDPEA-co-DMAEMA (Figure 5.12b) showed evidence of aggregation immediately after BSA addition, and complete peak disappearance after 1 h. This was attributed to be as result of the high positively charge density as confirmed by the zeta potential (+45 mV) promoting protein binding. Finally, the last BSA screening of the same series of HyB monomer was performed on EGDPEA-*b*-DMAEMA formulation (Figure 5.12c). As for the random copolymer, the presence of a high positive surface charge density similarly affected the interaction of the NPs with the protein leading to aggregation from 0h and complete trace disappearance after 1h. From this initial investigation, it seems that the architecture may not have a difference in the protein-binding kinetics. At this stage, the total surface charge may determine the protein binding rather than the architecture, and consequently, the possible different self-assembling.

In Figure 5.12d, HPhOPA-co-mPEGMA<sub>300</sub> formulation has initially shown a monomodal size distribution. However, once the NPs are in contact with the BSA solution a bimodal size distribution was detected for all the observation times. It can be speculated that due to the tendency of HPhOPA moiety to interact with BSA, as observed for the MPs prepared with the same

surfactant in Chapter 4, has likely contributed to the protein interaction process, thus, to the observed instability of the NPs. A faster and more relevant aggregation process was detected by the DLS when mPEGMA was substituted with the positively charged DMAEMA. As shown in Figure 5.12e, a large aggregate, with size around 650 nm (free surfactant 205 nm), was detected after 0 h of protein contact. Evidence of further aggregation and stability was observed after 24 h, likely due to the formation of BSA multilayers. To further investigate the interaction between the BSA with the different NPs, sizes reported, also, as Volume and Number. The Volume and Number distributions confirmed the size of the NPs before the BSA incubation, superimposing on the Intensity traces. When aggregates were forming because of the interaction with BSA, two different situations were observed, mono- or bimodal traces. This may confirm the formation of aggregates, as previously discussed.

The reported screening of NPs-BSA aggregation propensity has remarked not only the importance of the interplay among hydrophobic moiety natures, charge density and polymer architecture to effectively link NPs, thus NPs surfaces, characteristics with behaviours in biologically relevant conditions pre cell-attachment.

Due to time and instrument booking limitation, further investigations need to be carried out to shed light on the interaction of the bio-instructive surface with the model BSA and more related model proteins involved in biofilms formation.

## 5.4 Conclusions

In this chapter, it was shown that the method previously developed for the manufacturing of MPs, by using bespoke comb-graft PEG based surfactant, can be expanded to other chemistries. In the markets, the available polymeric surfactants have shown to have different chemistries (alkoxylated alkyl phenol condensates, polyamine derivatives of polyisobutenylsuccinic anhydride and polyalkylene glycol modified polyester) and different architectures (block, comb-graft, random, etc.). In light of this, the combined variation of 3D polymer architectures and chemistry were used, for the first time, to assess any differences in the self-assembling performance in the droplet microfluidics system. Amphiphilic cationic block and random copolymers were used as surfactant to both stabilise 1,6-hexanediol diacrylate emulsion in water and, produce monodisperse MPs. From the chemical characterisation ( $^1\text{H-NMR}$ ,  $^{13}\text{C-NMR}$  and GPC), it was demonstrated the successful design and production of these final materials with a target molar ratio 90:10 % mol/mol and a  $M_n$  below  $20,000 \text{ g mol}^{-1}$ . Their self-assembling properties were evaluated by calculating CAC *via* DLS method. Both block and random copolymers series showed CAC values one order of magnitude higher than the PEG polymeric systems. In this case, the presence of the positively charged DMAEMA may negatively affect the performance of these materials in acting as surfactants. Probably, not only the presence of the DMAEMA but its distribution along the chain may have a role in the final dilution stability.

When these materials were used in the microfluidics system, the MPs produced were overall monodispersed with size below 70  $\mu\text{m}$  and porosity throughout their surface. Nonetheless, the presence of the target chemistry of the HyB comonomers and DMAEMA was confirmed by ToF-SIMS. These latest observations indicated that the use of DMAEMA as hydrophilic alternative monomer was still successful for the production of 3D bio-instructive platform for the biomaterials screening.

Finally, DMAEMA was chosen to confer a positive charge to the surface of the MPs with the aim to investigate the cell- and protein-MPs outermost layer interaction. However, due to time limitations related to 19-COVID restrictions, biological assays (in particular the bacteria attachment assay) could not be successfully performed. In this regard, a preliminary study on the stability of the surface chemistry was performed to understand the interaction between our target chemistry and a model protein. A protein corona binding assay was carried out by incubating the nano formulations with BSA, used as protein model. The reported screening of NP-BSA aggregation propensity remarked not only the importance of the interplay among hydrophobic moiety natures, charge density and polymer architecture but to effectively link NP, thus, MPs surface characteristics with behaviours in biologically relevant conditions pre-cell attachment.

## 5.5 Appendix

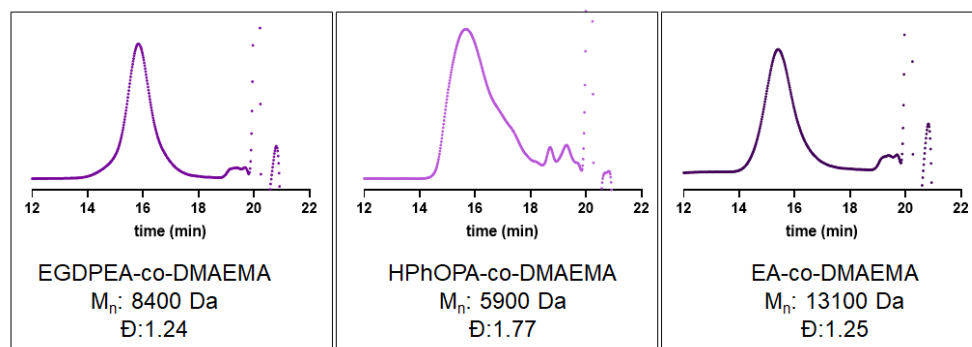


Figure Appendix 5-1 GPC chromatograms of the final pure random copolymers: EGDPEA-co-DMAEMA, HPhOPA-co-DMAEMA and EA-co-DMAEMA.

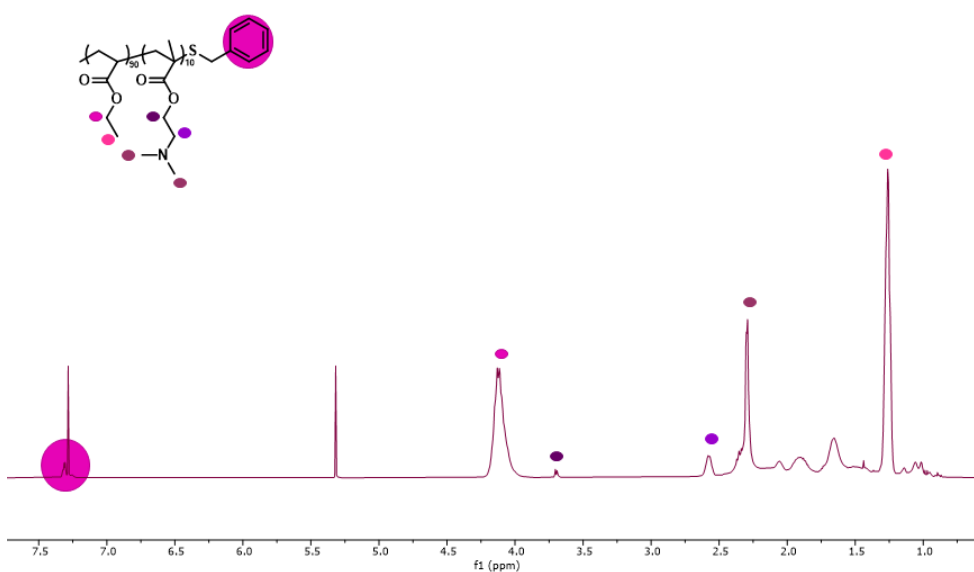


Figure Appendix 5-2  $^1\text{H-NMR}$  spectrum of the purified EA-co-DMAEMA.

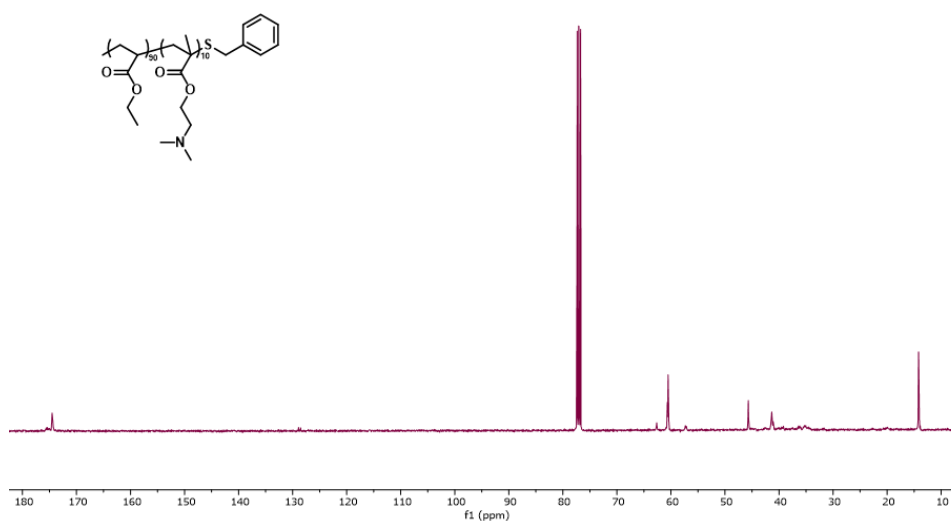


Figure Appendix 5-3  $^{13}\text{C-NMR}$  spectrum of the purified EA-co-DMAEMA

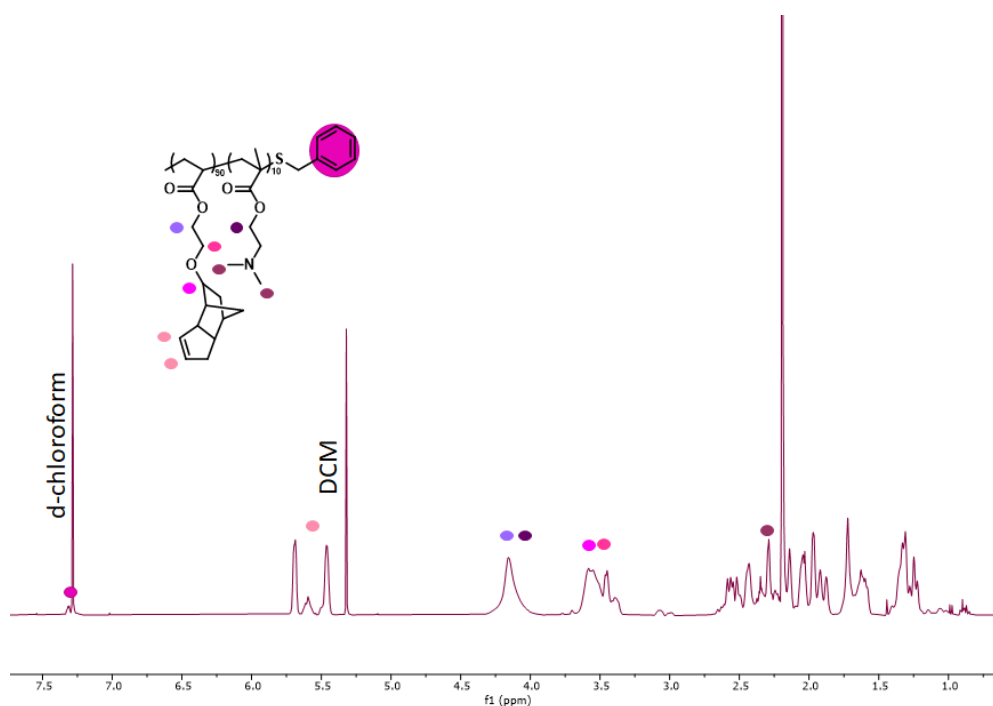


Figure Appendix 5-4 <sup>1</sup>H-NMR spectrum of the purified EGDPEA-co-DMAEMA

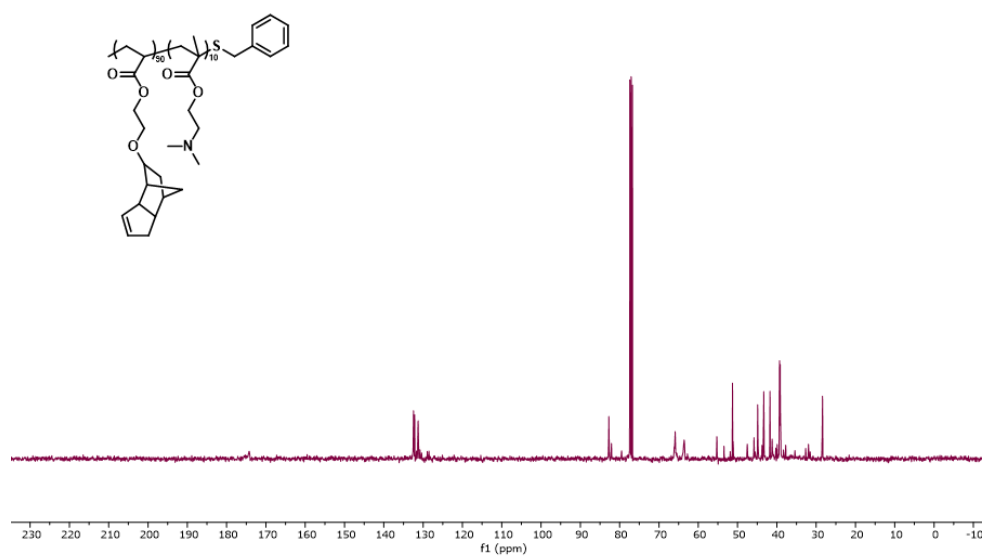


Figure Appendix 5-5 <sup>13</sup>C-NMR spectrum of the purified EGDPEA-co-DMAEMA

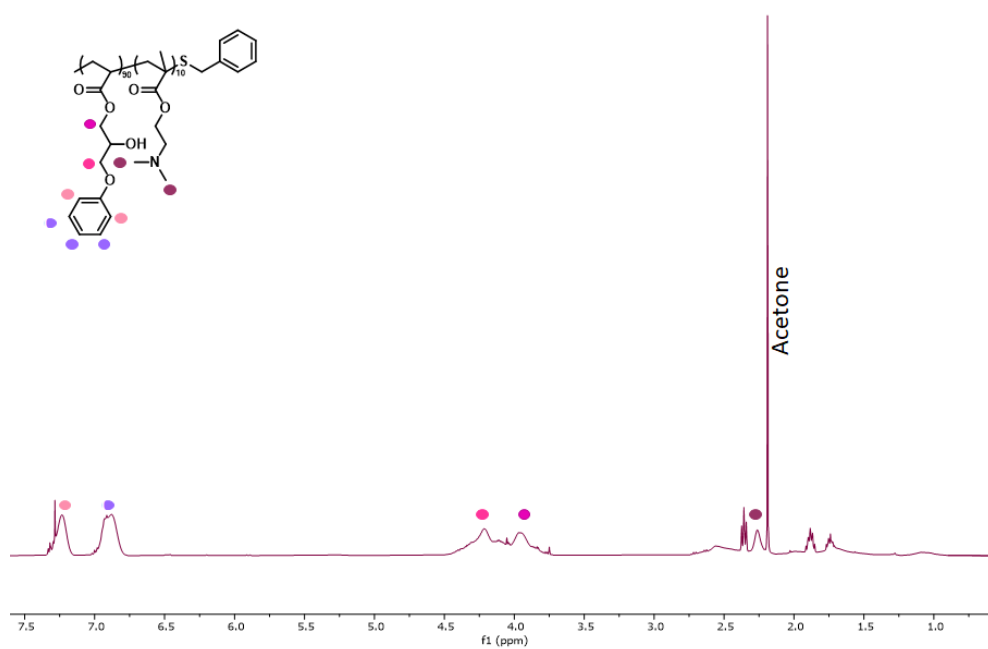


Figure Appendix 5-6  $^1\text{H-NMR}$  spectrum of the purified HPhOPA-co-DMAEMA

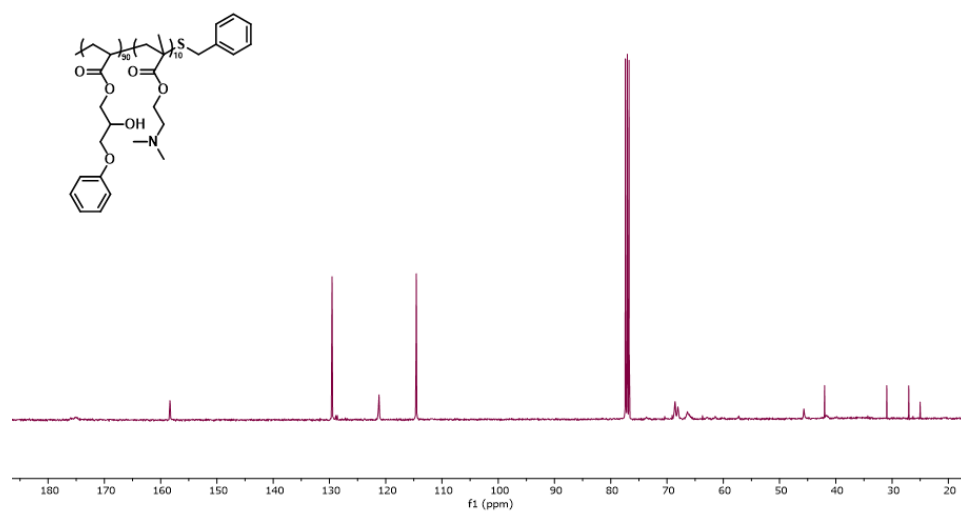


Figure Appendix 5-7  $^{13}\text{C-NMR}$  spectrum of the purified HPhOPA-co-DMAEMA

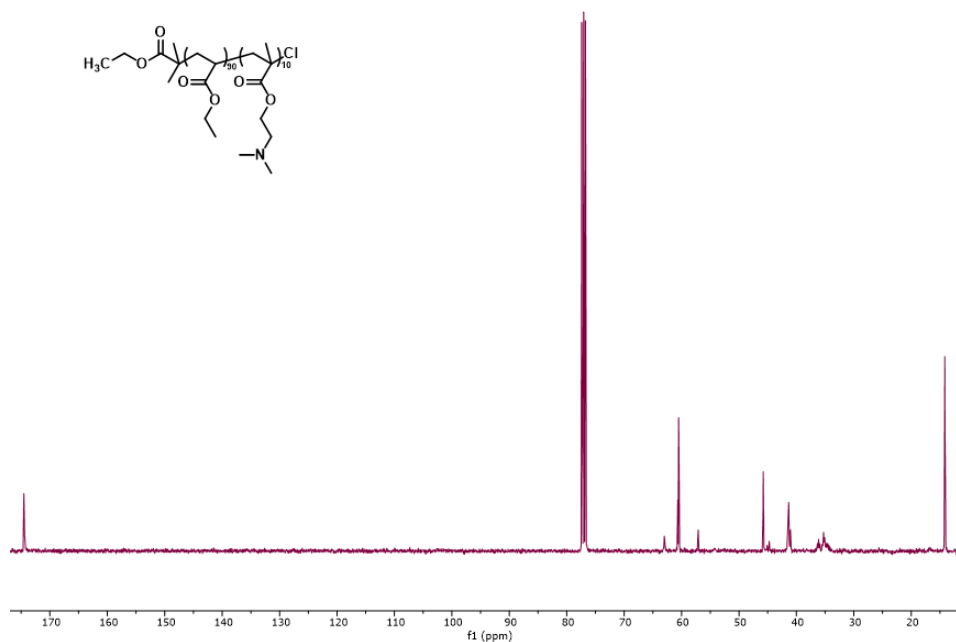


Figure Appendix 5-8 <sup>13</sup>C-NMR spectrum of the purified EA-b-DMAEMA

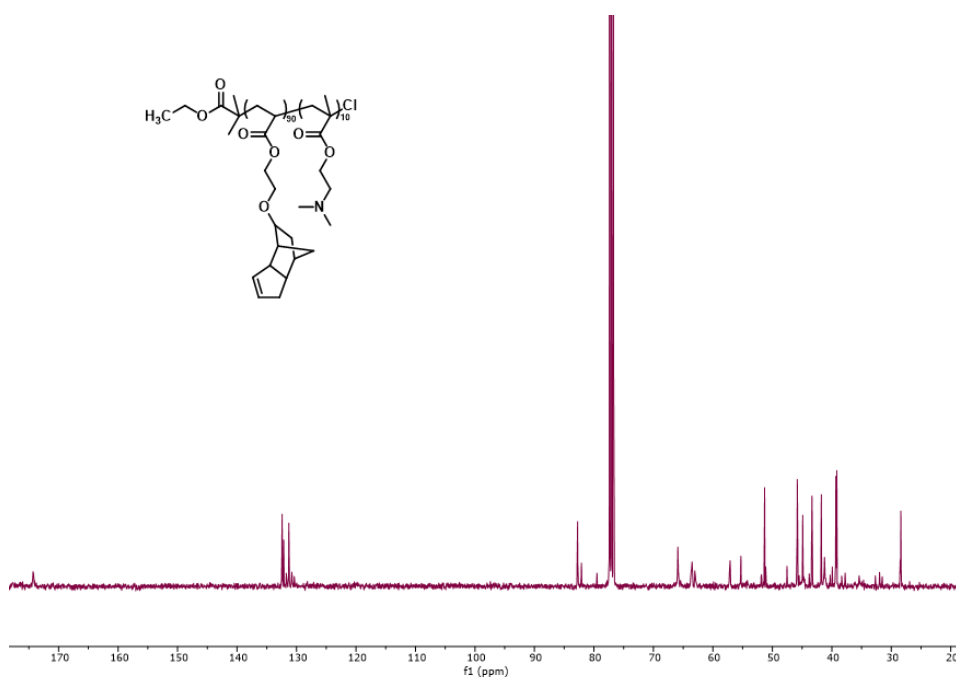


Figure Appendix 5-9 <sup>13</sup>C-NMR spectrum of the purified EGDPEA-b-DMAEMA

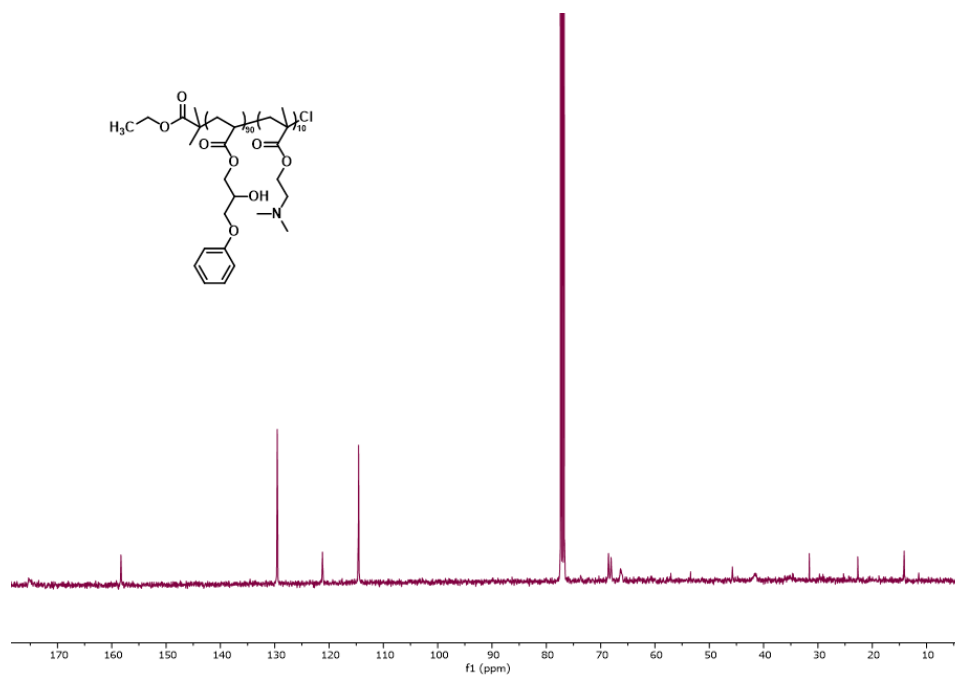


Figure Appendix 5-10 <sup>13</sup>C-NMR spectrum of the purified HPhOPA-b-DMAEMA

Table Appendix 5-1 Values of the flow rates for the aqueous ( $Q_c$ ) and the organic ( $Q_d$ ) phase adopted into the microfluidics for the random and block amphiphilic copolymers.

Entry	$Q_c$ (mL/h)	$Q_d$ (ml/h)
<b>EA-co-DMAEMA</b>	5	0.2
<b>EGDPEA-co-DMAEMA</b>	4	0.2
<b>HPhOPA-co-DMAEMA</b>	5	0.3
<b>EA-b-DMAEMA</b>	4.5	0.2
<b>EGDPEA-b-DMAEMA</b>	5.5	0.2
<b>HPhOPA-b-DMAEMA</b>	-	-

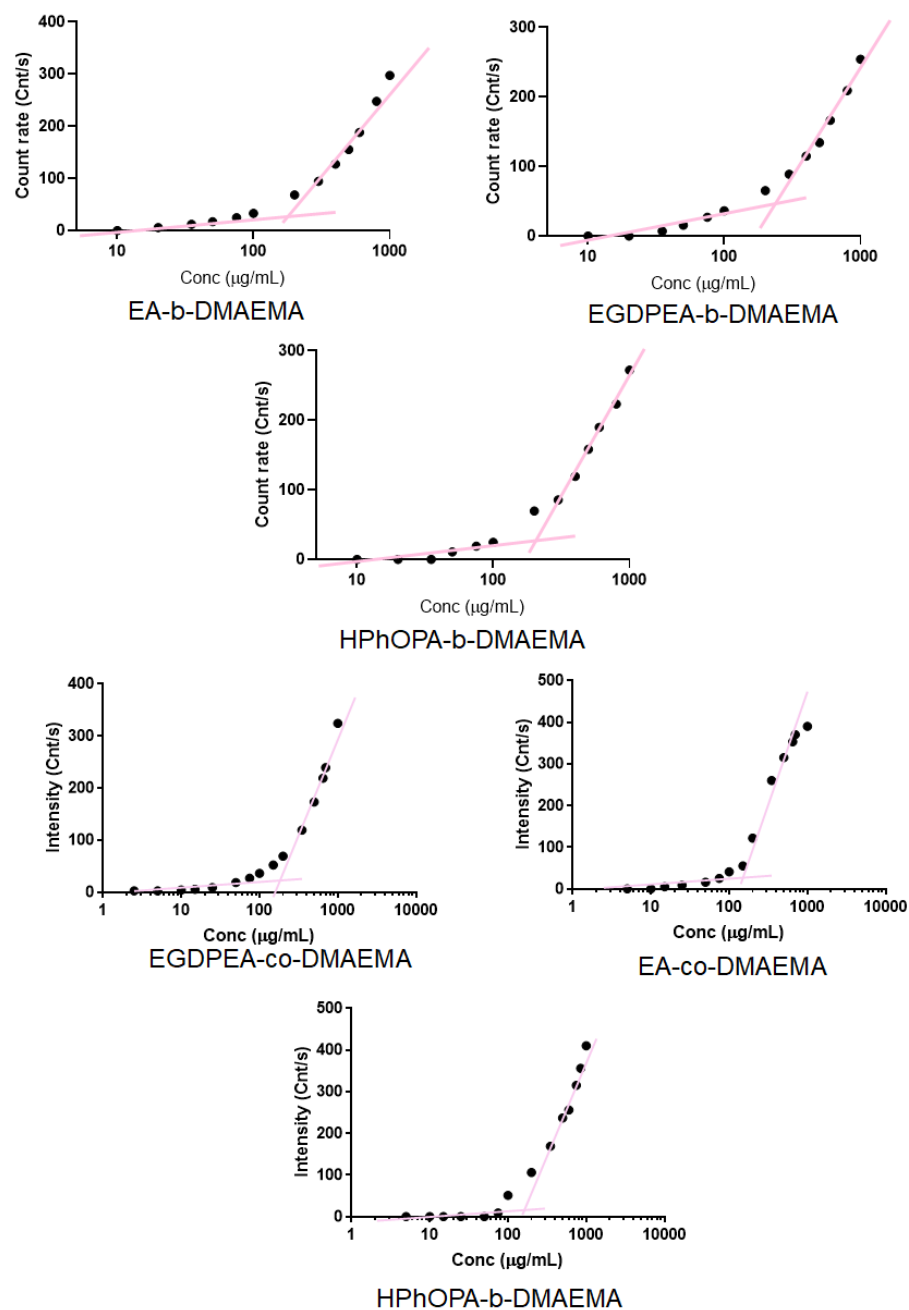


Figure Appendix 5-11 CAC of the 6 surfactants: EGDPEA-co-DMAEMA, EA-co-DMAEMA, HPhOPA-co-DMAEMA, EGDPEA-b-DMAEMA, EA-b-DMAEMA and HPhOPA-b-DMAEMA. The plots of the intensity of scattered light (kilo counts per second) as a function of concentration ( $\mu\text{g/mL}$ ). The data showed that the scattering detected for the surfactant concentrations below the CAC is similar to deionised water. After the CAC was reached, the scattering intensity shows a linear increase with concentration.

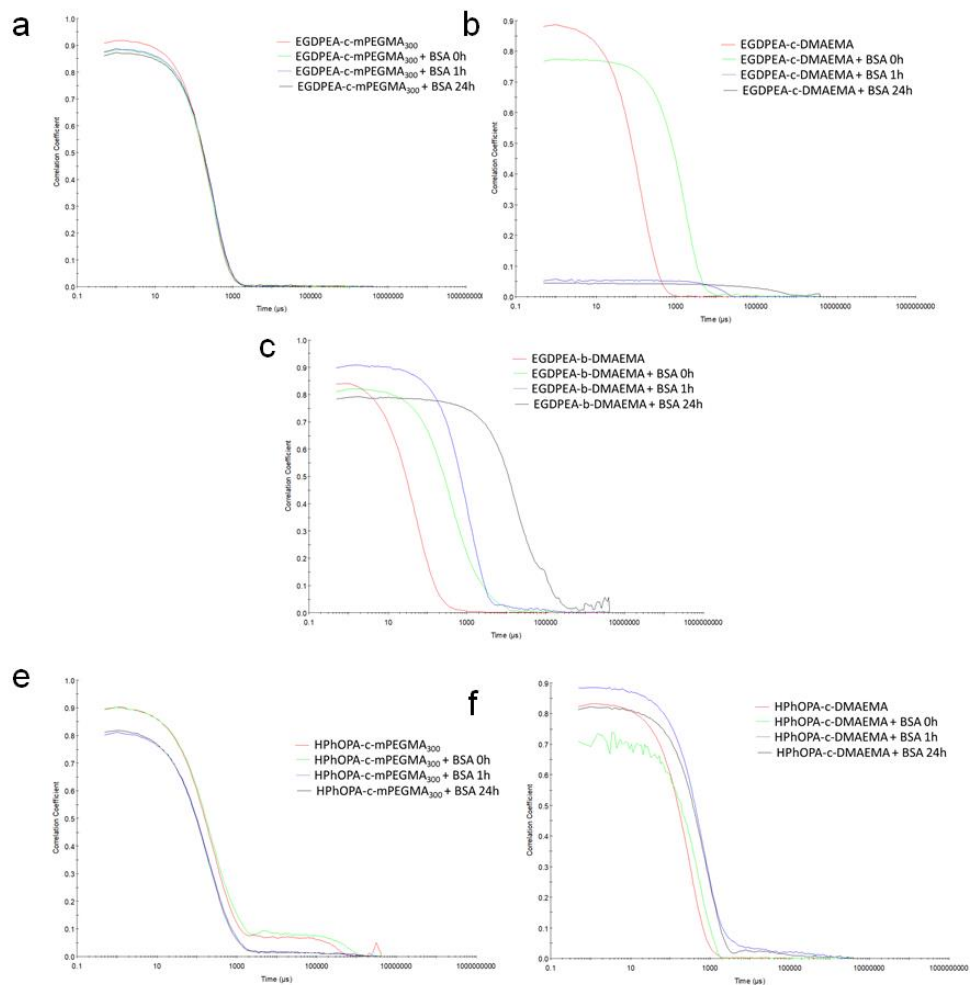


Figure Appendix 5-12 Correlograms of the DLS traces the protein corona binding studies of the follow copolymers a) EGDPEA-co-mPEGMA<sub>300</sub>, b) EGDPEA-co-DMAEMA, c) EGDPEA-b-DMAEMA, e) HPhOPA-co-mPEGMA<sub>300</sub> and f) HPhOPA-co-DMAEMA.

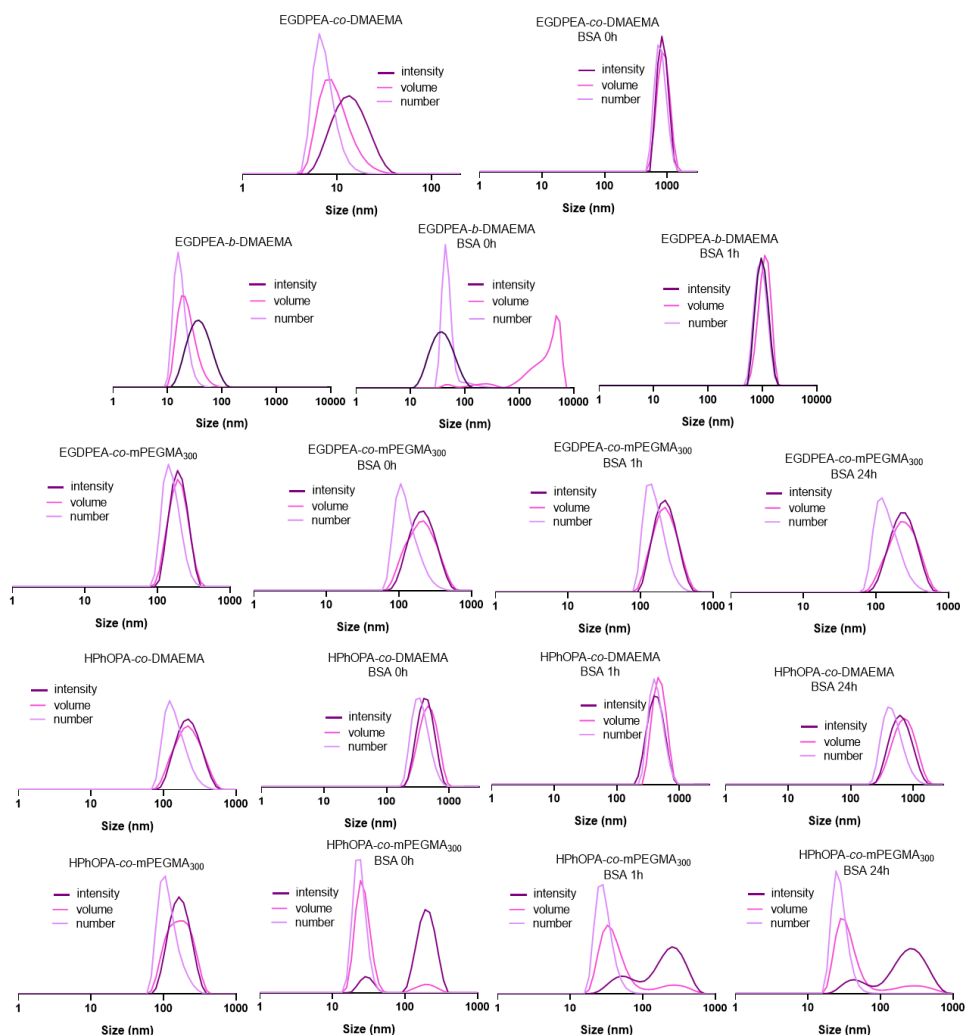


Figure Appendix 5-13 Sizes (nm) shown as Intensity, Volume and Number for the copolymers alone (EGDPEA-co-DMAEMA, EGDPEA-b-DMAEMA, EGDPEA-co-mPEGMA<sub>300</sub>, HPhOPA-co-DMAEMA, HPhOPA-co-mPEGMA<sub>300</sub>) and for the copolymers incubated with BSA at different time (0h, 1h, 24h). Data was not shown in case of absence of DLS traces.

## 6 Conclusions

### 6.1 Summary

The aim of this thesis work resided on the synthesis of a library of novel biologically active amphiphilic copolymers, with different 3D architectures and amphiphilic chemistries. For the first time, these amphiphilic copolymers were used as bespoke surfactants, in a droplets-based microfluidics device, to deliver surface functionalised monodisperse MPs. This developed method has potentially lower associated costs by reducing the quantity of expensive ‘bioactive’ polymers during the screening process. In fact, it requires only minimal amount of the expensive active materials (2% in wt/wt) in a microfluidic setup.

Previously, it has been shown that the utilisation of commercial surfactants is detrimental for biological applications.<sup>230</sup> When the surface of the MPs plays a key role in the chemistry/biology interface, it is important that the ‘active’ chemistry is completely exposed to the biological environment. In this regard, the use of unfunctionalized commercial surfactants, that stick on the surface during the emulsion stabilisation, might mask the specific biological properties of the target chemistry of MPs. The present work has emphasised how the investigation and rationalisation of the role of these amphiphilic species in the emulsion-based methods is still open.

In Chapter 3, it was reported for the first time the successful development of a HT pipeline to design, produce and characterise comb-graft amphiphilic

copolymers. This was possible thanks to the use in sequence of: a) an automated synthesiser, b) an ink-jet printer, c) a DLS plate-reader and d) a computational study. Overall, the automated synthesiser allowed to optimise the synthesis of twenty key bioinstructive functional copolymers, suitable for use as a surfactant, within a month. In addition, thanks to the use, for the first time, of the Catalytic Chain Transfer Polymerisation and the Thiol-mediated Free Radical polymerisation, a scale up reaction (10g) was successfully performed on 5 keys comb-graft copolymers, showing the high versatility of the automated synthesiser. To continue the HT pipeline, the combination of an ink-jet printer and a DLS plate reader was successful to establish the quality of the surfactants produced at well-plate scale. The CACs obtained were successfully compared with CMCs of common commercially available surfactants (Tween 80, Brij, etc.). Finally, this data from this property screen was then utilised to build a proof-of-concept computational model to assess the molecular descriptors that identified the four key molecular drivers that underpin the CAC properties of these types of complexes, comb-graft, architectural polymers.

Once the library of surfactants was completed, Chapter 4 was focused on the development of a method to produce MPs *via* droplets microfluidics. The surfactants worked as stabilisers of the 1,6-Hexanediol emulsion in water allowing the production of crosslinked MPs. During the stabilisation of the O/W emulsion, these surfactants stucked on the surface of the particles conferring a target biological activity represented by the particular

HyB monomer used. The developed system revealed to be effective in producing particles in a continuous flow with control over sizes, shapes and chemical nature. In fact, surface morphology studies conducted on these MPs showed mostly spherical and smooth materials with sizes of around 60  $\mu\text{m}$  and monodispersed. ToF-SIMS analysis confirmed the presence of unique ions for each 'hit' hydrophobic comonomers on the MPs surfaces. Therefore, the ability of the MPs to affect biological response was tested using *P. aruginosa* as the bacterial model and human skin fibroblast as the cellular model. From the different biological results, it was shown how these functional amphiphilic copolymers do modify the behaviour of bacteria and cells when on particle surfaces. This new method extends the utility and screening of biomaterials, discovered through the 2D polymer microarray platform, beyond currently used dip-coating applications. This will, therefore, enable the targeting of further biological applications where a 2D flat dip-coating procedure would be not realistic.

In Chapter 5, the chemistry and 3D architectures of these biological-active materials were further extended, beyond the comb-graft and the neutral PEG-based hydrophilic system. Amphiphilic block and random copolymers were synthesised with an alternative model hydrophilic positively charged comonomer, DMAEMA. The polymerisation strategies, i.e. ATRP and Thiol-mediated Free Radical Polymerisation, resulted successful in the production of the random and block copolymers. Also, these new amphiphilic linear cationic copolymers demonstrated to act as surfactants stabilising the O/W

emulsion and producing droplets in the previously developed flow-focusing microfluidics method. In fact, the MPs produced were overall monodispersed with size below 70  $\mu\text{m}$ . In addition, the presence of the target chemistry of the HyB comonomers and DMAEMA was confirmed by ToF-SIMS for all the produced MPs. However, it was observed that the presence of the DMAEMA, may negatively affect the performance of these materials to act as surfactants. On the other hand, thanks to the chemistry of the hydrophile it was showed an alteration of the surface charge of the nanosuspensions, thus, crucial for interactions with the external biological environment. These preliminary results can hint to the future production of 3D materials that not only have bacteria/cells anti- and pro-attachment properties but, also, bacteria killing and clustering features.

## 6.2 Recommendation for Future Work

The work throughout this thesis resulted multidisciplinary which involved the manufacturing and testing from different application view. Therefore, different future paths could be undertaken upon the work produced within this thesis.

From a synthetic point of view, the copolymers discussed in Chapter 5 need an improved design to enhance their amphiphilicity. For example, the synthesis of DMAEMA-based macromonomer (5-6 units) could mimic the stability observed from the mPEGMA surfactants showed in Chapter 3. Alternatively, the 3-(Dimethylamino)propyl acrylate monomer, presenting a similar amino functionality to DMAEMA but a longer alkyl chain, might play

an interesting role as hydrophile. In addition, the manufacturing microfluidics process, showed in the same chapter, can be modified to build up smooth particles reducing the detachment phenomena of the surfactants. In particular, as shown by Xu et al., the use of buffer (rather than DI water) in the collecting flask can change the solubility of the MPs components minimising aggregation and leaching.<sup>232</sup> In this regard, the possibility of exploiting different buffers (at different pH) in the collection flask can be explored to identify the best conditions to avoid porosity throughout the MPs. However, following the deep surface study performed by Rafati et al. on PLGA MPs, it would be interesting to use the same analytical techniques (ToF-SIMS dept profiling, AFM and Raman) to identify the distribution of the surfactants around the pore.<sup>397</sup> Similarly, the whole library of MPs, produced throughout this work of thesis, could be further investigated by ToF-SIMS dept profiling and XPS to assess whether the surfactants are evenly distributed on the surfaces as well as the outmost layer thickness.

Another aspect of this thesis work that needs to be further expanded is the protein attachment investigation performed in this thesis work. In fact, because of the disruption caused by the 19-COVID to the research work, it was impossible to develop in detail this part of the project as it was planned. The future work on protein attachment on particles, in particular BSA and fibronectin attachment, will involve the use of the 3D OrbiSIMS facility to study their dept distribution on the surface by following the work of

Kotowska et al. In addition, AFM could be performed on the MPs with adhered protein to investigate how the elasticity of the surface changed.<sup>398</sup>

Finally, a final aspect of this work could be the interest of moving from cross-linked core material for the MPs to a biodegradable and more biocompatible systems which would allow to expand the applications in the biomaterials field.

## 7 References

- (1) Staudinger, H. Über Polymerisation. *Berichte der Dtsch. Chem. Gesellschaft (A B Ser.* **1920**, *53* (6), 1073–1085. <https://doi.org/10.1002/cber.19200530627>.
- (2) Zhou, Y. N.; Li, J. J.; Wu, Y. Y.; Luo, Z. H. Role of External Field in Polymerization: Mechanism and Kinetics. *Chemical Reviews*. American Chemical Society March 11, 2020. <https://doi.org/10.1021/acs.chemrev.9b00744>.
- (3) Douka, A.; Vouyiouka, S.; Papaspyridi, L. M.; Papaspyrides, C. D. A Review on Enzymatic Polymerization to Produce Polycondensation Polymers: The Case of Aliphatic Polyesters, Polyamides and Polyesteramides. *Progress in Polymer Science*. Elsevier Ltd April 1, 2018, pp 1–25. <https://doi.org/10.1016/j.progpolymsci.2017.10.001>.
- (4) Yokozawa, T.; Yokoyama, A. Chain-Growth Polycondensation: The Living Polymerization Process in Polycondensation. *Progress in Polymer Science (Oxford)*. Pergamon January 1, 2007, pp 147–172. <https://doi.org/10.1016/j.progpolymsci.2006.08.001>.
- (5) Gurnani, P.; Blakney, A. K.; Yeow, J.; Bouton, C. R.; Shattock, R. J.; Stevens, M. M.; Alexander, C. An Improved Synthesis of Poly(Amidoamine)s for Complexation with Self-Amplifying RNA and Effective Transfection. *Polym. Chem.* **2020**, *11* (36), 5861–5869. <https://doi.org/10.1039/d0py00912a>.

- (6) Colombani, D. Chain-Growth Control in Free Radical Polymerization. *Progress in Polymer Science (Oxford)*. Elsevier Ltd January 1, 1997, pp 1649–1720. [https://doi.org/10.1016/S0079-6700\(97\)00022-1](https://doi.org/10.1016/S0079-6700(97)00022-1).
- (7) Matyjaszewski, K.; Davis, T. P. *Handbook of Radical Polymerization*; Wiley-Interscience, 2002.
- (8) Matyjaszewski, K.; Spanswick, J. Controlled/Living Radical Polymerization. *Mater. Today* **2005**, *8* (3), 26–33. [https://doi.org/10.1016/S1369-7021\(05\)00745-5](https://doi.org/10.1016/S1369-7021(05)00745-5).
- (9) Braunecker, W. A.; Matyjaszewski, K. Controlled/Living Radical Polymerization: Features, Developments, and Perspectives. *Progress in Polymer Science (Oxford)*. Pergamon January 1, 2007, pp 93–146. <https://doi.org/10.1016/j.progpolymsci.2006.11.002>.
- (10) Iwasaki, T.; Yoshida, J. I. Free Radical Polymerization in Microreactors. Significant Improvement in Molecular Weight Distribution Control. *Macromolecules* **2005**, *38* (4), 1159–1163. <https://doi.org/10.1021/ma048369m>.
- (11) Tulig, T. J.; Tirrell, M. On the Onset of the Trommsdorff Effect. *Macromolecules* **1982**, *15*, 459–463.
- (12) Burczyk, A. F.; O'Driscoll, K. F.; Rempel, G. L. Cobaloxime as a Catalytic Chain Transfer Agent. *J. Polym. Sci. Polym. Chem. Ed.* **1984**, *22* (11), 3255–3262. <https://doi.org/10.1002/pol.1984.170221142>.
- (13) Gridnev, A. 25Th Anniversary of Catalytic Chain Transfer. *J. Polym. Sci. Part A Polym. Chem.* **2000**, *38* (10), 1753–1766.

[https://doi.org/10.1002/\(SICI\)1099-0518\(20000515\)38:10<1753::AID-POLA600>3.0.CO;2-O](https://doi.org/10.1002/(SICI)1099-0518(20000515)38:10<1753::AID-POLA600>3.0.CO;2-O).

(14) Matyjaszewski, K. Overview: Fundamentals of Controlled/Living Radical Polymerization. *ACS Symp. Ser.* **1998**, *685*, 2–30. <https://doi.org/10.1021/bk-1998-0685.ch001>.

(15) Furuncuoğlu, T.; Uğur, I.; Değirmenci, I.; Aviyente, V. Role of Chain Transfer Agents in Free Radical Polymerization Kinetics. *Macromolecules* **2010**, *43* (4), 1823–1835. <https://doi.org/10.1021/ma902803p>.

(16) Davis, T. P. *Handbook of Radical Polymerization*; 2002. <https://doi.org/10.1002/0471220450>.

(17) Heuts, J. P. A.; Muratore, L. M.; Davis, T. P. Preparation and Characterization of Oligomeric Terpolymers of Styrene, Methyl Methacrylate and 2-Hydroxyethyl Methacrylate: A Comparison of Conventional and Catalytic Chain Transfer. *Macromol. Chem. Phys.* **2000**, *201* (18), 2780–2788. [https://doi.org/10.1002/1521-3935\(20001201\)201:18<2780::AID-MACP2780>3.0.CO;2-Z](https://doi.org/10.1002/1521-3935(20001201)201:18<2780::AID-MACP2780>3.0.CO;2-Z).

(18) Mayo, F. R. Chain Transfer in the Polymerization of Styrene: The Reaction of Solvents with Free Radicals 1. *J. Am. Chem. Soc.* **1943**, *65* (12), 2324–2329. <https://doi.org/10.1021/ja01252a021>.

(19) Jiang, L.; Huang, W.; Xue, X.; Yang, H.; Jiang, B.; Zhang, D.; Fang, J.; Chen, J.; Yang, Y.; Zhai, G.; Kong, L.; Wang, S. Radical Polymerization in the Presence of Chain Transfer Monomer: An Approach to Branched Vinyl Polymers. *Macromolecules* **2012**, *45* (10), 4092–4100. <https://doi.org/10.1021/ma300443g>.

- (20) Henríquez, C.; Bueno, C.; Lissi, E. A.; Encinas, M. V. Thiols as Chain Transfer Agents in Free Radical Polymerization in Aqueous Solution. *Polymer (Guildf)*. **2003**, *44* (19), 5559–5561. [https://doi.org/10.1016/S0032-3861\(03\)00581-0](https://doi.org/10.1016/S0032-3861(03)00581-0).
- (21) Lowe, A. B. Thiol-Ene “Click” Reactions and Recent Applications in Polymer and Materials Synthesis. *Polym. Chem.* **2010**, *1* (1), 17–36. <https://doi.org/10.1039/B9PY00216B>.
- (22) Cramer, N. B.; Scott, J. P.; Bowman, C. N. Photopolymerizations of Thiol-Ene Polymers without Photoinitiators. *Macromolecules* **2002**, *35* (14), 5361–5365. <https://doi.org/10.1021/ma0200672>.
- (23) Goethals, F.; Frank, D.; Du Prez, F. Protected Thiol Strategies in Macromolecular Design. *Progress in Polymer Science*. Elsevier Ltd January 1, 2017, pp 76–113. <https://doi.org/10.1016/j.progpolymsci.2016.09.003>.
- (24) Valdebenito, A.; Encinas, M. V. Thiophenols as Chain Transfer Agents in the Polymerization of Vinyl Monomers. *Polymer (Guildf)*. **2005**, *46* (24), 10658–10662. <https://doi.org/10.1016/j.polymer.2005.09.051>.
- (25) Dule, M.; Biswas, M.; Biswas, Y.; Mandal, K.; Jana, N. R.; Mandal, T. K. Cysteine-Based Amphiphilic Peptide-Polymer Conjugates via Thiol-Mediated Radical Polymerization: Synthesis, Self-Assembly, RNA Polyplexation and N-Terminus Fluorescent Labeling for Cell Imaging. *Polymer (Guildf)*. **2017**, *112*, 125–135. <https://doi.org/10.1016/j.polymer.2017.01.083>.
- (26) Kotal, A.; Si, S.; Paira, T. K.; Mandal, T. K. Synthesis of Semitelechelic POSS-Polymethacrylate Hybrids by Thiol-Mediated Controlled Radical

Polymerization with Unusual Thermal Behaviors. *J. Polym. Sci. Part A Polym. Chem.* **2008**, *46* (3), 1111–1123. <https://doi.org/10.1002/pola.22453>.

(27) Puertas-Bartolomé, M.; Fernández-Gutiérrez, M.; García-Fernández, L.; Vázquez-Lasa, B.; San Román, J. Biocompatible and Bioadhesive Low Molecular Weight Polymers Containing Long-Arm Catechol-Functionalized Methacrylate. *Eur. Polym. J.* **2018**, *98*, 47–55. <https://doi.org/10.1016/j.eurpolymj.2017.11.011>.

(28) Zana, R. Dimeric and Oligomeric Surfactants. Behavior at Interfaces and in Aqueous Solution: A Review. *Advances in Colloid and Interface Science*. Elsevier March 29, 2002, pp 205–253. [https://doi.org/10.1016/S0001-8686\(01\)00069-0](https://doi.org/10.1016/S0001-8686(01)00069-0).

(29) O'Brien, D. M.; Vallieres, C.; Alexander, C.; Howdle, S. M.; Stockman, R. A.; Avery, S. V. Epoxy-Amine Oligomers from Terpenes with Applications in Synergistic Antifungal Treatments. *J. Mater. Chem. B* **2019**, *7* (34), 5222–5229. <https://doi.org/10.1039/c9tb00878k>.

(30) Heuts, J. P. A.; Smeets, N. M. B. Catalytic Chain Transfer and Its Derived Macromonomers. *Polym. Chem.* **2011**, *2* (11), 2407. <https://doi.org/10.1039/c1py00224d>.

(31) Gridnev, A. The 25th Anniversary of Catalytic Chain Transfer. *J. Polym. Sci. Part A Polym. Chem.* **2000**, *38* (10), 1753–1766. [https://doi.org/10.1002/\(SICI\)1099-0518\(20000515\)38:10<1753::AID-POLA600>3.0.CO;2-O](https://doi.org/10.1002/(SICI)1099-0518(20000515)38:10<1753::AID-POLA600>3.0.CO;2-O).

(32) Heuts, J. P. A.; Davis, T. P.; Russell, G. T. Comparison of the Mayo and Chain Length Distribution Procedures for the Measurement of Chain

Transfer Constants. *Macromolecules* **1999**, *32* (19), 6019–6030.  
<https://doi.org/10.1021/ma990076j>.

(33) Gridnev, A. A.; Ittel, S. D. Catalytic Chain Transfer in Free-Radical Polymerizations. *Chem. Rev.* **2001**, *101* (12), 3611–3659.  
<https://doi.org/10.1021/cr9901236>.

(34) Wang, J. S.; Matyjaszewski, K. Controlled/“Living” Radical Polymerization. Atom Transfer Radical Polymerization in the Presence of Transition-Metal Complexes. *J. Am. Chem. Soc.* **1995**, *117* (20), 5614–5615.  
<https://doi.org/10.1021/ja00125a035>.

(35) Matyjaszewski, K.; Xia, J. Atom Transfer Radical Polymerization. *Chem. Rev.* **2001**, *101* (9), 2921–2990. <https://doi.org/10.1021/cr940534g>.

(36) Engelis, N. G.; Anastasaki, A.; Nurumbetov, G.; Truong, N. P.; Nikolaou, V.; Shegiwal, A.; Whittaker, M. R.; Davis, T. P.; Haddleton, D. M. Sequence-Controlled Methacrylic Multiblock Copolymers via Sulfur-Free RAFT Emulsion Polymerization. *Nat. Chem.* **2017**, *9* (2), 171–178.  
<https://doi.org/10.1038/NCHEM.2634>.

(37) Shegiwal, A.; Wemyss, A. M.; Liarou, E.; Town, J.; Patias, G.; Atkins, C. J.; Marathianos, A.; Lester, D. W.; Efstathiou, S.; Haddleton, D. M. Polymerisable Surfactants for Polymethacrylates Using Catalytic Chain Transfer Polymerisation (CCTP) Combined with Sulfur Free-RAFT in Emulsion Polymerisation. *Eur. Polym. J.* **2020**, *125*.  
<https://doi.org/10.1016/j.eurpolymj.2020.109491>.

- (38) Gridnev, A. A. Radical Polymerization of Methyl Methacrylate in the Presence of Cobaloximes and Benzoyl Peroxide. *Polym. J.* **1992**, *24* (7), 613–623. <https://doi.org/10.1295/polymj.24.613>.
- (39) Gridnev\*, A. A.; Ittel\*, S. D. Catalytic Chain Transfer in Free-Radical Polymerizations. **2001**. <https://doi.org/10.1021/CR9901236>.
- (40) Kukulj, D.; Davis, T. P. Mechanism of Catalytic Chain Transfer in the Free-Radical Polymerisation of Methyl Methacrylate and Styrene. *Macromol. Chem. Phys.* **1998**, *199* (8), 1697–1708. [https://doi.org/10.1002/\(SICI\)1521-3935\(19980801\)199:8<1697::AID-MACP1697>3.0.CO;2-Z](https://doi.org/10.1002/(SICI)1521-3935(19980801)199:8<1697::AID-MACP1697>3.0.CO;2-Z).
- (41) Haddleton, D. M.; Crossman, M. C.; Hunt, K. H.; Topping, C.; Waterson, C.; Suddaby, K. G. Identifying the Nature of the Active Species in the Polymerization of Methacrylates: Inhibition of Methyl Methacrylate Homopolymerizations and Reactivity Ratios for Copolymerization of Methyl Methacrylate/n-Butyl Methacrylate ... *Macromolecules* **1997**, *30* (97), 3992–3998. <https://doi.org/10.1021/ma970303m>.
- (42) Corrigan, N.; Jung, K.; Moad, G.; Hawker, C. J.; Matyjaszewski, K.; Boyer, C. Reversible-Deactivation Radical Polymerization (Controlled/Living Radical Polymerization): From Discovery to Materials Design and Applications. *Progress in Polymer Science*. Elsevier Ltd December 1, 2020, p 101311. <https://doi.org/10.1016/j.progpolymsci.2020.101311>.
- (43) Matyjaszewski, K. Atom Transfer Radical Polymerization (ATRP): Current Status and Future Perspectives. *Macromolecules* **2012**, *45* (10), 4015–4039. <https://doi.org/10.1021/ma3001719>.

- (44) Fetzer, L.; Toniazzi, V.; Ruch, D.; Di Lena, F. Transition-Metal Catalysts for Controlled Radical Polymerization: A First Update. *Israel Journal of Chemistry*. John Wiley & Sons, Ltd April 1, 2012, pp 221–229. <https://doi.org/10.1002/ijch.201100117>.
- (45) Tang, W.; Matyjaszewski, K. Effect of Ligand Structure on Activation Rate Constants in ATRP. *Macromolecules* **2006**, *39* (15), 4953–4959. <https://doi.org/10.1021/ma0609634>.
- (46) Tang, W.; Matyjaszewski, K. Effects of Initiator Structure on Activation Rate Constants in ATRP. *Macromolecules* **2007**, *40* (6), 1858–1863. <https://doi.org/10.1021/ma062897b>.
- (47) Patten, T. E.; Matyjaszewski, K. Atom Transfer Radical Polymerization and the Synthesis of Polymeric Materials. *Adv. Mater.* **1998**, *10* (12), 901–915. [https://doi.org/10.1002/\(SICI\)1521-4095\(199808\)10:12<901::AID-ADMA901>3.0.CO;2-B](https://doi.org/10.1002/(SICI)1521-4095(199808)10:12<901::AID-ADMA901>3.0.CO;2-B).
- (48) Dong, H.; Tang, W.; Matyjaszewski, K. Well-Defined High-Molecular-Weight Polyacrylonitrile via Activators Regenerated by Electron Transfer ATRP. *Macromolecules* **2007**, *40* (9), 2974–2977. <https://doi.org/10.1021/ma070424e>.
- (49) Konkolewicz, D.; Magenau, A. J. D.; Averick, S. E.; Simakova, A.; He, H.; Matyjaszewski, K. ICAR ATRP with Ppm Cu Catalyst in Water. *Macromolecules* **2012**, *45* (11), 4461–4468. <https://doi.org/10.1021/ma300887r>.
- (50) Konkolewicz, D.; Wang, Y.; Kryszewski, P.; Zhong, M.; Isse, A. A.; Gennaro, A.; Matyjaszewski, K. SARA ATRP or SET-LRP. End of Controversy? *Polymer*

*Chemistry*. Royal Society of Chemistry August 7, 2014, pp 4396–4417.  
<https://doi.org/10.1039/c4py00149d>.

(51) Min, K.; Gao, H.; Matyjaszewski, K. Use of Ascorbic Acid as Reducing Agent for Synthesis of Well-Defined Polymers by ARGET ATRP. *Macromolecules* **2007**, *40* (6), 1789–1791.  
<https://doi.org/10.1021/ma0702041>.

(52) Coessens, V.; Pintauer, T.; Matyjaszewski, K. Functional Polymers by Atom Transfer Radical Polymerization. *Progress in Polymer Science (Oxford)*. Pergamon April 1, 2001, pp 337–377. [https://doi.org/10.1016/S0079-6700\(01\)00003-X](https://doi.org/10.1016/S0079-6700(01)00003-X).

(53) Alvarez-Paino, M.; Amer, M. H.; Nasir, A.; Cuzzucoli Crucitti, V.; Thorpe, J.; Burroughs, L.; Needham, D.; Denning, C.; Alexander, M. R.; Alexander, C.; Rose, F. R. A. J. Polymer Microparticles with Defined Surface Chemistry and Topography Mediate the Formation of Stem Cell Aggregates and Cardiomyocyte Function. *ACS Appl. Mater. Interfaces* **2019**, *11* (38), 34560–34574. <https://doi.org/10.1021/acsami.9b04769>.

(54) YU, Y.; ZHAO, J.; Bayly, A. E. Development of Surfactants and Builders in Detergent Formulations. *Chinese J. Chem. Eng.* **2008**, *16* (4), 517–527.  
[https://doi.org/10.1016/S1004-9541\(08\)60115-9](https://doi.org/10.1016/S1004-9541(08)60115-9).

(55) Scheibel, J. J. The Evolution of Anionic Surfactant Technology to Meet the Requirements of the Laundry Detergent Industry. *Journal of Surfactants and Detergents*. Springer Verlag 2004, pp 319–328.  
<https://doi.org/10.1007/s11743-004-0317-7>.

- (56) Veldhuizen, E. J. A.; Haagsman, H. P. Role of Pulmonary Surfactant Components in Surface Film Formation and Dynamics. *Biochimica et Biophysica Acta - Biomembranes*. Elsevier August 25, 2000, pp 255–270.  
[https://doi.org/10.1016/S0005-2736\(00\)00256-X](https://doi.org/10.1016/S0005-2736(00)00256-X).
- (57) Mulligan, C. N. Environmental Applications for Biosurfactants. *Environ. Pollut.* **2005**, *133* (2), 183–198.  
<https://doi.org/10.1016/j.envpol.2004.06.009>.
- (58) Banat, I. M.; Makkar, R. S.; Cameotra, S. S. Potential Commercial Applications of Microbial Surfactants. *Applied Microbiology and Biotechnology*. Springer Verlag 2000, pp 495–508.  
<https://doi.org/10.1007/s002530051648>.
- (59) Bhardwaj, A.; Hartland, S. Applications of Surfactants in Petroleum Industry. *J. Dispers. Sci. Technol.* **1993**, *14* (1), 87–116.  
<https://doi.org/10.1080/01932699308943389>.
- (60) Czajka, A.; Hazell, G.; Eastoe, J. Surfactants at the Design Limit. **2015**.  
<https://doi.org/10.1021/acs.langmuir.5b00336>.
- (61) Rosen, M. J.; Kunjappu, J. T. *Surfactants and Interfacial Phenomena: Fourth Edition*; John Wiley and Sons, 2012.  
<https://doi.org/10.1002/9781118228920>.
- (62) Nagarajan, R.; Wang, C. C. Theory of Surfactant Aggregation in Water/Ethylene Glycol Mixed Solvents. *Langmuir* **2000**, *16* (12), 5242–5251.  
<https://doi.org/10.1021/la9910780>.
- (63) Yazhgur, P.; Vierros, S.; Hannoy, D.; Sammalkorpi, M.; Salonen, A. Surfactant Interactions and Organization at the Gas-Water Interface (CTAB

with Added Salt). *Langmuir* **2018**, *34* (5), 1855–1864.  
<https://doi.org/10.1021/acs.langmuir.7b03560>.

(64) He, Y.; Yazhgur, P.; Salonen, A.; Langevin, D. Adsorption-Desorption Kinetics of Surfactants at Liquid Surfaces. *Advances in Colloid and Interface Science*. Elsevier August 12, 2015, pp 377–384.  
<https://doi.org/10.1016/j.cis.2014.09.002>.

(65) Yunfei, H.; Yazhuo, S.; Honglai, L.; Dominique, L.; Anniina, S. Surfactant Adsorption onto Interfaces: Measuring the Surface Excess in Time. *Langmuir* **2012**, *28* (6), 3146–3151. <https://doi.org/10.1021/la2047454>.

(66) Sharma, R. Small-Molecule Surfactant Adsorption, Polymer Surfactant Adsorption, and Surface Solubilization: An Overview; 1996; pp 1–20.  
<https://doi.org/10.1021/bk-1995-0615.ch001>.

(67) Öztekin, N.; Erim, F. B. Determination of Critical Aggregation Concentration in the Poly-(Vinylpyrrolidone)–Sodium Dodecyl Sulfate System by Capillary Electrophoresis. *J. Surfactants Deterg.* **2013**, *16* (3), 363–367. <https://doi.org/10.1007/s11743-012-1411-7>.

(68) Tizzotti, M. J.; Sweedman, M. C.; Schäfer, C.; Gilbert, R. G. The Influence of Macromolecular Architecture on the Critical Aggregation Concentration of Large Amphiphilic Starch Derivatives. *Food Hydrocoll.* **2013**, *31* (2), 365–374. <https://doi.org/10.1016/j.foodhyd.2012.11.023>.

(69) Vincent, B. McBain and the Centenary of the Micelle. *Advances in Colloid and Interface Science*. Elsevier B.V. January 1, 2014, pp 51–54.  
<https://doi.org/10.1016/j.cis.2013.11.012>.

- (70) Kume, G.; Gallotti, M.; Nunes, G. Review on Anionic/Cationic Surfactant Mixtures. *J. Surfactants Deterg.* **2008**, *11* (1), 1–11. <https://doi.org/10.1007/s11743-007-1047-1>.
- (71) Cserháti, T.; Forgács, E.; Oros, G. Biological Activity and Environmental Impact of Anionic Surfactants. *Environ. Int.* **2002**, *28* (5), 337–348. [https://doi.org/10.1016/S0160-4120\(02\)00032-6](https://doi.org/10.1016/S0160-4120(02)00032-6).
- (72) Scheibel, J. J. The Evolution of Anionic Surfactant Technology to Meet the Requirements of the Laundry Detergent Industry. *Journal of Surfactants and Detergents*. Springer Verlag December 17, 2004, pp 319–328. <https://doi.org/10.1007/s11743-004-0317-7>.
- (73) St. Laurent, J. B.; De Buzzaccarini, F.; De Clerck, K.; Demeyere, H.; Labeque, R.; Lodewick, R.; Van Langenhove, L. Laundry Cleaning of Textiles. In *Handbook for Cleaning/Decontamination of Surfaces*; Elsevier, 2007; Vol. 1, pp 57–102. <https://doi.org/10.1016/B978-044451664-0/50003-6>.
- (74) Zhou, C.; Wang, Y. Structure–Activity Relationship of Cationic Surfactants as Antimicrobial Agents. *Current Opinion in Colloid and Interface Science*. Elsevier Ltd February 1, 2020, pp 28–43. <https://doi.org/10.1016/j.cocis.2019.11.009>.
- (75) Borse, M. S.; Devi, S. Importance of Head Group Polarity in Controlling Aggregation Properties of Cationic Gemini Surfactants. *Advances in Colloid and Interface Science*. Elsevier November 16, 2006, pp 387–399. <https://doi.org/10.1016/j.cis.2006.05.017>.
- (76) Bhattacharjee, S.; Chen, J.; Landers, J.; Baker, J. R. Zwitterionic Surfactant as a Promising Non-Cytotoxic Carrier for Nanoemulsion-Based

Vaccine Development. *ChemistrySelect* **2019**, *4* (31), 9027–9032.  
<https://doi.org/10.1002/slct.201902737>.

(77) FernLey, G. W. Zwitterionic Surfactants: Structure and Performance. *J. Am. Oil Chem. Soc.* **1978**, *55* (1), 98–103.  
<https://doi.org/10.1007/BF02673397>.

(78) Rapp, B. E. Surface Tension. In *Microfluidics: Modelling, Mechanics and Mathematics*; Elsevier, 2017; pp 421–444. <https://doi.org/10.1016/B978-1-4557-3141-1.50020-4>.

(79) Raffa, P.; Wever, D. A. Z.; Picchioni, F.; Broekhuis, A. A. Polymeric Surfactants: Synthesis, Properties, and Links to Applications. *Chemical Reviews*. 2015, pp 8504–8563. <https://doi.org/10.1021/cr500129h>.

(80) Raduan, N. H.; Horozov, T. S.; Georgiou, T. K. “comb-like” Non-Ionic Polymeric Macrosurfactants. *Soft Matter* **2010**, *6* (10), 2321–2329.  
<https://doi.org/10.1039/b926822g>.

(81) Alexandridis, P. Amphiphilic Copolymers and Their Applications. *Curr. Opin. Colloid Interface Sci.* **1996**, *1* (4), 490–501.  
[https://doi.org/10.1016/S1359-0294\(96\)80118-x](https://doi.org/10.1016/S1359-0294(96)80118-x).

(82) Torchilin, V. P. Structure and Design of Polymeric Surfactant-Based Drug Delivery Systems. *Journal of Controlled Release*. July 12, 2001, pp 137–172. [https://doi.org/10.1016/S0168-3659\(01\)00299-1](https://doi.org/10.1016/S0168-3659(01)00299-1).

(83) Blanazs, A.; Armes, S. P.; Ryan, A. J. Self-Assembled Block Copolymer Aggregates: From Micelles to Vesicles and Their Biological Applications. *Macromolecular Rapid Communications*. John Wiley & Sons, Ltd February 18, 2009, pp 267–277. <https://doi.org/10.1002/marc.200800713>.

(84) Adout, A.; Kang, S.; Asatekin, A.; Mayes, A. M.; Elimelech, M. Ultrafiltration Membranes Incorporating Amphiphilic Comb Copolymer Additives Prevent Irreversible Adhesion of Bacteria. *Environ. Sci. Technol.* **2010**, *44* (7), 2406–2411. <https://doi.org/10.1021/es902908g>.

(85) Asatekin, A.; Mayes, A. M. Oil Industry Wastewater Treatment with Fouling Resistant Membranes Containing Amphiphilic Comb Copolymers. *Environ. Sci. Technol.* **2009**, *43* (12), 4487–4492. <https://doi.org/10.1021/es803677k>.

(86) Raffa, P.; Broekhuis, A. A.; Picchioni, F. Polymeric Surfactants for Enhanced Oil Recovery: A Review. *Journal of Petroleum Science and Engineering*. Elsevier B.V. September 1, 2016, pp 723–733. <https://doi.org/10.1016/j.petrol.2016.07.007>.

(87) Kakde, D.; Taresco, V.; Bansal, K. K.; Magennis, E. P.; Howdle, S. M.; Mantovani, G.; Irvine, D. J.; Alexander, C. Amphiphilic Block Copolymers from a Renewable  $\epsilon$ -Decalactone Monomer: Prediction and Characterization of Micellar Core Effects on Drug Encapsulation and Release. *J. Mater. Chem. B* **2016**, *4* (44), 7119–7129. <https://doi.org/10.1039/c6tb01839d>.

(88) Wesslén, B.; Wesslén, K. B. Preparation and Properties of Some Water-soluble, Comb-shaped, Amphiphilic Polymers. *J. Polym. Sci. Part A Polym. Chem.* **1989**, *27* (12), 3915–3926. <https://doi.org/10.1002/pola.1989.080271204>.

(89) Alexandridis, P.; Lindman, B. *Amphiphilic Block Copolymers: Self-Assembly and Applications*; 2000.

- (90) Ianiro, A.; Wu, H.; van Rijt, M. M. J.; Vena, M. P.; Keizer, A. D. A.; Esteves, A. C. C.; Tuinier, R.; Friedrich, H.; Sommerdijk, N. A. J. M.; Patterson, J. P. Liquid–Liquid Phase Separation during Amphiphilic Self-Assembly. *Nat. Chem.* **2019**, *11* (4), 320–328. <https://doi.org/10.1038/s41557-019-0210-4>.
- (91) Mai, Y.; Eisenberg, A. Self-Assembly of Block Copolymers. *Chem. Soc. Rev.* **2012**, *41* (18), 5969–5985. <https://doi.org/10.1039/c2cs35115c>.
- (92) Riess, G. Micellization of Block Copolymers. *Prog. Polym. Sci.* **2003**, *28* (7), 1107–1170. [https://doi.org/10.1016/S0079-6700\(03\)00015-7](https://doi.org/10.1016/S0079-6700(03)00015-7).
- (93) Kojima, M.; Hirai, Y.; Yabu, H.; Shimomura, M. The Effects of Interfacial Tensions of Amphiphilic Copolymers on Honeycomb-Patterned Films. *Polym. J.* **2009**, *41* (8), 667–671. <https://doi.org/10.1295/polymj.PJ2009027>.
- (94) Carrot, G.; Hilborn, J.; Knauss, D. M. Synthesis, Characterization and Micelle Formation of Amphiphilic Graft Copolymers. *Polymer (Guildf)*. **1997**, *38* (26), 6401–6407. [https://doi.org/10.1016/S0032-3861\(97\)00203-6](https://doi.org/10.1016/S0032-3861(97)00203-6).
- (95) York, A. W.; Kirkland, S. E.; McCormick, C. L. Advances in the Synthesis of Amphiphilic Block Copolymers via RAFT Polymerization: Stimuli-Responsive Drug and Gene Delivery. *Advanced Drug Delivery Reviews*. Elsevier June 10, 2008, pp 1018–1036. <https://doi.org/10.1016/j.addr.2008.02.006>.
- (96) Mühlebach, A.; Gaynor, S. G.; Matyjaszewski, K. Synthesis of Amphiphilic Block Copolymers by Atom Transfer Radical Polymerization (ATRP). *Macromolecules* **1998**, *31* (18), 6046–6052. <https://doi.org/10.1021/ma9804747>.

(97) Zhang, W.; Dong, G.; Yang, H.; Sun, J.; Zhou, J.; Wang, J. Synthesis, Surface and Aggregation Properties of a Series of Amphiphilic Dendritic Copolymers. *Colloids Surfaces A Physicochem. Eng. Asp.* **2009**, *348* (1–3), 45–48. <https://doi.org/10.1016/j.colsurfa.2009.06.029>.

(98) Hadjichristidis, N.; Pitsikalis, M.; Iatrou, H.; Driva, P.; Chatzichristidi, M.; Sakellariou, G.; Lohse, D. Graft Copolymers. In *Encyclopedia of Polymer Science and Technology*; John Wiley & Sons, Inc.: Hoboken, NJ, USA, 2010. <https://doi.org/10.1002/0471440264.pst150.pub2>.

(99) Hadjichristidis, N.; Pispas, S.; Pitsikalis, M.; Iatrou, H.; Lohse, D. J. Graft Copolymers. In *Encyclopedia of Polymer Science and Technology*; John Wiley & Sons, Inc.: Hoboken, NJ, USA, 2002. <https://doi.org/10.1002/0471440264.pst150>.

(100) Ohno, S.; Matyjaszewski, K. Controlling Grafting Density and Side Chain Length in Poly(n-Butyl Acrylate) by ATRP Copolymerization of Macromonomers. *J. Polym. Sci. Part A Polym. Chem.* **2006**, *44* (19), 5454–5467. <https://doi.org/10.1002/pola.21669>.

(101) Tsarevsky, N. V; Bencherif, S. A.; Matyjaszewski, K. Graft Copolymers by a Combination of ATRP and Two Different Consecutive Click Reactions. *Macromolecules* **2007**, *40* (13), 4439–4445. <https://doi.org/10.1021/ma070705m>.

(102) Zhang, M.; Russell, T. P. Graft Copolymers from Poly(Vinylidene Fluoride-Co-Chlorotrifluoroethylene) via Atom Transfer Radical Polymerization. *Macromolecules* **2006**, *39* (10), 3531–3539. <https://doi.org/10.1021/ma060128m>.

- (103) Shinoda, H.; Miller, P. J.; Matyjaszewski, K. Improving the Structural Control of Graft Copolymers by Combining ATRP with the Macromonomer Method. *Macromolecules* **2001**, *34* (10), 3186–3194. <https://doi.org/10.1021/ma001943j>.
- (104) Patias, G.; Wemyss, A. M.; Efstathiou, S.; Town, J. S.; Atkins, C. J.; Shegiwal, A.; Whitfield, R.; Haddleton, D. M. Controlled Synthesis of Methacrylate and Acrylate Diblock Copolymers: Via End-Capping Using CCTP and FRP. *Polym. Chem.* **2019**, *10* (47), 6447–6455. <https://doi.org/10.1039/c9py01133a>.
- (105) Roos, S. G.; Müller, A. H. E.; Matyjaszewski, K. Copolymerization of Rc-Butyl Acrylate with Methyl Methacrylate and Pmma Macromonomers: Comparison of Reactivity Ratios in Conventional and Atom Transfer Radical Copolymerization. *Macromolecules* **1999**, *32* (25), 8331–8335. <https://doi.org/10.1021/ma9819337>.
- (106) Radke, W.; Roos, S.; Stein, H. M.; Müller, A. H. E. Acrylic Thermoplastic Elastomers and Comb-Shaped Poly(Methyl Methacrylate) via the Macromonomer Technique. *Macromol. Symp.* **1996**, *101* (1), 19–27. <https://doi.org/10.1002/masy.19961010105>.
- (107) Tsukahara, Y.; Hayashi, N.; Jiang, X. L.; Yamashita, Y. Radical Copolymerization Behavior of Macromonomers; Incompatibility Effect. *Polym. J.* **1989**, *21* (5), 377–391. <https://doi.org/10.1295/polymj.21.377>.
- (108) Hadjichristidis, N.; Pitsikalis, M.; Latrou, H.; Sakellariou, G. *Macromolecular Architectures by Living and Controlled/Living Polymerizations*; 2010. <https://doi.org/10.1002/9783527629091.ch7>.

(109) Hong, S. C.; Jia, S.; Teodorescu, M.; Kowalewski, T.; Matyjaszewski, K.; Gottfried, A. C.; Brookhart, M. Polyolefin Graft Copolymers via Living Polymerization Techniques: Preparation of Poly(*n*-Butyl Acrylate)-Graft-Polyethylene through the Combination of Pd-Mediated Living Olefin Polymerization and Atom Transfer Radical Polymerization. *J. Polym. Sci. Part A Polym. Chem.* **2002**, *40* (16), 2736–2749. <https://doi.org/10.1002/pola.10348>.

(110) Neugebauer, D.; Zhang, Y.; Pakula, T.; Sheiko, S. S.; Matyjaszewski, K. Densely-Grafted and Double-Grafted PEO Brushes via ATRP. A Route to Soft Elastomers. *Macromolecules* **2003**, *36* (18), 6746–6755. <https://doi.org/10.1021/ma0345347>.

(111) Shinoda, H.; Matyjaszewski, K.; Okrasa, L.; Mierzwa, M.; Pakula, T. Structural Control of Poly(Methyl Methacrylate)-*g*-Poly(Dimethylsiloxane) Copolymers Using Controlled Radical Polymerization: Effect of the Molecular Structure on Morphology and Mechanical Properties. *Macromolecules* **2003**, *36* (13), 4772–4778. <https://doi.org/10.1021/ma034064g>.

(112) Shinoda, H.; Matyjaszewski, K. Structural Control of Poly(Methyl Methacrylate)-*g*-Poly(Lactic Acid) Graft Copolymers by Atom Transfer Radical Polymerization (ATRP). *Macromolecules* **2001**, *34* (18), 6243–6248. <https://doi.org/10.1021/ma0105791>.

(113) Hawker, C. J.; Mecerreyes, D.; Elce, E.; Dao, J.; Hedrick, J. L.; Barakat, I.; Dubois, P.; Jérôme, R.; Volksen, W. “Living” Free Radical Polymerization of Macromonomers: Preparation of Well Defined Graft

Copolymers. *Macromol. Chem. Phys.* **1997**, *198* (1), 155–166.  
<https://doi.org/10.1002/macp.1997.021980112>.

(114) Pihtili, G.; Demirelli, K. Synthesis of Comb-Type Block Copolymers by Grafting through Method: Electrical Properties and Determination of Activation Energy via Conductivity. *J. Macromol. Sci. Part A Pure Appl. Chem.* **2019**.  
<https://doi.org/10.1080/10601325.2019.1706428>.

(115) Bo, G.; Wesslén, B.; Wesslén, K. B. Amphiphilic Comb-shaped Polymers from Poly(Ethylene Glycol) Macromonomers. *J. Polym. Sci. Part A Polym. Chem.* **1992**, *30* (9), 1799–1808.  
<https://doi.org/10.1002/pola.1992.080300903>.

(116) Feng, H.; Lu, X.; Wang, W.; Kang, N. G.; Mays, J. W. Block Copolymers: Synthesis, Self-Assembly, and Applications. *Polymers (Basel)*. **2017**, *9* (10). <https://doi.org/10.3390/polym9100494>.

(117) Matsen, M. W.; Bates, F. S. Origins of Complex Self-Assembly in Block Copolymers. *Macromolecules* **1996**, *29* (23), 7641–7644.  
<https://doi.org/10.1021/ma960744q>.

(118) Matyjaszewski, K.; Spanswick, J. Controlled/Living Radical Polymerization. *Mater. Today* **2005**, *8* (3), 26–33.  
[https://doi.org/10.1016/S1369-7021\(05\)00745-5](https://doi.org/10.1016/S1369-7021(05)00745-5).

(119) Hadjichristidis, N.; Pitsikalis, M.; Iatrou, H. Synthesis of Block Copolymers. *Advances in Polymer Science*. Springer, Berlin, Heidelberg 2005, pp 1–124. [https://doi.org/10.1007/12\\_005](https://doi.org/10.1007/12_005).

- (120) Khan, A. R.; Magnusson, J. P.; Watson, S.; Grabowska, A. M.; Wilkinson, R. W.; Alexander, C.; Pritchard, D. Camptothecin Prodrug Block Copolymer Micelles with High Drug Loading and Target Specificity. *Polym. Chem.* **2014**, *5* (18), 5320–5329. <https://doi.org/10.1039/c4py00369a>.
- (121) Ding, H.; Park, S.; Zhong, M.; Pan, X.; Pietrasik, J.; Bettinger, C. J.; Matyjaszewski, K. Facile Arm-First Synthesis of Star Block Copolymers via ARGET ATRP with Ppm Amounts of Catalyst. *Macromolecules* **2016**, *49* (18), 6752–6760. <https://doi.org/10.1021/acs.macromol.6b01597>.
- (122) Min, K.; Gao, H.; Matyjaszewski, K. Preparation of Homopolymers and Block Copolymers in Miniemulsion by ATRP Using Activators Generated by Electron Transfer (AGET). *J. Am. Chem. Soc.* **2005**, *127* (11), 3825–3830. <https://doi.org/10.1021/ja0429364>.
- (123) Min, K.; Gao, H.; Matyjaszewski, K. Use of Ascorbic Acid as Reducing Agent for Synthesis of Well-Defined Polymers by ARGET ATRP. *Macromolecules* **2007**, *40* (6), 1789–1791. <https://doi.org/10.1021/ma0702041>.
- (124) Kwak, Y.; Matyjaszewski, K. ARGET ATRP of Methyl Methacrylate in the Presence of Nitrogen-Based Ligands as Reducing Agents. *Polym. Int.* **2009**, *58* (3), 242–247. <https://doi.org/10.1002/pi.2530>.
- (125) Constantinou, A. P.; Lan, T.; Carroll, D. R.; Georgiou, T. K. Tricomponent Thermoresponsive Polymers Based on an Amine-Containing Monomer with Tuneable Hydrophobicity: Effect of Composition. *Eur. Polym. J.* **2020**, *130*, 109655. <https://doi.org/10.1016/j.eurpolymj.2020.109655>.

- (126) Duncan, R. The Dawning Era of Polymer Therapeutics. *Nature Reviews Drug Discovery*. Nature Publishing Group May 2003, pp 347–360. <https://doi.org/10.1038/nrd1088>.
- (127) Li, C.; Guo, C.; Fitzpatrick, V.; Ibrahim, A.; Zwierstra, M. J.; Hanna, P.; Lechtig, A.; Nazarian, A.; Lin, S. J.; Kaplan, D. L. Design of Biodegradable, Implantable Devices towards Clinical Translation. *Nature Reviews Materials*. Nature Research January 1, 2020, pp 61–81. <https://doi.org/10.1038/s41578-019-0150-z>.
- (128) Ekladios, I.; Colson, Y. L.; Grinstaff, M. W. Polymer–Drug Conjugate Therapeutics: Advances, Insights and Prospects. *Nat. Rev. Drug Discov*. <https://doi.org/10.1038/s41573-018-0005-0>.
- (129) Alves, N. M.; Pashkuleva, I.; Reis, R. L.; Mano, J. F. Controlling Cell Behavior through the Design of Polymer Surfaces. *Small*. October 18, 2010, pp 2208–2220. <https://doi.org/10.1002/sml.201000233>.
- (130) Chen, L.; Yan, C.; Zheng, Z. Functional Polymer Surfaces for Controlling Cell Behaviors. *Materials Today*. Elsevier B.V. January 1, 2018, pp 38–59. <https://doi.org/10.1016/j.mattod.2017.07.002>.
- (131) Park, S. Bin; Lih, E.; Park, K. S.; Joung, Y. K.; Han, D. K. Biopolymer-Based Functional Composites for Medical Applications. *Progress in Polymer Science*. Elsevier Ltd May 1, 2017, pp 77–105. <https://doi.org/10.1016/j.progpolymsci.2016.12.003>.
- (132) Maitz, M. F. Applications of Synthetic Polymers in Clinical Medicine. *Biosurface and Biotribology* **2015**, *1* (3), 161–176. <https://doi.org/10.1016/j.bsbt.2015.08.002>.

- (133) Gilbert, P. M.; Havenstrite, K. L.; Magnusson, K. E. G.; Sacco, A.; Leonardi, N. A.; Kraft, P.; Nguyen, N. K.; Thrun, S.; Lutolf, M. P.; Blau, H. M. Substrate Elasticity Regulates Skeletal Muscle Stem Cell Self-Renewal in Culture. *Science* (80-. ). **2010**, *329* (5995), 1078–1081. <https://doi.org/10.1126/science.1191035>.
- (134) Wen, J. H.; Vincent, L. G.; Fuhrmann, A.; Choi, Y. S.; Hribar, K. C.; Taylor-Weiner, H.; Chen, S.; Engler, A. J. Interplay of Matrix Stiffness and Protein Tethering in Stem Cell Differentiation. *Nat. Mater.* **2014**, *13* (10), 979–987. <https://doi.org/10.1038/nmat4051>.
- (135) Jones, D. S.; Djokic, J.; McCoy, C. P.; Gorman, S. P. Poly( $\epsilon$ -Caprolactone) and Poly( $\epsilon$ -Caprolactone)-Polyvinylpyrrolidone-Iodine Blends as Ureteral Biomaterials: Characterisation of Mechanical and Surface Properties, Degradation and Resistance to Encrustation in Vitro. *Biomaterials* **2002**, *23* (23), 4449–4458. [https://doi.org/10.1016/S0142-9612\(02\)00158-8](https://doi.org/10.1016/S0142-9612(02)00158-8).
- (136) Taresco, V.; Alexander, C.; Singh, N.; Pearce, A. K. Stimuli-Responsive Prodrug Chemistries for Drug Delivery. *Adv. Ther.* **2018**, *1* (4), 1800030. <https://doi.org/10.1002/adtp.201800030>.
- (137) Hrubý, M.; Filippov, S. K.; Štěpánek, P. Smart Polymers in Drug Delivery Systems on Crossroads: Which Way Deserves Following? *European Polymer Journal*. Elsevier Ltd April 1, 2015, pp 82–97. <https://doi.org/10.1016/j.eurpolymj.2015.01.016>.
- (138) Uludağ, H. Grand Challenges in Biomaterials. *Front. Bioeng. Biotechnol.* **2014**, *2* (OCT), 2–5. <https://doi.org/10.3389/fbioe.2014.00043>.

- (139) Peppas, N. A.; Langer, R. New Challenges in Biomaterials. *Science* (80- ). **1994**, 263 (5154), 1715–1720. <https://doi.org/10.1126/science.8134835>.
- (140) Hench, L. L.; Thompson, I. Twenty-First Century Challenges for Biomaterials. *Journal of the Royal Society Interface*. 2010. <https://doi.org/10.1098/rsif.2010.0151.focus>.
- (141) Hench, L. L. Biomaterials. *Science* (80- ). **1980**, 208 (4446), 826–831. <https://doi.org/10.1126/science.6246576>.
- (142) Ratner, B. D.; Bryant, S. J. Biomaterials: Where We Have Been and Where We Are Going. *Annual Review of Biomedical Engineering*. Annual Reviews August 15, 2004, pp 41–75. <https://doi.org/10.1146/annurev.bioeng.6.040803.140027>.
- (143) Hench, L. L.; Wilson, J. Surface-Active Biomaterials. *Science*. American Association for the Advancement of Science November 9, 1984, pp 630–636. <https://doi.org/10.1126/science.6093253>.
- (144) Hench, L. L.; Polak, J. M. Third-Generation Biomedical Materials. *Science*. American Association for the Advancement of Science February 8, 2002, pp 1014–1017. <https://doi.org/10.1126/science.1067404>.
- (145) Harris, J. J.; Lu, S.; Gabriele, P. Commercial Challenges in Developing Biomaterials for Medical Device Development. *Polym. Int.* **2018**, 67 (8), 969–974. <https://doi.org/10.1002/pi.5590>.
- (146) Hait, W. N. Anticancer Drug Development: The Grand Challenges. *Nature Reviews Drug Discovery*. Nature Publishing Group April 2010, pp 253–254. <https://doi.org/10.1038/nrd3144>.

- (147) Nair, L. S.; Laurencin, C. T. Biodegradable Polymers as Biomaterials. *Progress in Polymer Science (Oxford)*. 2007, pp 762–798. <https://doi.org/10.1016/j.progpolymsci.2007.05.017>.
- (148) Scopus preview - Welcome to Scopus <https://www.scopus.com/home.uri> (accessed Mar 30, 2020).
- (149) Pampaloni, F.; Reynaud, E. G.; Stelzer, E. H. K. The Third Dimension Bridges the Gap between Cell Culture and Live Tissue. *Nature Reviews Molecular Cell Biology*. Nature Publishing Group October 2007, pp 839–845. <https://doi.org/10.1038/nrm2236>.
- (150) Breslin, S.; O’Driscoll, L. Three-Dimensional Cell Culture: The Missing Link in Drug Discovery. *Drug Discovery Today*. Elsevier Current Trends March 1, 2013, pp 240–249. <https://doi.org/10.1016/j.drudis.2012.10.003>.
- (151) Fitzgerald, K. A.; Malhotra, M.; Curtin, C. M.; O’Brien, F. J.; O’Driscoll, C. M. Life in 3D Is Never Flat: 3D Models to Optimise Drug Delivery. *Journal of Controlled Release*. Elsevier October 10, 2015, pp 39–54. <https://doi.org/10.1016/j.jconrel.2015.07.020>.
- (152) Chitcholtan, K.; Asselin, E.; Parent, S.; Sykes, P. H.; Evans, J. J. Differences in Growth Properties of Endometrial Cancer in Three Dimensional (3D) Culture and 2D Cell Monolayer. *Exp. Cell Res.* **2013**, 319 (1), 75–87. <https://doi.org/10.1016/j.yexcr.2012.09.012>.
- (153) Algahtani, M. S.; Scurr, D. J.; Hook, A. L.; Anderson, D. G.; Langer, R. S.; Burley, J. C.; Alexander, M. R.; Davies, M. C. High Throughput

Screening for Biomaterials Discovery. *J. Control. Release* **2014**, *190*, 115–126. <https://doi.org/10.1016/j.jconrel.2014.06.045>.

(154) Bleicher, K. H.; Böhm, H.-J.; Müller, K.; Alanine, A. I. Hit and Lead Generation: Beyond High-Throughput Screening. *Nat. Rev. Drug Discov.* **2003**, *2* (5), 369–378. <https://doi.org/10.1038/nrd1086>.

(155) Selekman, J. A.; Qiu, J.; Tran, K.; Stevens, J.; Rosso, V.; Simmons, E.; Xiao, Y.; Janey, J. High-Throughput Automation in Chemical Process Development. *Annu. Rev. Chem. Biomol. Eng.* **2017**, *8* (1), 525–547. <https://doi.org/10.1146/annurev-chembioeng-060816-101411>.

(156) Hoogenboom, R.; Meier, M. A. R.; Schubert, U. S. Combinatorial Methods, Automated Synthesis and High-Throughput Screening in Polymer Research: Past and Present. *Macromol. Rapid Commun.* **2003**, *24* (1), 15–32. <https://doi.org/10.1002/marc.200390013>.

(157) Webster, D. C. Combinatorial and High-Throughput Methods in Macromolecular Materials Research and Development. *Macromol. Chem. Phys.* **2008**, *209* (3), 237–246. <https://doi.org/10.1002/macp.200700558>.

(158) Hoogenboom, R.; Fijten, M. W. M.; Meier, M. A. R.; Schubert, U. S. Living Cationic Polymerizations Utilizing an Automated Synthesizer: High-Throughput Synthesis of Polyoxazolines. *Macromol. Rapid Commun.* **2003**, *24* (1), 92–97. <https://doi.org/10.1002/marc.200390003>.

(159) Nasrullah, M. J.; Webster, D. C. Parallel Synthesis of Polymer Libraries Using Atom Transfer Radical Polymerization (ATRP). *Macromol. Chem. Phys.* **2009**, *210* (8), 640–650. <https://doi.org/10.1002/macp.200800578>.

- (160) Haven, J. J.; Guerrero-Sanchez, C.; Keddie, D. J.; Moad, G. Rapid and Systematic Access to Quasi-Diblock Copolymer Libraries Covering a Comprehensive Composition Range by Sequential RAFT Polymerization in an Automated Synthesizer. *Macromol. Rapid Commun.* **2014**, *35* (4), 492–497. <https://doi.org/10.1002/marc.201300459>.
- (161) Haven, J. J.; Baeten, E.; Claes, J.; Vandenberghe, J.; Junkers, T. High-Throughput Polymer Screening in Microreactors: Boosting the Passerini Three Component Reaction. *Polym. Chem.* **2017**, *8* (19), 2972–2978. <https://doi.org/10.1039/C7PY00360A>.
- (162) Guerrero-Sanchez, C.; Zhang, J.; Vitz, J.; Schubert, U. S. High-Throughput Synthesis of Polymers. In *Encyclopedia of Polymer Science and Technology*; John Wiley & Sons, Inc.: Hoboken, NJ, USA, 2018; pp 1–21. <https://doi.org/10.1002/0471440264.pst668>.
- (163) Rinckenauer, A. C.; Vollrath, A.; Schallon, A.; Tauhardt, L.; Kempe, K.; Schubert, S.; Fischer, D.; Schubert, U. S. Parallel High-Throughput Screening of Polymer Vectors for Nonviral Gene Delivery: Evaluation of Structure-Property Relationships of Transfection. *ACS Comb. Sci.* **2013**, *15* (9), 475–482. <https://doi.org/10.1021/co400025u>.
- (164) Mao, T.; Liu, G.; Wu, H.; Wei, Y.; Gou, Y.; Wang, J.; Tao, L. High Throughput Preparation of UV-Protective Polymers from Essential Oil Extracts via the Biginelli Reaction. *J. Am. Chem. Soc.* **2018**, *140* (22), 6865–6872. <https://doi.org/10.1021/jacs.8b01576>.
- (165) Alesso, S. M.; Yu, Z.; Pears, D.; Worthington, P. A.; Luke, R. W. A.; Bradley, M. Synthesis of Resins via Multiparallel Suspension

Polymerization. *J. Comb. Chem.* **2001**, *3* (6), 631–633.  
<https://doi.org/10.1021/cc010045b>.

(166) Baudis, S.; Lendlein, A.; Behl, M. High-Throughput Synthesis as a Technology Platform for Copolymer Libraries. In *Macromolecular Symposia*; Wiley-VCH Verlag, 2014; Vol. 345, pp 105–111.  
<https://doi.org/10.1002/masy.201400159>.

(167) Becer, C. R.; Paulus, R. M.; Hoogenboom, R.; Schubert, U. S. Optimization of the Nitroxide-Mediated Radical Polymerization Conditions for Styrene and tert-Butyl Acrylate in an Automated Parallel Synthesizer. *J. Polym. Sci. Part A Polym. Chem.* **2006**, *44* (21), 6202–6213.  
<https://doi.org/10.1002/pola.21694>.

(168) Zhang, H.; Marin, V.; Fijten, M. W. M.; Schubert, U. S. High-Throughput Experimentation in Atom Transfer Radical Polymerization: A General Approach toward a Directed Design and Understanding of Optimal Catalytic Systems. *J. Polym. Sci. Part A Polym. Chem.* **2004**, *42* (8), 1876–1885. <https://doi.org/10.1002/pola.20027>.

(169) Zhang, H.; Fijten, M. W. M.; Hoogenboom, R.; Reinierkens, R.; Schubert, U. S. Application of a Parallel Synthetic Approach in Atom-Transfer Radical Polymerization: Set-Up and Feasibility Demonstration. *Macromol. Rapid Commun.* **2003**, *24* (1), 81–86.  
<https://doi.org/10.1002/marc.200390002>.

(170) Fijten, M. W. M.; Meier, M. A. R.; Hoogenboom, R.; Schubert, U. S. Automated Parallel Investigations/Optimizations of the Reversible Addition-Fragmentation Chain Transfer Polymerization of Methyl

Methacrylate. *J. Polym. Sci. Part A Polym. Chem.* **2004**, *42* (22), 5775–5783.  
<https://doi.org/10.1002/pola.20346>.

(171) Pan, X.; Lathwal, S.; Mack, S.; Yan, J.; Das, S. R.; Matyjaszewski, K. Automated Synthesis of Well-Defined Polymers and Biohybrids by Atom Transfer Radical Polymerization Using a DNA Synthesizer. *Angew. Chemie - Int. Ed.* **2017**, *56* (10), 2740–2743. <https://doi.org/10.1002/anie.201611567>.

(172) Gurnani, P.; Floyd, T.; Tanaka, J.; Stubbs, C.; Lester, D.; Sanchez-Cano, C.; Perrier, S. PCR-RAFT: Rapid High Throughput Oxygen Tolerant RAFT Polymer Synthesis in a Biology Laboratory. *Polym. Chem.* **2020**, *11* (6), 1230–1236. <https://doi.org/10.1039/c9py01521c>.

(173) Potyrailo, R.; Rajan, K.; Stoewe, K.; Takeuchi, I.; Chisholm, B.; Lam, H. Combinatorial and High-Throughput Screening of Materials Libraries: Review of State of the Art. *ACS Combinatorial Science*. American Chemical Society November 14, 2011, pp 579–633.  
<https://doi.org/10.1021/co200007w>.

(174) Fernandes, T. G.; Diogo, M. M.; Clark, D. S.; Dordick, J. S.; Cabral, J. M. S. High-Throughput Cellular Microarray Platforms: Applications in Drug Discovery, Toxicology and Stem Cell Research. *Trends in Biotechnology*. Elsevier Current Trends June 1, 2009, pp 342–349.  
<https://doi.org/10.1016/j.tibtech.2009.02.009>.

(175) Díaz-Mochón, J. J.; Tourniaire, G.; Bradley, M. Microarray Platforms for Enzymatic and Cell-Based Assays. *Chemical Society Reviews*. 2007, pp 449–457. <https://doi.org/10.1039/b511848b>.

- (176) Hook, A. L.; Anderson, D. G.; Langer, R.; Williams, P.; Davies, M. C.; Alexander, M. R. High Throughput Methods Applied in Biomaterial Development and Discovery. *Biomaterials*. January 2010, pp 187–198. <https://doi.org/10.1016/j.biomaterials.2009.09.037>.
- (177) Amin, Y. Y. I.; Runager, K.; Simoes, F.; Celiz, A.; Taresco, V.; Rossi, R.; Enghild, J. J.; Abildtrup, L. A.; Kraft, D. C. E.; Sutherland, D. S.; Alexander, M. R.; Foss, M.; Ogaki, R. Combinatorial Biomolecular Nanopatterning for High-Throughput Screening of Stem-Cell Behavior. *Adv. Mater.* **2016**, *28* (7), 1472–1476. <https://doi.org/10.1002/adma.201504995>.
- (178) Patel, A. K.; Tibbitt, M. W.; Celiz, A. D.; Davies, M. C.; Langer, R.; Denning, C.; Alexander, M. R.; Anderson, D. G. High Throughput Screening for Discovery of Materials That Control Stem Cell Fate. *Current Opinion in Solid State and Materials Science*. The Authors 2016, pp 202–211. <https://doi.org/10.1016/j.cossms.2016.02.002>.
- (179) Hook, A. L.; Chang, C. Y.; Yang, J.; Luckett, J.; Cockayne, A.; Atkinson, S.; Mei, Y.; Bayston, R.; Irvine, D. J.; Langer, R.; Anderson, D. G.; Williams, P.; Davies, M. C.; Alexander, M. R. Combinatorial Discovery of Polymers Resistant to Bacterial Attachment. *Nat. Biotechnol.* **2012**, *30* (9), 868–875. <https://doi.org/10.1038/nbt.2316>.
- (180) Vallieres, C.; Hook, A. L.; He, Y.; Crucitti, V. C.; Figueredo, G.; Davies, C. R.; Burroughs, L.; Winkler, D. A.; Winkler, D. A.; Winkler, D. A.; Winkler, D. A.; Wildman, R. D.; Irvine, D. J.; Alexander, M. R.; Avery, S. V. Discovery of (Meth)Acrylate Polymers That Resist Colonization by Fungi

Associated with Pathogenesis and Biodeterioration. *Sci. Adv.* **2020**, *6* (23), eaba6574. <https://doi.org/10.1126/sciadv.aba6574>.

(181) Kohn, J. New Approaches to Biomaterials Design. *Nature Materials*. Nature Publishing Group 2004, pp 745–747. <https://doi.org/10.1038/nmat1249>.

(182) Anderson, D. G.; Levenberg, S.; Langer, R. Nanoliter-Scale Synthesis of Arrayed Biomaterials and Application to Human Embryonic Stem Cells. *Nat. Biotechnol.* **2004**, *22* (7), 863–866. <https://doi.org/10.1038/nbt981>.

(183) Celiz, A. D.; Smith, J. G. W.; Patel, A. K.; Hook, A. L.; Rajamohan, D.; George, V. T.; Flatt, L.; Patel, M. J.; Epa, V. C.; Singh, T.; Langer, R.; Anderson, D. G.; Allen, N. D.; Hay, D. C.; Winkler, D. A.; Barrett, D. A.; Davies, M. C.; Young, L. E.; Denning, C.; Alexander, M. R. Discovery of a Novel Polymer for Human Pluripotent Stem Cell Expansion and Multilineage Differentiation. *Adv. Mater.* **2015**, *27* (27), 4006–4012. <https://doi.org/10.1002/adma.201501351>.

(184) Sanni, O.; Chang, C. Y.; Anderson, D. G.; Langer, R.; Davies, M. C.; Williams, P. M.; Williams, P.; Alexander, M. R.; Hook, A. L. Bacterial Attachment to Polymeric Materials Correlates with Molecular Flexibility and Hydrophilicity. *Adv. Healthc. Mater.* **2015**, *4* (5), 695–701. <https://doi.org/10.1002/adhm.201400648>.

(185) Stone, H. A.; Stroock, A. D.; Ajdari, A. Engineering Flows in Small Devices. *Annu. Rev. Fluid Mech.* **2004**, *36* (1), 381–411. <https://doi.org/10.1146/annurev.fluid.36.050802.122124>.

- (186) Doufène, K.; Tourné-Péteilh, C.; Etienne, P.; Aubert-Pouëssel, A. Microfluidic Systems for Droplet Generation in Aqueous Continuous Phases: A Focus Review. *Langmuir* **2019**, *35* (39), 12597–12612. <https://doi.org/10.1021/acs.langmuir.9b02179>.
- (187) Liu, Z.; Fontana, F.; Python, A.; Hirvonen, J. T.; Santos, H. A. Microfluidics for Production of Particles: Mechanism, Methodology, and Applications. *Small* **2019**, *1904673*, 1–24. <https://doi.org/10.1002/sml.201904673>.
- (188) Sackmann, E. K.; Fulton, A. L.; Beebe, D. J. The Present and Future Role of Microfluidics in Biomedical Research. *Nature* **2014**, *507* (7491), 181–189. <https://doi.org/10.1038/nature13118>.
- (189) Serra, C. A.; Chang, Z. Microfluidic-Assisted Synthesis of Polymer Particles. *Chem. Eng. Technol.* **2008**, *31* (8), 1099–1115. <https://doi.org/10.1002/ceat.200800219>.
- (190) Eduati, F.; Utharala, R.; Madhavan, D.; Neumann, U. P.; Longerich, T.; Cramer, T.; Saez-Rodriguez, J.; Merten, C. A. A Microfluidics Platform for Combinatorial Drug Screening on Cancer Biopsies. *Nat. Commun.* **2018**, *9* (1), 1–13. <https://doi.org/10.1038/s41467-018-04919-w>.
- (191) Wong, A. H. H.; Li, H.; Jia, Y.; Mak, P. I.; Martins, R. P. D. S.; Liu, Y.; Vong, C. M.; Wong, H. C.; Wong, P. K.; Wang, H.; Sun, H.; Deng, C. X. Drug Screening of Cancer Cell Lines and Human Primary Tumors Using Droplet Microfluidics. *Sci. Rep.* **2017**, *7* (1), 1–15. <https://doi.org/10.1038/s41598-017-08831-z>.

- (192) Bonat Celli, G.; Abbaspourrad, A. Tailoring Delivery System Functionality Using Microfluidics. *Annu. Rev. Food Sci. Technol.* **2018**, *9* (1), 481–501. <https://doi.org/10.1146/annurev-food-030117-012545>.
- (193) Hussain, M.; Xie, J.; Hou, Z.; Shezad, K.; Xu, J.; Wang, K.; Gao, Y.; Shen, L.; Zhu, J. Regulation of Drug Release by Tuning Surface Textures of Biodegradable Polymer Microparticles. *ACS Appl. Mater. Interfaces* **2017**, *9* (16), 14391–14400. <https://doi.org/10.1021/acsami.7b02002>.
- (194) Vasiliauskas, R.; Liu, D.; Cito, S.; Zhang, H.; Shahbazi, M. A.; Sikanen, T.; Mazutis, L.; Santos, H. A. Simple Microfluidic Approach to Fabricate Monodisperse Hollow Microparticles for Multidrug Delivery. *ACS Appl. Mater. Interfaces* **2015**, *7* (27), 14822–14832. <https://doi.org/10.1021/acsami.5b04824>.
- (195) Bian, X.; Jing, F.; Li, G.; Fan, X.; Jia, C.; Zhou, H.; Jin, Q.; Zhao, J. A Microfluidic Droplet Digital PCR for Simultaneous Detection of Pathogenic Escherichia Coli O157 and Listeria Monocytogenes. *Biosens. Bioelectron.* **2015**, *74*, 770–777. <https://doi.org/10.1016/j.bios.2015.07.016>.
- (196) Petukhov, V.; Guo, J.; Baryawno, N.; Severe, N.; Scadden, D. T.; Samsonova, M. G.; Kharchenko, P. V. DropEst: Pipeline for Accurate Estimation of Molecular Counts in Droplet-Based Single-Cell RNA-Seq Experiments. *Genome Biol.* **2018**, *19* (1), 78. <https://doi.org/10.1186/s13059-018-1449-6>.
- (197) Nisisako, T.; Tonii, T. Formation of Biphasic Janus Droplets in a Microfabricated Channel for the Synthesis of Shape-Controlled Polymer

Microparticles. *Adv. Mater.* **2007**, *19* (11), 1489–1493.  
<https://doi.org/10.1002/adma.200700272>.

(198) Song, Y.; Liu, S.; Wang, B.; Shang, M.; Lin, L.; Su, Y. Continuous and Controllable Preparation of Polyaniline with Different Reaction Media in Microreactors for Supercapacitor Applications. *Chem. Eng. Sci.* **2019**, *207*, 820–828. <https://doi.org/10.1016/j.ces.2019.07.008>.

(199) Xu, S.; Nie, Z.; Seo, M.; Lewis, P.; Kumacheva, E.; Stone, H. A.; Garstecki, P.; Weibel, D. B.; Gitlin, I.; Whitesides, G. M. Generation of Monodisperse Particles by Using Microfluidics: Control over Size, Shape, and Composition. *Angew. Chemie - Int. Ed.* **2005**, *44* (5), 724–728. <https://doi.org/10.1002/anie.200462226>.

(200) Yu, Y. L.; Zhou, Z. H.; Yu, W. T.; Song, Y. Z.; Xie, M. Q. Preparation of Magnetic Porous Microspheres and Their Ability to Remove Oils. *Macromol. Mater. Eng.* **2020**, *305* (1), 1900452. <https://doi.org/10.1002/mame.201900452>.

(201) Maan, A. A.; Schroën, K.; Boom, R. Monodispersed Water-in-Oil Emulsions Prepared with Semi-Metal Microfluidic EDGE Systems. *Microfluid. Nanofluidics* **2013**, *14* (1–2), 187–196. <https://doi.org/10.1007/s10404-012-1037-0>.

(202) De Jong, J.; Lammertink, R. G. H.; Wessling, M. Membranes and Microfluidics: A Review. *Lab on a Chip*. Royal Society of Chemistry 2006, pp 1125–1139. <https://doi.org/10.1039/b603275c>.

(203) Teh, S. Y.; Lin, R.; Hung, L. H.; Lee, A. P. Droplet Microfluidics. *Lab Chip* **2008**, *8* (2), 198–220. <https://doi.org/10.1039/b715524g>.

- (204) Anna, S. L.; Mayer, H. C. Microscale Tipstreaming in a Microfluidic Flow Focusing Device. *Phys. Fluids* **2006**, *18* (12). <https://doi.org/10.1063/1.2397023>.
- (205) Garstecki, P.; Gitlin, I.; Diluzio, W.; Whitesides, G. M.; Kumacheva, E.; Stone, H. A. Formation of Monodisperse Bubbles in a Microfluidic Flow-Focusing Device. *Appl. Phys. Lett.* **2004**, *85* (13), 2649–2651. <https://doi.org/10.1063/1.1796526>.
- (206) Anna, S. L.; Bontoux, N.; Stone, H. A. Formation of Dispersions Using “Flow Focusing” in Microchannels. *Appl. Phys. Lett.* **2003**, *82* (3), 364–366. <https://doi.org/10.1063/1.1537519>.
- (207) Xu, S.; Nie, Z.; Seo, M.; Lewis, P.; Kumacheva, E.; Stone, H. A.; Garstecki, P.; Weibel, D. B.; Gitlin, I.; Whitesides, G. M. Generation of Monodisperse Particles by Using Microfluidics: Control over Size, Shape, and Composition. *Angew. Chemie* **2005**, *117* (5), 734–738. <https://doi.org/10.1002/ange.200462226>.
- (208) Nie, Z.; Xu, S.; Seo, M.; Lewis, P. C.; Kumacheva, E. Polymer Particles with Various Shapes and Morphologies Produced in Continuous Microfluidic Reactors. *J. Am. Chem. Soc.* **2005**, *127* (22), 8058–8063. <https://doi.org/10.1021/ja042494w>.
- (209) Xu, S.; Nisisako, T. Surfactant-Laden Janus Droplets with Tunable Morphologies and Enhanced Stability for Fabricating Lens-Shaped Polymeric Microparticles. *Micromachines* **2021**, *12* (1), 1–11. <https://doi.org/10.3390/mi12010029>.

- (210) Xu, Q.; Hashimoto, M.; Dang, T. T.; Hoare, T.; Kohane, D. S.; Whitesides, G. M.; Langer, R.; Anderson, D. G.; David, H. Preparation of Monodisperse Biodegradable Polymer Microparticles Using a Microfluidic Flow-Focusing Device for Controlled Drug Delivery. *Small* **2009**, *5* (13), 1575–1581. <https://doi.org/10.1002/smll.200801855>.
- (211) Seiffert, S.; Weitz, D. A. Controlled Fabrication of Polymer Microgels by Polymer-Analogous Gelation in Droplet Microfluidics. *Soft Matter* **2010**, *6* (14), 3184–3190. <https://doi.org/10.1039/c0sm00071j>.
- (212) Ballauff, M.; Lu, Y. “Smart” Nanoparticles: Preparation, Characterization and Applications. *Polymer*. Elsevier BV March 23, 2007, pp 1815–1823. <https://doi.org/10.1016/j.polymer.2007.02.004>.
- (213) Li, F.; Truong, V. X.; Fisch, P.; Levinson, C.; Glattauer, V.; Zenobi-Wong, M.; Thissen, H.; Forsythe, J. S.; Frith, J. E. Cartilage Tissue Formation through Assembly of Microgels Containing Mesenchymal Stem Cells. *Acta Biomater.* **2018**, *77*, 48–62. <https://doi.org/10.1016/j.actbio.2018.07.015>.
- (214) Guermani, E.; Shaki, H.; Mohanty, S.; Mehrali, M.; Arpanaei, A.; Gaharwar, A. K.; Dolatshahi-Pirouz, A. Engineering Complex Tissue-like Microgel Arrays for Evaluating Stem Cell Differentiation. *Sci. Rep.* **2016**, *6* (1), 1–8. <https://doi.org/10.1038/srep30445>.
- (215) Das, M.; Zhang, H.; Kumacheva, E. Microgels: Old Materials with New Applications. *Annu. Rev. Mater. Res.* **2006**, *36*, 117–142. <https://doi.org/10.1146/annurev.matsci.36.011205.123513>.

- (216) Rott, N. Note on the History of the Reynolds Number. *Annu. Rev. Fluid Mech.* **1990**, *22* (1), 1–12. <https://doi.org/10.1146/annurev.fl.22.010190.000245>.
- (217) Jakiela, S.; Makulska, S.; Korczyk, P. M.; Garstecki, P. Speed of Flow of Individual Droplets in Microfluidic Channels as a Function of the Capillary Number, Volume of Droplets and Contrast of Viscosities. *Lab Chip* **2011**, *11* (21), 3603–3608. <https://doi.org/10.1039/c1lc20534j>.
- (218) Christopher, G. F.; Bergstein, J.; End, N. B.; Poon, M.; Nguyen, C.; Anna, S. L. Coalescence and Splitting of Confined Droplets at Microfluidic Junctions. *Lab Chip* **2009**, *9* (8), 1102–1109. <https://doi.org/10.1039/b813062k>.
- (219) Marculescu, C.; Tincu, B.; Avram, A.; Burinaru, T.; Avram, M. Computational Prediction of Capillary Number Impact on Droplets Formation in Microchannels. In *Energy Procedia*; Elsevier Ltd, 2016; Vol. 85, pp 339–349. <https://doi.org/10.1016/j.egypro.2015.12.260>.
- (220) De menech, M.; Garstecki, P.; Jousse, F.; Stone, H. A. Transition from Squeezing to Dripping in a Microfluidic T-Shaped Junction. *J. Fluid Mech.* **2008**, *595*, 141–161. <https://doi.org/10.1017/S002211200700910X>.
- (221) Ren, K.; Zhou, J.; Wu, H. Materials for Microfluidic Chip Fabrication. *Acc. Chem. Res.* **2013**, *46* (11), 2396–2406. <https://doi.org/10.1021/ar300314s>.
- (222) Janasek, D.; Franzke, J.; Manz, A. Scaling and the Design of Miniaturized Chemical-Analysis Systems. *Nature*. Nature Publishing Group July 27, 2006, pp 374–380. <https://doi.org/10.1038/nature05059>.

- (223) Nge, P. N.; Rogers, C. I.; Woolley, A. T. Advances in Microfluidic Materials, Functions, Integration, and Applications. *Chemical Reviews*. April 10, 2013, pp 2550–2583. <https://doi.org/10.1021/cr300337x>.
- (224) Luo, X.; Su, P.; Zhang, W.; Raston, C. L. Microfluidic Devices in Fabricating Nano or Micromaterials for Biomedical Applications. *Advanced Materials Technologies*. Wiley-Blackwell December 21, 2019, p 1900488. <https://doi.org/10.1002/admt.201900488>.
- (225) Nisisako, T.; Torii, T.; Higuchi, T. Novel Microreactors for Functional Polymer Beads. *Chem. Eng. J.* **2004**, *101* (1–3), 23–29. <https://doi.org/10.1016/j.cej.2003.11.019>.
- (226) Seo, M.; Nie, Z.; Xu, S.; Mok, M.; Lewis, P. C.; Graham, R.; Kumacheva, E. Continuous Microfluidic Reactors for Polymer Particles. *Langmuir* **2005**, *21* (25), 11614–11622. <https://doi.org/10.1021/la050519e>.
- (227) Lu, B.; Tarn, M. D.; Pamme, N.; Georgiou, T. K. Tailoring PH-Responsive Acrylic Acid Microgels with Hydrophobic Crosslinks for Drug Release. *J. Mater. Chem. B* **2015**, *3* (22), 4524–4529. <https://doi.org/10.1039/c5tb00222b>.
- (228) Riechers, B.; Maes, F.; Akoury, E.; Semin, B.; Gruner, P.; Baret, J. C. Surfactant Adsorption Kinetics in Microfluidics. *Proc. Natl. Acad. Sci. U. S. A.* **2016**, *113* (41), 11465–11470. <https://doi.org/10.1073/pnas.1604307113>.
- (229) Baret, J. C. Surfactants in Droplet-Based Microfluidics. *Lab Chip* **2012**, *12* (3), 422–433. <https://doi.org/10.1039/c1lc20582j>.

- (230) Hüsler, A.; Haas, S.; Parry, L.; Romero, M.; Nisisako, T.; Williams, P.; Wildman, R. D.; Alexander, M. R. Effect of Surfactant on *Pseudomonas Aeruginosa* Colonization of Polymer Microparticles and Flat Films. *RSC Adv.* **2018**, *8* (28), 15352–15357. <https://doi.org/10.1039/C8RA01491D>.
- (231) Wagner, O.; Thiele, J.; Weinhart, M.; Mazutis, L.; Weitz, D. A.; Huck, W. T. S.; Haag, R. Biocompatible Fluorinated Polyglycerols for Droplet Microfluidics as an Alternative to PEG-Based Copolymer Surfactants. *Lab Chip* **2016**, *16* (1), 65–69. <https://doi.org/10.1039/c5lc00823a>.
- (232) Xu, Q.; Hashimoto, M.; Dang, T. T.; Hoare, T.; Kohane, D. S.; Whitesides, G. M.; Langer, R.; Anderson, D. G.; David, H. Preparation of Monodisperse Biodegradable Polymer Microparticles Using a Microfluidic Flow-Focusing Device for Controlled Drug Delivery. *Small* **2009**, *5* (13), 1575–1581. <https://doi.org/10.1002/smll.200801855>.
- (233) Han, F. Y.; Thurecht, K. J.; Whittaker, A. K.; Smith, M. T. Bioerodable PLGA-Based Microparticles for Producing Sustained-Release Drug Formulations and Strategies for Improving Drug Loading. *Frontiers in Pharmacology*. Frontiers Research Foundation June 28, 2016, p 185. <https://doi.org/10.3389/fphar.2016.00185>.
- (234) Adams, J. M. Particle Size and Shape Effects in Materials Science: Examples from Polymer and Paper Systems. *Clay Miner.* **1993**, *28* (4), 509–530. <https://doi.org/10.1180/claymin.1993.028.4.03>.
- (235) Dundas, A. A.; Cuzzucoli Crucitti, V.; Haas, S.; Dubern, J.; Latif, A.; Romero, M.; Sanni, O.; Ghaemmaghami, A. M.; Williams, P.; Alexander, M. R.; Wildman, R.; Irvine, D. J. Achieving Microparticles with Cell-

Instructive Surface Chemistry by Using Tunable Co-Polymer Surfactants.

*Adv. Funct. Mater.* **2020**, 2001821.

<https://doi.org/10.1002/adfm.202001821>.

(236) Berkland, C.; Kim, K.; Pack, D. W. Fabrication of PLG Microspheres with Precisely Controlled and Monodisperse Size Distributions. *J. Control. Release* **2001**, *73* (1), 59–74.

[https://doi.org/10.1016/S0168-3659\(01\)00289-9](https://doi.org/10.1016/S0168-3659(01)00289-9).

(237) Mishra, R. K.; Cherusseri, J.; Bishnoi, A.; Thomas, S. Nuclear Magnetic Resonance Spectroscopy. In *Spectroscopic Methods for Nanomaterials Characterization*; 2017; Vol. 2, pp 369–415.

<https://doi.org/10.1016/B978-0-323-46140-5.00013-3>.

(238) Becker, E. D. A BRIEF HISTORY OF NUCLEAR MAGNETIC RESONANCE. *Anal. Chem.* **1993**, *65* (6), 295A-302A.

<https://doi.org/10.1021/ac00054a716>.

(239) Bloch, F. Nuclear Induction. *Phys. Rev.* **1946**, *70* (7–8), 460–474.

<https://doi.org/10.1103/PhysRev.70.460>.

(240) Izunobi, J. U.; Higginbotham, C. L. Polymer Molecular Weight Analysis by <sup>1</sup>H NMR Spectroscopy. *J. Chem. Educ.* **2011**, *88* (8), 1098–1104.

<https://doi.org/10.1021/ed100461v>.

(241) Yu, Q.; Zhang, Y.; Wang, H.; Brash, J.; Chen, H. Anti-Fouling Bioactive Surfaces. *Acta Biomater.* **2011**, *7* (4), 1550–1557.

<https://doi.org/10.1016/j.actbio.2010.12.021>.

(242) Hook, A. L.; Chang, C. Y.; Yang, J.; Scurr, D. J.; Langer, R.; Anderson, D. G.; Atkinson, S.; Williams, P.; Davies, M. C.; Alexander, M. R.

Polymer Microarrays for High Throughput Discovery of Biomaterials. *J. Vis. Exp.* **2012**, No. 59, 1–7. <https://doi.org/10.3791/3636>.

(243) Anderson, D. G.; Levenberg, S.; Langer, R. Nanoliter-Scale Synthesis of Arrayed Biomaterials and Application to Human Embryonic Stem Cells. *Nat. Biotechnol.* **2004**, *22* (7), 863–866. <https://doi.org/10.1038/nbt981>.

(244) Vauthier, C.; Bouchemal, K. Methods for the Preparation and Manufacture of Polymeric Nanoparticles. *Pharmaceutical Research*. Springer New York December 24, 2009, pp 1025–1058. <https://doi.org/10.1007/s11095-008-9800-3>.

(245) Schubert, S.; Delaney, J. T.; Schubert, U. S. Nanoprecipitation and Nanoformulation of Polymers: From History to Powerful Possibilities beyond Poly(Lactic Acid). *Soft Matter*. The Royal Society of Chemistry March 7, 2011, pp 1581–1588. <https://doi.org/10.1039/c0sm00862a>.

(246) Mora-Huertas, C. E.; Fessi, H.; Elaissari, A. Influence of Process and Formulation Parameters on the Formation of Submicron Particles by Solvent Displacement and Emulsification-Diffusion Methods: Critical Comparison. *Advances in Colloid and Interface Science*. Elsevier B.V. April 14, 2011, pp 90–122. <https://doi.org/10.1016/j.cis.2011.02.005>.

(247) Styliari, I. D.; Conte, C.; Pearce, A. K.; Hüsler, A.; Cavanagh, R. J.; Limo, M. J.; Gordhan, D.; Nieto-Orellana, A.; Suksiriworapong, J.; Couturaud, B.; Williams, P.; Hook, A. L.; Alexander, M. R.; Garnett, M. C.; Alexander, C.; Burley, J. C.; Taresco, V. High-Throughput Miniaturized Screening of

Nanoparticle Formation via Inkjet Printing. *Macromol. Mater. Eng.* **2018**, 303 (8), 1800146. <https://doi.org/10.1002/mame.201800146>.

(248) Topel, Ö.; Çakir, B. A.; Budama, L.; Hoda, N. Determination of Critical Micelle Concentration of Polybutadiene-Block- Poly(Ethyleneoxide) Diblock Copolymer by Fluorescence Spectroscopy and Dynamic Light Scattering. *J. Mol. Liq.* **2013**, 177, 40–43. <https://doi.org/10.1016/j.molliq.2012.10.013>.

(249) Stetefeld, J.; McKenna, S. A.; Patel, T. R. Dynamic Light Scattering: A Practical Guide and Applications in Biomedical Sciences. *Biophysical Reviews*. Springer Verlag December 1, 2016, pp 409–427. <https://doi.org/10.1007/s12551-016-0218-6>.

(250) Bhattacharjee, S. DLS and Zeta Potential - What They Are and What They Are Not? *J. Control. Release* **2016**, 235, 337–351. <https://doi.org/10.1016/j.jconrel.2016.06.017>.

(251) Kirby, B. J.; Hasselbrink, E. F. Zeta Potential of Microfluidic Substrates: 1. Theory, Experimental Techniques, and Effects on Separations. *Electrophoresis*. January 2004, pp 187–202. <https://doi.org/10.1002/elps.200305754>.

(252) Goldstein, J. I.; Newbury, D. E.; Echlin, P.; Joy, D. C.; Fiori, C.; Lifshin, E. Scanning Electron Microscopy and X-Ray Microanalysis: A Text for Biologists, Materials Scientists, and Geologists. **1981**, 840.

(253) Benninghoven, A. Chemical Analysis of Inorganic and Organic Surfaces and Thin Films by Static Time-of-Flight Secondary Ion Mass Spectrometry (TOF-SIMS). *Angewandte Chemie International Edition in*

*English*. John Wiley & Sons, Ltd June 6, 1994, pp 1023–1043.

<https://doi.org/10.1002/anie.199410231>.

(254) Sodhi, R. N. S. Time-of-Flight Secondary Ion Mass Spectrometry (TOF-SIMS): - Versatility in Chemical and Imaging Surface Analysis. *Analyst* **2004**, *129* (6), 483–487. <https://doi.org/10.1039/b402607c>.

(255) Belu, A. M.; Graham, D. J.; Castner, D. G. Time-of-Flight Secondary Ion Mass Spectrometry: Techniques and Applications for the Characterization of Biomaterial Surfaces. *Biomaterials* **2003**, *24* (21), 3635–3653. [https://doi.org/10.1016/S0142-9612\(03\)00159-5](https://doi.org/10.1016/S0142-9612(03)00159-5).

(256) Baret, J.-C. Surfactants in Droplet-Based Microfluidics. *Lab Chip* **2012**, *12* (3), 422–433. <https://doi.org/10.1039/C1LC20582J>.

(257) Dai, B.; Leal, L. G. The Mechanism of Surfactant Effects on Drop Coalescence. *Phys. Fluids* **2008**, *20* (4). <https://doi.org/10.1063/1.2911700>.

(258) La Sorella, G.; Strukul, G.; Scarso, A. Recent Advances in Catalysis in Micellar Media. *Green Chem.* **2015**, *17* (2), 644–683. <https://doi.org/10.1039/c4gc01368a>.

(259) Lourdes Pérez, ‡; Josep Lluís Torres, §; Angeles Manresa, ||; Conxita Solans, ‡ and; Ma Rosa Infante\*, ‡. Synthesis, Aggregation, and Biological Properties of a New Class of Gemini Cationic Amphiphilic Compounds from Arginine, Bis(ArgS)†. **1996**. <https://doi.org/10.1021/LA960301F>.

(260) Chang, A. B.; Lin, T. P.; Thompson, N. B.; Luo, S. X.; Liberman-Martin, A. L.; Chen, H. Y.; Lee, B.; Grubbs, R. H. Design, Synthesis, and Self-

Assembly of Polymers with Tailored Graft Distributions. *J. Am. Chem. Soc.* **2017**, *139* (48), 17683–17693. <https://doi.org/10.1021/jacs.7b10525>.

(261) Adlington, K.; Nguyen, N. T.; Eaves, E.; Yang, J.; Chang, C. Y.; Li, J.; Gower, A. L.; Stimpson, A.; Anderson, D. G.; Langer, R.; Davies, M. C.; Hook, A. L.; Williams, P.; Alexander, M. R.; Irvine, D. J. Application of Targeted Molecular and Material Property Optimization to Bacterial Attachment-Resistant (Meth)Acrylate Polymers. *Biomacromolecules* **2016**, *17* (9), 2830–2838. <https://doi.org/10.1021/acs.biomac.6b00615>.

(262) Dundas, A. A.; Sanni, O.; Dubern, J. F.; Dimitrakis, G.; Hook, A. L.; Irvine, D. J.; Williams, P.; Alexander, M. R. Validating a Predictive Structure–Property Relationship by Discovery of Novel Polymers Which Reduce Bacterial Biofilm Formation. *Adv. Mater.* **2019**, *31* (49). <https://doi.org/10.1002/adma.201903513>.

(263) Hook, A. L.; Chang, C. Y.; Yang, J.; Atkinson, S.; Langer, R.; Anderson, D. G.; Davies, M. C.; Williams, P.; Alexander, M. R. Discovery of Novel Materials with Broad Resistance to Bacterial Attachment Using Combinatorial Polymer Microarrays. *Adv. Mater.* **2013**, *25* (18), 2542–2547. <https://doi.org/10.1002/adma.201204936>.

(264) Alexander, M. R.; Williams, P. Water Contact Angle Is Not a Good Predictor of Biological Responses to Materials. *Biointerphases* **2017**, *12*, 1–7. <https://doi.org/10.1116/1.4989843>.

(265) Biasutti, J. D.; Roberts, G. E.; Lucien, F. P. Substituent Effects in the Catalytic Chain Transfer Polymerization of 2-Hydroxyethyl

Methacrylate. *Eur. Polym. J.* **2003**, *39*, 429–435.

[https://doi.org/10.1016/S0014-3057\(02\)00251-3](https://doi.org/10.1016/S0014-3057(02)00251-3).

(266) Haddleton, D. M.; Depaquis, E.; Kelly, E. J.; Kukulj, D.; Morsley, S. R.; Bon, S. A. F.; Eason, M. D.; Steward, A. G. Cobalt-Mediated Catalytic Chain-Transfer Polymerization (CCTP) in Water and Water/Alcohol Solution.

*J. Polym. Sci. Part A Polym. Chem.* **2001**, *39* (14), 2378–2384.

<https://doi.org/10.1002/pola.1214>.

(267) Liu, S.; Srinivasan, S.; Grady, M. C.; Soroush, M.; Rappe, A. M. Backbiting and  $\beta$ -Scission Reactions in Free-Radical Polymerization of

Methyl Acrylate. *Int. J. Quantum Chem.* **2014**, *114* (5), 345–360.

<https://doi.org/10.1002/qua.24572>.

(268) Haddleton, D. M.; Maloney, D. R.; Suddaby, K. G. Competition between  $\beta$ -Scission of Macromonomer-Ended Radicals and Chain Transfer to Cobalt(II) in Catalytic Chain Transfer Polymerization (CCTP).

*Macromolecules* **1996**, *29* (1), 481–483.

<https://doi.org/10.1021/ma9507756>.

(269) Ander, P. Dependence of Molecular Weight of Polystyrene on Initiator Concentration an Introductory Physical Chemistry Experiment. *J.*

*Chem. Educ.* **1970**, *47* (3), 233–234. <https://doi.org/10.1021/ed047p233>.

(270) Mandal, P.; Choudhury, S.; Singha, N. K. Acrylic ABA Triblock Copolymer Bearing Pendant Reactive Bicycloalkenyl Functionality via ATRP and Tuning Its Properties Using Thiol-Ene Chemistry. *Polymer (Guildf)*. **2014**,

*55* (22), 5576–5583. <https://doi.org/10.1016/j.polymer.2014.08.051>.

- (271) Maupu, A.; Kanawati, Y.; Métafiot, A.; Maric, M. Ethylene Glycol Dicyclopentenyl (Meth)Acrylate Homo and Block Copolymers via Nitroxide Mediated Polymerization. *Materials (Basel)*. **2019**, *12* (9). <https://doi.org/10.3390/ma12091547>.
- (272) Mandal, P.; Singha, N. K. Selective Atom Transfer Radical Polymerization of 1,2,3,6-Tetrahydrobenzyl Methacrylate (THBMA) and Demonstration of Thiol-Ene Addition Reaction in the Pendant Cycloalkenyl Functional Group. *Eur. Polym. J.* **2015**, *67*, 21–30. <https://doi.org/10.1016/j.eurpolymj.2015.03.025>.
- (273) Kolitz, M.; Cohen-Arazi, N.; Hagag, H.; Katzhendler, J.; Domb, A. J. Biodegradable Polyesters Derived from Amino Acids. *Macromolecules* **2009**, *42* (13), 4520–4530. <https://doi.org/10.1021/ma900464g>.
- (274) Akar, I.; Keogh, R.; Blackman, L. D.; Foster, J. C.; Mathers, R. T.; O'Reilly, R. K. Grafting Density Governs the Thermoresponsive Behavior of P(OEGMA-Co-RMA) Statistical Copolymers. *ACS Macro Lett.* **2020**, *9* (8), 1149–1154. <https://doi.org/10.1021/acsmacrolett.0c00461>.
- (275) Taresco, V.; Suksiriworapong, J.; Styliari, I. D.; Argent, R. H.; Swainson, S. M. E.; Booth, J.; Turpin, E.; Loughton, C. A.; Burley, J. C.; Alexander, C.; Garnett, M. C. New N-Acyl Amino Acid-Functionalized Biodegradable Polyesters for Pharmaceutical and Biomedical Applications. *RSC Adv.* **2016**, *6* (111), 109401–109405. <https://doi.org/10.1039/C6RA21464A>.
- (276) Varnek, A.; Gaudin, C.; Marcou, G.; Baskin, I.; Pandey, A. K.; Tetko, I. V. Inductive Transfer of Knowledge: Application of Multi-Task

Learning and Feature Net Approaches to Model Tissue-Air Partition Coefficients. *J. Chem. Inf. Model.* **2009**, *49* (1), 133–144. <https://doi.org/10.1021/ci8002914>.

(277) Hook, A. L.; Chang, C.-Y.; Yang, J.; Lockett, J.; Cockayne, A.; Atkinson, S.; Mei, Y.; Bayston, R.; Irvine, D. J.; Langer, R.; Anderson, D. G.; Williams, P.; Davies, M. C.; Alexander, M. R. Combinatorial Discovery of Polymers Resistant to Bacterial Attachment. *Nat. Biotechnol.* **2012**, *30* (9), 868–875. <https://doi.org/10.1038/nbt.2316>.

(278) Patel, A. K.; Celiz, A. D.; Rajamohan, D.; Anderson, D. G.; Langer, R.; Davies, M. C.; Alexander, M. R.; Denning, C. A Defined Synthetic Substrate for Serum-Free Culture of Human Stem Cell Derived Cardiomyocytes with Improved Functional Maturity Identified Using Combinatorial Materials Microarrays. *Biomaterials* **2015**, *61*, 257–265. <https://doi.org/10.1016/j.biomaterials.2015.05.019>.

(279) Haddleton, D. M.; Depaquis, E.; Kelly, E. J.; Kukulj, D.; Morsley, S. R.; Bon, S. A. F.; Eason, M. D.; Steward, A. G. ( CCTP ) in Water and Water / Alcohol Solution. *Polym. Sci. Part A Polym. Chem.* **2001**, *39* (14), 2378–2384.

(280) Roldo, M.; Power, K.; Smith, J. R.; Cox, P. A.; Papagelis, K.; Bouropoulos, N.; Fatouros, D. G. N-Octyl-O-Sulfate Chitosan Stabilises Single Wall Carbon Nanotubes in Aqueous Media and Bestows Biocompatibility. *Nanoscale* **2009**, *1* (3), 366. <https://doi.org/10.1039/b9nr00151d>.

(281) Cheng, W.; Rajendran, R.; Ren, W.; Gu, L.; Zhang, Y.; Chuang, K.-H.; Liu, Y. A Facile Synthetic Approach to a Biodegradable Polydisulfide MRI

Contrast Agent. *J. Mater. Chem. B* **2014**, *2* (32), 5295–5301.  
<https://doi.org/10.1039/C4TB00413B>.

(282) Hait, S. K.; Moulik, S. P. Determination of Critical Micelle Concentration (CMC) of Nonionic Surfactants by Donor-Acceptor Interaction with Iodine and Correlation of CMC with Hydrophile-Lipophile Balance and Other Parameters of the Surfactants. *J. Surfactants Deterg.* **2001**, *4* (3), 303–309. <https://doi.org/10.1007/s11743-001-0184-2>.

(283) Patist, A.; Bhagwat, S. S.; Penfield, K. W.; Aikens, P.; Shah, D. O. On the Measurement of Critical Micelle Concentrations of Pure and Technical-Grade Nonionic Surfactants. *J. Surfactants Deterg.* **2000**, *3* (1), 53–58. <https://doi.org/10.1007/s11743-000-0113-4>.

(284) Alexandridis, P.; Athanassiou, V.; Fukuda, S.; Hatton, T. A. *Surface Activity of Poly(Ethylene Oxide)-6ZocA-Poly(Propylene Oxide)-6Zocfc-Poly(Ethylene Oxide) Copolymers*; 2604.

(285) Antoun, S.; Gohy, J. F.; Jérôme, R. Micellization of Quaternized Poly(2-(Dimethylamino)Ethyl Methacrylate)-Block-Poly(Methyl Methacrylate) Copolymers in Water. *Polymer (Guildf)*. **2001**, *42* (8), 3641–3648. [https://doi.org/10.1016/S0032-3861\(00\)00746-1](https://doi.org/10.1016/S0032-3861(00)00746-1).

(286) Hadjiyannakou, S. C.; Vamvakaki, M.; Patrickios, C. S. Synthesis, Characterization and Evaluation of Amphiphilic Diblock Copolymer Emulsifiers Based on Methoxy Hexa(Ethylene Glycol) Methacrylate and Benzyl Methacrylate. *Polymer (Guildf)*. **2004**, *45* (11), 3681–3692. <https://doi.org/10.1016/j.polymer.2004.03.079>.

- (287) Prakash, G. K. S.; Wang, F.; Rahm, M.; Shen, J.; Ni, C.; Haiges, R.; Olah, G. A. On the Nature of C-H···F-C Interactions in Hindered CF<sub>3</sub>-C(Sp<sup>3</sup>) Bond Rotations. *Angew. Chemie - Int. Ed.* **2011**, *50* (49), 11761–11764. <https://doi.org/10.1002/anie.201105288>.
- (288) Hirai, Y.; Terashima, T.; Takenaka, M.; Sawamoto, M. Precision Self-Assembly of Amphiphilic Random Copolymers into Uniform and Self-Sorting Nanocompartments in Water. *Macromolecules* **2016**, *49* (14), 5084–5091. <https://doi.org/10.1021/acs.macromol.6b01085>.
- (289) Imai, S.; Hirai, Y.; Nagao, C.; Sawamoto, M.; Terashima, T. Programmed Self-Assembly Systems of Amphiphilic Random Copolymers into Size-Controlled and Thermoresponsive Micelles in Water. *Macromolecules* **2018**, *51* (2), 398–409. <https://doi.org/10.1021/acs.macromol.7b01918>.
- (290) Mikulskis, P.; Hook, A.; Dundas, A. A.; Irvine, D.; Sanni, O.; Anderson, D.; Langer, R.; Alexander, M. R.; Williams, P.; Winkler, D. A. Prediction of Broad-Spectrum Pathogen Attachment to Coating Materials for Biomedical Devices. *ACS Appl. Mater. Interfaces* **2018**, *10* (1), 139–149. <https://doi.org/10.1021/acsami.7b14197>.
- (291) Labute, P. A Widely Applicable Set of Descriptors. *J. Mol. Graph. Model.* **2000**, *18* (4–5), 464–477. [https://doi.org/https://doi.org/10.1016/S1093-3263\(00\)00068-1](https://doi.org/https://doi.org/10.1016/S1093-3263(00)00068-1).
- (292) Bickerton, G. R.; Paolini, G. V.; Besnard, J.; Muresan, S.; Hopkins, A. L. Quantifying the Chemical Beauty of Drugs. *Nat. Chem.* **2012**, *4* (2), 90–98. <https://doi.org/10.1038/nchem.1243>.

- (293) Rogers, D.; Hahn, M. Extended-Connectivity Fingerprints. *J. Chem. Inf. Model.* **2010**, *50* (5), 742–754. <https://doi.org/10.1021/ci100050t>.
- (294) A Decade of Drug-Likeness. *Nature Reviews Drug Discovery*. Nature Publishing Group November 2007, p 853. <https://doi.org/10.1038/nrd2460>.
- (295) Pampaloni, F.; Reynaud, E. G.; Stelzer, E. H. K. The Third Dimension Bridges the Gap between Cell Culture and Live Tissue. *Nature Reviews Molecular Cell Biology*. Nature Publishing Group October 2007, pp 839–845. <https://doi.org/10.1038/nrm2236>.
- (296) Saeed, A.; Francini, N.; White, L.; Dixon, J.; Gould, T.; Rashidi, H.; Al Ghanami, R. C.; Hruschka, V.; Redl, H.; Saunders, B. R.; Alexander, C.; Shakesheff, K. M. A Thermoresponsive and Magnetic Colloid for 3D Cell Expansion and Reconfiguration. *Adv. Mater.* **2015**, *27* (4), 662–668. <https://doi.org/10.1002/adma.201403626>.
- (297) Lin, R. Z.; Chang, H. Y. Recent Advances in Three-Dimensional Multicellular Spheroid Culture for Biomedical Research. *Biotechnology Journal*. Wiley-VCH Verlag October 1, 2008, pp 1172–1184. <https://doi.org/10.1002/biot.200700228>.
- (298) Haycock, J. W. 3D Cell Culture: A Review of Current Approaches and Techniques. *Methods in molecular biology (Clifton, N.J.)*. Humana Press 2011, pp 1–15. [https://doi.org/10.1007/978-1-60761-984-0\\_1](https://doi.org/10.1007/978-1-60761-984-0_1).
- (299) Mirbagheri, M.; Adibnia, V.; Hughes, B. R.; Waldman, S. D.; Banquy, X.; Hwang, D. K. Advanced Cell Culture Platforms: A Growing Quest

for Emulating Natural Tissues. *Materials Horizons*. Royal Society of Chemistry January 1, 2019, pp 45–71. <https://doi.org/10.1039/c8mh00803e>.

(300) Candini, O.; Grisendi, G.; Foppiani, E. M.; Brogli, M.; Aramini, B.; Masciale, V.; Spano, C.; Petrachi, T.; Veronesi, E.; Conte, P.; Mari, G.; Dominici, M. A Novel 3D In Vitro Platform for Pre-Clinical Investigations in Drug Testing, Gene Therapy, and Immuno-Oncology. *Sci. Rep.* **2019**, *9* (1), 1–12. <https://doi.org/10.1038/s41598-019-43613-9>.

(301) Patiño, T.; Soriano, J.; Barrios, L.; Ibáñez, E.; Nogués, C. Surface Modification of Microparticles Causes Differential Uptake Responses in Normal and Tumoral Human Breast Epithelial Cells. *Sci. Rep.* **2015**, *5* (1), 1–12. <https://doi.org/10.1038/srep11371>.

(302) Kawaguchi, H. Functional Polymer Microspheres. *Prog. Polym. Sci.* **2000**, *25* (8), 1171–1210. [https://doi.org/10.1016/S0079-6700\(00\)00024-1](https://doi.org/10.1016/S0079-6700(00)00024-1).

(303) Hooker, J. P.; Feist, F.; Delafresnaye, L.; Barner, L.; Barner-Kowollik, C. Precisely Controlled Microsphere Design via Visible-Light Cross-Linking of Functional Prepolymers. *Adv. Funct. Mater.* **2020**, *30* (26), 1905399. <https://doi.org/10.1002/adfm.201905399>.

(304) Costerton, J. W.; Stewart, P. S.; Greenberg, E. P. Bacterial Biofilms: A Common Cause of Persistent Infections. *Science*. Walport May 21, 1999, pp 1318–1322. <https://doi.org/10.1126/science.284.5418.1318>.

(305) Smith, A. W. Biofilms and Antibiotic Therapy: Is There a Role for Combating Bacterial Resistance by the Use of Novel Drug Delivery Systems?

*Advanced Drug Delivery Reviews*. Elsevier July 29, 2005, pp 1539–1550.  
<https://doi.org/10.1016/j.addr.2005.04.007>.

(306) Davies, D. Understanding Biofilm Resistance to Antibacterial Agents. *Nature Reviews Drug Discovery*. Nature Publishing Group February 2003, pp 114–122. <https://doi.org/10.1038/nrd1008>.

(307) NIH. PA-06-537: Immunology of Biofilms (RO1), 2007.

(308) NIH. NIH Guide: RESEARCH ON MICROBIAL BIOFILMS. *National Institute of Health*. 2002.

(309) Omar, A.; Wright, J.; Schultz, G.; Burrell, R.; Nadworny, P. Microbial Biofilms and Chronic Wounds. *Microorganisms* **2017**, *5* (1), 9. <https://doi.org/10.3390/microorganisms5010009>.

(310) Khaton, Z.; McTiernan, C. D.; Suuronen, E. J.; Mah, T. F.; Alarcon, E. I. Bacterial Biofilm Formation on Implantable Devices and Approaches to Its Treatment and Prevention. *Heliyon* **2018**, *4* (12), e01067. <https://doi.org/10.1016/j.heliyon.2018.e01067>.

(311) Caillier, L.; de Givenchy, E. T.; Levy, R.; Vandenberghe, Y.; G ribaldi, S.; Guittard, F. Synthesis and Antimicrobial Properties of Polymerizable Quaternary Ammoniums. *Eur. J. Med. Chem.* **2009**, *44* (8), 3201–3208. <https://doi.org/10.1016/j.ejmech.2009.03.031>.

(312) Neetu Kumra Taneja; Jaya Sivaswami Tya. Resazurin Reduction Assays for Screening of Anti-Tubercular Compounds against Dormant and Actively Growing Mycobacterium Tuberculosis, Mycobacterium Bovis BCG and Mycobacterium Smegmatis. *J. Antimicrob. Chemother.* **2007**, *43* (1), 1–4. <https://doi.org/10.1093/JAC>.

- (313) Li, P.; Poon, Y. F.; Li, W.; Zhu, H. Y.; Yeap, S. H.; Cao, Y.; Qi, X.; Zhou, C.; Lamrani, M.; Beuerman, R. W.; Kang, E. T.; Mu, Y.; Li, C. M.; Chang, M. W.; Jan Leong, S. S.; Chan-Park, M. B. A Polycationic Antimicrobial and Biocompatible Hydrogel with Microbe Membrane Suctioning Ability. *Nat. Mater.* **2011**, *10* (2), 149–156. <https://doi.org/10.1038/nmat2915>.
- (314) Cunliffe, D.; Smart, C. A.; Alexander, C.; Vulfson, E. N. Bacterial Adhesion at Synthetic Surfaces. *Appl. Environ. Microbiol.* **1999**, *65* (11), 4995–5002. <https://doi.org/10.1128/aem.65.11.4995-5002.1999>.
- (315) Holmes, P. F.; Currie, E. P. K.; Thies, J. C.; Van Der Mei, H. C.; Busscher, H. J.; Norde, W. Surface-Modified Nanoparticles as a New, Versatile, and Mechanically Robust Nonadhesive Coating: Suppression of Protein Adsorption and Bacterial Adhesion. *J. Biomed. Mater. Res. - Part A* **2009**, *91* (3), 824–833. <https://doi.org/10.1002/jbm.a.32285>.
- (316) Cheng, G.; Zhang, Z.; Chen, S.; Bryers, J. D.; Jiang, S. Inhibition of Bacterial Adhesion and Biofilm Formation on Zwitterionic Surfaces. *Biomaterials* **2007**, *28* (29), 4192–4199. <https://doi.org/10.1016/j.biomaterials.2007.05.041>.
- (317) Maan, A. M. C.; Hofman, A. H.; de Vos, W. M.; Kamperman, M. Recent Developments and Practical Feasibility of Polymer-Based Antifouling Coatings. *Advanced Functional Materials*. Wiley-VCH Verlag August 1, 2020. <https://doi.org/10.1002/adfm.202000936>.
- (318) Magin, C. M.; Cooper, S. P.; Brennan, A. B. Non-Toxic Antifouling Strategies. *Mater. Today* **2010**, *13* (4), 36–44. [https://doi.org/10.1016/S1369-7021\(10\)70058-4](https://doi.org/10.1016/S1369-7021(10)70058-4).

- (319) Prime, K. L.; Whitesides, G. M. Self-Assembled Organic Monolayers: Model Systems for Studying Adsorption of Proteins at Surfaces. *Science* (80-. ). **1991**, *252* (5009), 1164–1167. <https://doi.org/10.1126/science.252.5009.1164>.
- (320) Prime, K. L.; Whitesides, G. M. Adsorption of Proteins onto Surfaces Containing End-Attached Oligo(Ethylene Oxide): A Model System Using Self-Assembled Monolayers. *J. Am. Chem. Soc.* **1993**, *115* (23), 10714–10721. <https://doi.org/10.1021/ja00076a032>.
- (321) Wang, P.; Dong, Y.; Zhang, S.; Liu, W.; Wu, Z.; Chen, H. Protein-Resistant Properties of Poly(N-Vinylpyrrolidone)-Modified Gold Surfaces: The Advantage of Bottle-Brushes over Linear Brushes. *Colloids Surfaces B Biointerfaces* **2019**, *177*, 448–453. <https://doi.org/10.1016/j.colsurfb.2019.02.030>.
- (322) Divandari, M.; Morgese, G.; Trachsel, L.; Romio, M.; Dehghani, E. S.; Rosenboom, J. G.; Paradisi, C.; Zenobi-Wong, M.; Ramakrishna, S. N.; Benetti, E. M. Topology Effects on the Structural and Physicochemical Properties of Polymer Brushes. *Macromolecules* **2017**, *50* (19), 7760–7769. <https://doi.org/10.1021/acs.macromol.7b01720>.
- (323) Morgese, G.; Trachsel, L.; Romio, M.; Divandari, M.; Ramakrishna, S. N.; Benetti, E. M. Topological Polymer Chemistry Enters Surface Science: Linear versus Cyclic Polymer Brushes. *Angew. Chemie - Int. Ed.* **2016**, *55* (50), 15583–15588. <https://doi.org/10.1002/anie.201607309>.

- (324) Hannan, R. T.; Peirce, S. M.; Barker, T. H. Fibroblasts: Diverse Cells Critical to Biomaterials Integration. *ACS Biomater. Sci. Eng.* **2018**, *4* (4), 1223–1232. <https://doi.org/10.1021/acsbiomaterials.7b00244>.
- (325) Martin, P. Wound Healing - Aiming for Perfect Skin Regeneration. *Science* (80-. ). **1997**, *276* (5309), 75–81. <https://doi.org/10.1126/science.276.5309.75>.
- (326) Wietecha, M. S.; DiPietro, L. A. Therapeutic Approaches to the Regulation of Wound Angiogenesis. *Adv. Wound Care* **2013**, *2* (3), 81–86. <https://doi.org/10.1089/wound.2011.0348>.
- (327) Doltra, A.; Dietrich, T.; Schneeweis, C.; Kelle, S.; Doltra, A.; Stawowy, P.; Fleck, E. Magnetic Resonance Imaging of Cardiovascular Fibrosis and Inflammation: From Clinical Practice to Animal Studies and Back Cardiovascular MRI View Project Magnetic Resonance Imaging of Cardiovascular Fibrosis and Inflammation: From Clinical Practice to Ani. *Biomed Res. Int.* **2013**, *676489* (10), 1–2. <https://doi.org/10.1155/2013>.
- (328) Nosenko, M. A.; Moysenovich, A. M.; Zvartsev, R. V.; Arkhipova, A. Y.; Zhdanova, A. S.; Agapov, I. I.; Vasilieva, T. V.; Bogush, V. G.; Debabov, V. G.; Nedospasov, S. A.; Moisenovich, M. M.; Drutskaya, M. S. Novel Biodegradable Polymeric Microparticles Facilitate Scarless Wound Healing by Promoting Re-Epithelialization and Inhibiting Fibrosis. *Front. Immunol.* **2018**, *9* (December), 1–11. <https://doi.org/10.3389/fimmu.2018.02851>.
- (329) Tang, L.; Eaton, J. W. Inflammatory Responses to Biomaterials. *American Journal of Clinical Pathology*. Oxford Academic April 1, 1995, pp 466–471. <https://doi.org/10.1093/ajcp/103.4.466>.

- (330) Martin, P. Wound Healing - Aiming for Perfect Skin Regeneration. *Science* (80-. ). **1997**, 276 (5309), 75–81. <https://doi.org/10.1126/science.276.5309.75>.
- (331) Barbosa, M. A.; Martins, M. C. L. *Peptides and Proteins as Biomaterials for Tissue Regeneration and Repair*; Elsevier Inc., 2017. <https://doi.org/10.1016/C2015-0-01811-1>.
- (332) Visalakshan, R. M.; Macgregor, M. N.; Sasidharan, S.; Ghazaryan, A.; Mierczynska-Vasilev, A. M.; Morsbach, S.; Mailänder, V.; Landfester, K.; Hayball, J. D.; Vasilev, K. Biomaterial Surface Hydrophobicity-Mediated Serum Protein Adsorption and Immune Responses. *ACS Appl. Mater. Interfaces* **2019**, 11 (31), 27615–27623. <https://doi.org/10.1021/acsami.9b09900>.
- (333) Liu, Y.; Strauss, J.; Camesano, T. A. Thermodynamic Investigation of Staphylococcus Epidermidis Interactions with Protein-Coated Substrata. *Langmuir* **2007**, 23 (13), 7134–7142. <https://doi.org/10.1021/la700575u>.
- (334) Balamurugan, S.; Ista, L. K.; Yan, J.; López, G. P.; Fick, J.; Himmelhaus, M.; Grunze, M. Reversible Protein Adsorption and Bioadhesion on Monolayers Terminated with Mixtures of Oligo(Ethylene Glycol) and Methyl Groups. *J. Am. Chem. Soc.* **2005**, 127 (42), 14548–14549. <https://doi.org/10.1021/ja054156g>.
- (335) Schilp, S.; Rosenhahn, A.; Pettitt, M. E.; Bowen, J.; Callow, M. E.; Callow, J. A.; Grunze, M. Physicochemical Properties of (Ethylene Glycol)-Containing Self-Assembled Monolayers Relevant for Protein and Algal Cell

Resistance. *Langmuir* **2009**, 25 (17), 10077–10082.  
<https://doi.org/10.1021/la901038g>.

(336) Rosso, M.; Nguyen, A. T.; De Jong, E.; Baggerman, J.; Paulusse, J. M. J.; Giesbers, M.; Fokkink, R. G.; Norde, W.; Schroën, K.; Van Rijn, C. J. M.; Zuilhof, H. Protein-Repellent Silicon Nitride Surfaces: UV-Induced Formation of Oligoethylene Oxide Monolayers. *ACS Appl. Mater. Interfaces* **2011**, 3 (3), 697–704. <https://doi.org/10.1021/am100985c>.

(337) Heydorn, A.; Nielsen, A. T.; Hentzer, M.; Sternberg, C.; Givskov, M.; Ersboll, B. K.; Molin, S. Quantification of Biofilm Structures by the Novel Computer Program COMSTAT. *Microbiology* **2000**.  
<https://doi.org/10.1099/00221287-146-10-2395>.

(338) Nie, Z.; Seo, M. S.; Xu, S.; Lewis, P. C.; Mok, M.; Kumacheva, E.; Whitesides, G. M.; Garstecki, P.; Stone, H. A. Emulsification in a Microfluidic Flow-Focusing Device: Effect of the Viscosities of the Liquids. *Microfluid. Nanofluidics* **2008**, 5 (5), 585–594. <https://doi.org/10.1007/s10404-008-0271-y>.

(339) Tolker-Nielsen, T. Biofilm Development. *Microbiol. Spectr.* **2015**, 3 (2). <https://doi.org/10.1128/microbiolspec.mb-0001-2014>.

(340) Weiner, L. M.; Webb, A. K.; Limbago, B.; Dudeck, M. A.; Patel, J.; Kallen, A. J.; Edwards, J. R.; Sievert, D. M. Antimicrobial-Resistant Pathogens Associated with Healthcare-Associated Infections: Summary of Data Reported to the National Healthcare Safety Network at the Centers for Disease Control and Prevention, 2011-2014. *Infect. Control Hosp. Epidemiol.* **2016**, 37 (11), 1288–1301. <https://doi.org/10.1017/ice.2016.174>.

- (341) O'Toole, G. A.; Wong, G. C. L. Sensational Biofilms: Surface Sensing in Bacteria. *Current Opinion in Microbiology*. Elsevier Ltd April 1, 2016, pp 139–146. <https://doi.org/10.1016/j.mib.2016.02.004>.
- (342) Petrova, O. E.; Sauer, K. Sticky Situations: Key Components That Control Bacterial Surface Attachment. *Journal of Bacteriology*. May 2012, pp 2413–2425. <https://doi.org/10.1128/JB.00003-12>.
- (343) Flemming, H. C.; Wingender, J.; Szewzyk, U.; Steinberg, P.; Rice, S. A.; Kjelleberg, S. Biofilms: An Emergent Form of Bacterial Life. *Nature Reviews Microbiology*. Nature Publishing Group September 1, 2016, pp 563–575. <https://doi.org/10.1038/nrmicro.2016.94>.
- (344) Li, X. M.; Reinhoudt, D.; Crego-Calama, M. What Do We Need for a Superhydrophobic Surface? A Review on the Recent Progress in the Preparation of Superhydrophobic Surfaces. *Chem. Soc. Rev.* **2007**, *36* (8), 1350–1368. <https://doi.org/10.1039/b602486f>.
- (345) Vasudevan, R. Biofilms: Microbial Cities of Scientific Significance. *J. Microbiol. Exp.* **2014**, *1* (3). <https://doi.org/10.15406/jmen.2014.01.00014>.
- (346) Abdul, J.; Salman, S.; Kadhemy, M. F. H. Effect of PVA, PVA/Biosurfactant on Some Pathogenic Bacteria in Glass and Plastic Plates. *Int. J. Curr. Microbiol. Appl. Sci.* **2014**, *3* (10), 301–309.
- (347) Herrwerth, S.; Eck, W.; Reinhardt, S.; Grunze, M. Factors That Determine the Protein Resistance of Oligoether Self-Assembled Monolayers - Internal Hydrophilicity, Terminal Hydrophilicity, and Lateral Packing

Density. *J. Am. Chem. Soc.* **2003**, *125* (31), 9359–9366.  
<https://doi.org/10.1021/ja034820y>.

(348) Chen, S.; Li, L.; Zhao, C.; Zheng, J. Surface Hydration: Principles and Applications toward Low-Fouling/Nonfouling Biomaterials. *Polymer*. Elsevier Ltd October 29, 2010, pp 5283–5293.  
<https://doi.org/10.1016/j.polymer.2010.08.022>.

(349) Cheng, Y.; Feng, G.; Moraru, C. I. Micro-and Nanotopography Sensitive Bacterial Attachment Mechanisms: A Review. *Frontiers in Microbiology*. Frontiers Media S.A. February 21, 2019, p 191.  
<https://doi.org/10.3389/fmicb.2019.00191>.

(350) Pringle, J. H.; Fletcher, M. Influence of Substratum Wettability on Attachment of Freshwater Bacteria to Solid Surfaces. *Appl. Environ. Microbiol.* **1983**, *45* (3), 811–817. <https://doi.org/10.1128/aem.45.3.811-817.1983>.

(351) Ista, L. K.; Mendez, S.; Lopez, G. P. Attachment and Detachment of Bacteria on Surfaces with Tunable and Switchable Wettability. *Biofouling* **2010**, *26* (1), 111–118. <https://doi.org/10.1080/08927010903383455>.

(352) Bain, C. D.; Whitesides, G. M. Depth Sensitivity of Wetting: Monolayers of  $\omega$ -Mercapto Ethers on Gold. *J. Am. Chem. Soc.* **1988**, *110* (17), 5897–5898. <https://doi.org/10.1021/ja00225a050>.

(353) Vogler, E. A. Structure and Reactivity of Water at Biomaterial Surfaces. *Adv. Colloid Interface Sci.* **1998**, *74* (1–3), 69–117.  
[https://doi.org/10.1016/S0001-8686\(97\)00040-7](https://doi.org/10.1016/S0001-8686(97)00040-7).

- (354) Vogler, E. A. Protein Adsorption in Three Dimensions. *Biomaterials* **2012**, *33* (5), 1201–1237. <https://doi.org/10.1016/j.biomaterials.2011.10.059>.
- (355) Alexander, M. R.; Williams, P. Water Contact Angle Is Not a Good Predictor of Biological Responses to Materials. *Biointerphases* **2017**, *12* (2), 02C201. <https://doi.org/10.1116/1.4989843>.
- (356) Yu, Q.; Zhang, Y.; Chen, H.; Wu, Z.; Huang, H.; Cheng, C. Protein Adsorption on Poly(N-Isopropylacrylamide)-Modified Silicon Surfaces: Effects of Grafted Layer Thickness and Protein Size. *Colloids Surfaces B Biointerphases* **2010**, *76* (2), 468–474. <https://doi.org/10.1016/j.colsurfb.2009.12.006>.
- (357) Chen, H.; Hu, X.; Zhang, Y.; Li, D.; Wu, Z.; Zhang, T. Effect of Chain Density and Conformation on Protein Adsorption at PEG-Grafted Polyurethane Surfaces. *Colloids Surfaces B Biointerphases* **2008**, *61* (2), 237–243. <https://doi.org/10.1016/j.colsurfb.2007.08.012>.
- (358) Yoshikawa, C.; Goto, A.; Tsujii, Y.; Fukuda, T.; Kimura, T.; Yamamoto, K.; Kishida, A. Protein Repellency of Well-Defined, Concentrated Poly(2-Hydroxyethyl Methacrylate) Brushes by the Size-Exclusion Effect. *Macromolecules* **2006**, *39* (6), 2284–2290. <https://doi.org/10.1021/ma0520242>.
- (359) Yang, W.; Chen, S.; Cheng, G.; Vaisocherová, H.; Xue, H.; Li, W.; Zhang, J.; Jiang, S. Film Thickness Dependence of Protein Adsorption from Blood Serum and Plasma onto Poly(Sulfobetaine)-Grafted Surfaces. *Langmuir* **2008**, *24* (17), 9211–9214. <https://doi.org/10.1021/la801487f>.

- (360) Sanni, O.; Chang, C. Y.; Anderson, D. G.; Langer, R.; Davies, M. C.; Williams, P. M.; Williams, P.; Alexander, M. R.; Hook, A. L. Bacterial Attachment to Polymeric Materials Correlates with Molecular Flexibility and Hydrophilicity. *Adv. Healthc. Mater.* **2015**, *4* (5), 695–701. <https://doi.org/10.1002/adhm.201400648>.
- (361) Epa, V. C.; Hook, A. L.; Chang, C.; Yang, J.; Langer, R.; Anderson, D. G.; Williams, P.; Davies, M. C.; Alexander, M. R.; Winkler, D. A. Modelling and Prediction of Bacterial Attachment to Polymers. *Adv. Funct. Mater.* **2014**, *24* (14), 2085–2093. <https://doi.org/10.1002/adfm.201302877>.
- (362) Mikulskis, P.; Hook, A.; Dundas, A. A.; Irvine, D.; Sanni, O.; Anderson, D.; Langer, R.; Alexander, M. R.; Williams, P.; Winkler, D. A. Prediction of Broad-Spectrum Pathogen Attachment to Coating Materials for Biomedical Devices. *ACS Appl. Mater. Interfaces* **2018**, *10* (1), 139–149. <https://doi.org/10.1021/acsami.7b14197>.
- (363) Navarro, M.; Benetti, E. M.; Zapotoczny, S.; Planell, J. A.; Vancso, G. J. Buried, Covalently Attached RGD Peptide Motifs in Poly(Methacrylic Acid) Brush Layers: The Effect of Brush Structure on Cell Adhesion. *Langmuir* **2008**, *24* (19), 10996–11002. <https://doi.org/10.1021/la800999y>.
- (364) Yu, Q.; Zhang, Y.; Wang, H.; Brash, J.; Chen, H. Anti-Fouling Bioactive Surfaces. *Acta Biomater.* **2011**, *7* (4), 1550–1557. <https://doi.org/10.1016/j.actbio.2010.12.021>.
- (365) Liu, S.; Guo, W. Anti-Biofouling and Healable Materials: Preparation, Mechanisms, and Biomedical Applications. *Adv. Funct. Mater.* **2018**, *28* (41), 1–25. <https://doi.org/10.1002/adfm.201800596>.

- (366) Wörz, A.; Berchtold, B.; Moosmann, K.; Prucker, O.; Rühle, J. Protein-Resistant Polymer Surfaces. *J. Mater. Chem.* **2012**, *22* (37), 19547–19561. <https://doi.org/10.1039/c2jm30820g>.
- (367) Hucknall, A.; Rangarajan, S.; Chilkoti, A. In Pursuit of Zero: Polymer Brushes That Resist the Adsorption of Proteins. *Adv. Mater.* **2009**, *21* (23), 2441–2446. <https://doi.org/10.1002/adma.200900383>.
- (368) Uhlig, K.; Wischerhoff, E.; Lutz, J. F.; Laschewsky, A.; Jaeger, M. S.; Lankenau, A.; Duschl, C. Monitoring Cell Detachment on PEG-Based Thermoresponsive Surfaces Using TIRF Microscopy. *Soft Matter* **2010**, *6* (17), 4262–4267. <https://doi.org/10.1039/c0sm00010h>.
- (369) Ostuni, E.; Chapman, R. G.; Liang, M. N.; Meluleni, G.; Pier, G.; Ingber, D. E.; Whitesides, G. M. Self-Assembled Monolayers That Resist the Adsorption of Proteins and the Adhesion of Bacterial and Mammalian Cells. *Langmuir* **2001**, *17* (20), 6336–6343. <https://doi.org/10.1021/la010552a>.
- (370) Ahrens, C. C.; Dong, Z.; Li, W. Engineering Cell Aggregates through Incorporated Polymeric Microparticles. *Acta Biomaterialia*. 2017, pp 64–81. <https://doi.org/10.1016/j.actbio.2017.08.003>.
- (371) Sart, S.; Tsai, A. C.; Li, Y.; Ma, T. Three-Dimensional Aggregates of Mesenchymal Stem Cells: Cellular Mechanisms, Biological Properties, and Applications. *Tissue Engineering - Part B: Reviews*. Mary Ann Liebert Inc. October 1, 2014, pp 365–380. <https://doi.org/10.1089/ten.teb.2013.0537>.
- (372) Abecasis, B.; Aguiar, T.; Arnault, É.; Costa, R.; Gomes-Alves, P.; Aspegren, A.; Serra, M.; Alves, P. M. Expansion of 3D Human Induced Pluripotent Stem Cell Aggregates in Bioreactors: Bioprocess Intensification

and Scaling-up Approaches. *J. Biotechnol.* **2017**, *246*, 81–93.  
<https://doi.org/10.1016/j.jbiotec.2017.01.004>.

(373) Samal, S. K.; Dash, M.; Vlierberghe, S. Van; Kaplan, D. L.; Chiellini, E.; Blitterswijk, C. van; Moroni, L.; Dubruel, P. Cationic Polymers and Their Therapeutic Potential. *Chem. Soc. Rev.* **2012**, *41* (21), 7147–7194.  
<https://doi.org/10.1039/c2cs35094g>.

(374) Putnam, D. Polymers for Gene Delivery across Length Scales. *Nature Materials*. Nature Publishing Group June 10, 2006, pp 439–451.  
<https://doi.org/10.1038/nmat1645>.

(375) Yang, Y.; Cai, Z.; Huang, Z.; Tang, X.; Zhang, X. Antimicrobial Cationic Polymers: From Structural Design to Functional Control. *Polymer Journal*. Nature Publishing Group November 1, 2018, pp 33–44.  
<https://doi.org/10.1038/pj.2017.72>.

(376) Bhattarai, N.; Gunn, J.; Zhang, M. Chitosan-Based Hydrogels for Controlled, Localized Drug Delivery. *Advanced Drug Delivery Reviews*. 2010, pp 83–99. <https://doi.org/10.1016/j.addr.2009.07.019>.

(377) Magennis, E. P.; Fernandez-Trillo, F.; Sui, C.; Spain, S. G.; Bradshaw, D. J.; Churchley, D.; Mantovani, G.; Winzer, K.; Alexander, C. Bacteria-Instructed Synthesis of Polymers for Self-Selective Microbial Binding and Labelling. *Nat. Mater.* **2014**, *13* (7), 748–755.  
<https://doi.org/10.1038/nmat3949>.

(378) Gurnani, P.; Blakney, A. K.; Terracciano, R.; Petch, J. E.; Blok, A. J.; Bouton, C. R.; McKay, P. F.; Shattock, R. J.; Alexander, C. The In Vitro , Ex Vivo , and In Vivo Effect of Polymer Hydrophobicity on Charge-Reversible

Vectors for Self-Amplifying RNA. *Biomacromolecules* **2020**, *21*, 3253.  
<https://doi.org/10.1021/acs.biomac.0c00698>.

(379) Cuzzucoli Crucitti, V.; Migneco, L. M.; Piozzi, A.; Taresco, V.; Garnett, M.; Argent, R. H.; Francolini, I. Intermolecular Interaction and Solid State Characterization of Abietic Acid/Chitosan Solid Dispersions Possessing Antimicrobial and Antioxidant Properties. *Eur. J. Pharm. Biopharm.* **2018**, *125*, 114–123. <https://doi.org/10.1016/j.ejpb.2018.01.012>.

(380) Georgiou, T. K.; Vamvakaki, M.; Patrickios, C. S.; Yamasaki, E. N.; Phylactou, L. A. Nanoscopic Cationic Methacrylate Star Homopolymers: Synthesis by Group Transfer Polymerization, Characterization and Evaluation as Transfection Reagents. *Biomacromolecules* **2004**, *5* (6), 2221–2229. <https://doi.org/10.1021/bm049755e>.

(381) Llopis-Hernández, V.; Cantini, M.; González-García, C.; Cheng, Z. A.; Yang, J.; Tsimbouri, P. M.; García, A. J.; Dalby, M. J.; Salmerón-Sánchez, M. Material-Driven Fibronectin Assembly for High-Efficiency Presentation of Growth Factors. *Sci. Adv.* **2016**, *2* (8), 1–10. <https://doi.org/10.1126/sciadv.1600188>.

(382) Förster, S.; Abetz, V.; Müller, A. H. E. Polyelectrolyte Block Copolymer Micelles. *Advances in Polymer Science*. Springer, Berlin, Heidelberg 2004, pp 173–210. <https://doi.org/10.1007/b11351>.

(383) Kumar, S.; Acharya, R.; Chatterji, U.; De, P. Side-Chain Amino-Acid-Based Ph-Responsive Self-Assembled Block Copolymers for Drug Delivery and Gene Transfer. *Langmuir* **2013**, *29* (49), 15375–15385. <https://doi.org/10.1021/la403819g>.

- (384) Förster, S.; Antonietti, M. Amphiphilic Block Copolymers in Structure-Controlled Nanomaterial Hybrids. *Adv. Mater.* **1998**, *10* (3), 195–217. [https://doi.org/10.1002/\(SICI\)1521-4095\(199802\)10:3<195::AID-ADMA195>3.0.CO;2-V](https://doi.org/10.1002/(SICI)1521-4095(199802)10:3<195::AID-ADMA195>3.0.CO;2-V).
- (385) Mori, T.; Hashizume, A.; Sato, T. Micellization Behavior of an Amphiphilic Statistical Copolymer in Water-Methanol Mixtures. *Polym. J.* **2009**, *41* (3), 189–194. <https://doi.org/10.1295/polymj.PJ2008223>.
- (386) Huang, J.; Cusick, B.; Pietrasik, J.; Wang, L.; Kowalewski, T.; Lin, Q.; Matyjaszewski, K. Synthesis and in Situ Atomic Force Microscopy Characterization of Temperature-Responsive Hydrogels Based on Poly(2-(Dimethylamino)Ethyl Methacrylate) Prepared by Atom Transfer Radical Polymerization. *Langmuir* **2007**, *23* (1), 241–249. <https://doi.org/10.1021/la061683k>.
- (387) Datta, H.; Bhowmick, A. K.; Singha, N. K. Atom Transfer Radical Polymerization (ATRP) of Ethyl Acrylate: Its Mechanistic Studies. In *Macromolecular Symposia*; John Wiley & Sons, Ltd, 2006; Vol. 240, pp 245–251. <https://doi.org/10.1002/masy.200650830>.
- (388) Pearce, A. K.; Anane-Adjei, A. B.; Cavanagh, R. J.; Monteiro, P. F.; Bennett, T. M.; Taresco, V.; Clarke, P. A.; Ritchie, A. A.; Alexander, M. R.; Grabowska, A. M.; Alexander, C. Effects of Polymer 3D Architecture, Size, and Chemistry on Biological Transport and Drug Delivery In Vitro and in Orthotopic Triple Negative Breast Cancer Models. *Adv. Healthc. Mater.* **2020**, *9* (22), 2000892. <https://doi.org/10.1002/adhm.202000892>.

- (389) Phan, H.; Minut, R. I.; McCrorie, P.; Vasey, C.; Larder, R. R.; Krumins, E.; Marlow, M.; Rahman, R.; Alexander, C.; Taresco, V.; Pearce, A. K. Role of Self-Assembly Conditions and Amphiphilic Balance on Nanoparticle Formation of PEG-PDLLA Copolymers in Aqueous Environments. *J. Polym. Sci. Part A Polym. Chem.* **2019**, *57* (17), 1801–1810. <https://doi.org/10.1002/pola.29451>.
- (390) Suk, J. S.; Xu, Q.; Kim, N.; Hanes, J.; Ensign, L. M. PEGylation as a Strategy for Improving Nanoparticle-Based Drug and Gene Delivery. *Advanced Drug Delivery Reviews*. Elsevier B.V. April 1, 2016, pp 28–51. <https://doi.org/10.1016/j.addr.2015.09.012>.
- (391) Mandal, P.; Singha, N. K. Tailor-Made Polymethacrylate Bearing Bicyclo-Alkenyl Functionality via Selective ATRP at Ambient Temperature and Its Post-Polymerization Modification by “thiol-Ene” Reaction. *RSC Adv.* **2014**, *4* (11), 5293–5299. <https://doi.org/10.1039/c3ra43801e>.
- (392) Horn, M.; Matyjaszewski, K. Solvent Effects on the Activation Rate Constant in Atom Transfer Radical Polymerization. *Macromolecules* **2013**, *46* (9), 3350–3357. <https://doi.org/10.1021/ma400565k>.
- (393) Giernoth, R. Solvents and Solvent Effects in Organic Chemistry. 4th Ed. By Christian Reichardt and Thomas Welton. *Angew. Chemie Int. Ed.* **2011**, *50* (48), 11289–11289. <https://doi.org/10.1002/anie.201105531>.
- (394) Xu, J. H.; Luo, G. S.; Li, S. W.; Chen, G. G. Shear Force Induced Monodisperse Droplet Formation in a Microfluidic Device by Controlling Wetting Properties. *Lab Chip* **2006**, *6* (1), 131–136. <https://doi.org/10.1039/b509939k>.

- (395) Dreyfus, R.; Tabeling, P.; Willaime, H. Ordered and Disordered Patterns in Two-Phase Flows in Microchannels. *Phys. Rev. Lett.* **2003**, *90* (14), 4. <https://doi.org/10.1103/PhysRevLett.90.144505>.
- (396) Endres, T. K.; Beck-Broichsitter, M.; Samsonova, O.; Renette, T.; Kissel, T. H. Self-Assembled Biodegradable Amphiphilic PEG–PCL–LPEI Triblock Copolymers at the Borderline between Micelles and Nanoparticles Designed for Drug and Gene Delivery. *Biomaterials* **2011**, *32* (30), 7721–7731. <https://doi.org/10.1016/J.BIOMATERIALS.2011.06.064>.
- (397) Rafati, A.; Boussahel, A.; Shakesheff, K. M.; Shard, A. G.; Roberts, C. J.; Chen, X.; Scurr, D. J.; Rigby-Singleton, S.; Whiteside, P.; Alexander, M. R.; Davies, M. C. Chemical and Spatial Analysis of Protein Loaded PLGA Microspheres for Drug Delivery Applications. *J. Control. Release* **2012**, *162* (2), 321–329. <https://doi.org/10.1016/j.jconrel.2012.05.008>.
- (398) Aylott, J. W.; Trindade, G. F.; Shard, A. G.; Mendes, P. M.; Williams, P. M.; Alexander, M. R.; Scurr, D. J. Protein Identification by 3D Orbitrap SIMS to Facilitate in Situ Imaging and Depth Profiling. *Nat. Commun.* **2020**, *11* (2020), 1–8. <https://doi.org/10.1038/s41467-020-19445-x>.